CONF-8305107

PROCEEDINGS

17th Asilomar Conference on Fire and Blast Effects of Nuclear Weapons

May 30–June 3, 1983

Asilomar Conference Center
Pacific Grove, California

Sponsored by
The Federal Emergency Management Agency (FEMA)

Organized by
The Lawrence Livermore National Laboratory (LLNL)

FEMA Contract No. EMW-E-0883
Work Unit Unit No. 2561C

This report has been reviewed by Lawrence Livermore National Laboratory for the Federal Emergency Management Agency and has been approved for publication. Approval does not signify that the contents necessarily reflect the views and policies of the Federal Emergency Management Agency.

Work performed under the auspices of the U.S. Department of Energy by Lawrence Livermore National Laboratory under Contract W-7405-Eng-48.

CONF-8305107

PROCEEDINGS

17th Asilomar Conference on Fire and Blast Effects of Nuclear Weapons

May 30–June 3, 1983

Asilomar Conference Center
Pacific Grove, California

Edited by
Robert G. Hickman
Carol A. Meier

Sponsored by
The Federal Emergency Management Agency (FEMA)

Organized by
The Lawrence Livermore National Laboratory (LLNL)

LAWRENCE LIVERMORE LABORATORY
University of California • Livermore, California • 94550

COMPONENT PART NOTICE

THIS PAPER IS A COMPONENT PART OF THE FOLLOWING COMPILATION REPORT:

(TITLE): Proceedings. Asilomar Conference on Fire and Blast Effects of Nuclear Weapons (17th), May 30-June 3, 1983. Asilomar Conference Center, Pacific Grove, California,

(SOURCE): Lawrence Livermore National Lab. (390999).

TO ORDER THE COMPLETE COMPILATION REPORT USE AD-A132 780.

THE COMPONENT PART IS PROVIDED HERE TO ALLOW USERS ACCESS TO INDIVIDUALLY AUTHORED SECTIONS OF PROCEEDINGS, ANNALS, SYMPOSIA, ETC. HOWEVER, THE COMPONENT SHOULD BE CONSIDERED WITHIN THE CONTEXT OF THE OVERALL COMPILATION REPORT AND NOT AS A STAND-ALONE TECHNICAL REPORT.

THE FOLLOWING COMPONENT PART NUMBERS COMPRISE THE COMPILATION REPORT:

AD#:	TITLE:
AD-P001 799	Direct Course Blast Shelter Entranceway and Blast Door Experiments.
AD-P001 800	Failure Criteria for Blast Loads Structures - A Review.
AD-P001 801	Effects of Multiple Bursts on Structural Response.
AD-P001 802	Hydrocode Studies of Flows Generated by Large Area Fires.
AD-P001 803	Firestorm Formation and Environment Characteristics after a Large-Yield Nuclear Burst.
AD-P001 804	Criteria for Onset of Firestorms.
AD-P001 805	Analysis of the Large Urban Fire Environment.
AD-P001 806	The Large Urban Fire Environment: Trends and Model City Predictions.
AD-P001 807	Reliability of Engineered Basements as Blast Shelters.
AD-P001 808	Reliability of Residential Basements as Blast Shelters.
AD-P001 809	Design Validation Experiments for the Key Workers Blast Shelter.
AD-P001 810	Structural Response of the SATCOM Antenna to a Blast Loading.
AD-P001 811	Air Gun Test Facility.
AD-P001 812	Wind-Aided Flame Spread Across Strewn Debris.
AD-P001 813	Modeling Urban Fire Growth.
AD-P001 814	Flashover Modeling for Direct Course.
AD-P001 815	Spontaneous Ignition of Solids Subjected to Linearly Time-Dependent Radiant Exposure.
AD-P001 816	Global-Scale Obscuration by Mass Fire Smoke.
AD-P001 817	Fire in Targeting Urban/Industrial Areas.
AD-P001 818	Thermal Radiation from a Nuclear Weapon Burst.

COMPONENT PART NOTICE (CON'T)

AD#:	TITLE:
AD-P001 819	Direct Course Industrial Hardening Experiment and Predictions.
AD-P001 820	Blast Loading Computations Over Complex Structures.
AD-P001 821	Design of Blast Simulators for Nuclear Testing.

SECURITY CLASSIFICATION OF THIS PAGE (When Data Entered)

REPORT DOCUMENTATION PAGE		READ INSTRUCTIONS BEFORE COMPLETING FORM
1. REPORT NUMBER	2. GOVT ACCESSION NO.	3. RECIPIENT'S CATALOG NUMBER
4. TITLE (and Subtitle) Proceedings 17th Asilomar Conference on Fire and Blast Effects of Nuclear Weapons		5. TYPE OF REPORT & PERIOD COVERED 1983 Conference Proceedings 6. PERFORMING ORG. REPORT NUMBER Conf.-8305107
7. AUTHOR(s) Robert G. Hickman Carol A. Meier (eds.)		8. CONTRACT OR GRANT NUMBER(s) EMW-E-0883
9. PERFORMING ORGANIZATION NAME AND ADDRESS Lawrence Livermore National Laboratory P.O. Box 808 Livermore CA 94550		10. PROGRAM ELEMENT, PROJECT, TASK AREA & WORK UNIT NUMBERS FEMA Work Unit 2561C
11. CONTROLLING OFFICE NAME AND ADDRESS Federal Emergency Management Agency Washington DC 20472		12. REPORT DATE July 1983 13. NUMBER OF PAGES 287
14. MONITORING AGENCY NAME & ADDRESS (if different from Controlling Office) Lawrence Livermore National Laboratory P.O. Box 808 Livermore CA 94550		15. SECURITY CLASS. (of this report) Unclassified 15a. DECLASSIFICATION/DOWNGRADING SCHEDULE

16. DISTRIBUTION STATEMENT (of this Report)

Approved for Public Release: Distribution Unlimited

17. DISTRIBUTION STATEMENT (of the abstract entered in Block 20, if different from Report)

18. SUPPLEMENTARY NOTES

19. KEY WORDS (Continue on reverse side if necessary and identify by block number)

Blast/Fire interaction research, fire initiation, extinction of fire by blast, blast response of urban structures, fire spread, fire hazards, fire countermeasures.

20. ABSTRACT (Continue on reverse side if necessary and identify by block number)

This report summarizes the proceedings of the 17th Asilomar Conference on Fire and Blast Effects of Nuclear Weapons. The conference, sponsored by the Federal Emergency Management Agency (FEMA) and organized by the Lawrence Livermore National Laboratory (LLNL, was held from May 30 through June 3, 1983 at the Asilomar Conference Center in Pacific Grove, California.

The objective of the 1983 conference was to provide for the technical

DD FORM 1 JAN 73 1473 EDITION OF 1 NOV 65 IS OBSOLETE

SECURITY CLASSIFICATION OF THIS PAGE (When Data Entered)

20. ABSTRACT (cont.)

exchange of ideas relating to the science and technology of the immediate effects of nuclear weapon explosions. This exchange was accomplished through the presentation of technical papers, as well as through formal group discussions on pertinent topics. Those attending the conference included individuals from Sweden and the United Kingdom, as well as those individuals from government, industry, and academia in the United States.

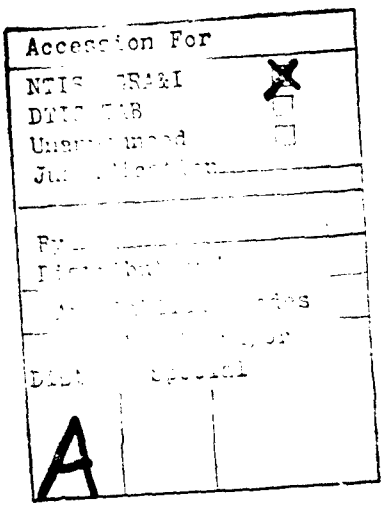

CONTENTS

ABSTRACT

This report summarizes the proceedings of the 17th Asilomar Conference on Fire and Blast Effects of Nuclear Weapons. The conference, sponsored by the Federal Emergency Management Agency (FEMA) and organized by the Lawrence Livermore National Laboratory (LLNL), was held from May 30 through June 3, 1983 at the Asilomar Conference Center in Pacific Grove, California.

The objective of the 1983 conference was to provide for the technical exchange of ideas relating to the science and technology of the immediate effects of nuclear weapon explosions. This exchange was accomplished through the presentation of technical papers, as well as through formal group discussions on pertinent topics. Those attending the conference included individuals from Sweden and the United Kingdom, as well as those individuals from government, industry, and academia in the United States.

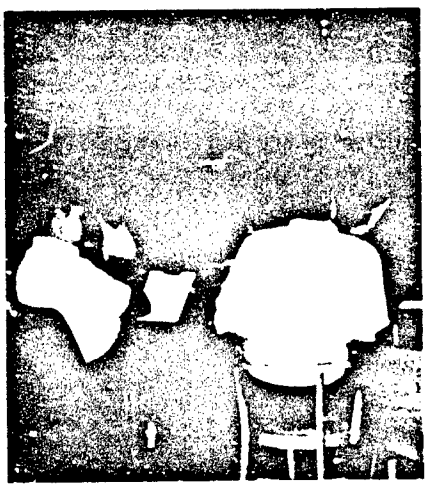

Conference Candids

CONFERENCE COMMITTEE

Lawrence Livermore National Laboratory

Conference Chairperson
Robert Hickman

Conference Coordinator
Camille Minichino

Publications Chairperson
Carol Meier

Coordinating Secretary
Jackie Meeks

TECHNICAL REVIEW COMMITTEE

Lawrence Livermore National Laboratory

Robert Hickman

Sang-Mook Kang

Shyam Shukla

Tom Reitter

OPENING REMARKS

AND

AGENCY OVERVIEWS

1983 Asilomar Conference

Opening Remarks
by
Jim Kerr

I think it's important to look in both directions in meetings like this. A lot of distinguished alumni are back. The direct lineage of these meetings goes back to early meetings with the fire research contractors that we held with our contractors at IITRI in 1962. Various sponsorships, or managing organizations, were represented at the original 1962 meeting and at the Forest Service when we met in Riverside and at NRDL in San Francisco. We first came to Asilomar about 1966. Outside of some state agencies, we have had the longest run of any organization meeting at Asilomar. About 20% of you are here for the first time, and that fraction of new people every year is quite healthy; otherwise, the program tends to get a little stale and we can't have that. We think that gatherings of this type are absolutely essential to educate us. We regard this as an important management tool for the FEMA research management people. Certainly we have to exchange information and cross-fertilize.

FEMA started under the Carter Administration by putting 5 agencies together. Under the Reagan Administration FFMA does have a mandate to succeed and that is of real importance. We are supposed to move ahead and make the pieces fit together with the mission that we have. As some of you heard me say, we are responsible for everything from "hang-nails to holocaust" and everything between. It's an incredibly broad mission, and at the same time Dr. Giuffrida feels that he does have a mandate from the President to succeed. The President feels that having the civil population prepared to cope with disaster, of whatever flavor, is in fact a part of the strategic equation. He also feels that it is very important that we have our international connections, so we have people here from across the water.

The Research Office is in the National Preparedness Program Directorate of FEMA. FEMA has three principal program areas, the training and fire programs, the State and Local Programs Directorate which interface with the state and local authorities to carry out programs. The National Preparedness Program Directorate is supposed to be at the cutting edge, the place where all the brains are and where the program and policies are developed. There is a very good rationale for having this office in with our brethren who take care of other national programs, industrial preparedness, and that sort of thing. The Research Office with all this coverage sits there with all these National Preparedness Programs. It's supposed to provide basic science input to all the rest of the agency. Each element of FEMA has both the privilege and the duty of funding its own applied research program. For example, if Don Bettge, who is in the Civil Defense Division, wants to do something along the lines of countermeasures, say blast hardening, it's up to him to fund it, and you go after him for money, not me. If he runs these things through me, I have a ccomputer search done, and then we can find out where some other work has been done, because if its applied science, it is not run through the Research Office. So if Don finds that he can't do his countermeasure program, because the physics haven't been done yet, then he's free to call on the Research Office to see about funding the physics.

The Research Office does have to do the coordination of R&D for FEMA. It serves as a focal point for science and technology support. Those are our principal jobs and that's where we spend most of our time. Part of our R&D program is performed within FEMA, resulting in papers which we prepare ourselves, as distinguished from contract work. There is now a working group in FEMA known as the Issues Group. These are presidential appointees, of which we have four or five, and they meet every week to address real issues. Some of the issues, of course, are how do we play the R&D game, how do we allocate funds, and how do we manage. It's also interesting to look at the history. The best history and certainly the oldest agency of the five that went together to form FEMA was the Civil Defense Agency. We had the Berlin Crisis and the Cuban Missile Crisis. Budgets responded to political events rather than scientific breakthroughs.

How should we mobilize the nation in time of stress and crises and international tension? The President decides that he wants to upgrade our preparedness. What should the research role be? We look at the history of World War II, and we find that President Roosevelt discovered that there was science around, and that the science industry was going to start expanding. There had to be a fairly respectable establishment with a management role. This was put together on a crash basis, and the legacy that we have is the excellent R&D program of today. We have a Science Advisor in the White House with a half dozen other staff, and nobody else worrying about science in the civil sector. We have a bit of an in-house study going on right now. Capt. Jarratt is working on that problem, and we think that that's a place where the National Defense Executive Reserve could play a big role. I thank those of you who responded last year to my recruiting pitch to sign up for the Executive Reserve. It is sort of like the National Guard without a uniform. The mobilization is something that FEMA has to work out; I hope our plan will hit the streets by the end of the year.

What is the keynote? I have suggested that we concentrate on the pursuit of excellence. That's not a bad way to start this conference again, but perhaps that's a little too vague. I think that we have to concentrate on collating our knowledge, synthesizing what we believe and understand, and looking ahead in a fashion so that we can provide the scientific guidance that not just FEMA but people who work in the civil areas can use. We have opportunities here: there are all the papers which you will hear; and the workshops that are the heart of the week's work. The heart of the conference is the interaction that we achieve, and that happens most in the workshops.

The proceedings are evidence of where we think we stand on any given subject. We read them carefully and those of us here naturally have an awareness of what is going on, but people throughout the Agency look at what's been said in the workshops, and this does tend to move science down the road.

BOB LEVINE - NBS
Opening Remarks

Our role is going to be limited pretty much to the more scientific areas of fire science in the future. Right now we have about 100 people on our staff. In terms of budget, we get about $3.5M from other agencies (including FEMA) and about $5M internally. With our internal funding, we operate a grants program that amounts to $2M which goes to universities. Thus, our in-house program ends up as about half contract work. We try to stay in close contact with the real world, by being in direct contact with people who must comply with regulations.

We perform fire property tests on full-scale rooms with real materials and furnishings. We also serve on a number of advisory panels. Our organization is made up of groups, each of which represents a thrust area. Some are very basic, such as fire gas toxicology, and others are more applied, aimed at getting materials properties that can be put into computer models. Other thrust areas include, but are not limited to, extinguishment and suppression phenomena and techniques, development of a more quantitative fire safety evaluation system, and quantitative fire risk analysis. This has many tasks, similar to the nuclear people, but we are trying to go beyond the simple cost effectiveness justification. We also perform laboratory work in support of arson studies.

Some recent tests include flame spread rates as a function of impinging radiant heat flux, and these results can go into computer models, too. The expression developed works on a number of different kinds of materials, including those found in airplanes. In the area of 3D field equations applied to plumes, our Center of Applied Mathematics within the Bureau has developed a model for use in rooms in conjunction with Fendell and Carrier.

In our grants program, which is $2M as I mentioned earlier, we have about a 25% turnover each year. Flame spread, sooting, turbulent diffusion flames, charring, entrained flow in corridors, radiation from flames, combustion efficiency, and radiation from soot are typical study areas that are currently funded. We monitor these activities with people who are doing similar research in-house, so close contact is maintained.

We are also putting more effort into working with the fire community in a more organized way rather than just hoping it will happen.

HAL ANDERSON - U S. Forestry Service
Opening Pemarks

I'll describe briefly what has occurred in the past three years and what we anticipate in the coming year. The Forestry Service is made up of three branches, one of which is Research. The funding has declined some in the past few years. In the fire area, we have 77 people at the research stations throughout the country. There are another 38 fire-related scientists who are funded from other parts of the Forestry Service. Our fire research budget in FY83 is $8M, or about $2M less than in FY81, and we anticipate another decline of about $1M in FY84.

Our station, the Intermountain Station at Missoula, Montana, received about $2.5M this year, and fire behavior received about $1M. We are trying to speed the utilization of research compared to our typical technology transfer rates of the past. We have developed predictive fire models for slope effects, moisture effects, and wind-driven fires. This model is being used in officer training and in the training of other specialists to make it operational by next year. Fire effects R&D work deals with recovery of a burned over area, mostly from the viewpoint of the biologist. The fate of fauna, vegetation, seeds, micro-organisms in the soil, are each important.

We have two other fire labs in the US: one at Riverside, California, and one in Macon, Georgia. At Riverside, they are looking at fire in chaparral. They study fire management, economics, fire prevention, and meteorological effects. At the Macon lab, there are three projects: combustion processes that involves toxicity and particulates production; adaptation of fire science developed in the West to the needs of the East; and fire-weather data systems. We also have several stations around the country doing other kinds of forestry research.

We're trying very hard to do the best work we can and take advantage of information exchanges such as this to make the most of our shrinking budgets, just as others have probably experienced.

SESSION I

STRUCTURAL RESPONSE A

BLAST LOADING OF CLOSURES FOR USE ON SHELTERS

George A. Coulter

U.S. Army Ballistic Research Laboratory
U.S. Army Armament Research and Development Command
Aberdeen Proving Ground, Maryland 21005

ABSTRACT

The work reported here is a part of a study funded by the Federal Emergency Management Agency (FEMA) under Work Unit 1123C to upgrade existing shelters in key worker and host areas. The objective of this portion of the study is to determine closures suitable for shelters in these two areas. Ultimate failure of closures (breakout) was determined by dynamic loading tests performed at the BRL 2.44 m blast simulator. Test results are given for three types of closures. Load ratios of ultimate failure to allowable static design loads were found dynamically to be about four for the wood beam/plywood skin closures. This would make it acceptable for both host and key worker shelter areas.

I. INTRODUCTION

The work described here is a part of a study funded by FEMA under Work Unit 1123C to upgrade existing shelters. The objective of the Interagency Agreement No. EMW-E-0699 with the Ballistic Research Laboratory (BRL) was to design and test a series of closures made from readily available materials that might be suitable for use in host and key worker areas. A major requirement was that the materials could be obtained at local suppliers. Also, the closures should be useable for opening sizes from small pipe vents to entryways for underground shelters.

Previous work sponsored by FEMA at BRL (1), (2) had verified design procedures (3) indicating that plywood panels and plywood stressed-skin panels were satisfactory expedient closures for the low pressure host area. They were also effective closures for small, pipe vent type openings in the higher pressure risk area if used with suitable supporting fixtures. The need, therefore, was to design and test closures intended for entryway-size openings in the risk area.

Accordingly, three types of closures were prepared for testing at the BRL 2.44 m (8 ft) shock tube: commercial steel doors, steel grating/plywood closures, and wood beam/plywood skin closures. The method of testing is described in the next section.

II. TEST PROCEDURE

Details of the test flange, closures, and recording instrumentation are described briefly in this section.

A. TEST FLANGE AND CLOSURES

The test flange and the closures are shown in Figures 1-4. All tests were conducted with the closures mounted in the vertical position. Wooden frames were used to mask each of the closures to give a smooth wall effect for the test. The clearance of about 0.5 cm that separated the closure from the frame was covered with strips of rubber, with a loose edge left on the closure side.

The beam closure shown in Figure 2 was made of 3.81 × 8.89 cm (2 × 4's) joists on edge, sandwiched and nailed, between sheets of 1.27 cm thick plywood. The short ends were supported with a length of 7.62 cm during the tests of this closure. The face grain of the plywood sheets ran in the direction of the 2 × 4's to give the greatest strength.

Figure 3 shows ordinary steel grating, covered on one side with plywood (0.635 or 1.27 cm) to contain the blast pressure. The grating normally is sold in a standard width of 0.91 m, so two widths were attached to cover the end flange opening of 1.219 × 1.676 m. Grating was supported 7.12 cm on all sides.

The third closure tested is shown as Figure 4. The doors were full-flush steel, no cut-outs, and had internal bracing with a filler of rock wool for insulation. The doors were supported on all four edges.

All closures were tested to ultimate failure, where major portions, or all of the closure was blown from the end flange opening (1.219 × 1.676 m).

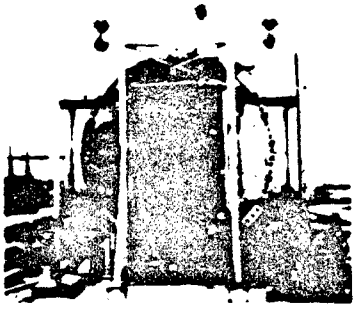

Figure 1. Test fixture, 2.44 m shock tube.

Figure 2. Wood beam closure, Shot 8-82-25.

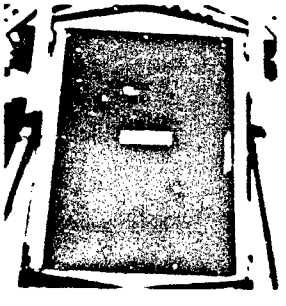

Figure 3. Grating closure, Shot 8-82-31.

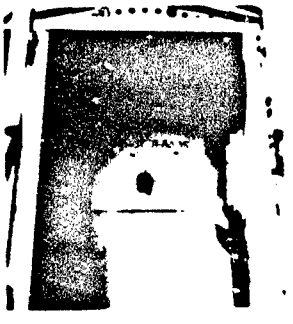

Figure 4. Steel door, Shot 8-82-35.

B. INSTRUMENTATION

The blast pressure load applied to the closure was measured at a point on the wooden masking frame 11.43 cm from the long edge of the flange opening. The transducer was approximately centered vertically along the heighth of the frame. The output from the transducer (PCB Model 113A24) was suitably amplified and recorded by an CEC FM 3300 tape recorder. Records were available for a quick-look from an on-site oscillograph for immediate recording changes for following tests.

The displacement of the closure was tracked with an OPTRON Model 501 Electro Optical Displacement Follower (4). A light cardboard target, painted black was attached with an aluminum holder to the center of the closure. The target was optically tracked and converted to displacement-time records by the recorder.

A high speed camera (Red Lakes HYCAM) operated at 1000 pictures per second supplemented the displacement follower when it was over ranged.

III. RESULTS

The results are summarized with a data table and typical loading/deflection-time records.

A. DATA TABLE

Table 1 summarizes the resulting loading pressure, transient center deflection, vibration frequency, and damage to the closures.

TABLE 1. LOADING DATA FOR CLOSURES

SHOT NO.	CLOSURES	LOAD, kpa	DISPL., cm	FREQ., Hz	ULTIMATE FAILURE / ALLOWABLE LOAD	DAMAGE
8-82-25	Wood beam	239	3.14	121/19	-----	2×4 broken.
8-82-26		300	----	------	-----	Half panel out.
8-82-27		278	3.40	102/16	4	Skin broken.
8-82-29	Steel grating	174	----	-----	-----	Walls broken.
8-82-30		215	----	-----	-----	Grating out.
8-82-31		192	----	-----	7	Grating bulged.
8-82-33		53	5.50	75/15	1.2	Bulged.
8-82-34		57	> 5.75	-----	-----	Door bent.
8-82-35		52	8.75	83/15	-----	Bulged.

The wood beam/plywood closures (Shots 8-82-25 to 8-82-27) were tested through a range of loading pressures (reflected) from 239 kPa (34.7 psi) to 300 kPa (43.5 psi). Slight damage by bulging occurred at the low end of the loading range. At 300 kPa (43.5 psi), the closure was in place and effective. Two frequencies of vibration were measured - 102 to 121 Hz and 16-20 Hz. Near ultimate failure the vibrations tend to damp out.

The loading range for the steel grating (Shots 8-82-29 to 8-82-31) varied between 174 kPa (25.2 psi) and 215 kPa (31.2 psi). When the two sections of grating were held together with U-bolts the closure remained together at a load of 174 kPa (25.2 psi). At 215 kPa (31.2 psi), the closure was blown completely away from the shock tube. Successful operation was found at an intermediate load of 192 kPa (27.8 psi).

The third type of closure, the commercial steel door was weak even when supported on all four sides. The doors tested behaved inconsistently but failed at about 57 kPa (8.3 psi). None survived load ranges comparable to either the wood beam or the grating closure.

B. LOADING AND DEFLECTION PLOTS

Figures 5 and 6 show some typical pressure and deflection plots as a function of time during the blast loading period. The pressure record (upper trace) was modified as damage occurred to the closure letting the blast wave vent. When the closure remained intact, the deflection record follows the loading-pressure well. See Shots 8-82-25, 31, and 35 for no venting. Venting is shown by Shots 8-82-26, 29, and 34.

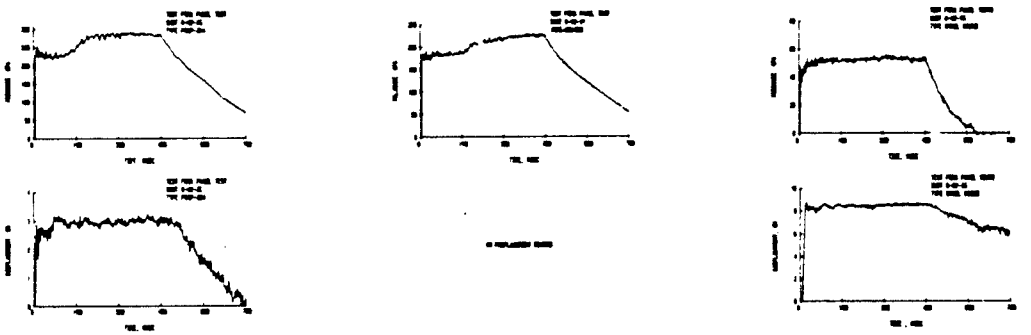

Figure 5. Records for effective closures.

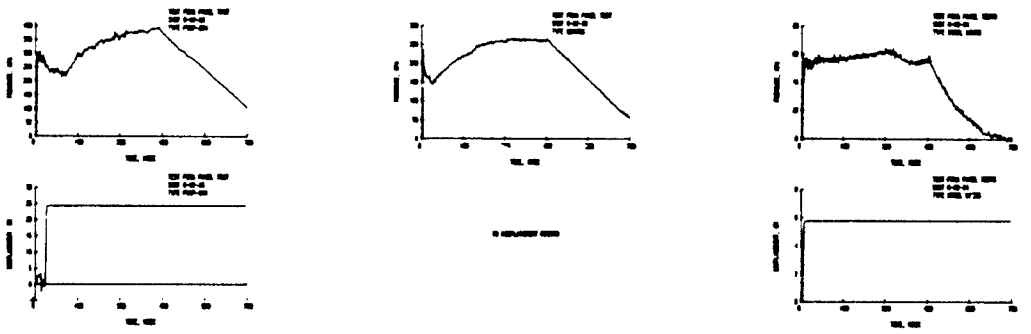

Figure 6. Records for vented closures.

IV. ANALYSIS

The analysis will follow the methods given in the design procedures of (3). This procedure was used for predicting the ultimate failure of the wood beam/plywood closures and also for the steel doors. Table values from (5) were used for the allowable static load for the steel grating/plywood closure.

A. WOOD BEAM/PLYWOOD CLOSURES

The horizontal shear mode was judged to be weakest for the wood beam/plywood closures. Accordingly, the total load-horizontal shear, P_v, was calculated following the procedures given in (3).

$$P_v = (2(\Sigma F_v t)/(\ell\ell' Q_v))(EI_g/E_{stringer}), \quad (1)$$

where F_v = allowable stress (6) in stringers horizontal shear (655 kPa), t = sum of stringer width (167.6 cm), EIg = stiffness factor (17.46×10^{10} kPa $-cm^4$), E_{skin} = modulus of elasticity for plywood skins (7) (13.64×10^6 kPa). $E_{stringer}$ = modulus of elasticity for stringer (12.77×10^6 kPa), ℓ = clear span of stringers (121.9 cm), ℓ' = clear width of closure (167.9 cm), and Q_v = the statical moment (2029.07 cm^3). The allowable load, P_v, is 72.42 kPa (10.5 psi).

The dynamic load, P_{dm}, needed to cause ultimate failure is found from Equation 2.

$$P_{dm} = 4P_v\ (1 - \frac{1}{2\mu}), \quad (2)$$

where the ductility ratio, μ, is taken as 2. P_{dm} is 217.3 kPa (31.5 psi).

B. STEEL GRATING/PLYWOOD CLOSURES

The allowable load was taken as the safe load given (5) for the steel grating (27.8 kPa, 4.03 psi). The plywood sheet (0.635 cm) cover for the grating was neglected. The dynamic load for ultimate failure was calculated from Equation 2 with a μ of 10 used for steel. P_{dm} = 105.6 kPa (15.31 psi).

C. COMMERCIAL STEEL DOORS

Calculations were made for the steel door assuming it would act like a stressed skin panel under deflection (3). The allowable static load for panel deflection, P_d, is found from Equation 3.

$$P_d = 1/[C\ell\ell'(\frac{5}{384}\frac{\ell^2}{(EIg)} + \frac{0.15}{AG})] + DL, \quad (3)$$

where C = factor (360), EIg = stiffness factor (5.07×10^{10} kPa-cm^4), A = cross section of internal braces (15.58 cm^2), G = modulus of rigidity of stringers (79.57×10^6 kPa), ℓ = clear span of panel in direction of stringers

(167.64 cm), and ℓ' = clear width of panel (109.4 cm). The dead weight (DL) was set to zero since the doors were tested as upright wall panels. P_d = 21.0 kPa (3.04 psi). For support on all four sides, P_d is modified by a factor of 2.139 times. The allowable load is 44.92 kPa (6.52 psi). No attempt was made to calculate ultimate failure.

IV. SUMMARY AND CONCLUSIONS

Three types of closures were tested to ultimate failure at the BRL 2.44 m blast simulator: (1) wood beam/plywood skin panels, (2) steel grating/plywood closures, and (3) commercial steel doors. Compared to allowable safe static loads, the grating closures were about seven times stronger, the wood beam panels about four times stronger, and the steel doors only about twenty percent above the allowable static loads. The wood beam closures and grating closures withstood loads that would probably allow both to be used in the key worker areas. The commercial doors tested withstood loads which would make them suitable only for host areas.

REFERENCES

1. George A. Coulter, "Debris Hazard from Blast Loaded Plywood Sheet Closures," Memorandum Report ARBRL-02917, Ballistic Research Laboratory, March 1979 (AD# A071460).

2. George A. Coulter, "Blast Loading of Construction Materials and Closure Designs," Memorandum Report ARBRL-02947, Ballistic Research Laboratory, August 1979 (AD# A077116).

3. H. L. Murphy, "Upgrading Basements for Combined Nuclear Effects: Predesigned Expedient Options II," SRI Project 6876 Technical Report, July 1980.

4. See company manual "Model 501 Optical Displacement Follower," OPTRON, Div. of Univ. Tech. Inc., 30 Hazel Terrace, Woodbridge, CT 06525.

5. "Marco Safe Load Data-Fed. Spec. RRG-661a," McMaster-Carr Supply, 640 West Lake St., Chicago, IL.

6. "Design Values for Wood Construction - A Supplement to the 1977 Edition of National Design Specification for Wood Construction," National Forest Products Assoc., 1619 Mass. Ave., N.W., Washington, DC 20036, April 1980.

7. "Plywood Design Specifications," American Plywood Assoc., P.O. Box 2277, Tacoma, Washington 98401, December 1978.

DIRECT COURSE Blast Shelter Entranceway and Blast Door Experiments

by

S. A. Kiger and D. W. Hyde
USAE Waterways Experiment Station
Vicksburg, Miss.

ABSTRACT

The DIRECT COURSE Event is a high-explosive simulation of a 1-kt height-of-burst nuclear weapon. DIRECT COURSE is sponsored by the Defense Nuclear Agency and is scheduled for September 1983 at the White Sands Missile Range, New Mexico. Three entranceway experiments will be fielded, one full size complete with two blast doors to document structural response and loading in the simulated 1-kt blast environment. Also, two 1/10-scale models, one double and one single entrance configuration, will be used to obtain blast pressure data that can be scaled to a 1-Mt blast environment. Results from these experiments will be used to evaluate and improve structural response calculations for the 1-kt environment, and to obtain loading data for a 1-Mt environment. These data will be used to design entranceways and blast doors for the key worker blast shelter.

INTRODUCTION

Several blast shelter entranceways, some including blast doors, were tested in the aboveground atomic tests at the Nevada Test Site during the 1950's, see for example References 1-7. The blast doors, or closures, tested were either massive reinforced concrete doors (4 and 5), vertical shaft entranceways with a submarine-type hatch (1, 2, and 3), steel doors with beam stiffeners (6), or doors tested at less than 10 psi (7). More recent tests have re-examined the steel door (8) and the vertical shaft with a hatch at ground level (9).

The most cost efficient closure and entranceway system, and one whose survivability has clearly been demonstrated, is the vertical shaft with a hatch-type closure. However, if a vertical entranceway is used for a large shelter, 100-person capacity or larger, it may not be possible to get everyone into the shelter in the allotted time (normally 15 min.). Therefore a cost efficient, walk down, entranceway and blast door design is needed for blast shelters such as the deliberate, 100-person capacity, Key Worker blast shelter that is currently being designed for FEMA by the USAE Huntsville Division.

OBJECTIVES

1. Evaluate the design of an entryway, complete with blast door, in a 1-kt simulated 50 psi airblast environment.

2. Obtain 1-Mt airblast loading data for single tunnel, dead end and double tunnel, pass through entryway systems using tenth-scale models.

3. Design and evaluate alternate blast door configurations.

ANALYSIS

A full-scale, single tunnel, dead end entranceway, as shown schematically in Figure 1, will be tested. Anticipated maximum pressures on the structure at the 50 psi overpressure range are shown in Figure 2 where the pressures shown are horizontal soil stresses at midstructure height, internal airblast pressures, and peak reflected pressure, P_r , at the tunnel dead end. The worst case loading of the entrance tunnel will occur with the entrance facing away from ground zero, thus loading the exterior of the tunnel with soil transmitted pressures before the tunnel becomes pressurized. Therefore, the loads used for tunnel design calculations were the soil transmitted pressures.

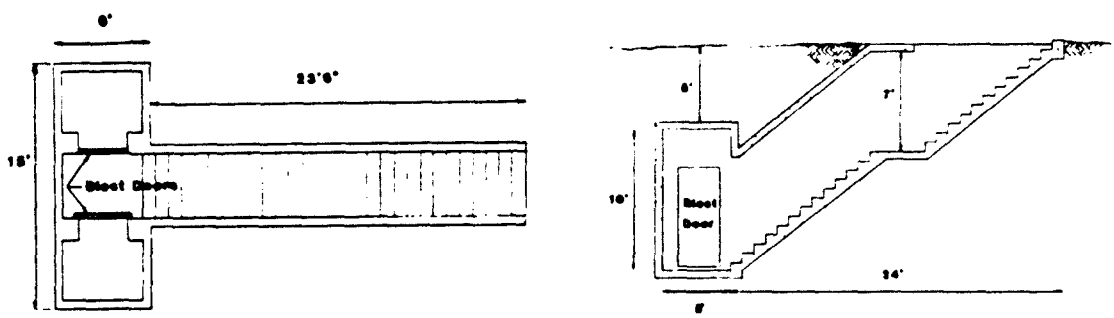

a. Plan view b. Elevation

Figure 1. Full-scale entranceway configuration.

The worst case loading for the blast door occurs with the tunnel facing ground zero, as shown in Figure 2, therefore, this will be the orientation for the DIRECT COURSE Test. Pressures in the tunnel were computed by Mr. Bob Britt, WES, using References 10 and 11. The pressure-time history computed at the center of the blast door, and used for the blast door response analysis, is shown in Figure 3.

The blast door was designed with the objectives that it be relatively inexpensive (less than about $500) and that it be constructable at the construction site to save transportation cost. A reasonable approach would be to preconstruct the formwork and then pour concrete in the door at the construction site. Four types of doors, with cross sections shown in Figure 4, were considered. To withstand the blast loads, the door must have a flexural capacity of approximately 150 psi. To minimize the cost of hinges and make handling easier, it should weigh no more than about 1500 lb, and it should transmit no more than about 50 rads of prompt radiation. The use of high-density concrete was considered because of its increased radiation protection. Reference 12 was used for radiation calculations. Based on a 1-Mt weapon at a range of 5000 ft (50 psi overpressure), gamma radiation in front of the door is about 9.6×10^3 rads. Based on the analysis results in Table 1, a Type 4 door, 3 inches thick, and using standard concrete was selected. Maximum deflection for this door, with the loading shown in Figure 3, and a negative steel reinforcement ratio of 1.1 percent, is 0.39 in., which is a ductility (ratio of maximum to elastic deflection) of 1.4.

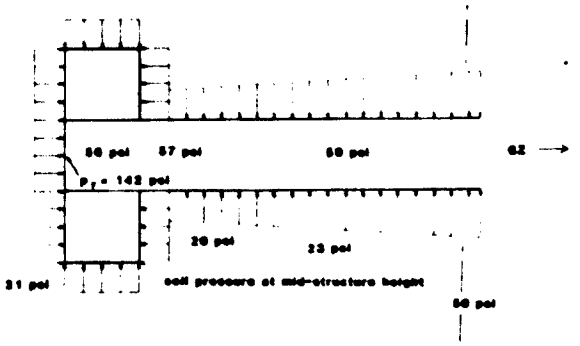

Figure 2. Entranceway loading at the 50 psi overpressure range from 1-kt airburst.

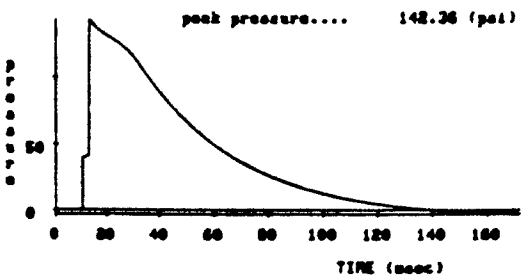

Figure 3. Computed pressure at the center of the blast door.

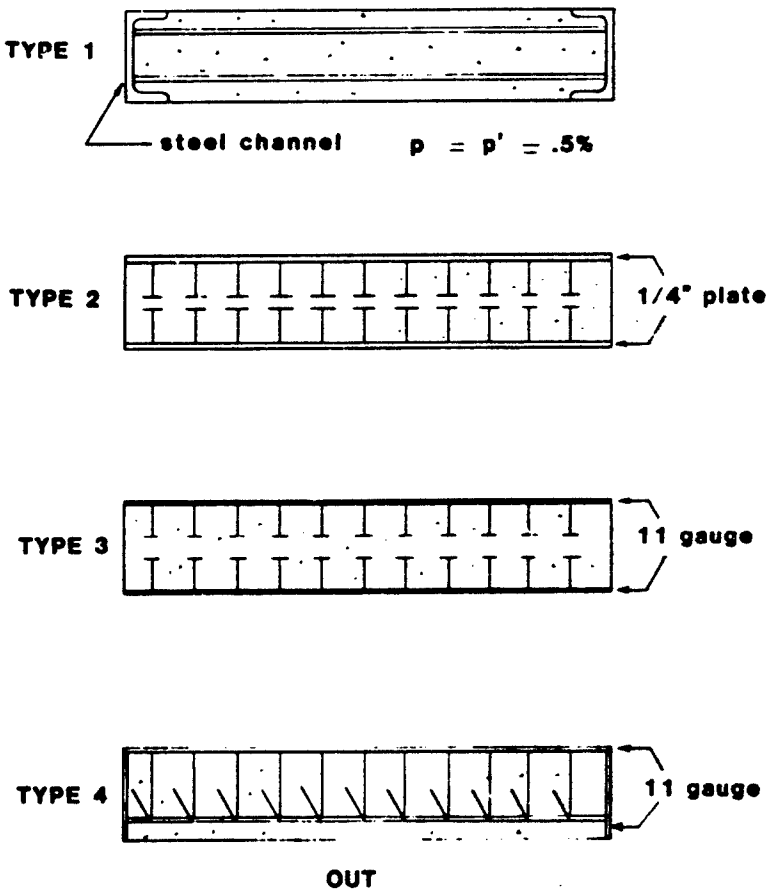

Figure 4. Blast door cross sections considered (not to scale).

Table 1. Blast Door Analysis Results

Slab Thickness in.	Type 1			Type 2			Type 3			Type 4		
	WT lb	R psi	$\gamma_{in.}$ rads	WT lb	R psi	$\gamma_{in.}$ rads	WT lb	R psi	$\gamma_{in.}$ rads	WT lb	R psi	$\gamma_{in.}$ rads
					Standard Concrete, 150 lb/ft^3							
6	2300	110	14									
5	1910	70	20									
3				1630	532	26	1330	244	40	1210	180	48
2				1280	369	46	980	166	71			
					High-Density Concrete, 200 lb/ft^3							
6	2975	110	6									
5	2470	70	9									
3				1980	532	17	1680	244	23	1560	180	31
2				1510	369	34	1210	166	48			

A standard steel fire door with supports as shown in Figure 5 will also be tested. Three W 6 x 12 beams will support the door. The pins, shown going through the door, will attach to the support beams and prevent rebound forces from opening the door.

Two 1/10-scale nonresponding entranceway models, one single tunnel similar to the full-scale structure and one pass-through tunnel, will be tested. These models will be instrumented with airblast gages to obtain airblast loading data. These data can then be scaled, using cube root scaling, to a 1-Mt event and used for design calculations.

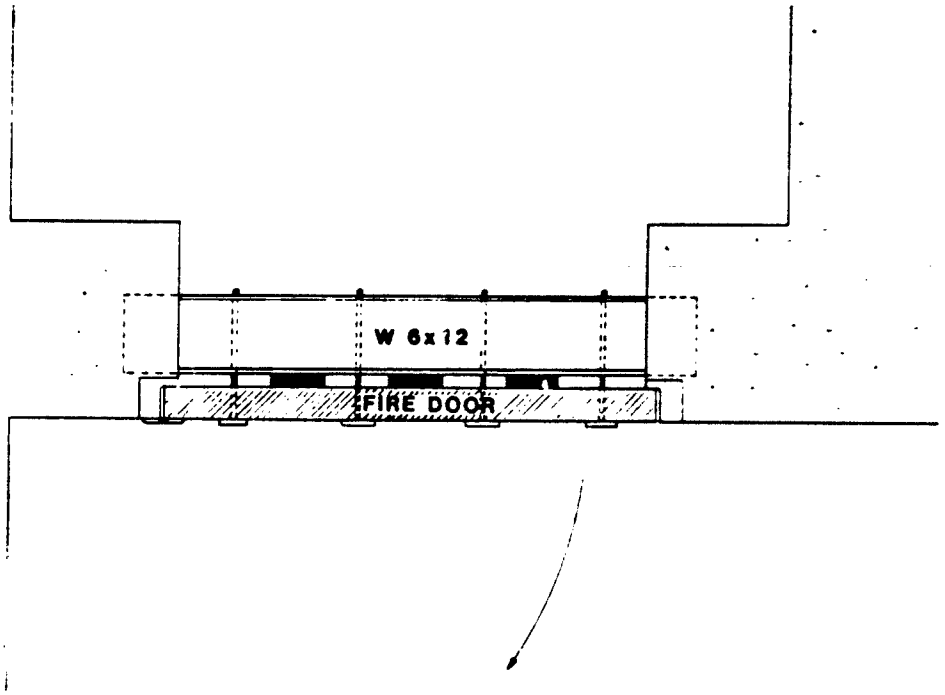

Figure 5. A supported steel fire door.

REFERENCES

1. W. J. Flathau, Project Officer, R. A. Breckenridge, and C. K. Wiehle, U. S. Army Engineer Waterways Experiment Station, Corps of Engineers, Vicksburg, Miss., and U. S. Naval Civil Engineering Laboratory, Port Hueneme, Calif., June 1959. "Blast Loading and Response of Underground Concrete-Arch Protective Structures," Report WT-1420, Operation Plumbbob, Project 3.1.

2. G. H. Albright, LTJG, CEC, USNR, Project Officer, J. C. LeDoux, LCDR, CEC, USNR, and R. A. Mitchell, LTJG, CEC, USNR, Bureau of Yards and Docks, Washington, D. C., and U. S. Naval Civil Engineering Laboratory, Port Hueneme, Calif., July 14, 1960. "Evaluation of Buried Conduits as Personnel Shelters," Report WT-1421, Operation Plumbbob, Project 3.2.

3. G. H. Albright, LTJG, CEC, USNR, Project Officer, E. J. Beck, J. C. LeDoux, LCDR, CEC, USN, and R. A. Mitchell, LTJG, CEC, USNR, Bureau of Yards and Docks, Navy Department, Washington, D. C., and U. S. Naval Civil Engineering Laboratory, Port Hueneme, Calif., Feb. 28, 1961. "Evaluation of Buried Corrugated-Steel Arch Structures and Associated Components," Report WT-1422, Operation Plumbbob. Project 3.3.

4. E. Cohen, E. Laing, and A. Bottenhofer, Ammann & Whitney, Consulting Engineers, New York, N. Y., September 15, 1962. "Response of Dual-Purpose Reinforced-Concrete Mass Shelter," Report WT-1449, Operation Plumbbob, Project 30.2.

5. E. Cohen, E. Laing, and A. Bottenhofer, Ammann & Whitney, Consulting Engineers, New York, N. Y., May 28, 1962. "Response of Protective Vaults to Blast Loading," Report WT-1451, Operation Plumbbob, Project 30.4.

6. E. Cohen and A. Bottenhofer, Ammann & Whitney, Consulting Engineers, New York, N. Y., June 25, 1962. "Test of German Underground Personnel Shelters," Report WT-1454, Operation Plumbbob, Project 30.7.

7. N. FitzSimons, Federal Civil Defense Administration, Washington, D. C., August 22, 1958. "Evaluation of Industrial Doors Subjected to Blast Loading," Report ITR-1459, Operation Plumbbob, Project 31.4.

8. R. S. Cummins, Jr., "Blast Door Tests for the Federal Republic of Germany," Miscellaneous Paper N-76-13, September 1976, U. S. Army Engineer Waterways Experiment Station, CE, Vicksburg, Miss.

9. Donn Incorporated Staff: J. L. Petras: Project Engineer; A. H. Hoffer: Project Manager; R. F. Worley: VP, Engr. & Research; K. C. Brown: VP, Chief Project Officer. "Test of the Donn Corporation Blast Shelters, A Condensed Version of the Final Report Structures Tested in the Misers Bluff Event, November 1978."

10. G. A. Coulter, BRL Report No. 1809, "Attenuation of Peaked Air Shock Waves in Smooth Tunnels," November 1966.

11. S. Hikida and C. E. Needham, S-CUBED-R-81-5067, DNA #5863Z, "Low Altitude Multiple Burst (LAMB) Model Volume 1: Shock Description," S-CUBED, Albuquerque, N. M., June 1981.

12. T. E. Kennedy, et. al., "Expedient Field Fortifications For Use Against Nuclear Weapons," Technical Report N-74-7, September 1974, U. S. Army Engineer Waterways Experiment Station, CE, Vicksburg, Miss.

TESTS AND ANALYSES OF 1/4-SCALE UPGRADED NINE-BAY REINFORCED CONCRETE BASEMENT MODELS

By
Stanley C. Woodson
USAE Waterways Experiment Station
Vicksburg, Mississippi

ABSTRACT

Two nine-bay prototype structures, a flat plate and two-way slab with beams, were designed in accordance with the 1977 ACI code. A 1/4-scale model of each prototype was constructed, upgraded with timber posts, and statically tested. The development of the timber posts placement scheme was based upon yield-line analyses, punching shear evaluation, and moment-thrust interaction diagrams of the concrete slab sections. The flat plate model and the slab with beams model withstood approximate overpressures of 80 and 40 psi, respectively, indicating that required hardness may be achieved through simple upgrading techniques.

BACKGROUND

Under the current civil defense program called Crisis Relocation Planning (CRP), keyworkers and officials would remain in target areas during a time of international crisis when a nuclear war would be imminent until it became necessary to take cover in a nearby hardened shelter. One concept for development of these hardened shelters consists of upgrading basements in existing buildings with additional structural members to withstand a peak overpressure from a 1 Mt weapon of 50 pounds per square inch (psi). A study on the upgrading of two-way R/C slabs (1) indicated that it may be possible to upgrade two-way R/C slabs, but revealed the need for more tests and evaluation in this area.

DESCRIPTION OF TEST SPECIMENS AND UPGRADING SCHEMES

Two specific slab types were chosen to be studied: a flat plate structure and a two-way slab with beams structure. A prototype structure of each of the two types was designed according to the 1977 ACI code (2). Nine-bay prototype structures consisted of three 20-foot spans in each direction in order to include corner, exterior, and interior slab panels. The perimeter of each structure was supported with R/C walls and columns. Four R/C columns supported the interior region of the structure. A 1/4-scale model of each prototype structure was then constructed and statically tested in the Large Blast Load Generator test facility located at the U. S. Army Engineer Waterways Experiment Station (3). Four and one-half inches of sand were placed over the roof of the model to simulate a soil layer serving as a barrier to radiation. The walls and columns were cast monolithically with the slabs, and the model structures were bolted to a base slab to produce a considerable degree of fixity. In the model with beams, the beams spanned from each column to adjacent columns, except that beams did not span from exterior column to exterior column. The material properties for the design of the structures used a steel having a minimum yield strength of 60,000 psi and concrete with a minimum compressive strength of 4,000 psi.

The study discussed in (1) utilized composite wooden upgrading columns consisting of four 4-in. by 4-in. dimensioned timbers. The encouraging results of the previous studies influenced the decision to use wooden timbers in the current study for upgrading the model slabs. Since the models were 1/4-scale structures, a composite wooden column was represented by a single 4-in. by 4-in. dimensioned timber. Effort was taken to design a placement spacing scheme for the upgrading columns that would harden the structures as required. A ductile flexural-type failure was considered to be more desirable than a brittle shear-type failure. The types of design calculations and analyses performed for different spacings of the upgrading columns included: yield-line analyses, punching shear evaluations, and a study of shear and moment-thrust interaction diagrams generated by the computer program called Reinforced Concrete Column Analysis (4). In the analyses, the slabs were considered to be continuous over the upgrading columns which were considered to act as simple supports. After various spacings were studied, a spacing of 15 inches on-center (60 inches in the prototype) was chosen for the upgrading columns in the flat plate model. A spacing of 20 inches (80 inches in the prototype) was used in the two-way R/C slab with beams model. The two-way R/C slab with beams model was tested after the flat plate model was tested. The results of the flat plate model test showed that the 15-inch spacing was conservative. Consequently a 20-inch o.c. spacing was used for the upgrading columns in the two-way R/C slab with beams model.

INSTRUMENTATION

The loading pressure in each of the two tests was measured with two gages mounted inside the test chamber. Three interface stress gages were used to measure the load applied normal to a basement wall of each model. Eight linear variable displacement transducers were used to measure slab deflections, and two were used to measure wall deflections. Five soil-stress gages were used to investigate load transfer through the soil cover and backfill. Three of the gages were placed on top of a 1/4-inch-thick layer of soil on top of the model's surface, and the remaining two were placed in the backfill approximately 12 inches from the model's wall.

Ten strain gages were used in the flat plate model test, and twelve were used in the slab with beams model test. In each model, two gages were mounted on vertical wall steel, and four were mounted on vertical steel in one of the interior columns. In the flat plate model, four gages were mounted on reinforcement in the slab at an interior column. In the slab with beams model, four gages were mounted on reinforcement in the beams at an interior column, and two were mounted on slab reinforcement in an exterior bay near a beam's midspan and perpendicular to the beam.

EXPERIMENTAL RESULTS

The flat plate model was statically loaded with water pressure until the maximum pressure attainable from the commercial water line was reached at 79 psi. Figure 1 is an overhead view of the tested model. Top and bottom surface yield lines are indicated by solid and dashed lines, respectively.

The two-way slab with beams model was statically loaded until rupture occurred at a pressure of about 39.5 psi as shown in Figure 2. Top and bottom surface yield lines are indicated by solid and dashed lines, respectively.

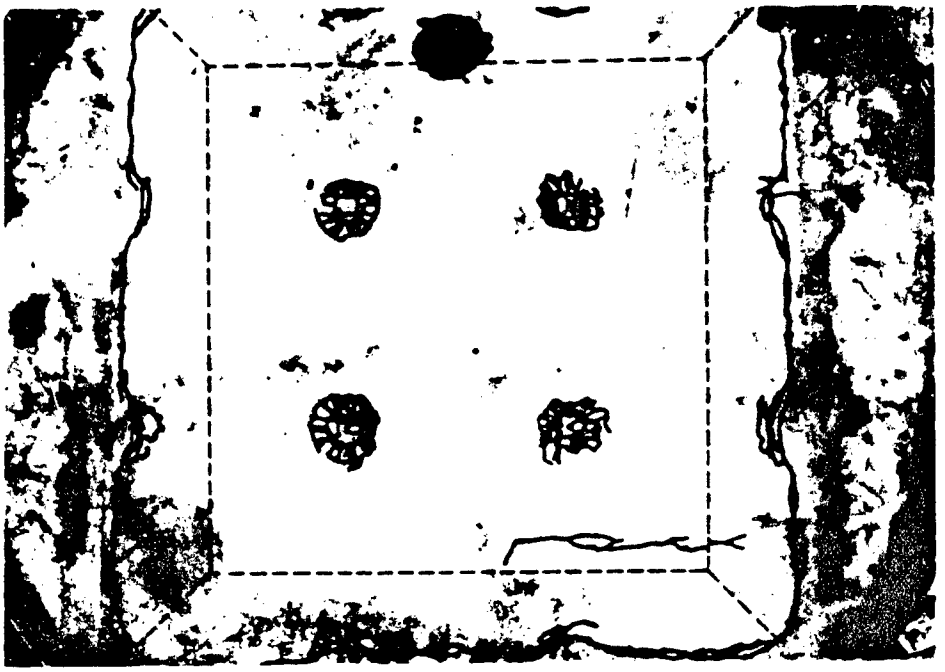

Figure 1

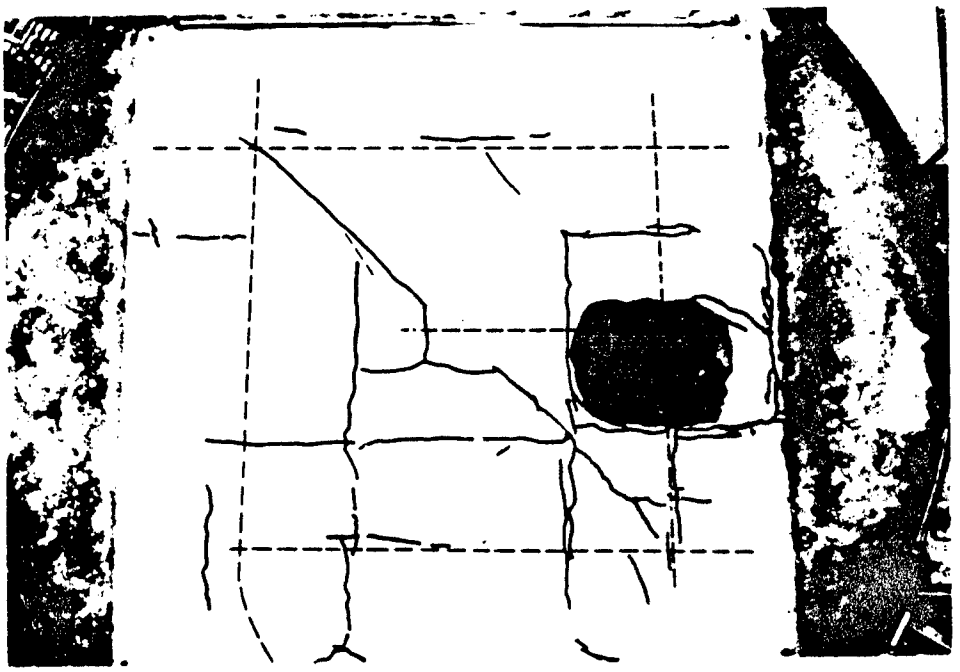

Figure 2

DISCUSSION

FLAT PLATE MODEL

When the water pressure loading reached a value of approximately 40 psi abrupt changes occurred in the measurements of deflection, strain in the slab at an interior concrete column, and soil-stress over an interior column. The rate of deflection of the slab increased under a constant rate of loading. However, the strain readings decreased to a value of zero and the soil-stress reading decreased to a value of zero also; this indicated that a punching shear failure had occurred at the interior columns.

Although the punching shear failure occurred at the concrete columns, it did not occur at the wooden upgrading columns. The wooden wedges used to secure the upgrading columns in place compressed, allowing the slab to move downward thereby redistributing load to the concrete columns. The load-deflection behavior of the wooden upgrading columns was investigated by loading two of the specimens in an Olson Universal Testing Machine. Since deflections were measured at upgrading columns in the region where yield lines occurred, the load on an upgrading column in the region could be determined from the load-deflection curve developed from the specimens tested in the Universal Testing Machine. An effective upgrading column spacing could then be determined from the expression

$$\ell = \left(\frac{P}{w}\right)^{1/2} \tag{1}$$

where

ℓ = upgrading column spacing (inches)

P = column load (pounds)

w = slab load (pounds/inch^2)

For the region where yield lines occurred, the value of ℓ determined by equation 1 was approximately equal to 28 inches. Since the actual spacing used in the test was 15 inches, the calculated effective spacing of 28 inches implies that the upgrading columns at the yield-line region received a greater portion of the slab load than expected. Limited instrumentation prohibits similar evaluations for all regions of the model.

It is probable that the upgrading column load was greater than anticipated in the yield-line region due to the formation of the yield mechanisms and the midspan deflection between the upgrading columns. It is evident from the soil-stress data that soil-arching did exist. The deflections of the 15-inch span along with deflections due to punching of the concrete columns may have caused a redistribution of the load on the model's surface such that the upgrading columns at the regions where yield lines occurred did receive more load than those at other regions of the model.

Consideration of the slab acting as a continuous member simply supported by the wooden upgrading columns and with fixed ends at the walls and concrete columns would include the assumption that the midspan and support moment values would be equivalent to $w\ell^2/24$ and $w\ell^2/12$, respectively

where

w = uniform load

ℓ = span between upgrading columns

Moment-thrust interaction diagrams were developed for support and midspan conditions of the 15-inch span between upgrading columns in the region of the slab where yield lines occurred. Load paths based upon thrusts and moments determined from wall and roof pressure records were plotted on the interaction diagrams. The load path for the support conditions intersected its respective interaction diagram at moment and thrust values compatible to a slab surface load of approximately 6 psi. The initiation of yielding at the upgrading columns allowed the 15-inch span to behave as a simply supported member with concentrated moments at the supports. The load path for the midspan conditions intersected its respective interaction diagram at moment and thrust values compatible to a slab surface load of 21 psi.

Data records indicate that plastic deformation was continuing to occur when the test was terminated at an overpressure of 79 psi. The 58 psi difference between the load at yield and the maximum load applied may be explained by the assumptions used in the analysis. The load was assumed to be uniform over a continuous member spanning over simple supports and with fixed ends. However, as previously discussed, a redistribution of the load by soil arching occurred over the model's surface. Some two-way action occurred as the upgrading columns deflected, and flexibility of the walls allowed rotations at the assumed fixed ends. Therefore, there may not have been a 58 psi load difference between the loads at yield of the 15-inch span's midspan and test termination due to the interaction of the upgrading columns and the soil cover with the structure.

TWO-WAY SLAB WITH BEAMS MODEL

As expected, data indicated that the thrust in the slab was similar to the thrust in the flat plate model for any given overpressure loading. It is evident from strain gage data that changes in the structure's response behavior began to occur at an overpressure loading of approximately 15 psi. Strain gages in the slab reinforcement steel near and perpendicular to the beams showed considerable increase in the rate of tension strains for a constant rate of water pressure loading. The strain gages in the beams and near the interior column indicated low values of strain as was the case for the flat plate test prior to punching shear failure at the column when the water loading pressure was about 40 psi. At an overpressure of approximately 22 psi, the deflection data and the soil-stress data indicated that the rate of deflections was increasing and that soil-arching was occurring. When the water loading pressure reached a value of approximately 39.5 psi, punching shear failure had not occurred at the concrete columns. The presence of the beams joining the columns increased the shear area beyond that which existed in the flat plate model test. Therefore, punching shear failure at the concrete columns was avoided, although the upgrading column spacing was greater than that

used in the flat plate test. However, rupture did occur in an exterior bay. The ruptured area was bounded on two sides by beams and seemed to follow rows of upgrading columns on the other two sides. The location was such that the center of the rupture area was supported by one upgrading column. It is probable that either punching shear failure occurred at the upgrading column, or the upgrading column slipped out of position leaving the slab unsupported over a span of 40 inches.

Criswell (5) studied the behavior of slab-column connections subjected to static loadings. Criswell indicated that the ACI code expression for shear strength underestimates by 25 percent the shear strength in connections having a r/d ratio of 2

where

r = square column side dimension

d = effective depth of the slab

The r/d ratio in the current study is 2.1, therefore, Criswell's results may be appropriate. If the ACI code underestimates the shear strength by 25 percent, a punching shear force capacity of approximately 18.6 kips would be expected. Deflection measurements were taken at an upgrading column which was probably loaded similarly to the upgrading column at the ruptured area. Application of the deflection data to the previously mentioned load-deflection curve developed from two upgrading column specimens indicates that the column load at the time the slab ruptured was approximately 28.8 kips.

Criswell (5) also stated that punching shear failure is likely to occur at connections where general flexural yielding has occurred. Such flexural-shear failures occurred in some tests at less than 60 percent of the shear capacity calculated according to the ACI code. In the current study, 60 percent of the calculated shear strength is equivalent to approximately 8.4 kips. A corner bay next to the bay where rupture occurred showed several yield lines beginning to congest near an upgrading column, indicating that the slab may have been susceptible to flexural-shear failure. If flexural shear failure did occur at the ruptured area, the data records imply that it occurred at a shear capacity approximately 165 percent of that calculated according to the ACI code.

CONCLUSIONS

The ability of the upgraded flat plate model slab to deflect without punching shear failure occurring at the upgrading columns allowed the model to withstand overpressures greater than expected. The test was terminated when the upgrading column load was approximately 190 percent of the shear strength capacity calculated according to the ACI code.

Punching shear failure at the upgrading columns was the controlling parameter used in the design of the upgrading scheme. However, the flat plate test indicated that more concern should be directed to punching shear failure at the concrete columns and to flexural failure between upgrading columns. Load redistribution from soil arching in the flat plate test caused some upgrading columns to support about 3.5 times the load generally expected

to equal the load applied to the square area with a side dimension equivalent to the span length.

The rupture that occurred in the model slab with beams was the consequence of either an upgrading column punching into the slab or the slippage of the column such that it no longer supported the slab. If shear failure did occur at the upgrading column, it occurred at an upgrading column load of approximately 165 percent of the shear strength capacity calculated according to the ACI code. Numerous yield lines had formed on the model's surface, and a corner bay appeared to be susceptible to flexural-shear failure. A better balance between shear failure and flexural failure seemed to have occurred in the slab with beams test when compared to the flat plate test. The possibility that the upgrading column slipped implies that effort should be taken to secure upgrading columns in place.

The 15-inch upgrading column spacing was conservative in the flat plate model, and the 20-inch spacing was inadequate in the model slab with beams for a CRP requirement of an overpressure load capacity of 50 psi. The two tests did indicate that basement structures may be upgraded by practical methods to withstand overpressures near 50 psi.

REFERENCES

1. S. C. Woodson and M. K. McVay, "Tests and Evaluation of Upgraded Flat Plate and Waffle Slab Floor Systems" (In preparation), U. S. Army Engineer Waterways Experiment Station, Vicksburg, Mississippi, 1983.

2. American Concrete Institute, Building Code Requirements for Reinforced Concrete, ACI 318-77, Detroit, Michigan, 1977.

3. W. L. Huff, "Test Devices, Blast Load Generator Facility," Miscellaneous Paper N-69-1, U. S. Army Engineer Waterways Experiment Station, Vicksburg, Mississippi, 1969.

4. S. A. Mahin and V. V. Bertero, "RCCOLA, A Computer Program for Reinforced Concrete Column Analysis, User's Manual and Documentation," Department of Civil Engineering, University of California, Berkeley, California, 1977.

5. M. E. Criswell, "Strength and Behavior of Reinforced Concrete Slab-Column Connections Subjected to Static and Dynamic Loadings," Technical Report No. N-70-1, U. S. Army Engineer Waterways Experiment Station, Vicksburg, Mississippi, 1970.

STRUCTURAL RESPONSE OF UPGRADED FLAT SLAB

James F. Beck
James E. Beck and Associates
4216 Los Palos Avenue
Palo Alto, California 94306

In Beck (1980) analytical analyses were performed on "as built" slabs-over-basement areas to determine if the slabs had the potential to be upgraded to resist blast overpressures of between 30 and 50 psi resulting from a 1-Mt nuclear explosion. These analyses were performed with the assumption that the upgrading support system was "adequate" to develop the full upgrading potential of the slab. Specifically, rigid intermediate support columns and beams were assumed as outlined in various upgrading schemes. This study was not charged with developing recommendations for upgrading schemes, it was limited in scope to determining whether the slabs could be upgraded to usable values. The study predicted that 18% of the NSS buildings evaluated could be upgraded to withstand overpressures in the desired overpressure range. Therefore, with "adequate" support, many NSS buildings could potentially be upgraded to the standards desired by FEMA. However, the assumption of rigid supports gives an upper bound on the upgrading strength potential of a system, and it does not predict the actual strength of the upgraded system with real (non-rigid) supports.

In many real upgraded situations one would not find supports that would meet the required rigidity standards to produce the upper limits of the floor system's upgraded potential strength. Therefore, a dynamic-single-degree-of-freedom (DSDOF) analytical model previously developed for FEMA (Wiehle 1973) was modified (Beck 1982) so that a wooden post (non-rigid support) upgraded flat slab could be analyzed for response to a blast type of loading. After being modified the analytical model was compared with the results of an experiment performed at the US Army Waterways Engineer Experiment Station (WES) (Woodson 1981). The analytical model, as originally constructed, over-predicted the strength of the upgraded WES test structure (Beck 1982). The original predictions were based on assuming design properties for the strength of the wooden columns. Inspection of the WES test data revealed that the columns were considerably less stiff than normally used design strength parameters would predict, notably the modulus of elasticity was over-estimated by a factor of about four. As a second attempt to predict the strength of the upgraded structure, the observed values of the column load-deflection function were then used in the analytical model. This new set of calculated deflections faithfully predicted the response of the upgraded floor system. This experience has shown that there is a potentially serious problem of simply using design calculations for evaluating the strength of a floor system for upgrading.

This work indicates that not only must element ultimate strengths be considered in upgrading structural systems, but also the relative stiffnesses of the members must be considered. Currently, this is not done, and strength predictions based on not looking at the "true" relative stiffness of the upgraded system can result in one over-predicting the strength of the upgraded system by a factor of between 2 and 8 times greater than that of the actual system. This can, therefore, be of considerable interest when considering the upgrading potential of a structural system.

REFERENCES

Beck, J. E., "Summary of Dynamic Analyses of Selected NSS Buildings," SRI International (for the Federal Emergency Management Agency) Menlo Park, California, July 1980.

Beck, J. E., "Structural Analyses of Buildings in the National Shelter Survey," James E. Beck and Associates (for the Federal Emergency Management Agency) Palo Alto, California, September 1982.

Wiehle, C. K. and J. L. Bockholt, "Dynamic Analysis of Reinforced Concrete Floor Systems," Stanford Research Institute (for the Defense Civil Preparedness Agency), Menlo Park, California, July 1973.

Woodson, S., "Data Summary of Tests on Upgraded Center Portion of a Waffle Slab and a Flat Plate," US Army Engineer Waterways Experiment Station, Vicksburg, Mississippi, July 1981.

FAILURE CRITERIA FOR BLAST LOADS STRUCTURES - A REVIEW

A. Longinow*, S.A. Guralnick** and J. Mohammadi***

INTRODUCTION

The reliable rating of protective structures in a blast environment depends to a large extent on the ability to predict the magnitude and duration of the blast load required to produce incipient collapse. Such ability is best developed on the basis of experimental data on the failure of structures. At the present time experimental data on this subject is very limited. Also, the field of predicting incipient collapse of structures is mostly in its infancy.

This paper briefly reviews the state-of-the-art of predicting the incipient collapse of structures subjected to blast loads and presents a suggested experimental and analytic, probability based program capable of producing the required data and criteria by the use of full-scale tests and model studies. The emphasis of this review is on reinforced concrete structures.

REVIEW OF EXPERIMENTAL WORK

The interest in the behavior of structures when subjected to high intensity blast loads had its beginning shortly after the detonation of the first nuclear device. In the 1950's, a series of nuclear weapon field tests was conducted. The specimens were full-scale structures, scale model structures and structural components. The emphasis was on the development of reliable and economical design and analysis methods for protective construction. These tests produced a wealth of data. Among other things, it was demonstrated that structures located below the ground surface, even in a shallow burial, survived significantly better than those directly exposed to the blast. In fact many of the buried structures (including conventional basements) survived at surface overpressures several times the specified design overpressure. This first series of tests also demonstrated a need for further tests, and the need to develop analytic methods capable of simulating actual structural response to blast loads.

Since these early tests a great deal of additional work has been devoted to the simulation of weapon effects, mostly in the laboratory (2-13). Concurrently with experimental studies, research upon the development of analytic methods aimed at predicting structural response was initiated (14-20). Field tests are still being conducted on a periodic basis. These, however, are less extensive in scope than the previous test series. Loading is usually produced using conventional exposives simulating a low yield nuclear device. Also, most of the current tests conducted are mainly in the category of proof tests.

* Associate Professor of Civil Engineering, Illinois Institute of Technology, Chicago, IL 60616
** Perlstein Distinguished Professor of Engineering, Illinois Institute of Technology, Chicago, IL 60616
*** Assistant Professor of Civil Engineering, Illinois Institute of Technology, Chicago, IL 60616

The development of reliable and economic design methods requires accurate knowledge of the loads (intensities and distributions) experienced by a given structure and the conditions leading to collapse (i.e. failure criteria). Yield line theory (21) is extensively used to predict the collapse loads of reinforced concrete slabs. This theory has proved to be effective in predicting the initial loads causing hinges to form for slabs with negligible membrane forces. However, such slabs are relatively uncommon in actural hardened construction. Roof and wall slabs are generally restrained to some degree and the yieldline approach therefore, is only partially applicable. The importance of restraint on slab load carrying capacity has been studied by a number of investigators both within and outside the defense community (2,3,22-31). It has been demonstrated that in laterally restrained slabs two types of membrane action may occur. Compressive membrane action, the so-called arching effect, occurs at the early stages of deflection. This is then followed by tensile membrane action at more advanced stages of loading. Arching action is produced because compressive forces at the center of the slab act above the slab mid-depth. Compressive forces thus follow the pressure line of a shallow arch. Due to this action, the load-carrying capacity of the slab may well be substantially greater than that predicted by yield-line theory. As the deflection of the slab increases further, cracking of the concrete occurs and the membrane action in the central region shifts from compressive to tensile. Thereafter, the slab carries load by the reinforcement acting as a plastic tensile membrane, with cracking penetrating the slab thickness. The ultimate tensile membrane capacity is reached when the reinforcement is at incipient rupture. The load-displacement relationship (resistance function) depends on the degree of restraint along the edges, the quantity of reinforcement and extent to which the reinforcement is embedded beyond the slab boundaries.

The incipient collapse of a reinforced concrete slab is generally related to its midpoint deflection. This failure deflection, δ_u, is empirically expressed as a function of the short-direction span length of the slab. For example, Park (22) and Keenan (2) suggest that $\delta_u = 0.1\ell_s$, where ℓ_s is the short direction span length. Black (3), calims that this value is too conservative and suggests that $\delta_u = 0.15\ell_s$. Herzog (23) suggests that $\delta_u = 0.31\ell_s \sqrt{\varepsilon_u}$ where ε_u is the rupture strain of reinforcement. A Portland Cement Association study (27) suggests that $\delta_u = k\ell_s \sqrt{\varepsilon_u}$ where k is a factor which accounts for the non-uniform distribution of strain along the length of the reinforcing bars.

These failure criteria apply to a fully restrained condition and are assumed to be independent of concrete strength and slab geometry. Two-way action in the slab is neglected and no distinction is made between static and dynamic loads. Obviously a great deal of research remains to be done in this area.

Certain types of slabs, by virtue of their size, type of support conditions and loading, will fail primarily in shear. Certain column supported slabs are in this category and many types have been studied with respect to conventional static loads. Data that can be used to define a dynamic resistance function for reinforced concrete slabs are very limited (32-36). For building construction, the primary interest is in the peak shear capacity and, therefore, no attempt has been made in tests to determine post peak behavior of members failing in shear or flexure. Failure analyses make use of the modified ACI formula (37) when considering shear as a mode of failure. Some recent studies performed at NCEL (38) have used shear ductility in the analysis of dynamically loaded reinforced concrete slabs. In this approach it is

assumed that prior to shear failure a shear hinge is formed analogous to the formation of a plastic hinge prior to flexural failure. This failure criterion is also very tentative.

Structural members such as columns, beam-columns, slabs subjected to lateral and in-plane loads, shear walls (39-42), structural assembiies (43,44), connections (45), etc. have received very little attention as far as incipient collapse is concerned. Some full-scale structures have been tested and these test data do exist (1). This includes arches and rectangular structures both buried and above ground. However, these appear as mostly special cases in terms of load environment and type of structure. Very little duplication of experiments for control purposes has been performed.

SUGGESTED RESEARCH

After some thirty years of testing in the field and the laboratory, widely acceptable failure criteria for structures subjected to blast loads do not exist. The need to develop failure criteria still exits.

A coordinated, long-term experimental-analytic study aimed at the development of failure criteria for structures subjected to dynamic loads is recommended. It should involve the following topics:

1. A review and categorization of all pertinents experimental data.

2. The development of an experimental plan to include full-scale structures, scale model structures and individual components.

3. A comparison of test results with predictions of behavior using analytic statistical-probabilistic techniques.

It is important to emphasize that a long-term coordinated (five to ten years) effort is recommended. The major failure of the studies performed during the past thirty years was the lack of continuity and coordination between the individual studies. Since both the Department of Defense and non-defense related agencies would benefit from such an effort, it is recommended that a multi-agency program be set up to pursue the stated objectives.

REFERENCES

1. Beck, C., ed., "Nuclear Weapons Effects Tests of Blast Type Shelters", A documentary compendium of test reports, Civil Effects Branch, Division of Biology and Medicine, U.S. Atomic Energy Commission, Washington, D.C., June 1969.
2. Keenan, W.A., "Strength and Behavior of Restrained Reinforced Concrete Slabs Under Static and Dynamic Load," Technical Report R-621, U.S. Naval Civil Engrg. Lab. Port Hueneme, Cal., April 1969.
3. Black, M.S., "Ultimate Strength Study of Two-Way Concrete Slabs," ASCE Journal of Structural Division, Vol. 101, STi, pp. 311-324, Jan. 1975.
4. Huff, W.L., "Collapse Strength of a Two-Way-Reinforced Concrete Slab Contained Within a Steel Frame Structure", U.S. Army Engineer Waterways Experimental Station, Report #N-75-2, June 1975.
5. Criswell, M.E., "Design and Testing of a Blast-Resistant Reinforced Concrete Slab System", U.S. Army Engineer Waterways Experiment Station, Report #N-72-10, November 1972.

6. Kiger, S.A., "Static Test of a Hardened Shallow-Buried Structure", U.S. Army Engineer Waterways Experimental Station, Report #N-78-7, October 1978.
7. Brown, W.M., and Black, M.S., "Dynamic Strength Study of Small Fixed-Edge Longitudinally Restrained Two-Way-Reinforced Concrete Slabs", U.S. Army Engineer Waterways Experimental Station, Report #N-73-8, Dec. 1973.
8. Criswell, M.E., "Strength and Behavior of Reinforced Concrete Slab-Column Connections Subjected to Static and Dynamic Loadings", U.S. Army Engineer Waterways Experimental Station, Report #N-70-1, December 1970.
9. Denton, D.R., "A Dynamic Ultimate Strength Study of Simply Supported Two-Way Reinforced Concrete Slabs", U.S. Army Engineer Waterways Experimental Station, Report #1-789, July, 1967.
10. Murtha, R., and Crawford, J., "Dynamic Shear Failure Predictions of Shallow-Buried Reinforced-Concrete Slabs", Civil Engineering, Lab., Naval Construction Battalion Center, Tech. Memorandum, #M-51-81-04, May 1981.
11. McVay, M., "Test and Analysis of Upgraded One-Way-Reinforced Concrete Floor Slabs", U.S. Army Engineer Waterways Experimental Station, Report #SL-81, April 1981.
12. Kiger, S.A., and Getchell, J.V., "Vulnerability of Shallow-Buried Flat-Roof Structures", U.S. Army Engineer Waterways Experimental Station, Report #SL-80-7, September, 1980.
13. Balsara, J.P., "Similitude Study of Flexible Buried Arches Subjected to Blast Loads", Technical Report #1-807, U.S. Army Engineer Waterway Experimental Station, January 1968.
14. Ferritto, J.M., "Optimum Dynamic Design of Nonlinear Reinforced Concrete Slab Under Blast Loading", Civil Eng. Lab., Naval Construction Battalion Center, Tech. Note #N-1494, July, 1977.
15. Ferritto, J.M., "Evaluation of Blast Resistant Design Procedures Using Finite Element Analysis", Civil Eng. Lab., Naval Construction Battalion Center, Tech. Note Memorandum #M-51-77-9, July, 1977.
16. Ferritto, J.M., "An Evaluation of the Accuracy of Material Model Representation of Reinforced Concrete", Civil Eng. Lab., Naval Construction Battalion Center", Tech. Memorandum #51-78-18, July, 1978.
17. Ferritto, J.M., "Development of a Computer Program for the Dynamic Nonlinear Response of Reinforced Concrete Slabs Under Blast Loading", Civil Eng. Lab., Naval Construction Battalion Center, Tech. Note #N-1434, April, 1976.
18. Haltiwanger, J.D., Hall, W.J. and Newmark, N.M., "Approximate Methods for the Vulnerability Analysis of Structures Subjected to the Effects of Nuclear Blast", Vol. I and II, N.M. Newmark Consulting Eng. Services. Report #U-275-76, June 1976.
19. Brode, J.L., "A Review of Nuclear Explosion Phenomena Pertinent to Protective Construction", Report #R-425-PR. The RAND Corporation, May 1964.
20. Anderson, F.E., et al., "Design of Structures to Resist Nuclear Weapon Effects", ASCE Manuals of Engineering Practice No. 42, ASCE, N.Y., 1961.
21. Johansen, K.W., "Yield-Line Theory," Cement and Concrete Assn. London, 1962.
22. Park, R., "Tensile Membrane Behavior of Uniformly Loaded Rectangular Reinforced Concrete Slabs with Fully Restrained Edges," Concrete Research Vol. 16, No. 46, pp. 39-44, March 1964.
23. Herzog, M., "Membrane Effect in Reinforced Concrete Slabs According to Tests", Beton und Stahlbetonbau, Vol. 11(71), pp. 270-275, 1976.

24. Hawkins, N.M., and Mitchell, D., "Progressive Collapse of Flat Plate Structures", ACI Journal, Vol. 76, No. 7, pp. 775-808, July, 1979.
25. Takayanagi, T., Derecho, A.T. and Igbal, M., "Design Criteria for Deflection Capacity of Conventionally Reinforced Concrete Slabs - Phase II: Design and Construction Requirements", Prepared for Naval Civil Engineering Lab., Port Hueneme, California, PCA, Skokie, IL. Jan. 1980.
26. Igbal, M. and Derecho, A.T., "Desing Criteria for Deflection Capacity of Conventionally Reinforced Concrete Slabs - Phase I: State-of-the-Art", Prepared for Naval Civil Engineering Lab., Port Hueneme, California, PCA, Skokie, IL, May 1979.
27. Takayanagi, T., and Derecho, A.T., "Design Criteria for Deflection Capacity of Conventionally Reinforced Concrete Slabs", Phase III - Summary of Design Criteria and Design and Construction Details - Design Examples, Prepared for Naval Civil Eng. Lab., Prot Hueneme, Cal., PCA, Skokie, IL, May 1980.
28. Hopkins, D.C. and Park, R., "Test on a Reinforced Concrete Slab and Beam Floor Designed with Allowance for Membrane Action", Cracking, Deflection and Ultimate Load of Concrete Slab Systems, ACI, SP-30, pp. 251-269, 1971.
29. Powell, D.S., "The Ultimate Strength of Concrete Panels Subjected to Uniformily Distributed Loads", Thesis, Cambridge Univ, 1956.
30. Brotchie, J.F. and Holley, M.J., "Membrane Action in Slabs", in Cracking, Deflection and Ultimate Load of Concrete Slab Systems, ACI, SP-30, pp. 345-377, 1971.
31. Brotchie, J.F., Jacobson, A., and Okubo, S., "Effect of Membrane Action on Slab Behavior", MIT-Dept. of Civil Engineering, Report #R-65-25, August, 1965,
32. Guralnick, S.A, and LaFraugh, "Laboratory Study of a 45-Foot-Square Flat Plate Structure", Proc. American Concrete Inst. Vol. 60, pp. 1107-1185, Sept. 1963.
33. Keenan, W.A., "Shear Stress in One-Way Slabs Subjected to Blast Load", Civil Eng. Lab., Naval Construction Battalion Center, Port Hueneme, Cal.
34. Sozen, M.A., and Siess, C.P., "Investigation of Multiple-Panel Reinforced Concrete Floor Slabs: Design Methods, Their Evaluation and Comparison", Proc. American Concrete Inst., Vol. 60, pp. 999-1027, Aug, 1963.
35. Corley, W.G., and Hawkins, N.M., "Shearhead Reinforcement for Slabs", Proc. American Concrete Inst. Vol. 65, pp. 811-824, Oct. 1968.
36. Ford, R.D., and Vanderbilt, M.D., "Analysis of Shear Test Structure". Structureal Research Report #4, Civil Eng. Dept. Colorado State Univ., Fort Collins, Colorado, June 1970.
37. Crawford, R.E., et al., "The Air Force Manual for Design and Analysis of Hardened Structures", AFWL-TR-74-1C2, Air Force Weapons Laboratory, Oct. 1974.
38. Murtha, R.M. and Holland, T.J., "Analyses of WES FY82 Dynamic Shear Test Structures", TM No. 51-83-02, Naval Civil Engineering Laboratory, Port Hueneme, California, December 1982.
39. Benjamin, J.R. and Williams, H., "The Behavior of One-Story Reinforced Concrete Shear Walls,"Journal of the Structural Division, ASCE, Vol. 83, ST3, pp. 1-49, May, 1957.
40. Benjamin, J.R. and Williams, H., "The Behavior of One-Story Reinforced Concrete Shear Walls Containing Openings", Journ. ACI, Vol. 55, No. 11, pp. 605-618.
41. Beekhuis, W.J., "An Experimental Study of Squat Shear Walls", Master of Engineering Repts., Dept. of Civil Eng., Univ. of Canterbury, Christ-Church, New Zealand, 1971.

42. Bakos, J.D., "Dynamic Response of a Small Shear Wall Structure", U.S. Army Engineer Waterways Experimental Station, Rept. #N-69-7, Nov. 1969.
43. Beaufait, F., and Williams, R.R., "Experimental Study of Reinforced Concrete Frames Subjected to Alternating Sway Forces", Jour. ACI, Vol. 65, No. 11 pp. 980-984, Nov. 1968.
44. Ockleston, A.J., "Load Tests on a Three-Story Reinforced Concrete Building in Johannesburg", Structural Engineer, Vol. 33, Oct. 1955.
45. Simmonds, S.H., "Flat Slabs Supported on Columns Elongated in Plan", Proc American Concrete Concrete Inst., Vol. 67, No. 12, pp 967-975, Dec. 1970.

EFFECTS OF MULTIPLE BURSTS ON STRUCTURAL RESPONSE

J. Mohammadi*, A. Longinow**, H.S. Napandensky***

INTRODUCTION

In performing casualty/survivability studies in the civil defense area, it has been customary to consider the hazards produced by a single, 1-MT size weapon. A vast majority of the casualty estimates available today are based on the 1-MT weapon assumption. In real cases, however, there are situations where a given personnel shelter may be subjected to the effects of multiple bursts. This is likely to occur when the target area containing the shelter is subjected to more than one attack. This may also occur when the given shelter is located between several potential targets. In such a case, when each of the targets is attacked at different times, then the shelter will experience as many blast loadings as the combined number of attacks.

Generally, a shelter structure is designed to withstand a predetermined "design" blast load. The structure will experience damage to the extent that a given blast load is more intense than the design blast load. The extent of additional damage from subsequent loadings will be in direct proportion to the "available" strength of the structure, i.e., to the extent to which its strength has been degraded due to previous blast loadings. The collapse will take place once the available strength is below the limit determined by the designer.

This paper describes the problem of structural failure (collapse) as a result of a multiple blast load condition. Due to the non-deterministic nature of the problem, the method described herein considers the failure probability of the structure after each blast. The structure is modeled as a single degree of freedom dynamic system with a resistance function which provides for degradation of strength. The method considers uncertainties in both structural and blast load parameters. Probability of structural collapse is determined for a series of attack conditions separated in time for which the ratio of blast load to resistance of the structure is greater than 1.0. Practical applications of the approach are illustrated along with further recommended applications.

GENERAL ASSUMPTIONS

(i) The structure is modeled as a single-degree of freedom system

(ii) The applied load is assumed to consist of a series of step loads (see Fig. 1) of different peak intensities, F_i.

(iii) The resistance capacity of the structure is represented by means of an elasto-plastic resistance shown in Fig. 2. The yield and maximum displacements are represented respectively, by X_y and X_m. The stiffness of the elastic part is $k = R(X_y)^{-1}$ in which R is the resistance capacity.

* Assistant Professor of Civil Engrg., Ill. Inst. of Tech., Chicago, Il.
** Associate Professor of Civil Engrg., Ill. Inst. of Tech., Chicago, Il.
*** Manager, Fire and Explosion Research, IIT Research Inst., Chicago, Il.

(iv) The applied blast load will leave the structure undamaged if the ratio of the load to resistance is less than 1/2, i.e. $F_i/R \leq 1/2$.

BASIC FORMULATION

The resistance function shown in Fig. 2 is further idealized by means of an "effective" linear resistance function shown in Fig. 3. The effective displacement X_e is found by equating the energy corresponding to elasto-plastic case and that of the corresponding linear curve (1). Such linearization yields

$$X_e^2 = X_y^2 (2 X_m/X_y - 1) \tag{1}$$

Introducing the ductility ratio $Z_i = X_m/X_y$, Eq. (1) may be written as

$$X_e^2 = X_y^2 (2 Z_i - 1) \tag{2}$$

or

$$Z_i = X_e^2/2 X_y^2 + 1/2 \tag{3}$$

Given the step load shown in Fig. 1, the maximum response of the linear system is (1).

$$X_e = 2 F_i/k = 2 F_i X_y/R \tag{4}$$

In the light of Eq. (4), Eq. (3) becomes

$$Z_i = (2F_i X_y/R)^2/2X_y^2 + 1/2 = 2/(R/F_i)^2 + 1/2 = 2/\theta_i^2 + 1/2 \tag{5}$$

where $\theta_i = R/F_i$.

Damage is likely to occur if $F_i \geq R/2$. This corresponds to $Z_i \geq 1$. Thus the probability of damage P(D) is:

$$P(D) = P(Z_i > 1) \tag{6}$$

Using arbitrarily a lognormal probability distribution for θ_i (2), the probability of damage is:

$$P(D) = \Phi\left(\frac{\ell n\ \bar{Z}_i}{\Omega_{Z_i}}\right) \tag{7}$$

Where Φ (.) = the standard normal probability function, $\bar{Z}_i$ = the mean of Z_i and Ω_{Z_i} = the coefficient of variation (C.O.V.) of Z_i representing the

uncertainty in Z_i. If $\bar{\theta}_i$ and Ω_{θ_i} are respectively the mean and C.O.V. of θ_i, $\bar{Z}_i$ and Ω_{Z_i} are calculated as (3):

$$\bar{Z}_i = 2/\bar{\theta}_i^2 + 1/2 \tag{8}$$

$$\Omega_{Z_i} = 8\ \Omega_{\theta_i}/(4 + \bar{\theta}_i^2) \tag{9}$$

in which (Ref. 2)

$$\bar{\theta}_i = \bar{R}/\bar{F}_i \tag{10}$$

and $$\Omega_{\theta_i} = (\Omega_R^2 + \Omega_i^2)^{1/2} \tag{11}$$

where $\bar{R}$ and $\bar{F}$ are, respectively the means of R and F_i and Ω_R and Ω_{F_i} are the respective C.O.V.'s.

COLLAPSE OF THE SYSTEM

The collapse of the structure may be defined as a ductility level above which the system suffers extensive damage so that failure is certain. If M represents this ductility level, collapse is represented by $\mu_i > M$ where μ_i is the overall ductility of the system at time of the ith blast load, whereas Z_i is the ductility because of ith blast only. The value of μ_i depends on the previous ductilities μ_1, μ_2, ... μ_{i-1}. The probability of collapse, $P(C_i)$ at the ith blast load depends on whether or not $Z_i > 1$. From the total probability theorem (Ref. 2), the probability of collapse is:

$$P(C_i) = P(C_i \mid Z_i > 1)\ P(Z_i > 1) + P(C_i \mid Z_i \leq 1)\ P(Z_i \leq 1) \tag{12}$$

where $P(C_i \mid Z_i > 1) = P(\mu > M)$; whereas $P(C_i \mid Z_i < 1)$ depends on the ductility at (i-1)th blast. This can be postulated as $P(C_i \mid Z_i \leq 1)$ $P(\mu_{i-1} > M)$. Eq. (12), therefore, becomes:

$$P(C_i) = P(\mu_i > M)\ P(Z_i > 1) + P(\mu_{i-1} > M)\ P(Z_i \geq 1) \tag{13}$$

The probability $P(\mu_i > M)$ may be calculated as follows.

After application of load F_{i-1} as part of a series of loads F_1, F_2, ... F_n if $Z_{i-1} > 1$, a permanent displacement $X_{p_{i-1}}$ will be produced. This displacement will be added to the displacement produced by load F_i (see Fig. 3).

For an equivalent linear system, under the action of F_i the system starts from rest with a permanent displacement $X_{p_{i-1}}$, and the total displacement X_{e_i} (see Fig. 4) is

$$X_{e_i} = X_{p_{i-1}} + 2F_i/k \tag{14}$$

If $\mu_i = X_{m_i}/X_y$ (see Fig. 4), a relationship between μ_i and μ_{i-1} may then be derived based on equalizing the energy of the elasto-plastic system and that of the linear one, i.e.

$$\mu_i = \mu_{i-1} + 2/\theta_i^2 - 1/2 \tag{15}$$

For a special condition of i=1, there is no previous permanent displacement. This condition will lead to $\bar{\mu}_0 = 1$ so that Eq. (15) may still be used for i=1. Assuming lognormal distributions for μ_i and Z_i the collapse probability at ith blast may then be calculated in terms of $\bar{\mu}_i$ and Ω_{μ_i} the C.O.V. of μ_i

$$P(C_i) = \{1-\Phi[(1/\Omega_{\mu_i})\, \ell n(M/\bar{\mu}_i)]\}\, \Phi[(1/\Omega_{Z_i})\, \ell n(Z_i)] + \{1-\Phi[(1/\Omega_{\mu_{i-1}})\, \ell n(M/\bar{\mu}_{i-1})]\}\, \{[1-\Phi(\ell n\, Z_i)/\Omega_{Z_i}]\} \tag{16}$$

SPECIAL CASES

For a large $\bar{\theta}_i$, $\bar{\mu}_i$ may be smaller than $\bar{\mu}_{i-1}$. This is, of course, not possible. It is, therefore, more appropriate to set $\bar{\mu}_i \geq \bar{\mu}_{i-1}$ as a necessary condition in this formulation.

If for every blast, $\bar{\theta}_i > 2$. $\bar{\mu}_i$ remains constant and equal to 1. Although Ref. (4) specifies this condition as a no failure case, the present formulation still yields a value for failure probability. This is because of the uncertainties associated with F_i and R.

NUMERICAL ILLUSTRATION

For a shelter under repeated identical loads, the collapse probabilities for different $\bar{\theta}_i$ ranging from 1.0 to 2.0 were obtained using the above formulations. The uncertainties associated with F_i and R are taken as 20%. Furthermore a ductility level M=2 is assumed for defining the borderline between failure and no failure. The results (see Fig. 5) show that even for relatively large $\bar{\theta}_i$ (i.e. $\bar{\theta}_i = 2.0$) the collapse probability may become sign-

ificant after the 3rd or fourth attack.

CONCLUSIONS

A method was formulated for studying the probability of failure of structures when subjected to repeated blast loads. It was applied to the analysis of a structure subjected to a series of identical blast loads and several different ranges from ground zero. Results indicate that even as few as three repeated blast loads can significantly increase the probability of failure even for cases with a relatively high R/F. (The R/F ratio can be looked at as indicating the relative strength of the structure or as an indication of its range from the point of detonation.)

This method can be extended to consider a variety of different loading and resistance functions and attack conditions. For the civil defender, this method is a potentially useful tool for evaluating the effectiveness of different shelter mixes. For the targeteer it is a useful tool for evaluating the effectiveness of different attack conditions.

REFERENCES

1. Newmark, N.M. and Rosenblueth, E., Fundamentals of Earthquake Engineering, Prentice-Hall, Inc. Englewood Cliffs, N.J. 1971.

2. Ang, A. H-S., "Structural Risk Analysis and Reliability-Based Design," Journal of Structural Division, ASCE, Vol. 99, ST9, Sept., 1973, pp. 1891-1910.

3. Ang, A. H-S., and Tang, W.H., Probability Concepts in Engineering Planning and Design, Vol. I - Basic Principles, John Wiley and Sons, N.Y. 1975.

4. Weidlinger, P., "Structures Under Repeated Blast Loads," Rand Corporation, March, 1961.

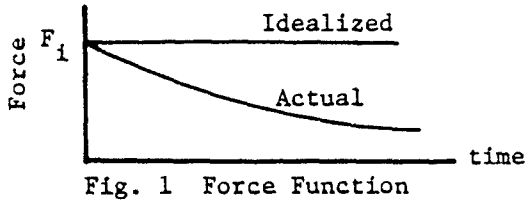

Fig. 1 Force Function

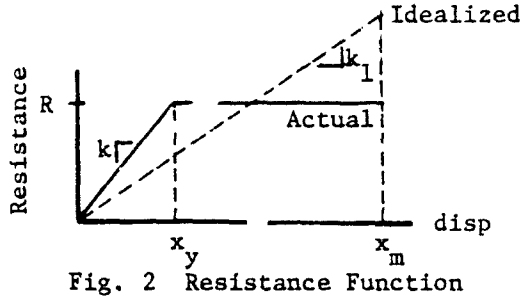

Fig. 2 Resistance Function

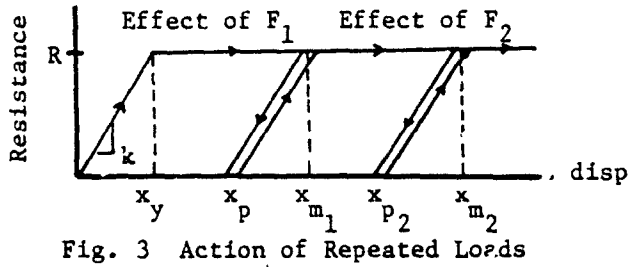

Fig. 3 Action of Repeated Loads

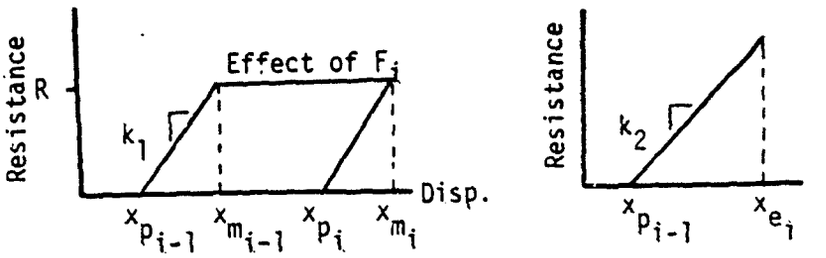

Fig. 4 Elasto-Plastic and Equivalent Linear System

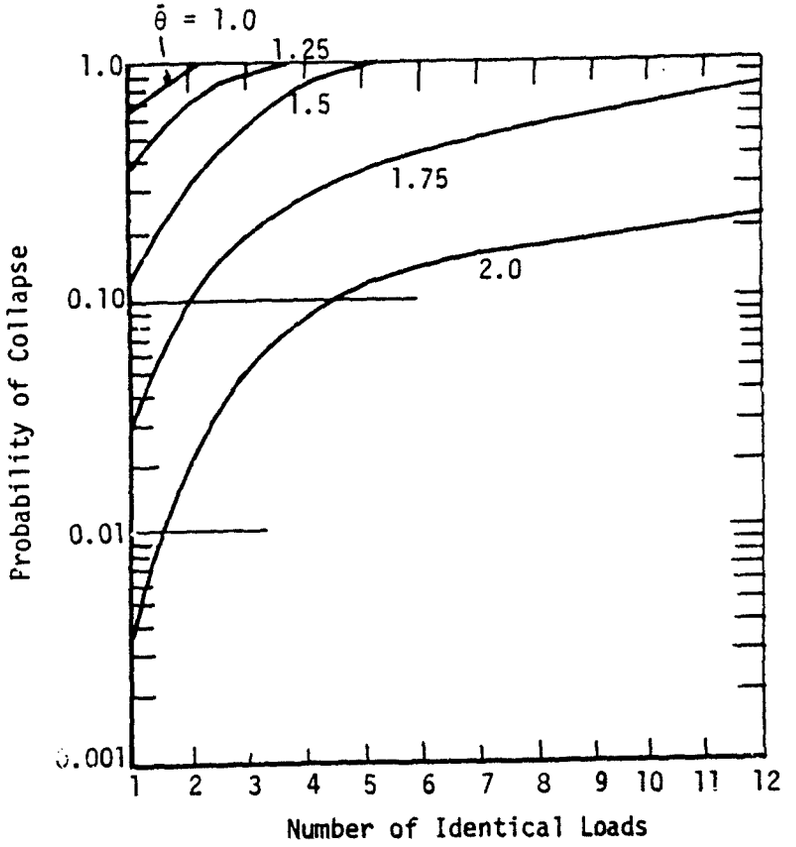

Fig. 5 Numerical Illustration

SESSION II

MASS FIRE AND RELATED TOPICS

SOME OBSERVATIONS ON THE EFFECT OF TURBULENCE MODELING IN NUMERICAL SIMULATIONS OF MULTIPLE-BURST FLOW FIELDS

E. J. Chapyak

Energy Division, Los Alamos National Laboratory, MS K559,
P.O. Box 1663, Los Alamos, New Mexico 87545

ABSTRACT

We describe some preliminary attempts to calculate the development of a simple class of axisymmetric multiple-burst environments. Our primary interest is in the intermediate time regime, during which the characteristic plume structures stabilize and begin to spread horizontally. Employing a standard two-equation description of turbulent entrainment, we find that the maximum extent of plume penetration into the atmosphere is sensitive to details of the turbulence modeling. Some interesting dynamic features of the plume stabilization process are also observed. These results are discussed together with supporting analysis and used to identify generic differences between single-and multiple-burst environments.

INTRODUCTION

Continuing developments in strategic-warfare technology toward more compact and accurate delivery systems have emphasized the importance of multiple burst scenarios to both military and civil defense planners. A prime example of this trend is the recent attention given the survivability of the proposed closely-spaced basing mode for the MX missile system. Clearly, any survivability assessment for this system must involve detailed examinations of a wide spectrum of threat scenarios that involve detonations spaced closely in both space and time.

One of the most important considerations for the viability of closely-spaced basing is the concept of fratricide, whereby a portion of the MX system survives because late-arriving reentry vehicles are incapacitated by weapon effects generated by earlier-arriving ones. Before an evaluation of fratricide can be attempted, the evolution and spatial characteristics of dust clouds and related aspects of multiple-burst flowfields must be known to some degree of accuracy. Thus, the purpose of this study was to see if realistic, but inexpensive, calculations of relatively late-time (tens-of-minutes) multiburst environments could be made with existing capabilities. Although a definitive answer to this problem was not obtained during the short period allotted for the study, we nevertheless have identified some interesting differences between single-burst and multiple-burst environments and the requisite modeling required for their realistic prediction.

PROBLEM DESCRIPTION

The intent of the work presented here is to make a preliminary analysis of the simplest multiple-burst problem — a sequence of near-surface bursts detonated at the same position, but delayed in time by a constant interval. In particular, we consider the successive near-surface detonations of one-MT weapons at an interval of twenty seconds.

The initial atmosphere for these calculations was taken to be isothermal, with both pressure and density falling off exponentially with height. The numerical grid was 26 km high by 14 km in radius. A total of 864 variable-sized zones were employed with the smallest zone size set at 0.25 km. Boundary conditions at the top of the atmosphere included a constant pressure condition, with unimpeded flow permitted across the boundary.* Radial boundary conditions were those of unimpeded flow. No attempt was made to describe the effect of water vapor, dust entrainment or radiation transport.

The code used in these calculations is the SIMMER-II code (1), developed at Los Alamos for nuclear reactor safety analysis. It is a derivative of the KACHINA code (2), and uses a form of the Implicit-Compressible-Eulerian (ICE) numerical solution technique. SIMMER has also been generalized for turbulent, reactive-flow applications. The version of the code used here contains the k-ϵ, two-equation description of turbulent mixing, unmodified for buoyancy effects. This simplification appears to be reasonable for the types of flow structures described here.

SOURCE CHARACTERIZATION

Because the time scale of interest for these problems is long compared with the time between bursts, our description of the individual detonations is necessarily limited to an approximate description of fireball development, rise, and interaction with the next burst. We found that an energy deposition rate of 2×10^6 J/kg-s over a cylinder 0.75 km high and 0.75 km in radius (about one-tenth the volume of the fireball's maximum size) existing for a total of two seconds produced a good approximation to a single, near-surface, one-MT fireball (see below). Whether this deposition produces an adequate description of fireball development in a perturbed atmosphere (i.e., after many bursts have occurred) is an unresolved issue.

---

*All variables, except for pressure, are reflected across the top boundary. This is somewhat unrealistic for atmospheric problems where significant density gradients exist, and can give rise to unphysical effects near the boundary. Likewise, the constant pressure condition can also generate such disturbances. Our belief is that these perturbations do not significantly affect the primary flows generated by fireball buoyancy.

Figure 1 shows a comparison between a one-MT, surface-burst fireball density profile taken from Brode (3) at 2.6 s after detonation with a surface fireball density profile from the present study at 4.0 s after detonation. Recalling that, whereas the energy deposition in a real fireball is practically instantaneous, the deposition in this study occurs over a two-second period, we find the agreement remarkably good. Clearly, if the Brode calculation were extended to 4.0 s, even better agreement would be observed. This comparison could probably be improved by depositing the same total energy in a smaller time window; however, as the energy spike is sharpened, a much more dynamic expansion takes place, causing the calculation to take longer to run. We feel that the current formulation is a good compromise between accuracy and efficiency.

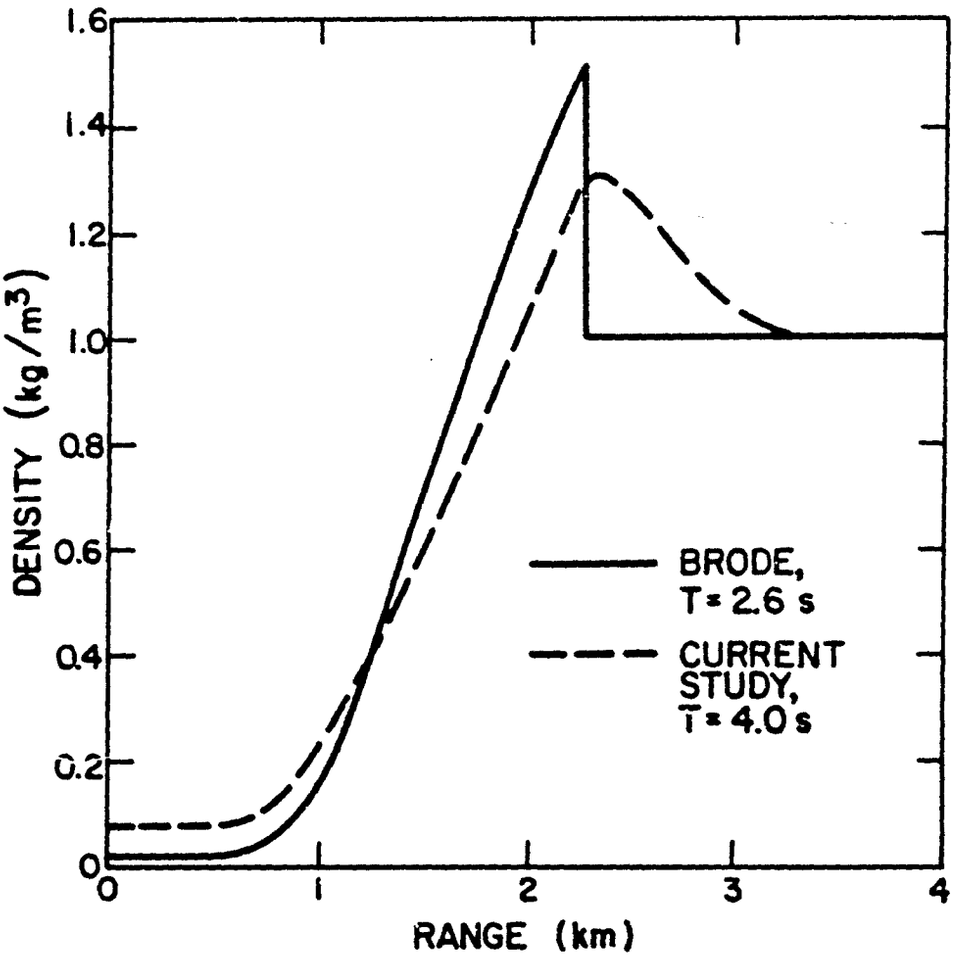

Fig. 1. Comparison of Fireball Density Profiles

PRELIMINARY STUDY

Before proceeding with the multiburst calculations, we wanted to test both the source characterization model and the general numerical formulation with a single-burst simulation. The early-time results from this calculation were discussed in the previous section. As the fireball forms and begins to rise, a classical vortex structure develops. Eventually the fireball reminant overshoots its equilibrium altitude, the vortex reverses, and a downward motion is initiated. In short, these reslts suggest a typical single fireball evolutionary sequence. No noticeable adverse effects attributable to boundary conditions were observed. Unfortunately, space limitiations prevent us from including graphical displays that form the basis of our comments and conclusions.

The next step was to proceed with the multiburst simulation. Naturally, during early times, these results were not dramatically different from the single-burst results. However, as soon as several detonations occurred significant differences were apparent. In fact, we observed the rapid development of a narrow plume structure that quickly penetrated the top of the calculational mesh. Further, high velocities generated in the plume were characteristic of very low entrainment rates.

PLUME STUDIES

The observation of a low-entrainment-rate plume in the multiburst calculation motivated us to investigate in more systematic detail the role of turbulence modeling in the development of such structures. To accomplish this economically, we lowered the energy release rate from 3 MT/min to 3 KT/min, and allowed the release to be continuous in time. Also, to improve resolution in the radial direction we reduced the radial extend of the problem from 14 km to 7 km. With these modifications, we hoped to keep all flow disturbances well within the calculational boundaries.

For reference, we first performed an effectively inviscid calculation of the 3 KT/min steady-release-rate case, starting from quiescent conditions. The quasi-steady-state result was a highly penetrating plume that extended to approximately 18 km in height with intense fallback occurring immediately outside the narrow upward moving core. The height at which horizontal spreading took place appeared to be in the range of 6–7 km.

This can be contrasted to the behavior of a high-turbulence-level case, where the initial turbulent dynamic viscosity was taken to be 0.01 kg/m-s and turbulent kinetic energy was set at $10^{-6} m^2/s^2$. As suggested in the next section, these initial conditions promote rapid generation of turbulence from the mean motion of the plume, and by inference significant entrainment. The result was a plume that penetrated to only about 11 km, with horizontal spreading occurring at about 6 km.

We subsequently investigated an intermediate case, where the initial turbulent dynamic viscosity was set at 0.001 kg/m-s. Here, the plume initially penetrated to heights close to those observed in the inviscid case, but then collapsed back down to about 14 km. The ultimate horizontal spreading height was again about 6 km. A detailed examination of the evolution of turbulent kinetic energy in the two turbulent calculations showed that the high-initial-turbulence-level case generated entrainment quickly, while the lower-initial-turbulence-level case did not generate significant entrainment for some time. Once it did, however, the turbulence levels were actually higher than in the former case.

AN EXPLANATION

The standard k-ε transport equations of Launder and Spalding (4) are

$$\frac{\partial \rho k}{\partial t} + \nabla.(\rho k v) = \nabla\left(\frac{\mu}{a} \nabla k\right) + 2\mu e^{ij} e^{ij} - 2/3\ \rho k \nabla.v - \rho\varepsilon \tag{1}$$

$$\frac{\partial \rho \varepsilon}{\partial t} + \nabla.(\rho \varepsilon v) = \nabla\left(\frac{\mu}{b} \nabla \varepsilon\right) + \frac{c\varepsilon}{k} + 2\mu e^{ij} e^{ij} - 1/3 \rho\varepsilon \nabla \cdot v - d\rho\varepsilon^2/k. \tag{2}$$

The constants a, b, c, and d are of order unity. An important quantity in the above quations is the so-called eddy viscosity defined by the Kolmogonov relation, $\mu = c_\mu \rho k^2/\varepsilon$. The variable μ is generally orders of magnitude larger than the molecular viscous coefficient. The strain rate deviator tensor e^{ij} is defined by

$$e^{ij} = 1/2\ \left(\frac{\partial v^i}{\partial x_j} + \frac{\partial v^j}{\partial x_i}\right) - 1/3\ \nabla.v\ \delta^{ij}. \tag{3}$$

A qualitative appreciation for these equations can be obtained by neglecting all spatial derivatives, letting $c = d = 1$, and taking ρ as a constant. We then have two ordinary differential equations:

$$\frac{dk}{dt} = c_\mu \frac{k^2 s(t)}{\varepsilon} - \varepsilon \tag{4}$$

and

$$\frac{d\varepsilon}{dt} = c_\mu k\ s(t) - \frac{\varepsilon^2}{k}, \tag{5}$$

where $s(t) = 2\ e^{ij} e^{ij}$. The solution to these equations is

$$T = T_i \exp\left[\int_o^t (\nu_i s(\tau) - \varepsilon_i) d\tau / k_i\right], \tag{6}$$

where T is any of k, ε, or μ, $\nu = \mu/\rho$, and the subscript denotes initial values.

Equation 6 suggests an explanation for the plume results described above. The growth rate of say μ, for a given mean shear $s(t)$, is sensitive to the initial parameters ν_j and k_j. A large ν_j and small k_j will ensure that turbulence is generated very quickly. The calculations comprising the preliminary study were set up with low ν_j and relatively large k_j, so that turbulence never had a chance to develop, and essentially laminar, low-entrainment, behavior was observed. Exacerbating the problem was an effective numerical upper limit on the shear that could be developed due to the relatively large zone sizes employed.

We do not, incidently, claim that such behavior is necessarily physical. Certainly, problems exist in matching an inherently turbulent description in one region of the flow to a non-turbulent description in an adjacent region. Other entrainment models and/or much finer zoning, may prove to be more appropriate for the types of problems considered here.

CONCLUSIONS

These observations point to an interesting contrast between single- and multiple-burst simulations. Calculations of single-fireball dynamics do not appear to require entrainment modeling to achieve a reasonable degree of accuracy, probably because numerical diffusion is inherently present. On the other hand, it appears that multiple-fireball calculations, particularly of the type that give rise to narrow, plume-like structures, are much more sensitive to details in the turbulence modeling. This contrast is perhaps not so mysterious if we recall that most of the entrainment in plumes and jets occurs across their radial boundaries. At those boundaries very little radial motion is occurring, so that numerical diffusion is relatively ineffective in creating entrainment (5). Thus, some type of entrainment model is required to provide an adequate account of mixing in the plume-like structures so common to multiple-burst scenarios.

REFERENCES

1. L. L. Smith, SIMMER-II: A Computer Program for LMFBR Disrupted Core Analysis, Los Alamos National Laboratory, Los Alamos, New Mexico, LA-7215-M (1978).

2. A. A. Ansden and F. H. Harlow, KACHINA: An Eulerian Computer Program for Multifield Fluid Flows, Los Alamos National Laboratory, Los Alamos, New Mexico, LA-5680 (1974).

3. H. L. Brode, "Review of Nuclear Weapons Effects," Annual Review of Nuclear Science 18, 153 (1968).

4. B. E. Launder and D. B. Spalding, Lectures in Mathematical Models of Turbulence (Academic Press, New York, 1972).

5. E. J. Chapyak, et al., "Verification Studies of Entrained-Flow Gasification and Combustion Systems with the SIMMER-II Code," in Proc. 10th IMACS World Congress (Montreal, Canada, 1982), Vol. 4, pp. 71-74.

HYDROCODE STUDIES OF FLOWS GENERATED BY LARGE AREA FIRES

H. L. Brode, D. A. Larson and R. D. Small

Pacific-Sierra Research Corporation
12340 Santa Monica Boulevard
Los Angeles, California 90025

ABSTRACT

The global computational approach to the simulation of the meso-scale motions generated by a large area fire is described. Existing hydrocode solutions are reviewed and ongoing calculations discussed. Assumptions applied in many hydrocode solutions are assessed, and modeling requirements based on recent analytical efforts are defined.

INTRODUCTION

The flow system generated by a large area fire is characterized by a high-speed radial inflow near the ground and a very large free-convection column. For fires as large or larger than the World War II firestorms (1, 2), the low-level inflows are expected to be of hurricane force, and the convection columns are expected to ascend through much of the atmosphere. Perturbations of such magnitude should additionally induce significant meso-scale motions outside the column. Such motions might, for example, be vortex-like and pump air in towards the fire, increasing the fire-wind inflow (3, 4).

This paper reviews the large hydrocode approach to the simultaneous simulation of all components (inflow, column upflow, far field) of the fire-generated flow system. The complexities inherent in adopting this approach are discussed, and progress made to date is summarized. The alternative analytical approach is to consider individual flow components separately and match them together in a suitable manner (3). Although significant results concerning the near-fire inflow have been developed (5) and modifications of standard plume theory may (or may not (3)) provide a suitable description of the weakly-buoyant column flow, no component analysis of the far field has yet been completed. Such an analysis may of necessity be computational and involve hydrocode usage.

HYDROCODE ANALYSIS

Conceptually, the full Navier-Stokes, energy, continuity, species, and combustion equations (6) can be solved numerically and the fire-generated flow field defined in an infinite domain. For many problems of interest, current models of the burning processes, flow chemistry, and turbulent structure do not justify such a rigorous modeling. Accordingly, a number of simplifying assumptions have been used (4, 7-10). They include an isothermal boundary condition to model the heat release by combustion (7 - 9), the Boussinesq approximation (7 - 10), either a constant eddy diffusivity (4, 7 - 9) or k-ε model (10) to describe the turbulent structure and a finite-volume heat source (4).

With the heat addition modeled by an isothermal condition at the ground, the production of buoyancy depends on the diffusion of energy from the boundary. Coupled with the Boussinesq approximation, use of an isothermal condition

restricts the solution to weakly buoyant motions similar in principle to flows generated by urban heat islands (11, 12). Such motions tend to form very thin columns, unlike actual fire systems in which the highly-turbulent, strongly-buoyant near-fire flow produces a column whose width is comparable to that of the fuel bed (13). In order to adequately simulate the qualitative aspects of large-fire flows, hydrocode models must therefore treat the near-fire (or source) region with some care.

A fine zoning of the source region is of course a necessity. Beyond that, the use of a finite-volume heat source is recommended, and more accurate turbulence modeling may be considered. Recent studies (14) of the source-region flow component indicate that it depends strongly on the height of the heating region (see Fig. 1), but is relatively insensitive to the spatial distribution of the heat release. The use of a finite-volume heat release should thus not be restricted by a limited data base, but should greatly improve the modeling. The level of turbulence in the source region should be greater than that in the slower-moving, overhead column, and much greater than outside the column. An adequate definition of the source-region turbulence is at present lacking, however, and current models are correspondingly crude. The current radiation models are simple graybody losses, which are also quite approximate. Radiation should play a negligible role over most of the flow field, but is expected to be of importance in the early (low-level) decay of the high-temperature source flow to the weakly-buoyant column flow.

Current hydrocode solutions all show large fire-wind inflows near the source region. Smith, Morton and Leslie (8) relate the induced fire winds to the dynamic pressure field generated by the buoyancy. The pressure gradients are greatest in the neighborhood of the fire zone and decay rapidly with distance from the fire perimeter. The generation of a high-velocity inflow near the fire by pressure gradients rather than by viscous entrainment is consistent with the observations of Cox and Chitty (15).

An interesting feature of several large-scale solutions has been the development of well-defined vortex structures. Delage and Taylor (12) describe early-time roll motions above an urban heat island as well as the development of a meso-scale recirculation (cf. 3, 11). Luti and Brzustowski (9) examine the generation of lee-side vortices by a heat source in cross flow.

Larson, Brode, and Small (4) consider the strongly buoyant flow produced by area fire of 10 km radius, and describe the time history of several vortex motions. The volume heat addition generates several rotating cells in the source region (Fig. 2). The continued, constant production of buoyancy generates a strengthening inflow that gradually imposes a radially directed flow in the source region (Fig. 3). As the inflow strengthens, a strong vortex develops above the fire perimeter (Fig. 4) and is eventually shed. The outward motion of that vortex produces a stronger inflow that extends approximately one fire radius beyond the fire boundary. As the vortex moves to infinity, the inflow weakens and roll motions reappear in the burning region. The cycle repeats at approximately 20 minute intervals in this particular case. In related, ongoing hydrocode studies, similar results are being obtained (16).

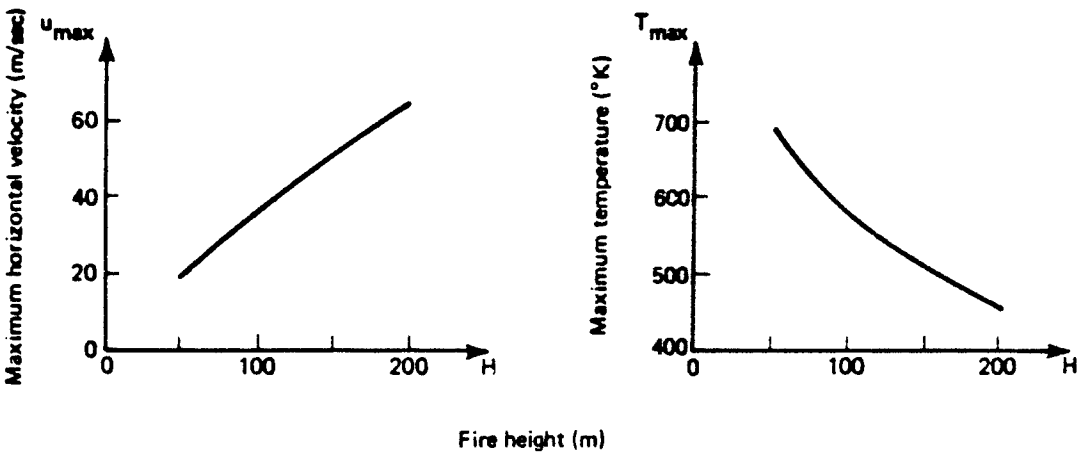

Fig. 1. Dependence of maximumradial velocity and temperature on fire height.

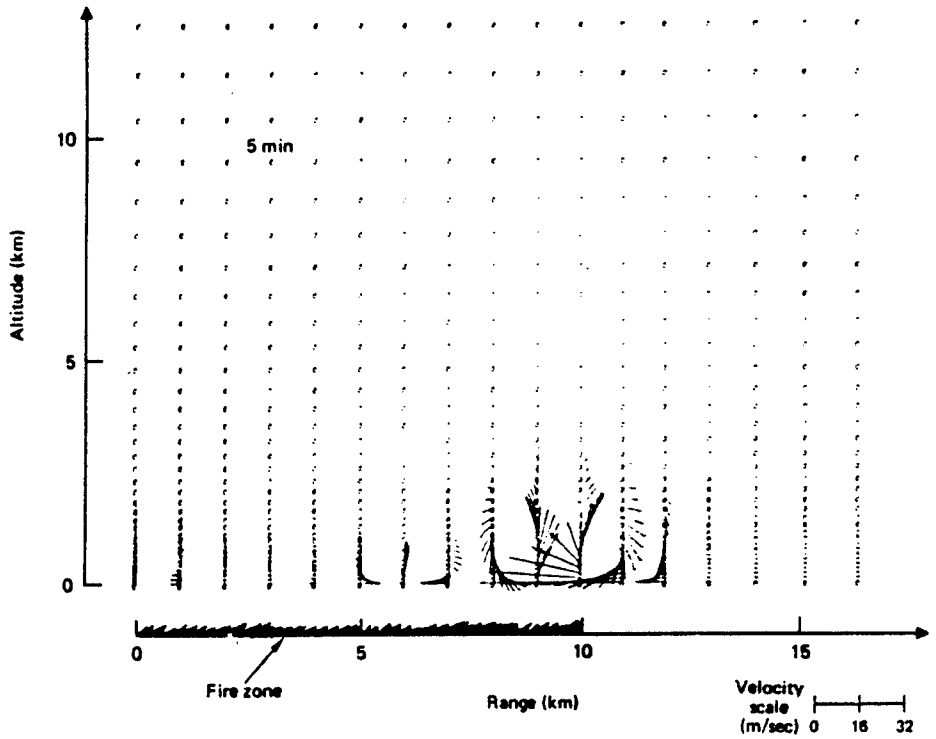

Fig. 2. Simulated flow field at 5 min. after ignition for sample 10 km fire.

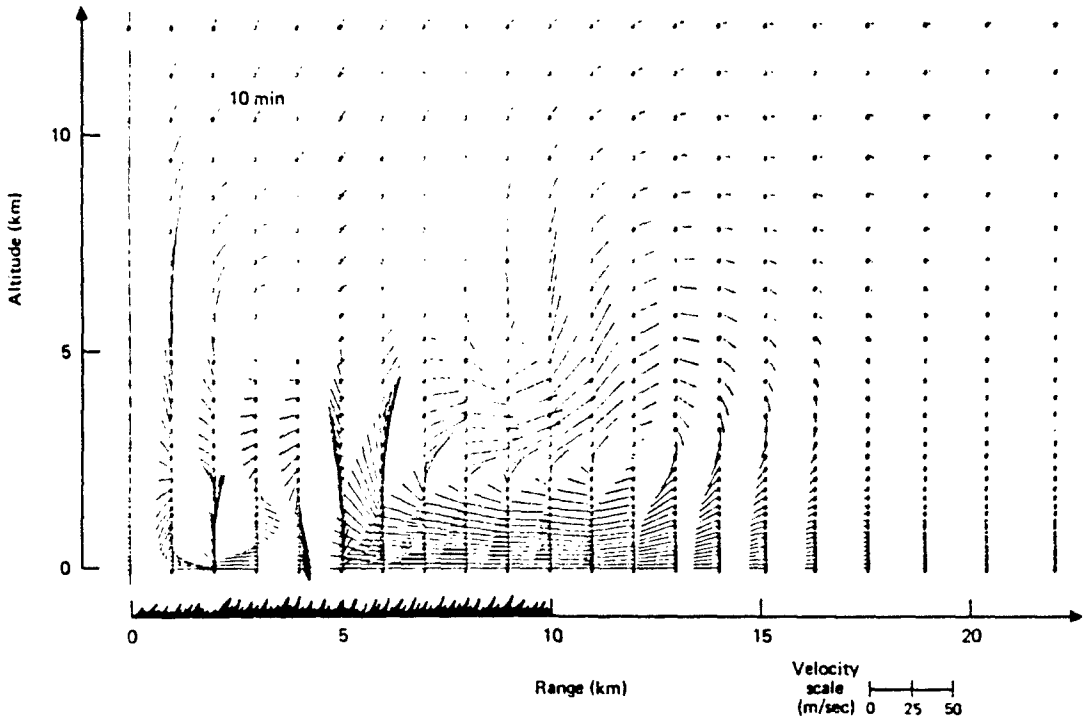

Fig. 3. Simulated flow field at 10 min. for sample 10 km fire.

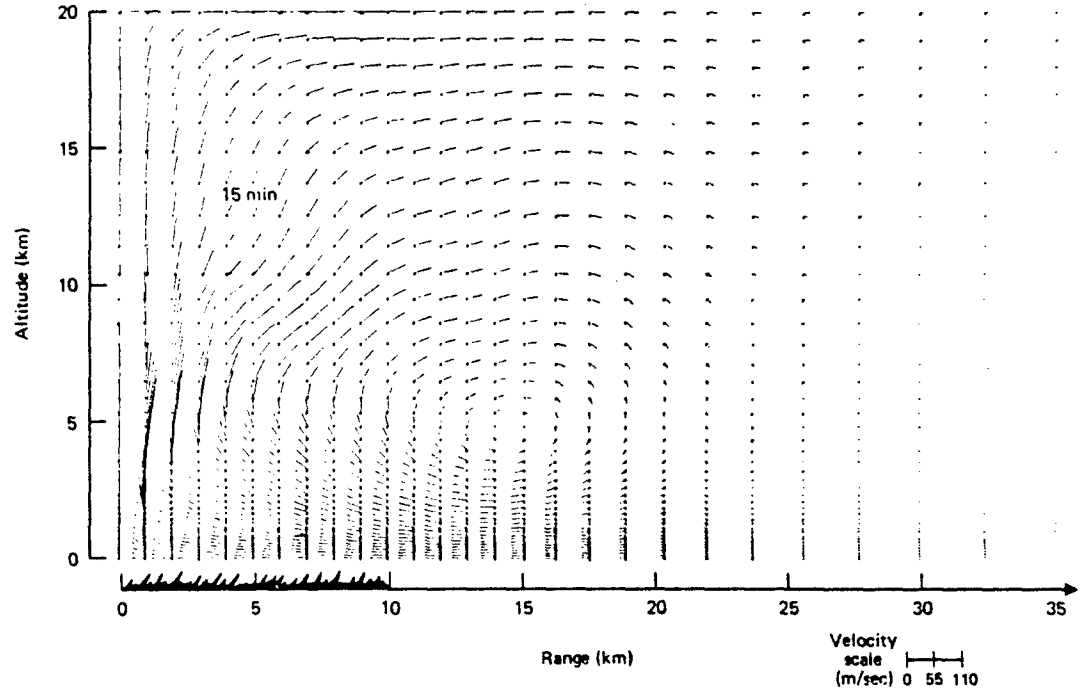

Fig. 4. Simulated flow field at 15 min for sample 10 km fire.

In those studies, the dependence of solutions on boundary conditions, level of turbulence and other data is being investigated. In addition, we are investigating the type of hydrocode modeling that is required to simulate the fire flows generated by the Project Flambeau experiments (13), the largest fires for which at least a limited data base is available. Such a simulation would provide a test case against which further computational work could be validated. Such work should consider larger fires, improved turbulence and radiation modeling, and the effect of condensation on the column flow and far-field forcing.

DISCUSSION

Thus far, numerical simulations of flows generated by large fires have been somewhat limited, but they have contributed to the understanding of the dynamics of such flows and the interaction between flow components. Conversely, individual study of the component flows has provided ideas for improved hydrocode modeling. It is expected that refinements in both types of analysis will be fostered by a continued interchange of results.

The burning fuel bed provides the driving force for the overall flow, and it is in and around the fuel bed that knowledge of the flow field is of most interest. A careful modeling of the high-speed surface inflow and strongly buoyant upflow thus requires fine zoning of the source region and treatment of the effects of turbulence and radiation. Current modeling efforts are addressing those issues.

ACKNOWLEDGEMENT

This review was sponsored by the Defense Nuclear Agency, monitored by Dr. Michael J. Frankel.

REFERENCES

1. D. Irving, Destruction of Dresden, Kimber, London, England (1963).

2. M. Middlebrook, The Battle of Hamburg, Scribner, New York (1981).

3. R. D. Small, D. A. Larson, and H. L. Brode, Analysis of Large Urban Fires, Pacific-Sierra Research Corporation, Los Angeles, California, PSR Report 1122 (September 1981).

4. H. L. Brode, D. A. Larson, and R. D. Small, Time-Dependent Model of Flows Generated by Large Area Fires, Pacific-Sierra Research Corporation, Los Angeles, California, PSR Note 482 (July 1982).

5. D. A. Larson and R. D. Small, Analysis of the Large Urban Fire Environment, Part I: Theory, Pacific-Sierra Research Corporation, Los Angeles, California, PSR Report 1210 (July 1982).

6. F. Williams, "Scaling of Mass Fires," Fire Research Abstracts and Reviews, Vol. 11, p. 1 (1969).

7. H. J. Nielsen, Mass Fire Data Analysis, ITT Research Institute, Chicago, Illinois, DASA Report No. 2018 (January 1970).

8. R. K. Smith, B. R. Morton, and L. M. Leslie, "The Role of Dynamic Pressure in Generating Fire Winds," Journal of Fluid Mechanics, Vol. 68, pp. 1-19 (1975).

9. F. M. Luti and T. A. Brzustowski, "Flow Due to a Two-Dimensional Heat Source with Cross Flow in the Atmosphere," Combustion Science and Technology, Vol. 16, pp. 71-87 (1977).

10. F. M. Luti and T. A. Brzustowski, "Some Characteristics of a Two-Dimensional Starting Mass Fire with Cross Flow," Combustion Science and Technology, Vol. 26, pp. 25-33 (1981).

11. M. A. Estoque and C. M. Bhumralkar, "Flow Over a Localized Heat Source," Monthly Weather Review, Vol. 97, pp. 850-859 (1969).

12. Y. Delage and P. A. Taylor, "Numerical Studies of Heat Island Circulation," Boundary Layer Meteorology, Vol. 1, pp. 201-226 (1970).

13. C. M. Countryman, PROJECT FLAMBEAU...An Investigation of Mass Fire (1964-1967), Vol. 1, U.S. Forest Service, Berkeley, California (1969).

14. D. A. Larson and R. D. Small, Analysis of the Large Urban Fire Environment, Part II: Parametric Analysis and Model City Simulations, Pacific-Sierra Research Corporation, Los Angeles, California, PSR Report 1210 (November 1982).

15. G. Cox and R. Chitty, "A Study of the Deterministic Properties of Unbounded Fire Plumes," Combustion and Flame, Vol 39, pp. 191-199 (1980).

16. M. Rossenblatt, P. Hassig, and D. Kanne, private communication (March 1983).

FIRESTORM FORMATION AND ENVIRONMENT CHARACTERISTICS AFTER A LARGE-YIELD NUCLEAR BURST

Paul J. Hassig and Martin Rosenblatt

31 May 1983

1. INTRODUCTION

The ignition and propagation of fires after a large-yield HOB detonation represent a potentially important nuclear weapons effect. Urban areas, with many ignition sources, are particularly susceptible to fires and to the rapid spread and possible coalescence of individual fires distributed over a large area. Under some circumstances, a firestorm may develop.

The objectives of this study are to numerically simulate:

1. the physical conditions leading to a firestorm, and
2. the velocity and pressure fields inside and outside a "representative" firestorm.

2. METHODOLOGY

The development of a firestorm involves mutual interactions between the fire combustion/propagation and the atmosphere winds/temperatures. In view of the many uncertainties in the distribution of ignition points and available fuel, the mutual interactions will be analyzed using the DICE code (1) with simple combustion/propagation models.

DICE is an Eulerian code which solves the dynamic two-dimensional (2-D) axisymmetric atmospheric equations of motion using an implicit finite difference technique. The code can accept a general model detailing the the release of chemical energy due to combustion. For the numerical simulations described in this study, a simple model which adds combustion energy at a constant rate of $q_b = 0.25$ MJ/m^2/s uniformly along the ground is assumed. The combustion region is assumed circular with a radius of 10 km. Heat loss due to thermal radiation from hot gas and smoke is simulated in some of the calculations.

3. RESULTS

In order to gain some understanding into the phenomenology of a large mass fire, several coarsely zoned numerical simulations were performed. Table 1 lists the cases along with the relevant parameters which were varied.

The objective of these calculations was to provide some understanding of the effects of varying initial and boundary conditions.

Table 1. Numerical Simulation Cases of a Large Mass Fire

Case	Thermal Loss	Atmosphere	Rigid Boundary Upper	Rigid Boundary Radial	Zoning
125	< 1%	standard	no	no	coarse
126	< 1%	standard	yes	no	coarse
127	< 1%	adiabatic	yes	no	coarse
128	< 1%	adiabatic	yes	yes	coarse
129	45%	adiabatic	yes	no	coarse
3C1	30%	standard	no	no	fine

The coarsely zoned Cases F-125 to F-129 consisted of 1 km wide cells in the radial direction to a radius of 13 km. Each cell beyond 13 km was larger than the previous one by 9%, to a maximum radius of at least 100 km for the rigid boundary case. The vertical dimension of the first six cells is 100 m, with an increase of 9% for each additional cell upward. A rigid upper boundary occurs at 20 km altitude; Case F-125 has a transmissive upper boundary at 49 km altitude. Rigid boundaries were used for comparisons with prior work (2) and for computational simplicity.

The most pronounced difference is seen between Case F-126, which used a U.S. Standard Atmosphere (-6.5 K/km tropospheric lapse rate) and Case F-127, which had a constant dry adiabatic lapse rate (-9.8 K/km) atmosphere. Figure 1 compares the vertical temperature profiles of each atmosphere. Figure 2 compares the velocity fields at t = 15 min after the start of combustion. Note the formation of a much stronger vortex flow field for Case F-127 centered above and beyond the edge of the fire region. The tropopause tends to confine the vortex below 12 km altitude for Case F-126.

Figure 3 compares the velocity fields at t = 15 min for Case F-126 (rigid upper boundary at 20 km altitude) and Case F-125 (transmissive upper boundary at 49 km altitude). Note that the rigid upper boundary in Case F-126 causes a strong outward flow from the axis at 20 km altitude. However, below 15 km altitude the velocity fields appear identical.

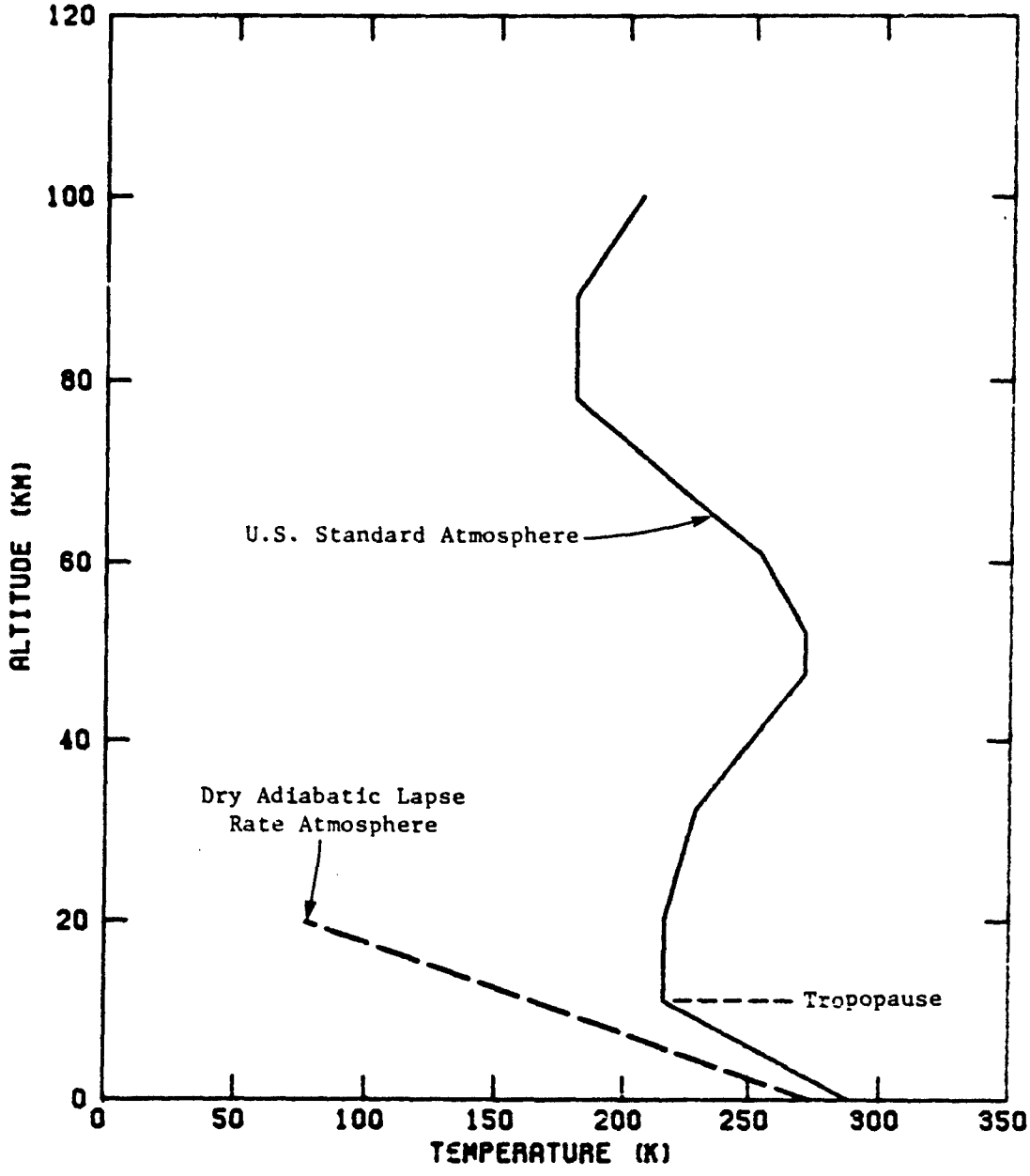

Figure 1. Vertical Temperature Profile Comparison for a U.S. Standard Atmosphere and a Dry Adiabatic Lapse Rate Atmosphere.

(a) Case F-127 (adiabatic atmosphere)

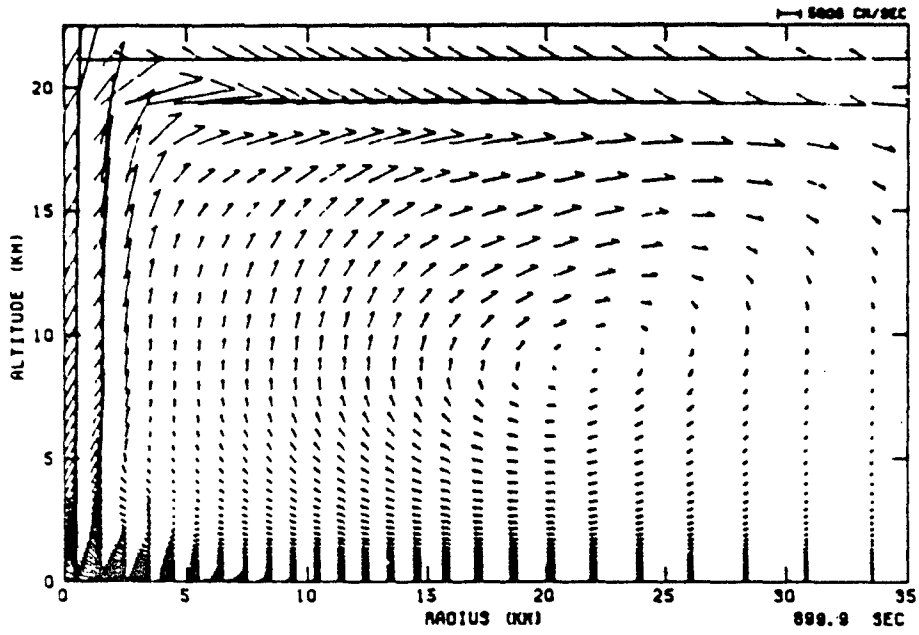

(b) Case F-126 (U.S. Standard Atmosphere)

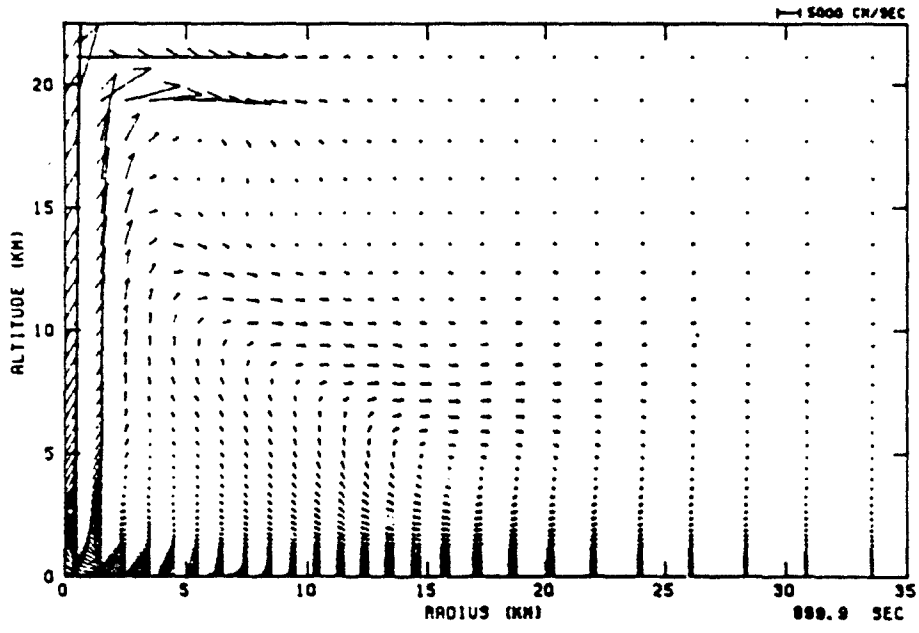

Figure 2. Particle Velocity Field at t = 15 min for
(a) Case F-127 (adiabatic atmosphere) and
(b) Case F-126 (U.S. Standard Atmosphere).

(a) Case F-126 (rigid upper boundary at 20 km altitude)

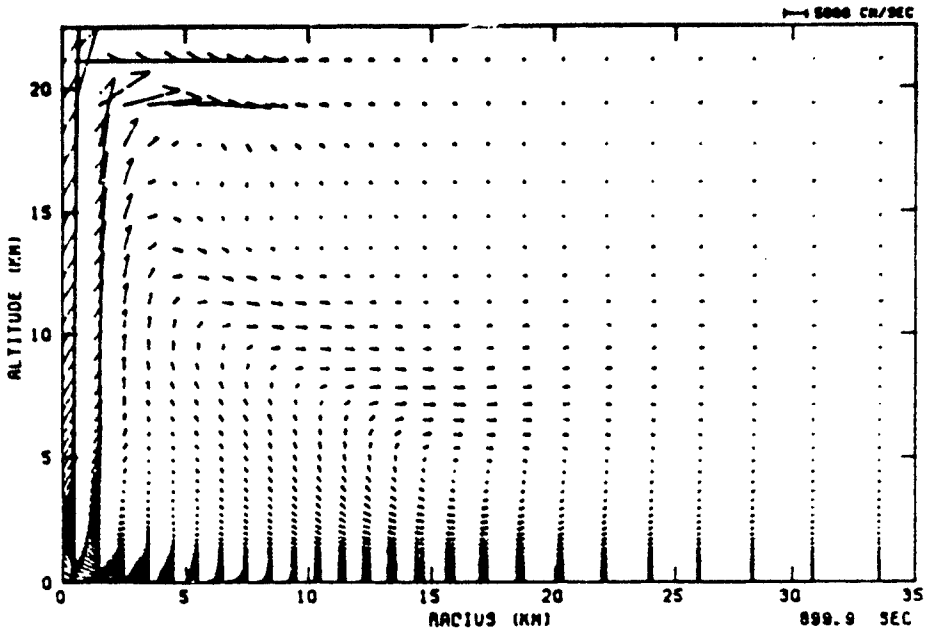

(b) Case F-125 (transmissive upper boundary at 49 km altitude)

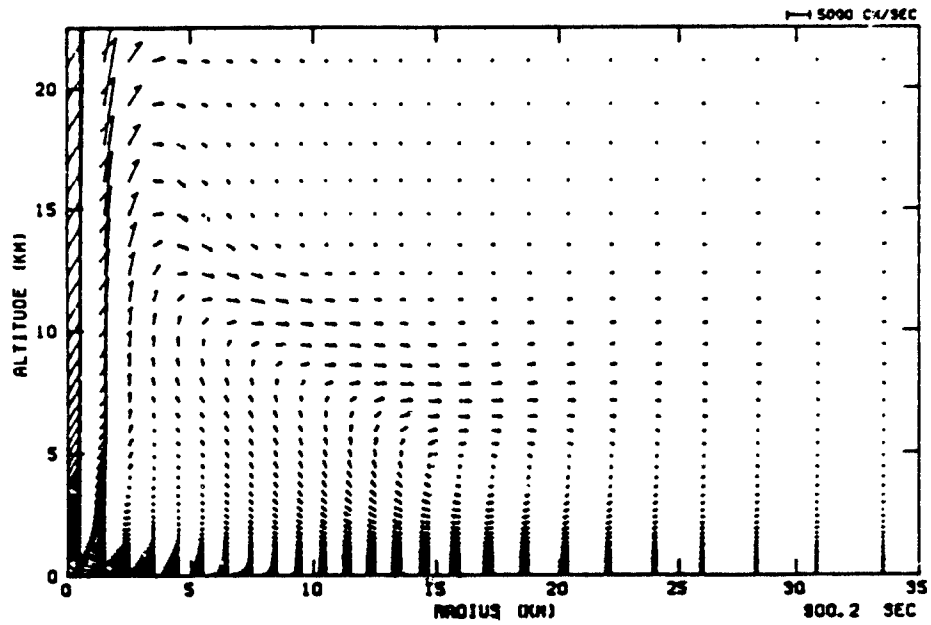

Figure 3. Particle Velocity Field at t = 15 min for

(a) Case F-126 (rigid upper boundary at 20 km altitude) and
(b) Case F-125 (transmissive upper boundary at 49 km altitude).

Figure 4 shows the horizontal velocity versus radius along the ground at t = 15 min for Case P-125. Peak inward velocities of nearly 100 m/s occur at 2 km radius. At the edge of the fire region -20 m/s velocities are evident, and extend to over 15 km radius. The shape of this velocity profile along the ground is maintained to t = 25 min, with variations on the order of 10 m/s.

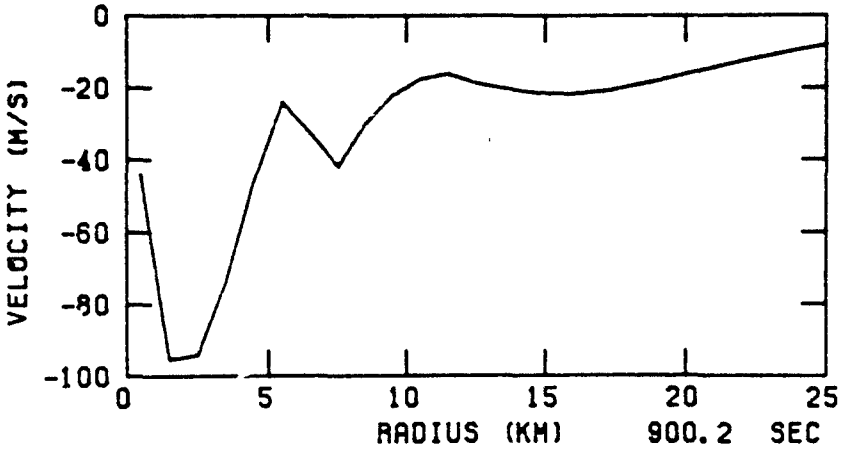

Figure 4. Radial Velocity vs. Range Along the Ground at t = 15 min for Case P-125

A more finely zoned numerical simulation is currently in progress, the results of which will be presented at the conference. Initial conditions include the U.S. Standard Atmosphere, and a linear build-up in time of the combustion rate to its full value (q_b = 0.25 MJ/m^2/s) between t = 0 and t = 15 min. The simulation will be carried out to t = 120 min.

REFERENCES

1. Rosenblatt, M., G.E. Eggum, P.J. Hassig, and R.J. Schlamp, DICE Code developed under U.S. Government contracts, California Research & Technology, Inc., 1972-1983.

2. Brode, H.L., D.I. Larson, and R.D. Small: Time-Dependent Model of Flows Generated by Large Area Fires, Pacific-Sierra Research Corporation, Note 483, July 1982.

CRITERIA FOR ONSET OF FIRESTORMS

G. F. Carrier, F. E. Fendell, and P. S. Feldman
TRW Space and Technology Group, Redondo Beach, CA 90278

Quantitative criteria are evolved for onset of firestorms, severe stationary (nonpropagating) holocausts arising via merger of fires from multiple simultaneous ignitions in a heavily fuel-laden urban environment. Within an hour, surface-level radial inflow from all directions sustains a large-diameter convective column that eventually reaches altitude of about 10 km (e.g., Hamburg, Dresden, Hiroshima). As the firestorm achieves peak intensity (2-3 hours after the ignitions), inflow speeds are inferred to attain 25-50 m/s; typically 12 km^2 are reduced to ashes, before winds relax to ambient levels in six-to-nine hours. Here the firestorm is interpreted to be a mesocyclone (rotating severe local storm). Even with exceedingly large heat release sustained over a concentrated area, in the presence of a very nearly autoconvectively unstable atmospheric stratification, onset of vigorous swirling on the scale of two hours requires more than concentration of circulation associated with the rotation of the earth; rather, a preexisting, if weak, circulation appears necessary for firestorm cyclogenesis.

NOMENCLATURE

$B(z,t)$ = radius of preexisting mesoscale vortex, m
$B_o(z) = B(z,0)$, m
$b(z,t)$ = e-folding radial distance for plume variables, m
$b_i = b(0,t)$, m
c_p = specific heat capacity at constant pressure for air, m^2/s^2-K
E = time-average strength of maintained heat source, W
g = gravitational acceleration, m/s^2
r = cylindrical radial coordinate, m
$S(z,t)$ = angular momentum per mass derived from earth rotation, m^2/s
$T(r,z,t)$ = temperature, K
t = time, s
$V(z)$ = swirl speed of preexisting mesoscale vortex, m/s
$v(r,z,t)$ = azimuthal velocity component, m/s
$W(z,t)$ = centerline axial velocity component, m/s
z = axial distance above ground, m
z_i = distance from subterranean point source to ground, m

GREEK

$\alpha(r,z,t)$ = entrainment functional
α_o = value of α in the absence of rotation
$\Gamma_o(z) = 3_o(z)\ V(z)$, m^2/s
ε = volumetric-flux equivalent of E, m^3/s
$\rho(r,z,t)$ = density, kg/m^3
Ω = component of angular velocity of earth locally perpendicular to surface, s^{-1}

SUBSCRIPTS

a = ambient quantity (function of z only)
i = initial, i.e., pertaining to z = 0
o = ambient quantity (function of z only)

INTRODUCTION

In the aftermath of the atomic bombing of Hiroshima, (1,2) and of the massive incendiary bombing of Hamburg (3-6) and Dresden (7), particularly virulent, long-lived, uncontrolled burning occurred that had few if any recorded precedents. About one-half hour after multiple simultaneous ignitions (in a heavily fuel-laden urban environment)(2,8), the fires merged to form a rather uniformly burning area of many square kilometers. Whereas the ambient winds were less than 5-6 m/s, the mass fire engendered radially inward winds at street level from all directions; about 2-3 hours after the initiating bombing, these winds reached a peak intensity of about 20 m/s, with some estimates by professional firefighters of 50 m/s. The radially inward wind apparently precluded spread beyond the initially ignited area, though virtually everything combustible within this region was burned before the winds subsided to moderate in speed and variable in direction about six hours after initiation. A single huge central convective column, into which the hot product gases flowed, rose to about 10 km. This rare nonpropagating fire, so distinct from more common ambient-wind-aided spreads, is termed a firestorm. The goal of the present investigation is to delineate, from thermohydrodynamic modeling, quantitative criteria for the onset of a firestorm; detailed description of the event at peak intensity is not the prime objective.

In the interpretation given here, the term firestrom is apt. In a conventional meteorological context, storm suggests cyclonic wind about a center of low surface pressure, with precipitation from convectively induced advection [i.e., from buoyancy-caused ascent and saturation of warm moist air, with (1) radial influx under continuity, and (2) possible attendant spin-up under conservation of angular momentum associated with earth rotation or some locally enhanced level]. Hence a firestorm is a "heat cyclone" (9), a mesolow in which the exothermicity of combustion, as distinguished from the condensation of water vapor, induces free convection. Just as firestorms are exceptional fire events, so mesolows (thunderstorms with organized rotation, also referred to as tornado cyclones and supercells) are uncommon relative to the total number of thunderstorms, and are characterized by horizontal scale of several kilometers and lifespan of about six hours (10). Further, just as the mesolow is characterized by towering cumulonimbi ascending through the depth of the troposphere to the tropopause, so the firestorm is characterized by a convective column ascending to exceptionally great height, e.g., 10-13 km at Hamburg.

The observation at low altitudes of appreciable radial influx from all directions toward the base of the centrally sited convective column corroborates, rather than contradicts, the primarily rotating nature of the bulk of the air motion. Investigation of the near-surface inflow layer near the center of a vigorously rotating airmass over a fixed flat surface shows that strong, purely swirling motion is altered to equally strong, purely radial influx near the ground, though immediately at the ground the non-slip constraint holds (11-13).

The firestorm is the exceptional event in that diffusive mechanisms normally relax spin-up, such that swirling is either modest or nil (14). Allusions to the parallel between firestorms and tropospheric storms in the general sense of strong convection accompanied by strong surface winds are frequent. However, pertinence of the dynamic characteristics of a rapidly rotating airmass above a relatively fixed flat surface plane has been

emphasized by Ebert (9), Emmons (15) and Long (16); Ebert and Emmons suggest that the rotation of the air surrounding the plume suppresses entrainment such that the buoyant plume rises to exceptional altitude, while Emmons and Long note that radial near-surface inflow is consistent with rapid higher-level swirling. Here, quantitative description seeking onset criteria is undertaken. It may be remarked that the well-known propensity for long-range, spotting-type (discontinuous) spread of free-burning fire via firebrands in the event of firewhirls (17, 18) suggests that the spatially confined character of recorded firestorms yet may have exceptions.

ANALYSIS

If one neglects plume-scale rotation during spin-up, then, for adopted Gaussian-type profiles, the angular momentum is

$$rv(r,z,t)=S(z,t)\left\{1-\exp[-r^2/b^2(z,t)]\right\} + \Gamma_0(z)\left\{1-\exp[-r^2/B^2(z,t)]\right\},$$

where the angular momentum $\Gamma_0(z)$ of a (prescribed) preexisting mesoscale vortex is taken as invariant in time over the span of interest in firestorm onset. Applying conservation of angular momentum yields

$$\frac{\partial S}{\partial t} = 2\Omega\alpha bW, \quad \frac{\partial B^2}{\partial t} = -2\alpha bW. \tag{2}$$

Since initially, $B(z,0) = B_0(z)$ and $\Gamma_0(z)$ is finite (see Table 1 for parameter values), since $S(z,0) = 0$ and $\Omega = O[(6h)^{-1}]$, and since the entrainment constant $\alpha = O(0.1)$ in a nonrotating atmosphere, it follows that spin-up times based on concentrating angular momentum derived from earth rotation occurs over too long a span to explain reported firestorm phenomena. Thus, the term involving S in (1) is discarded; the convectively induced advection engendered by the intense exothermicity serves to concentrate a preexisting vortex. Plausibility for such a preexisting vortex at Hamburg (derived in part from earlier air raids) is furnished by the fact that prior winds of 4-6 m/s were reported about 10 km from the firestorm site, but the site itself was in virtual calm (6,9).

The similarity solution for a buoyant plume from a point source of heat at $z = z_i$ in an adiabatic (neutrally stable) atmosphere (in which density variation with altitude is ignored to afford a closed-formed expression) is given by (19)

$$b = \frac{6}{5}\alpha_0(z+z_i), \quad W = \frac{5}{6\alpha_0}\left[\frac{18}{5\pi}\left(\frac{\alpha_0\varepsilon g}{z+z_i}\right)\right]^{1/3}, \tag{3}$$

where the entrainment constant α is given its classical value, and

$$\varepsilon = \frac{E}{\rho_a(0)c_pT_a(0)}, \quad b_i = \frac{6}{5}\alpha_0 z_i. \tag{4}$$

The subterranean site of the virtual source $(-z_i)$ has been chosen such that plume has (assigned) plausible radial scale b_i at ground level z=0; this procedure does admit finite mass and momentum flux, as well as buoyant flux. Equations (3)-(4) are used in (2) over the time interval before spin-up alters plume structure via introduction of an axial pressure gradient. The decrease of B^2 in time at fixed z, from (2), implies increased swirl v in time at fixed r and z, from (1). Computations for the parametric assignments of Table 1 suggest swirl speeds of O(20 m/s) are readily achieved for the lower troposphere just outside the plume. Presumably $\alpha = O(\alpha_0/10^2)$ after spin-up, such that reduction in entrainment results in roughly a doubling of the plume height. Some results are given in Figure 1.

CONCLUSIONS

Current estimates for firestorm-onset criteria are as follows: "(1) at least 8 pounds of combustible per square foot of fire area, (2) at least half of the structures in the area on fire simultaneously, (3) a wind of less than 8 miles per hour at the time, and (4) a minimum burning area of about half a square mile" (2, pp. 299-300). On the basis of the study described above, the following alternate criteria are proposed: (1) a localized heat release of order 10^{19} ergs/s sustained for at least 2-3 hours; (2) a preexisting weak vortex characterized near ground level by swirl of 4 m/s at about 8 km, such that preexisting angular momentum (per unit mass) near ground level is $3.2 \cdot 10^4$ m^2/s; (3) absence of a strong ambient crosswind, with less than 4 m/s perhaps being adequate constraint, but with total absence being even more conducive to firestorm onset; and (4) a very nearly dry-adiabatic lapse rate holding for the lowest few kilometers of the atmosphere. Lower-tropospheric spin-up to about 20 m/s within 2-3 h seems plausible under such criteria. If the exothermicity of combustibles is taken to be that of dry woody matter consumed readily in forest fires, which is $1.86 \cdot 10^4$ J/g or so, then the requisite fuel loading appears to be about four times the 8 pounds per square foot cited earlier, if an area of 12 km^2 is entailed and the burning continues at high intensity for 6 h (as reported at Hamburg). The onset of swirling near the convective-column edge may be abrupt in that it can rise from nearly nil levels to 20 m/s or so within a half hour. The background angular momentum associated with the rotation of the earth is inadequate for spin-up to the cited swirl speed on the scale of 2 hours or so.

Further work on plumes whose base temperatures are $O(10^3 K)$ and which are accompanied by significant swirl is impeded by the current absence of answers to the questions: (1) is the entrainment rate more properly related to mass entrainment [i.e., $\rho_a \lim_{r \to \infty} (ru)$] per unit of axial mass flux [$bW \lim_{r \to 0} \rho$], or to volume entrained [$\lim_{r \to \infty} (ru)$] per unit of axial volume flux (bW); (2) by how much is the entrainment coefficient reduced by an increase in swirl. Answers can be furnished experimentally only. In fact, it is clear from already published laboratory experiments on firewhirls (20) that reduction in entrainment with swirl is highly significant.

ACKNOWLEDGMENT

The authors are grateful to technical monitors Mike Frankel and Tom Kennedy for the opportunity to pursue this investigation. This work was supported by the Defense Nuclear Agency under contract DNA001-81-C-0111.

REFERENCES

1. H. Bond, ed., Fire and the Air War (National Fire Protection Agency, Boston, MA, 1946).

2. S. Glasstone and P. J. Dolan, eds., The Effects of Nuclear Weapons, 3rd ed. (U.S. Department of Defense and U.S. Department of Energy, Washington, D.C., 1977).

3. M. Caidin, The Night Hamburg Died (Ballantine, New York, NY, 1960).

4. G. Musgrove, Operation Gomorrah--The Hamburg Firestorm Raids (Jane's, New York, NY, 1981).

5. M. Middlebrook, The Battle of Hamburg--Allied Bombers against a German City in 1943 (Charles Scribner's Sons, New York, NY, 1981).

6. H. Brunswig, Feuersturm über Hamburg (Motorbuch, Stuttgart, Germany, 1981).

7. D. Irving, The Destruction of Dresden (Ballantine, New York, NY, 1965).

8. G. J. B. Fisher Incendiary Warfare (McGraw-Hill, New York, NY, 1946).

9. C. H. V. Ebert, "The Meteorological Factor in the Hamburg Fire Storm," Weatherwise 16, 70-75 (1963).

10. E. Brandes, "Mesocyclone Evolution and Tornadogenesis," Monthly Weather Review 106, 995-1011 (1978).

11. G. F. Carrier, "Swirling Flow Boundary Layers," Journal of Fluid Mechanics 49, 133-144 (1971).

12. O. R. Burggraf, K. Stewartson, and R. Belcher, "Boundary Layer Induced by a Potential Vortex," Physics of Fluids 14, 1821-1833 (1971).

13. G. F. Carrier and F. E. Fendell, "Analysis of the Near-Ground Wind Field of a Tornado with Steady and Spatially Varying Eddy Viscosity," in Wind Field and Trajectory Models for Tornado-Propelled Objects, Electric Power Research Institute, Palo Alto, CA, Report NP-748 (1978), pp. A-1--A-45.

14. P. Dergarabedian and F. Fendell, "Parameters Governing the Generation of Free Vortices," Physics of Fluids 10, 2293-2299 (1965).

15. H. W. Emmons, "Fundamental Problems of the Free Burning Fire," in Tenth Symposium (International) on Combustion (Combustion Institute, Pittsburgh, PA, 1965), pp. 951-964.

16. R. R. Long, "Fire Storms," Fire Research Abstracts and Reviews 9, 53-68 (1966).

17. H. E. Graham, "Fire Whirlwinds," Bulletin of the American Meteorological Society 36, 99-103 (1955).

18. S. L. Lee and J. M. Hellman, "Heat and Mass Transfer in Fire Research," in Advances in Heat Transfer, Vol. 10 (Academic, New York, NY, 1974), pp. 219-284.

19. B. R. Morton, G. Taylor, and J. S. Turner, "Turbulent Gravitational Convection from Maintained and Instantaneous Sources," Proceedings of the Royal Society A234, 1-23 (1956).

20. H. W. Emmons and S.-J. Ying, "The Fire Whirl," in Eleventh Symposium (International) on Combustion (Combustion Institute, Pittsburgh, PA, 1967), pp. 475-488.

21. S.-J. Ying, "The Fire Whirl," Engineering Sciences Laboratory, Division of

Engineering and Applied Physics, Harvard University, Cambridge, MA (1965).

22. P. Schubert, "Examination of the Building Density and Fuel Loading in the Districts Eimsbüttel and Hammerbrook in the City of Hamburg as of July 1948," Stanford Research Institute, Menlo Park, CA, translation under Project MU-6464 (1969).

Table 1 NOMINAL VALUES FOR PARAMETERS

$B_o(0)$	$8.00 \cdot 10^5$ cm	α_o	$9.30 \cdot 10^{-2}$
b_i	$5.00 \cdot 10^4$ cm	$\Gamma_o(0)$	$3.20 \cdot 10^8$ cm^2/s
c_p	$1.00 \cdot 10^7$ cm^2/s^2-K	ε	$2.60 \cdot 10^{12}$ cm^3/s
E	$9.05 \cdot 10^{18}$ erg/s	γ	1.40
g	$9.80 \cdot 10^2$ cm/s^2	$\rho_a(0)$	$1.16 \cdot 10^{-3}$ g/cm^3
$T_a(0)$	$3.00 \cdot 10^2$ K		

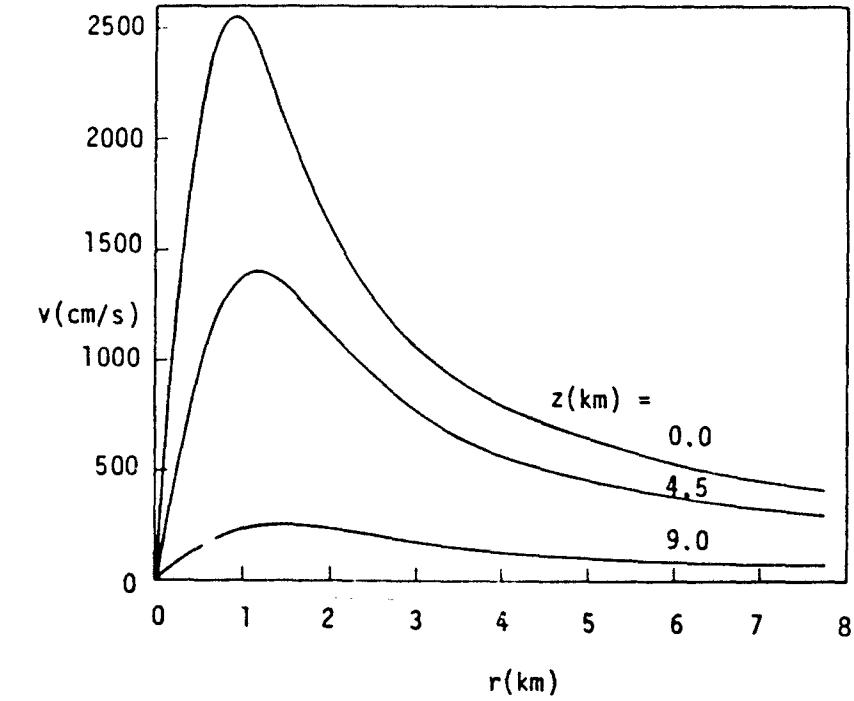

Figure 1 Swirl speed v, at time t=2.5 h at three altitudes z, vs. radial distance from the axis of symmetry r. The peak swirl occurs at r=1.12B, for fixed altitude and time, for the Oseen-type vortex adopted. Parameter values are those of Table 1 except here the volumetric flux of the heat source $\varepsilon = 2.586 \cdot 10^{12}$ cm^3/s.

PROJECT FLAMBEAU EXPERIMENTAL FIRE MEASUREMENTS

Thomas Y. Palmer
SWETL Inc., P.O. 278
Fallbrook, CA 92028

I. INTRODUCTION

The general Project Flambeau and Mass. Fire Systems experiments have been detailed elsewhere (Countryman, 1969, Palmer 1981) and will not be redescribed here. Other large fire experiments include those of Dessens in France and Project Euroka in Australia. The Project Flambeau experiments were the nearest approach to an instrumented experimental investigation of firestorms, mass fires and conflagrations that have been attempted, the other experiments being either to small or of to low an intensity. Fire conditions are important in both a military and civilian context, but in spite of the long relationship between fire and man, few measurements of large free-burning fires have been made. It is only since World War II that any attempts at fire modelling have been made, while computer simulation has only occurred in the last ten years. Progress in this area has been handicaped by a lack of experimental data to verify model results.

II. MODELS OF FIRE

Until recently most large fire models have been based upon the similarity approach to convection first developed by Morton, et al, (1956) for laboratory convective plumes simulating atmospheric convection. This approach has been extended to fires by many investigators (c.f. Byram, 1966, Morton, 1967, Smith et al, 1975), while overall descriptive models have been proposed by Countryman, (1969), Haines, (1982) and in the numerous fire reports of the state and federal fire agencies.

The numerous partial differential equations describing the physico-chemical processes in free combustion in the atmosphere have been summarized by Emmons, (1970). While in principle they offer a complete description of the mass fire-conflagration they require the use of appropriate initial and boundary conditions before any solution can progress. They require the application of very large computers and investigators include Stein, (1974) Luti, (1981) and Brode, 1982). Progress in this area has been limited by experimental verification. Important information relative is implicit in the Project Flambeau measurements if they are analyzed in light of recent theoretical and laboratory measurements.

III. REALITY-PROJECT FLAMBEAU

The first series of Project Flambeau experiments as described by Countryman, (1969) and Palmer, (1969) were heavily oriented towards understanding fuel combustion in the large fire environment. Although general wind and temperature measurements were made during the experiments the primary emphasis was on finding rates of combustion by measuring weight loss from large platforms and relating these measurements to laboratory experiments. Locally intensive airflow measurements, temperature calorimetric and radiation

measurements were made. It is now apparent that there was relatively little difference between these variables during the Project Flambeau experiment except relative to the porosity of the fuel (Palmer, unpublished, ms.). There was some theory due to Byram (personal communication) and outdoor experiments with large pans of fuel which indicated that ignition patterns and fuel arrangments could influence the behavour of large fires. Consequently a second series of experiments using the remaining fuel piles were instrumented for wind and rearranged and ignited in various patterns to study these effects. These experiments culminated in the Plot 6 and Plot 10 fires.

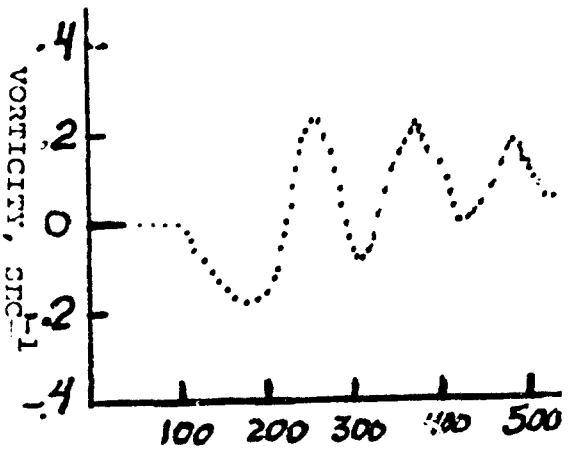

Fig. 2. Vorticity variation inside of Fire 6.

Temperature was not measured in these experiments because of instrumentation and data aquisition systems limitations.

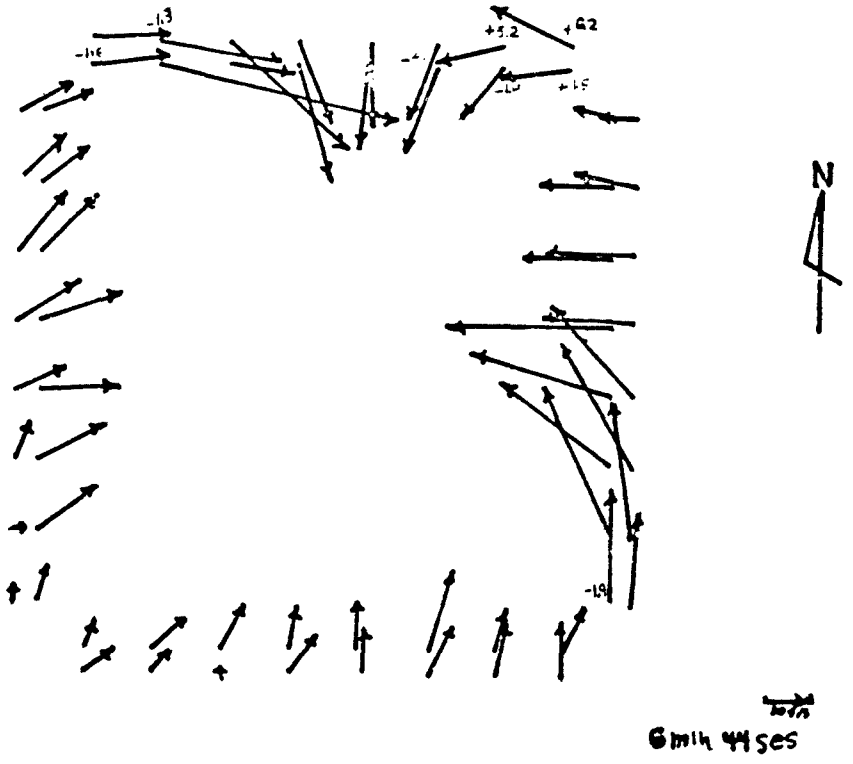

Figure 1. Exterior winds about Project Flambeau Fire 10. The two vortices varied in strength in a regular manner. A lateral gust is beginning on the western margin of the fire.

Time lapse cartoons of the wind field around Fire 10 (an example of one frame is given in Fig 1) clearly shows two centers of rotation. The rotating vortex pair varied in strength in a regular manner similar to the rotating patterns in the interior of Fire 6, as shown if Fig. 2. The period of the oscillating vortices was about fifty seco 's in both fires. An intense firewhirl was noted from an aircraft approximately at the center of the east vortex.

These time lapse plots of the wind fields and vorticity analysis clearly shows the following features of these fires:

A. The fires are clearly three dimensional
B. Large oppositely rotating centers of vorticity (spin) formed inside the fire on the downwind side when wind were weak.
C. Occasional lateral gusts moved into the fire area
D. The vortices, oscillated in strength in a periodic manner
E. There was mass and momentum exchange between the atmosphere and the fire

This combination of observed phenomena indicates that these large stationary fires can be described in the context of turbulent burst-intermittant-turbulence, layer replacement theory.

IV. INTERMITTANT TURBULENCE

The treatment of turbulence as an intermittant phenomena was apparently first formulated by Higbie in 1935, (although the standard reference to his work is erroneous.). The discription of boundary layer replacement and vorticity generation using this formulation has been used in chemical engineering to describe boiling and heat transfer from pipes for many years. The first formulation of the theory as a stochastic process was presented by Bulling and Dukler (1972). Although there is still controversy about how to treat the downward penetration of the free air gusts, there has been an increasing congruence between theoretical fluid mechanical approaches and this empirical engineering approach.

Observations of the Project Flambeau fires presented here and elsewhere (Palmer, 1981) and the observations of horizontal roll vortices in large forest conflagrations by Haines (1982) clearly show for the first time that there are two types of circulations in large fires with sufficiently large energy and a third type in fires of low energy:

A. Large energy fires
   (1) ones which generate vertical vortices as in Fig. 3, (with light winds)
   (2) ones which generate horizontal roll vortices as in Fig. 4, (strong winds)
B. Low energy fires
   (3) fires which produce small or no vortex motions with extensive direct mixing from the fire into the flames.

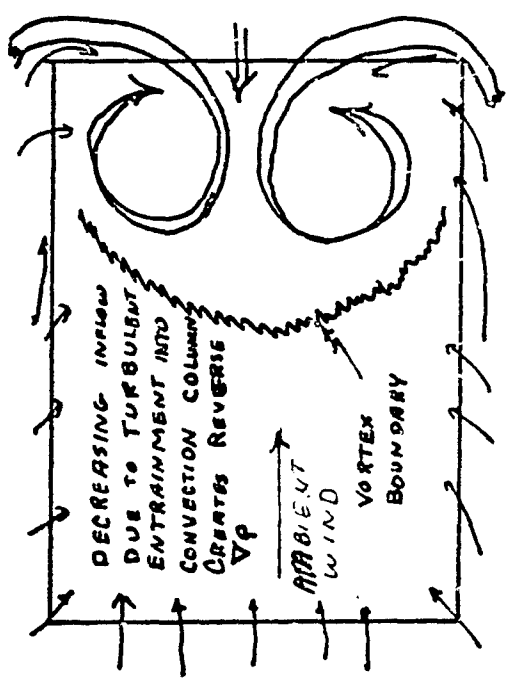

Figure 4. Downward view of vortex pair generated by fire in light winds.

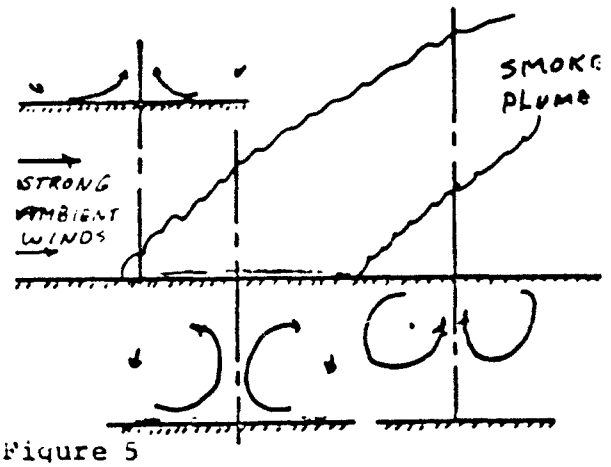

Figure 5

Cross-sections through a counter rotating, stream-wise vortex pair associated with strong winds.

The vortex pairs and the downward penetrating turbulent eddies in flows such as in catagory A-1 are strongly affected by the high-speed fluid in the outer flow field (Blackwelder and Eckelmann, 1979), There is usually a critical Rayleigh number associated with this kind of convection which seperates the differing states.

V. CONCLUSIONS

This preliminary analysis and model formulation of the Project Flambeau fires taken together taken together with other information, seems to indicate that mass fires and conflagrations are three-dimensional and oscillatory in nature. Large area fires seem to naturally fall into a strong fire generated vortices. The vortices oscillated with a period of about 50 seconds in these fires.

VI. REFERENCES.

Blackwelder and Eckelmann, 1979: Streamwise vortices associated with the bursting phenomena, Jour. Fluid Mech, 94 p577-94.

Brode, H.L, Larson, D.A. and Small, R. D., 1982: Time dependent model of flows generated by large area fires., Pac Sierra Res Corp, Note 483, Los Angeles CA

Bullin, J.S. and Dukler, A.E., 1972: Random eddy models for surface renewal: formulation as a stochastic process. Chem Eng Science, 27, pp 439=442.

Countryman, C.M. 1969: Project Flambeau, an investigation of mass fire (1964-1969) Final Rpt Vol I, Pac Sw Forest and Range Exp Stn, Berkeley, CA, 68p.

Emmons, H.W., 1970: Fluid mech- and combustion, 13th Symp (Intl) on combustion, The Combustion Inst., Philadelphia, PA

Haines, D. A., 1982: Horizontal roll vortices and crown fires, Jour App Meteo, 21 p 751-763.

Luti, F. M., 1981: Some characteristics of a two-dimensional starting mass fire with cross-flow. Comb. and Flame, 26 p25-33.

Morton, B. R. 1967: On the dynamics of fire plume convection. Proc. Mass Fire Res. Symp. Washington, DASIAC Special Report 59

Morton, B. R., Taylor, G. I. and Turner, J. S., 1956: Turbulent gravitational convection from maintained and instantaneous sources Proc. R. Soc A p 1-23.

Palmer, T.Y., 1981: Large fire winds gases and smoke. Atmos Env 15, p 2079-2090.

Smith. B.K.,Morton, B.R. and Leslie, L.M., 1975: The role of dynamic pressure in generating fire wind. J. Fluid Mech p 1-19.

Stein,A.M., Sullivan, J.G. and Murray, F. W., 1974: Physical models of fires and their associated environment AIAA Paper 74-8, 4pg., New York.

Thomas, L. C., 1978: A formulation for α_M and α_h based on the surface renewal principle, A I Ch E Jour. 24, p 101-105.

Turner, J. S. 1973: Buoyancy Effects in Fluids, Cambridge Press, Cam. Univ. Press, 367 p.

ANALYSIS OF THE LARGE URBAN FIRE ENVIRONMENT

R. D. Small and D. A. Larson

Pacific-Sierra Research Corporation
12340 Santa Monica Boulevard
Los Angeles, California 90025

ABSTRACT

An analysis describing the high temperature and velocity environment of a large urban area fire is presented. The boundary value problem treats the burning region in detail. A novel prescription of the boundary conditions at the fire periphery allows the burning-region analysis to be uncoupled from analyses of the free-convection column and the far field. The relationship between burning rate, buoyancy, pressure gradients, and the creation of high velocity fire winds is described. Sample results simulate the burning-region environemnt for the 1943 Hamburg firestorm.

INTRODUCTION

The high-velocity inflow generated by an area fire and the characteristics of the initial free-convection flow are determined by the burning-region interactions. Formulation of an appropriate equation set to describe the flow physics depends on the scale of the heat addition and the size of the burning region. As opposed to weakly heated flows controlled by the diffusion of momentum and energy, the volume heat addition implies a strong coupling of buoyancy forces and inertia.

The size of the burning region governs the ordering of terms in the conservation equations. For a heat addition volume defined by a mean flame height H and a fuel bed radius R, conservation of mass implies

$$\frac{u}{v} \sim \frac{R}{H} \quad .$$

If $R/H \sim O(1)$, the radial (u) and axial (v) velocities and the corresponding acceleration terms are of similar order. For $R >> H$, the characteristic radial velocity is much greater than the mean axial velocity and the governing momentum equations may be simplified.

This paper considers the class of flows generated by an asymptotically large fire ($R >> H$). An analytical model for the axisymmetric, quasi-steady flow in and around the burning region is developed (1), and sample results are presented.

EQUATIONS

For the large fires considered, the turbulent motion is expected to limit the flame heights (2) such that a more or less uniform heating-zone height H may be defined. A spatially-dependent volume heat function $Q \times q(r, y)$ is used to model the combustion processes in that (finite) region. Q represents the mean rate of heat release and $q(r, y)$ is an $O(1)$ variable describing its spatial distribution. Since $O(1)$ changes in temperature and density are expected, all density derivatives are retained.

The conservative equations are scaled using ambient (ground-level) thermodynamic values (P_a, ρ_a, T_a) and the characteristic burning-region lengths, H and R. The asymptotically-large burning region is thus represented by an order-one domain with comparable radial (r/R) and axial (y/H) dimensions. The disparate scaling lengths introduce a small parameter,

$$\varepsilon = \frac{H}{R} \quad , \qquad \varepsilon << 1 \quad , \tag{2}$$

which can be used to order terms. The burning-region aspect ratio is ε^{-1}.

Radial velocities are scaled with an arbitrary velocity U and, in order to preserve the two-dimensional structure of the continuity equation, axial velocities are scaled by εU. Since a subsonic flow is expected, the thermodynamic pressure $\hat{P}$ is defined as

$$\frac{\hat{P}}{P_a} = 1 + \delta P \quad , \quad \delta = \frac{U^2}{P_a/\rho_a} \quad , \tag{3}$$

where P represents a perturbation pressure. In scaled variables, the leading-order set of conservation and state equations (3) is

$$\frac{\partial}{\partial r}(r\rho u) + \frac{\partial}{\partial y}(r\rho v) = 0 \quad , \tag{4a}$$

$$\rho\left(u\frac{\partial u}{\partial r} + v\frac{\partial u}{\partial y}\right) = -\frac{\partial P}{\partial r} + M_1\left(\frac{1}{r}\frac{\partial}{\partial r}\left(r\frac{\partial u}{\partial r}\right) - \frac{u}{r^2}\right) + M_2\frac{\partial^2 u}{\partial y^2} \quad , \tag{4b}$$

$$\frac{\partial P}{\partial y} + A\rho = 0 \quad , \tag{4c}$$

$$\rho\left(u\frac{\partial T}{\partial r} + v\frac{\partial T}{\partial y}\right) = B\left(q(r, y) - \sigma(T^4 - 1)\right) + K_1\left(\frac{1}{r}\frac{\partial}{\partial r}\left(r\frac{\partial T}{\partial r}\right)\right) + K_2\frac{\partial^2 T}{\partial y^2} \quad , \tag{4d}$$

$$\rho T = 1 \quad , \tag{4e}$$

where

$$A = \frac{gH}{U^2} \quad , \quad B = \frac{\gamma - 1}{\gamma}\left(\frac{QR}{P_a U}\right) \quad ,$$

$$M_i = \frac{\varepsilon^{3-2i}\mathcal{L}_i}{\rho_a UH} \quad , \quad K_i = \frac{\varepsilon^{3-2i}k_i}{\rho_a c_p UH} \quad ,$$

$$\sigma = 4\pi\hat{\sigma}k^* \frac{T_a^4}{Q} = 4\pi\hat{\sigma}T_a^4\left(\frac{k^*H}{QH}\right) \quad . \tag{5}$$

$\mathcal{E}_i$ and k_i are dimensional mixing coefficients, the specific heat capacity c_p is assumed constant, $\hat{\sigma}$ is Stefan's constant, and k^* is the reciprocal of the radiation mean free path (assumed constant). In this formulation, eddy viscosities are used to model the turbulent transport of momentum and energy, and the graybody approximation (4) is used to specify the radiative cooling of the hot gas/smoke mixture.

An appropriate value for the radial velocity scale U is found by balancing the terms for convective transport and heat addition in the energy equation so as to properly represent the physics of a flow driven by combustive heating. Accordingly, setting B = 1,

$$U = \frac{\gamma - 1}{\gamma}\left(\frac{QR}{P_a}\right) \equiv \frac{\gamma - 1}{\gamma}\left(\frac{QH}{P_a \varepsilon}\right) . \tag{6}$$

BOUNDARY CONDITIONS

The type of boundary value problem to be solved depends on the relative magnitudes of the coefficients M_i and K_i, i = 1, 2. Measurements defining the magnitudes of relative values of the turbulent exchange coefficients have not been performed. However, observations of experimental burns simulating large area fires (5, 6) indicate that the flow is highly turbulent and that the convection column thickness is comparable to the fuel bed radius.

Above several flame heights, the flow asymptotes to the weakly buoyant flow characteristic of the convection column, implying that M_2, $K_2 \ll M_1$, K_1. Radial shear should also characterize the flow near the center of the fire. Except in a thin sublayer near the ground, the radial diffusion of momentum and energy should dominate the axial diffusion. Accordingly, we assume M_2, $K_2 = 0$ and consider solution of the nearly parabolic boundary value problem prescribed by Eqs. (4) and the following boundary conditions.

At the symmetry axis and at the ground, the boundary conditions are

$$u = \frac{\partial T}{\partial r} = 0 \qquad \text{on } r = 0 \ , \tag{7a}$$

$$v = 0 \qquad \text{on } y = 0 \ . \tag{7b}$$

The asymptotic conditions to be used above many flame heights should reflect the restructuring of a high-velocity, high-temperature, radial flow to a slower-moving, weakly buoyant, nearly vertical flow characteristic of the free-convection column. Based on a formal matching of asymptotic expansions (3) (in the limit $\varepsilon \to 0$) for the separate strongly-buoyant and convection column flows, it is found that the necessary condition is

$$P + Ay \to 0 \quad \text{as} \quad y \to \infty \ , \quad r \leq 1 \ . \tag{7c}$$

It can be shown that Eq. (7c) also implies $u \to 0$, $T \to 1$ as $y \to \infty$.

At the fire/column periphery ($r \approx 1$), large gradients in temperature, pressure (7), and the level of turbulence are expected. Jump conditions at $r = 1$ are used to analyze this local behavior. Writing Eqs. (4) in conservation form and integrating from $r = 1^-$ to $r = 1^+$ yields the following jumps

in mass, momentum, and energy at the periphery:

$$[\rho u] = 0 \quad ,$$

$$[\rho u^2] = [P] + \left[M_1 \frac{\partial u}{\partial r}\right] \quad ,$$

$$[\rho u T] = \left[K_1 \frac{\partial T}{\partial r}\right] \quad ,$$

where $[W] = W^+ - W^-$. Since the leading-order ambient density and temperature are $\rho^+ = T^+ = 1$, integration of Eq. (4c) yields $P^+ = - Ay$ on $r = 1^+$. Expanding the jump conditions, using the leading-order thermodynamic properties and assuming M_1^+, $K_1^+ << M_1^-$, K_1^-, the boundary conditions applicable at $r = 1$ are:

$$\frac{\partial u}{\partial r} = \frac{1}{M_1} \{P + Ay + \rho u^2(1 - \rho)\} \quad ,$$

$$\frac{\partial T}{\partial r} = \frac{1}{K_1} u(1 - \rho) \quad . \tag{7d}$$

The boundary value problem defined By Eqs. (4) (with M_2, $K_2 = 0$) and Eqs. (7) is independent of both the far-field and the free-convection-column flows. Such an uncoupling implies that the mechanics of the source region is controlled principally by the heat release and the resulting pressure gradients produced by the strong buoyancy.

RESULTS

For the special case of weak heating (q small), relatively small temperature changes and velocities are expected, and a leading-order description of those perturbations is provided by a linearization of Eqs. (4) and (7) about the ambient, no-flow state (1). The resulting, simplified equations are decoupled and may be solved in succession for the perturbation temperature (T_1), density (ρ_1), pressure (P_1), radial velocity (u_1) and vertical velocity (v_1) (1). This solution provides a concise description of the basic interchanges of energy and momentum in and around the burning zone as well as illustrating the structure of the solution.

For example, with $\nu << 1$, $q(r, y) = \nu$ in the burning zone and $q(r, y) = 0$ elsewhere, solution of the simplified energy equation (see Ref. (1)) yields a temperature increase

$$T_1 = \nu/4\sigma \quad . \tag{8a}$$

Sequential solution of the linearized state, momentum, and continuity equations yields

$$\rho_1 = - T_1 = - \nu/4\sigma \quad , \tag{8b}$$

$$P_1 = - A(1 - y)/4\sigma \quad , \tag{8c}$$

$$u_1 = - \nu P_1 r/M_1 = - \nu A(1 - y)r/4\sigma M_1 \quad , \tag{8d}$$

$$v_1 = \nu A(y - y^2/2)/2\sigma M_1 \quad . \tag{8e}$$

Solving each equation in turn suggests the following physical interpretation. The heat release increases the temperature (T_1) and thus the buoyancy (decrease in density). The buoyancy produces a pressure gradient (Eq. (8c)) which induces the fire-wind inflow u_1. Finally, the inflow is kinematically turned upward (v_1) to form the initial part of the convection column.

In general, Eqs. (4) and (7) are solved (1) by a numerical procedure that involves repeated iteration to find a pressure distribution consistent with the asymptotic condition Eq. (7c). Figures 1-5 show typical results obtained for the 1943 Hamburg firestorm (8). For that case, the fire dimensions and heat release were (approximately) R = 1500 m, H = 60 m, and QH = 57 kcal/m^2-sec (8, 9). The radiation mean free path was taken as 20 m and M_1, K_1 as 2.0. For those values, the velocity scale U is 16.8 m/sec, A and σ are 2.08 and 0.066, respectively.

The temperature rise and subsequent pressure drop in and around the fire due to the combustion heating are shown in Figs. 1 and 2. The changes are maximal in the center of the fire, where the high-speed radial inflow stagnates, but decay rapidly with increasing height. Above several flame heights, a state of weak buoyancy is attained. The induced radial inflow and the resulting vertical upflow are shown in Figs. 3 and 4. The turning of the strong inflow in the source region to form a low velocity, free-convection column is shown in Fig. 5.

DISCUSSION

The model developed here describes the velocity and thermodynamic fields generated by a large urban fire. The analysis focuses on the turning region, which includes the burning zone and the region below the established free-convection column. Such an approach allows estimates to be made of the conditions necessary for shelter design and of the environment facing survivors and rescue workers.

A finite-volume heat source is used to model the combustion processes, and large changes in temperature and density are allowed. A one-parameter eddy-viscosity model is used to describe the turbulent stresses, and a gray-body approximation employed to model radiative losses. Jump conditions are derived to describe rapid changes in physical quantities at the fire periphery. Those conditions effect model problem closure, allowing the induced fire winds to be computed directly, without extensive far-field calculations.

Sample results illustrate the generation of high-speed fire winds by the heat release and buoyancy production, and simulate the velocity and thermodynamic fields created in the Hamburg firestorm. Extensions of the theoretical treatment could include predictions of specie concentrations (1) as well as the extent beyond the fire region of the high-velocity radial inflow.

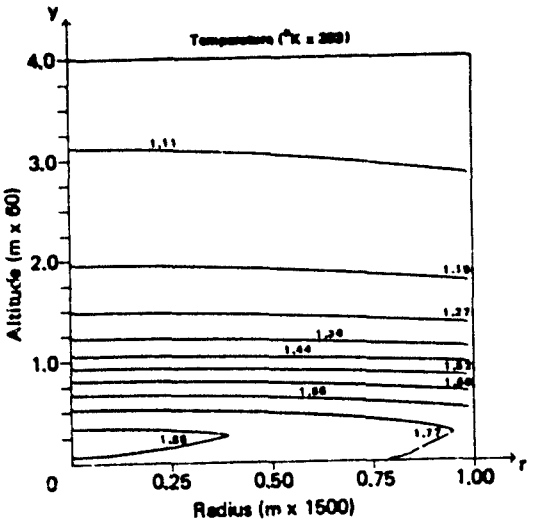

Fig. 1. Temperature contours Hamburg firestorm.

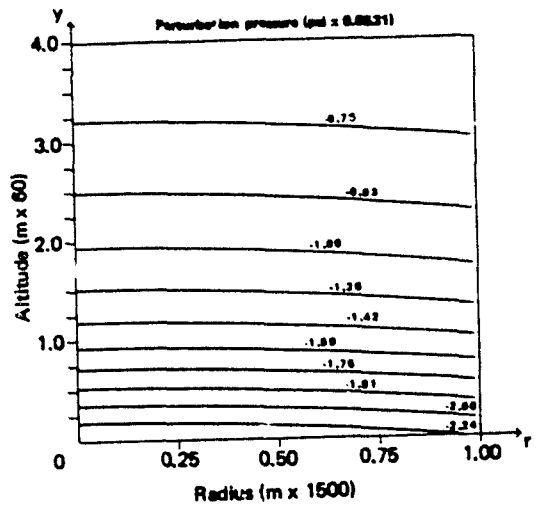

Fig. 2. Pressure contours, Hamburg firestorm.

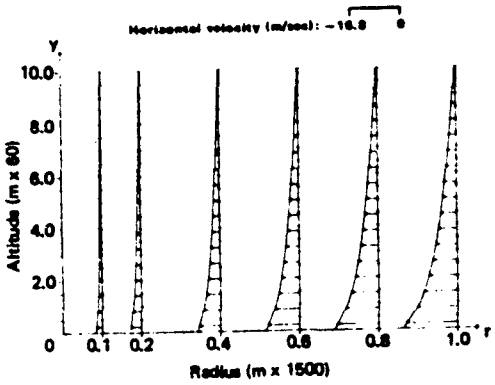

Fig. 3. Radial velocity profiles, Hamburg firestorm.

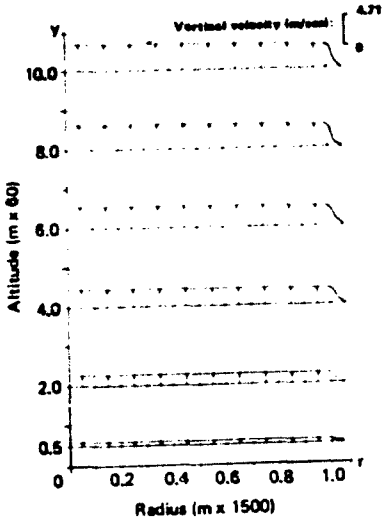

Fig. 4. Vertical velocity profiles, Hamburg firestorm.

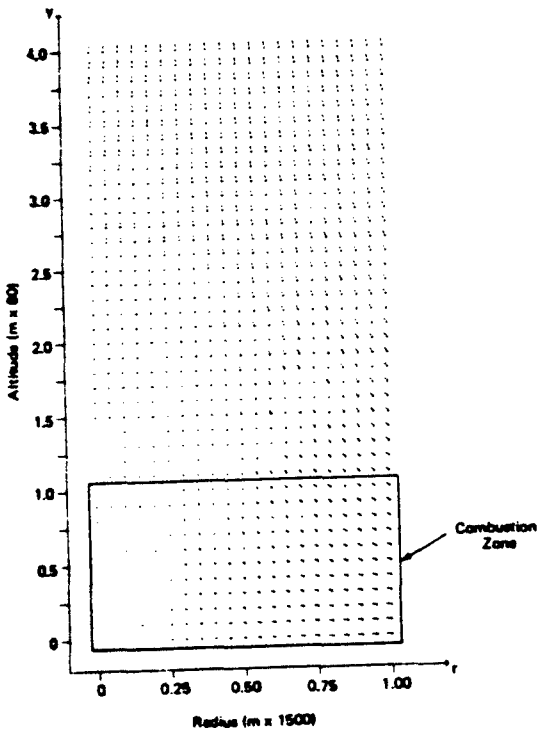

Fig. 5. Velocity field, Hamburg firestorm.

ACKNOWLEDGEMENT

This research was sponsored by the Federal Emergency Management Agency, Office of National Preparedness, monitored by Dr. David Bensen and the Defense Nuclear Agency, Dr. Michael J. Frankel, Project Monitor.

REFERENCES

1. D. A. Larson and R. D. Small, Analysis of the Large Urban Fire Environment, Part I: Theory, Pacific-Sierra Research Corporation, Los Angeles, California, PSR Report 1210 (July 1982).

2. P. H. Thomas, "The Size of Flames from Natural Fires," Ninth Symposium (International) on Combustion, The Combustion Institute, pp. 844-859 (1963).

3. R. D. Small, D. A. Larson and H. L. Brode, Analysis of Large Urban Fires, Pacific-Sierra Research Corporation, Los Angeles, California, PSR Report 1122 (September 1981).

4. M. P. Murgai and H. W. Emmons, "Natural Convection Above Fires," Journal of Fluid Mechanics, Vol. 8, pp. 611-624 (1960).

5. H. J. Nielsen, Mass Fire Data Analysis, ITT Research Institute, Chicago, Illinois, DASA Report 2018 (January 1970).

6. C. M. Countryman, PROJECT FLAMBEAU...An Investigation of Mass Fire (1964-1967), U.S. Forest Service, Berkeley, California, Vol. 1 (1969).

7. R. K. Smith, B. R. Morton and L. M. Leslie, "The Role of Dynamic Pressure in Generating Fire Wind," Journal of Fluid Mechanics, Vol. 68, pp. 1-19 (1975).

8. M. Middlebrook, The Battle of Hamburg, Scribner, New York (1981).

9. T. E. Lommasson, R. K. Miller, R. G. Kirkpatrick and J. A. Keller, A "Firestorm" Existence and Buildup Hypothesis, The Dikewood Corporation, Albuquerque, New Mexico, DC-FR-1058.0 (also DASA 2174) (September 1968).

THE LARGE URBAN FIRE ENVIRONMENT: TRENDS AND MODEL CITY PREDICTIONS

D. A. Larson and R. D. Small

Pacific-Sierra Research Corporation
12340 Santa Monica Boulevard
Los Angeles, California 90025

ABSTRACT

The urban fire environment that would result from a megaton-yield nuclear weapon burst is considered. The dependence of temperatures and velocities on fire size, burning intensity, turbulence, and radiation is explored, and specific calculations for three model urban areas are presented. In all cases, high velocity fire winds are predicted. The model-city results show the influence of building density and urban sprawl on the fire environment. Additional calculations consider large-area fires with the burning intensity reduced in a blast-damaged urban center.

INTRODUCTION

Large urban fires have resulted from natural disasters, explosions, and wartime actions. In many cases, entire urban areas were totally destroyed despite firefighters' efforts to contain the flames. The World War II fire-bombing raids on European and Japanese population centers caused immense damage and hundreds of thousands of casualties. Several ignited firestorms, with hurricane-force winds, high street-level temperatures, high concentrations of carbon monoxide, and complete burning of all combustible materials within the fire boundaries. Firestorms also produced a high number of casualties, seldom ameliorated even by concerted rescue efforts.

Large urban fires are a much greater threat in the age of nuclear weapons then ever before. Hundreds of square kilometers of an urban (or wildland) area can be ignited simultaneously by a single-megaton nuclear weapon. Indeed, superfires of unprecedented size could dwarf the tremendous fires of World War II.

This paper presents predictions of the temperatures, pressures, and high-speed winds created by large urban fires (1). The dependence of those quantities on fire size, burning rate, and various other parameters is explored, and fires in model U.S. cities are examined. Simulations in which fires are extinguished in the center by blast are compared with those in which the fires continue to burn. The analysis used (2) may also be extended to obtain estimates of oxygen depletion and noxious gas buildup.

MODEL

The predictive model employed (2) focuses on the strongly buoyant flow generated in and around a large area fire. A finite-volume heat source is used to approximate the net effect of the combustion kinetics. A one-parameter eddy-viscosity model describes the turbulent stresses, and a graybody approximation is employed to model hot gas and smoke radiation. Jump conditions describe the rapid changes in physical quantities at the fire periphery. Those conditions allow the induced fire winds to be calculated directly without extensive far-field computations.

The model depends parametrically on the radius R and height H of the fire, the scale Q and spatial distribution q(r, y) of the heat addition rate, the radiation mean-free path $1/k^*$, and the eddy coefficients of momentum and heat transfer $\bar{\xi}_1$, $\bar{k}_1$. A range of parameter values are used in the calculations.

SOLUTION DEPENDENCE ON FIRE SIZE, HEAT RELEASE, TURBULENCE, AND RADIATION

As a baseline case, a megaton-yield burst is assumed and the fire characterized by the following parameters (1, 3):

$$R = 10 \text{ km} \quad , \quad H = 100 \text{ m} \quad , \quad QH = 57 \text{ kcal/m}^2\text{-sec}$$

$$q(r, y) = \begin{cases} 1.6 & \text{for } y \leq 25 \text{ m} \\ 1.6\left(\dfrac{100 - y}{75}\right) & \text{for } 25 \text{ m} \leq y \leq 100 \text{ m} \\ 0 & \text{for } y \geq 100 \text{ m} \end{cases} \quad , \qquad (1)$$

$$k^{*-1} = 20 \text{ m} \quad , \quad M_1 = K_1 = 0.2 \quad ,$$

M_1 and K_1 are the dimensionless eddy coefficients defined by

$$M_1 = \bar{\xi}_1/UR \quad , \quad K_1 = \bar{k}_1/UR \quad , \quad U = (\gamma - 1)QR/\gamma P_a \qquad (2)$$

with γ the ratio of specific heats and P_a the ground-level ambient pressure. The above values are representative of the model cities considered in the next section.

The near-fire velocity and temperature fields predicted for the baseline case are shown in Figs. 1 and 2. These plots are typical of the results obtained for the model cities. In all cases, the induced inflow is strongly turned upward across the width of the burning region, and the high temperatures in the fire region decay rapidly with altitude.

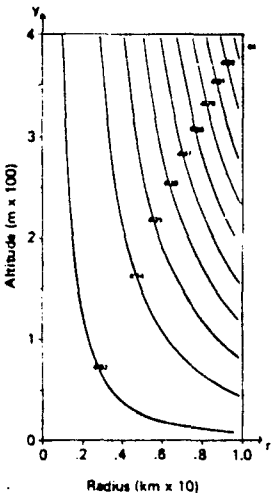

Fig. 1. Flow field strcamlines, baseline fire.

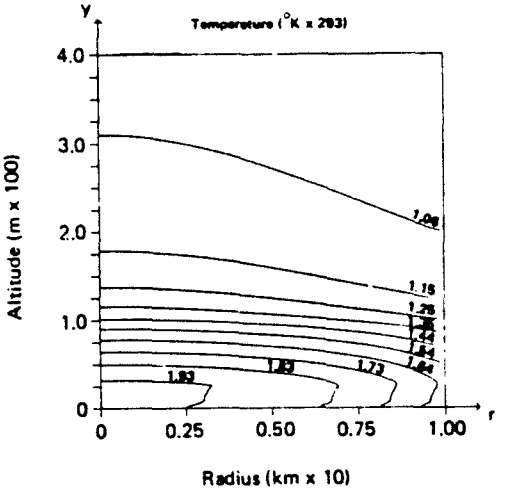

Fig. 2. Temperature contours, baseline fire.

The dependence of the fire-wind velocity and temperature with fire size, heat release, turbulence, and radiation is summarized in Figs. 3 and 4, and Table 1. The maximum induced velocity u_{max} and the maximum temperature T_{max} both increase with either radius (fire size) or intensity (fuel loading). The increases are nearly linear for relatively small radii and heating rates, but tail off markedly at larger radii and higher intensities.

Table 1 describes the basic dependence of fire winds and temperatures on the remaining factors: fire height, spatial distribution of the heat release, turbulence, and radiation. As expected, temperatures and velocities are increased when the radiation is reduced ($1/k^*$ increased (2)), and velocities are decreased when the turbulent stresses (i.e., M_1) are increased. The fire-wind environment is relatively insensitive to changes in the turbulent heat transfer (K_1), implying that the burning-region energy balance is principally controlled by the combustive heat release, convection and radiation. When the fire height H (QH fixed) is increased, temperatures drop. Correspondingly lower velocities do not occur, however, since a smaller fraction of the heat release QH is radiated away at the lower temperatures and higher kinetic energies are supported. This basic dependence on the fire-wind environment on fire height suggests that hydrocode simulations of the environment should employ a volume heat source instead of a prescribed heat influx at the ground surface.

Several variations in heat release distribution have been considered (1). As expected, relatively high frequency perturbations have little effect on the fire-wind environment. At lower frequencies, forced oscillations in the temperature field develop but the velocity field is still relatively unaffected. The gross features of fire-wind flows (e.g., velocity and temperature maxima) are thus primarily dependent on the total heat-release rates and not details of the fuel bed. The data base required to make predictions for specific cities may thus be minimized.

An additional excursion compares the results for the fully-circular (10 km radius) baseline fire with those for a similar but annular fire of inner radius 5 km. The results are quite similar. The annular-fire winds also blow in toward the symmetry axis and upward at all points. This suggests that the environment generated by nuclear-weapon-ignited urban fires may be relatively insensitive to changes in the geometry and loading of the central, blast-damaged region. In addition, as sketched in Fig. 5, a cluster of separated large fires, such as could result from multiple nuclear bursts over a large city, might coalesce and engulf much of the intervening region.

MODEL CITY PREDICTIONS

Predictions of the large-fire environment are made for three model U.S. cities, which we refer to as W, M, and E. City W is lightly built-up, and intended to represent new, sprawling cities. City E is heavily built-up, and intended to represent old, congested cities. City M is of intermediate building density. For each city, two cases are considered: a baseline fire and one modified by blast. In all cases, the fire radius is taken to 12 km (corresponding to a 1 Mt burst (3)).

Few metropolitan areas are axisymmetric. Nevertheless, most cities have a main business district with high-rise office and apartment buildings,

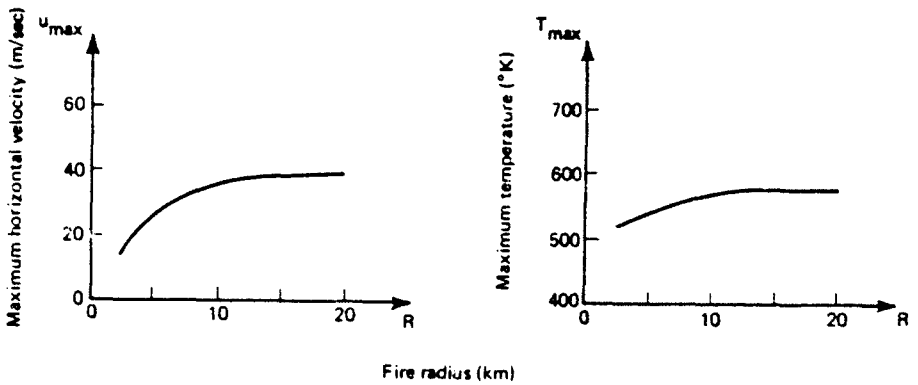

Fig. 3. Dependence of maximum radial velocity and temperature on fire radius.

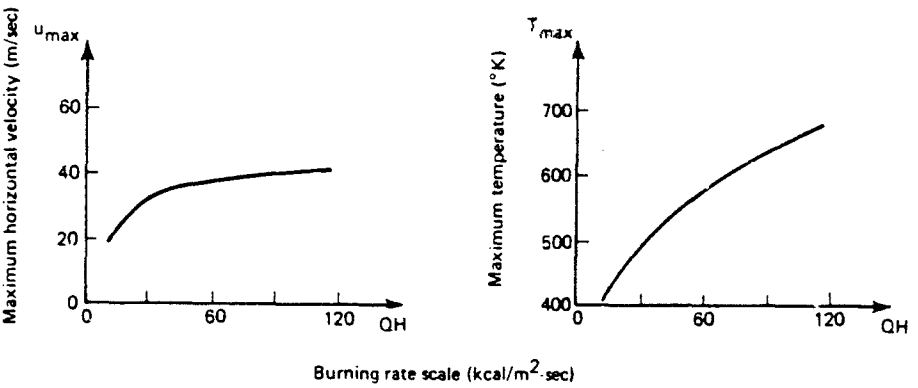

Fig. 4. Dependence of maximum radial velocity and temperature on burning rate scale.

Table 1--Dependence of temperature and radial velocity on other parameters

Parameter	Variation	Resulting Change in T--Temperature	Resulting Change in U--Radial Velocity
H--Fire Height	Increase	Decrease	Increase
q(r, y)--Heat Release Distribution	Radial Oscillations of Various Types	Oscillations	None
M_1--Eddy Coefficient: Momentum	Increase	None	Decrease
K_1--Eddy Coefficient: Heat	Increase	None	None
k^{*-1}--Radiation Mean Free Path	Increase	Increase	Increase

surrounded by lower density tracts. Each model city considered has three regions: a tall central city; a residential/industrial belt of intermediate height around the central city; and a low, primarily residential outer belt.

The basic dimensions and heat release characteristics of the model cities are defined (1) in Figs. 6-8. In each figure, the shaded area represents the assumed fuel zone (one building story ~ 3 m) and the hatched area represents the resulting combustion zone (2.4 to 5.0 times the fuel-bed height). For each baseline region, the areal heating rates are computed from assumed average values for the building land to total land ratio (0.15 to 0.40), the number of building stories, the fuel loading per story (16 to 20 lb/ft^2), and the overall burn rate for combustibles (90% of the weight in 3 hrs).

For the blast-modified cases, the weapon burst is assumed to occur over the city center, leveling many buildings in the central city and inner belt. The height of each fuel zone is thus assumed constant and equal to its baseline outer-belt value. The total height of the combustion zone is chosen similarly. The areal heating rate is not however independent of radius. The combustibles of the central city and inner belt would be spread radially by

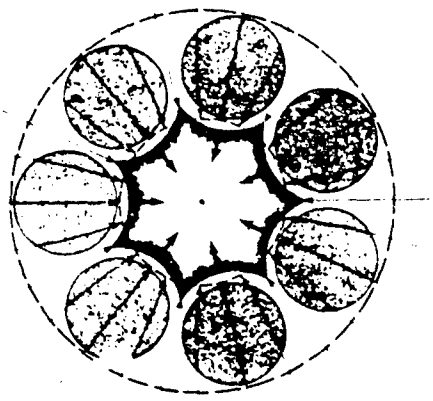

Fig. 5. Radial airflow and fire spread patterns suggested for annular cluster of large area fires.

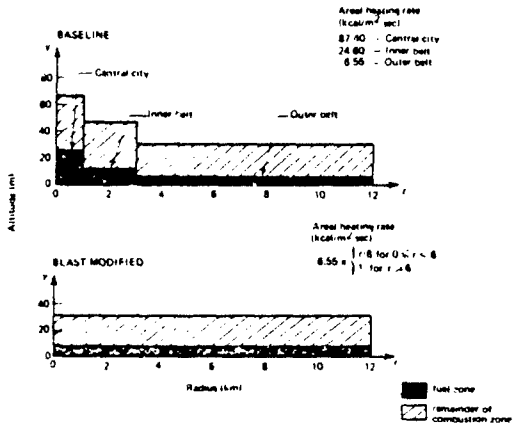

Fig. 6. Fire schematic for baseline and blast modified city W.

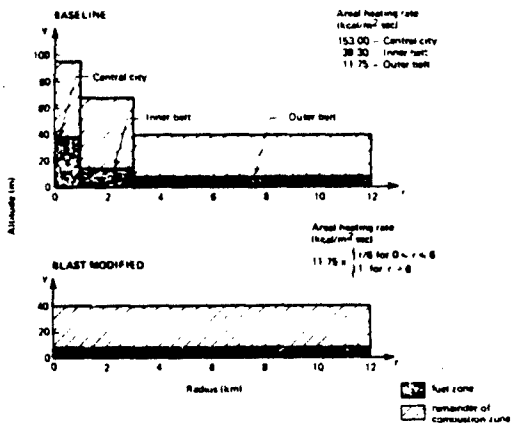

Fig. 7. Fire schematic for baseline and blast modified city M.

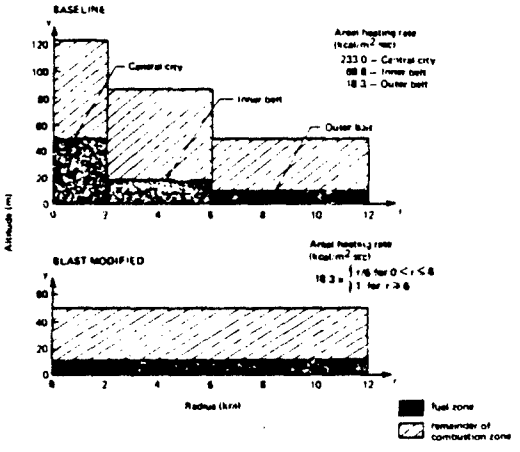

Fig. 8. Fire schematic for baseline and blast modified city E.

the blast, and piled up in a debris field. Since some combustibles in that zone may be buried under layers of nonflammable materials (e.g., concrete, brick, metal), the areal heating rate is not expected to be correspondingly higher and may in fact be relatively small. We thus assume that the heating rate is zero at the city center, increases linearly with radius over a debris zone extending out 6 km from the center (3), and equals its baseline outer-belt value for radii greater than 6 km.

The resulting model city predictions are summarized in Table 2. As expected, the baseline predictions are uniformly larger than the blast-modified ones. The differences are significant for the temperature, pressure and vertical velocity, but small for the radial velocity. The winds and wind damage resulting from nuclear-weapon-ignited fires may be relatively insensitive to the blast disruption of the fuel bed.

The predictions in Table 2 indicate that the winds generated by a large urban fire will in themselves constitute a major threat. Although most of the velocities in the table are less than hurricane force (more than 30 m/sec), it should be noted that those values represent *means*. Near street level, where fire winds will be channeled between buildings, hurricane force winds may be typical. The winds may be even greater than those encountered in the 1943 Hamburg firestorm (2).

The velocity, temperature, and pressure predictions in Table 2 are all greatest for city E (the tallest and densest) and least for city W (the shortest and sparsest). For a given fire, therefore, the threat will be most severe for the most congested cities. In general, however, the shorter cities sprawl out over greater areas than do taller ones of comparable population, and are thus capable of supporting more widespread fires. Multiple weapon bursts can greatly increase the fire severity in such cities.

Table 2--Velocity, temperature, and perturbation pressure maxima in model city simulations

	City			City		
	W	M	E	W	M	E
	Radial Velocity (m/sec)			*Vertical Velocity (m/sec)*		
Baseline	20.2	26.3	39.0	0.89	3.12	12.48
Blast-Modified	17.9	23.9	28.5	0.37	1.56	4.32
	Temperature (°K)			*Perturbation Pressure (psi)*		
Baseline	577	619	704	0.056	0.113	0.271
Blast-Modified	455	485	510	0.011	0.044	0.076

DISCUSSION

The results presented here provide basic predictions of the fire-wind velocities and temperatures that would occur in and around large urban fires caused by megaton-yield nuclear weapon bursts. The dependence of winds and temperatures on fire size, heat release, and other parameters is described,

and model-city simulations are summarized. The results should be applicable to fire damage evaluations, rescue planning, and definition of shelter requirements.

In general, hurricane-force winds are predicted. Velocities increase with fire width and the magnitude of the heat-release rate, but are rather insensitive to spatial variations in that rate. Predicted flow fields are all qualitatively the same, with the fire winds directed (radially) inward and upward everywhere. Such winds are expected to spread the flames into central, blast-extinguished regions, and to foster fire spread between clusters of fires caused by multiple weapon bursts.

In the model-city simulations, a range of fuel distributions and heat-release rates were developed to explore the effects of varying city construction and fuel loading. Those distributions and rates were sectionally uniform, but could easily be replaced in further simulations by more refined quantities based on surveys of actual cities. The most severe fires should occur in the higher density cities, though even low density regions can support hurricane-force winds if they are large enough. Application of these results to definition of shelter hardness (thermal) would imply different criteria for the different types of cities.

ACKNOWLEDGEMENT

This research was sponsored by the Federal Emergency Management Agency, Office of National Preparedness, monitored by Dr. David Bensen and the Defense Nuclear Agency, Dr. Michael J. Frankel, Project Monitor.

REFERENCES

1. D. A. Larson and R. D. Small, Analysis of the Large Urban Fire Environment, Part II: Parametric Analysis and Model City Simulations, Pacific-Sierra Research Corporation, Los Angeles, California, PSR Report 1210 (1982).

2. D. A. Larson and R. D. Small, Analysis of the Large Urban Fire Environment, Part I: Theory, Pacific-Sierra Research Corporation, Los Angeles, California, PSR Report 1210 (1982).

3. L. E. Johnson and D. A. Larson, Neglected Effects in Nuclear Warfare Simulation, Pacific-Sierra Research Corporation, Los Angeles, California, PSR Note 438 (May 1982).

SESSION III

PLENARY SESSION

THE STRATEGIC THREAT

Robert B. Barker
Assistant Associate Director, Arms Control
Lawrence Livermore National Laboratory

The Soviet Union is today recognized as having a strategic nuclear weapon capability either equivalent to, or by some, as superior to that of the United States. The Soviets have spent two decades of unprecedented military buildup to ensure that they are not and will not in the future be perceived as militarily inferior to the United States. One must look with awe at their routine modernization of intercontinental ballistic missiles, their Typhoon ballistic missile submarine, their ALFA attack submarine - the world's most technologically advanced submarine, and their newest Blackjack bomber. All these systems were designed, developed, and deployed as the United States proposed, debated, and delayed comparable systems.

Whether one believes there is relative parity between the United States and the Soviet Union or whether one believes in Soviet superiority, one must address the "why" of Soviet accomplishments. Is the Soviet objective a balance of nuclear terror - acceptance of Mutual Assured Destruction, the so-called MAD doctrine? Or, is their objective the attainment of a nuclear first strike capability against the United States - the ability to destroy U.S. nuclear delivery systems so effectively that the Soviet Union can escape damage in return?

It is surprising how difficult it is to find objective evaluations of Soviet national security accomplishments with the specific purpose of assessing whether in toto their aim is "deterrence" or "first strike". Let us then try to establish the basic criteria for each objective and compare the characteristics of the Soviet national security posture against them. Ultimately, national "intent" determines whether deterrence or first strike is the objective. But in the absence of such knowledge of Soviet national intent, as is the very real current case, prudence must cause us to assume that the intended use of a military capability is what it appears to be designed to accomplish.

Deterrent nuclear forces require survivability and destructive capability. The overall objective is to convince the adversary that he can achieve no net gain by launching a nuclear strike, in fact that his very existence as a nation will cease as a result of a retaliatory strike. Survivability requires that sufficient weapons survive an initial nuclear strike. Historically, in the United States, survivability has been achieved through diversification of the strategic nuclear force into the Triad of land-based missiles, sea-based missiles, and aircraft delivered weapons. Each of the three "legs" of the Triad has achieved survivability by different techniques. The land-based missiles have achieved survival through "hardness", through concrete and steel silos strong enough to protect the missile from nearby nuclear explosions. The sea-based missiles achieve survival through the invisibility of the ballistic missile submarines which travel quietly, deep beneath the sea. The aircraft delivered weapons have achieved survival through their ability to fly out from under an enemy nuclear attack and their ability to avoid or confuse the enemy's air defense capability.

Destructive capability, the second criterion of deterrence, requires that the numbers, accuracy, and yield of the surviving weapons be sufficient to destroy that which "matters" to the potential attacker who must be deterred. What matters? Historically, the United States has assumed that if it can threaten destruction of the political and military leadership, of the industrial base, and of conventional military capability the Soviets will be deterred from nuclear attack on the United States. If that spectrum of targets can be successfully destroyed after absorbing on initial strike, then it is hoped no sane or even insane leader could conclude that any post-strike objective could be enjoyed by the leaders of the country initiating the first strike.

Deterrence then depends upon survival and destructive capability. Survival can be achieved in a variety of ways but must be fundamentally responsive, in order to retain survivability as the capabilities of the potential attacker change and undermine the survivability which one once had. Destructive capability is also responsible since it too must change to defeat any protective measures initiated by the potential attacker.

A first strike force has distinctly different features. Survivability is not a first order issue since one intends to go first, and by the definition of first strike, go first so effectively that no serious damage will be suffered in return. (If there is concern that one's first strike intentions may be detected and, if the capability exists, a pre-emptive disarming strike attempted, then the first strike force must also have some survivability.) The primary criterion of a first strike force is fast and total destruction of the victim's nuclear delivery capability. To the extent that perfection is hard to achieve, the initiator of a first strike must defend and protect "what matters" from whatever few nuclear weapons of the victim might survive.

With these different criteria in mind, let us examine the Soviet Union's national security posture. The Soviets, at first glance, have a Triad structure similar to that of the United States, land-based missiles, sea-based missiles, and bomber-delivered weapons. When looked at in detail, however, there are dramatic differences in the seriousness with which the two countries have addressed survivability.

The Soviet long-range bomber force consists of some 150 aircraft, the newest having been deployed in 1974. Only if the new Blackjack bomber, now under development, reaches significant production levels can the Soviets be credited with a serious bomber leg of their Triad.

The Soviet sea-based missile force consists of 950 missiles aboard 62 submarines. However, only a small fraction of Soviet submarines are routinely at sea, leaving the majority of submarine warheads potentially vulnerable in a few ports. U.S. concerns for the survivability of its sea-based missiles have led it to routinely keep two-thirds of its submarines hidden at sea while the remaining one-third undergo maintenance.

The Soviet land-based missiles carry 70 percent of Soviet warheads. The missiles are stored in concrete and steel silos. The Soviets here, in sharp contrast to their practices with bombers and submarines, seem to take survivability seriously. However, here again, when evaluated more closely

the "survivability" scorecard again does not look too good. For the last decade we in the United States have known that the era of the survivability of any "fixed" target is over; that the accuracy of missiles will be such that a nuclear detonation will be so close that no structure of concrete and steel can survive. In this environment the Soviets continue to base the majority of its nuclear delivery capability aboard these fixed land-based missiles.

So when assessing the characteristics of Soviet nuclear forces against the criteria of survivability, the cornerstone of a deterrent force, one comes away not very impressed with Soviet efforts in this area. Destructive capability on the other hand is clearly substantiated, given survivability.

Now lets look at how the Soviet posture compares with the first strike criterion. The need for a first strike to be fast and lethal means that the Soviet bombers and submarines are, to first order, not relevant to the assessment. The Soviets, using only two-thirds of their SS-18 force, now or in the near future will have the ability to attack each U.S. land-based silo with two accurate, high yield warheads. Therefore, only 200 out of a total of 1400 Soviet land-based missiles will be needed to destroy the ICBM leg of the U.S. Triad. In the case of the SS-19, 500 missiles would be required, leaving almost 1000 missiles for other purposes.

The few U.S. bases where sea-based missile submarines are in maintenance will require only one warhead each for total destruction of one-third of our sea-based leg of the Triad, an easy accomplishment for the Soviets.

The bomber leg of the U.S. Triad is based at less than twenty bases. One high yield Soviet warhead each is sufficient to destroy each base. But some, maybe even all, the bombers can be launched between the time of the detection of Soviet missile launch and warhead arrival. Once airborne, the U.S. bombers can reach the Soviet Union. There they will come up against the world's most awesome air defense capability. The Soviets are credited with over 12,000 surface-to-air missiles in addition to the interceptor aircraft and the Soviet airborne warning and control (AWAC) aircraft designed to guide the interceptors to their targets. The U.S. Air Force will tell you that today they are confident that sufficient bombers can defeat that defense - but it is not for Soviet lack of trying and lack of investment. The Soviets seem committed to negating the deterrent capability of the bomber leg of the United States.

Returning to the U.S. submarine force, we left two-thirds of the submarines at sea, twenty submarines carrying over 350 missiles with over 3500 warheads. The Soviets have a substantial anti-submarine warfare activity and the United States has gone to considerable expense to dilute its effectiveness. The Trident submarine deployment at $18 per submarine is solely directed at making it harder for the Soviets to locate and destroy our sea-based leg of the Triad. Anti-submarine warfare is the most shrouded in secrecy of all military technology - and for very good reason. A submarine, if well located is trivial to destroy with conventional weaponry; if less well located it can be destroyed with one or several nuclear weapons. Yet the ability to localize may be easily defeated by active or passive countermeasures. The Soviets have every motivation to keep as their

darkest of secrets their progress in finding and destroying U.S. ballistic missile submarines.

If we look back at what we have just covered, we find that the Soviet land-based missile force looks as much like an element of a first strike as it is possible to look. We cannot conclude that the Soviets have an overall first strike capability because the U.S. bombers and submarines have a high survivability against missile attack. But Soviet air defense and anti-submarine warfare activities, if successful, would provide missing elements of a first strike capability.

One other attribute of a first strike posture is the ability to defend against and survive whatever very small force has escaped destruction. We have already noted the air-defense capability of the Soviets. We must also note the Soviet's limited but real antiballistic missile defense capability around Moscow, the center of Soviet political and military leadership. One can also note the shelter systems for the Soviet elite and the general civil defense preparedness. If one postulates that a first strike capability is a Soviet objective, that it would be exercised only when the Soviets had high confidence of destroying virtually all U.S. nuclear delivery capability and needed an ABM and civil defense only for unlikely surviving nuclear capability, then the military and civil defense of the Soviets seems to be of what they would need in such a scenario.

We have compared the Soviet posture today with the requirements for a deterrent force and found it wanting. We have compared their posture with the requirements for a first strike and found it wanting. We have looked at the directions in which they seem to be moving and found a better match for a first strike force then for a deterrent force.

What is Soviet intent? We don't know! We can conclude that the best fit - a first strike objective - is right. We can look for excuses for their deterrent posture failings and conclude that deterrence is their objective. What is to be avoided is letting wishful thinking determine our conclusion. We should not flee the uncomfortable feeling of being sized up for attack by inventing other reasons for the Soviet program.

We must present the Soviets with the opportunity of removing the ambiguity of their intent. The administration has done this by seeking agreement via the Strategic Arms Reduction Talks (START) in placing a priority on the reduction of fixed land-based missiles. Soviet acceptance will clearly signal a lessening interest in first strike.

But waiting for arms control agreements is not enough. We must give serious consideration to the protection of this country from any Soviet first strike plans. We must support modernization of the strategic deterrent to reduce its vulnerability. We must protect this country's citizens and resources. This is your difficult job.

"Hardened Structures"

presented by

Mr. E. Sevin
Defense Nuclear Agency

Text not available for publication.

WHAT GOOD IS OPERATIONS RESEARCH AFTER AN EMERGENCY?

Laurence L. George
Lawrence Livermore National Laboratory
P. O. Box 808, L-140
Livermore, CA 94550 U.S.A.

What is Operations Research?

Operations Research is the application of mathematics to solve problems. The problems are "word problems", real problems converted into mathematical form and solved. The mathematics are "applications" according to real mathematicians.

Operations Research is needed after emergencies because there will be plenty of problems. There may not be much time to solve them, but Operations Research already has solutions to fit the problems.

Operations Researchers want to solve problems. They will be attracted to and challenged by problems that arise after emergencies because of their motivation to restore order, because the problems are different from everyday problems, and because of the challenge to get quick solutions.

Operations Research requires computers because the days of simple solutions to simple problems have gone. There are still simple solutions, but they are applied to so much data that computers must store inputs and execute the simple solutions. The availability of personal computers makes Operations Research convenient after emergencies.

This is how an Operations Researcher solves a problem. The Manager and Operations Researcher formulate the problem and describe alternatives. Then the Operations Researcher abstracts the problem into a mathematical or computer model, solves the model and suggests the solution to the Manager. That solution may not solve the manager's problem because it is a solution to an abstract model. With some iteration, the Manager and the Operations Researcher can usually improve the solution. They might even find alternatives that had been overlooked. This problem solving process can be employed during and after emergencies

The Operations Researcher usually forces the problem into a standard form and uses standard solutions. Some solutions are preprogrammed so that problem solving amounts to gathering the data, applying the standard solution and reporting the results. The difficulties lie in problem formulation and data collection.

Operations Research, Management Science and Systems Science are similar. The publications are similar. Table 1 lists the main topics of the core journals in each field. Table 2 describes some typical Operations Research problems.

How does Operations Research help after emergencies? The obvious answer is it solves problems. Some solutions are already available. They were obtained in the course of designing systems for emergencies (Section 2) or allocating resources after emergencies (Section 3). But applications are scarce judging from the small number of references. This is due to the infrequency of emergencies relative to the frequency of everyday problems.

For example, a characteristic of mathematical programming makes it an attractive problem solving method after emergencies. The first step in mathematical programming is to find feasible solutions. After an emergency, feasible solutions may be scarce and all that is needed.

Table 1: Divisions of Some Leading Journals

Operations Research (Area Editors)	Management Science (Departments)	International Journal of Systems Science
Mathematical Programming & Optimization	Mathematical Programming and Networks	Math. Modeling
Distribution Networks & Facilities	Logistics, Distribution & Inventory	Optimization
Production	Production and Operations Management	Industry
Simulation	Simulation	Simulation
Decision Analysis	Decision Analysis	Control
Stochastic Processes & Queuing	Applied Stochastic Processes	
Social Systems, Health & Service	Public Sector Applications	Bio.Systems
Natural Resources & Energy	Finance; Information Systems and Accounting	Environment
Reliability	Marketing; Organization Analysis	
Military Oper. Research	Planning and Design; R & D and Innovation; Planning, Forecasting and Applied Game Theory	

Table 2. Typical Problems in Some Divisions

1. Mathematical Programming
   Find the best alternative to maximize one function subject to constraints on other functions of the alternatives.
2. Probability and Stochastic Processes
   Find the probabilities of some events or find the values of some functions of these probabilities.
3. Simulation
   Build a computer model of the problem and see what happens to the model when we change it.
4. Game Theory
   Find strategies to satisfy some objective in competition with adversaries.
5. Multi-objective Decision Analysis
   Satisfy several objectives simultaneously as well as possible.

What Has Operations Research Been Used for Prior to Emergencies? Operations Research has been applied extensively in planning, design and operation of production, distribution and service industries. Some of these applications are planning for emergencies:

1. design power generation and transmission systems for reliability in case of earthquake or fire (54, 55, 62),
2. allocate resources, plan inventories, and distribute supplies (blood, food, etc.) (24, 44, 45, 47, 48, 65, 66, 67),
3. design queuing, service and communication systems to handle overload or withstand electromagnetic pulse (63, 67, 63),
4. estimate reliability of lifeline networks (16, 17, 18, 19, 20, 21, 22, 48),
5. construct models of contagion, epidemics and disasters for assessment of their effects (25, 26, 37, 38, 39, 43, 61, 68, 69),
6. locate and dispatch emergency services such as health, police, fire and shelter (1, 23, 28, 29, 30, 31, 33, 41, 42),
7. estimate insurance premiums and the value of life (53, 56, 57, 58, 59, 60),
8. plan fire control strategies (2, 3, 4, 5, 6, 7, 8, 9, 10, 11, 12, 13, 26, 35, 36, 46),

The design for reliability of power, water and communication systems recently shifted emphasis. Systems have always been designed to avoid breakdown due to wearout or internal malfunction. But the need to withstand external shocks has been recently emphasized. Shocks could be earthquakes which shutdown power plants, knock over transmission towers, and break water mains. They could be electromagnetic pulses which scramble circuits. They could be storms which interrupt communications and cause damage. They could be fires inside nuclear power plants which can't be fought aggressively because of inaccessibility. Operations Research helps design for reliability in case of shocks and emergencies by estimating reliability of components and systems.

The typical model of component failure due to shock is that some load, mechanical, electromagnetic, or thermal, exceeds the component's capacity to withstand the load. The load and the component's capacity to withstand the load are modeled as random variables to represent inherent randomness. Component failure probability is

$$P[\text{Load} > \text{Strength}] = P[X > Y] = \int_0^\infty (1-F_Y(x))f_X(x)dx \qquad (1)$$

where $F_Y(x) = P[\text{Strength} < x]$ and $f_X(x)dx \cong P[x < \text{Load} < x+dx]$.

The probability a system survives (reliability) is the probability that some combinations of components survive. System reliability is not the product of component reliabilities because components are dependent. They are dependent because the component loads are all caused by the same external load.

For example, suppose two identical relays are used for redundancy in a circuit. Circuit failure probability is the probability both relays fail. Suppose the relays are in two different cabinets to reduce the probability that both are damaged by a fire. Suppose a fire occurs in the room containing the cabinets. Assume the relays fail if the peak temperatures in their cabinets exceed the capacities of their wiring insulations to withstand heat. Denote X_1 and X_2 the peak temperatures and Y_1 and Y_2 the capacities. Assume they are independent pairs of correlated normal random variables. The peak temperatures are correlated because they are due to the same fire. The probability of circuit failure increases with the correlation between X_1 and X_2. Incorrectly assuming X_1 and X_2 are uncorrelated underestimates circuit failure probability.

The recent shift in emphasis of reliability analysis has required that dependence be accounted for. This is done (64). In addition to handling dependence, the shift in emphasis requires that the effect of secondary threat following a shock, such as fire following earthquake, be accounted for.

For example, suppose earthquake load and subsequent fire can cause relay failures. Assume a relay fails if either the earthquake load exceeds the mechanical stsrength or if the fire temperature exceeds the insulation capacity. Let E and F denote earthquake and fire random variables. Then component failure probability is

$$P[X_1(E) > Y_1(E) \text{ or } X_1(F) > Y_1(F)]. \qquad (2)$$

If there is deterioriation due to earthquake, component failure probability is

$$P[X_1(E) > Y_1(E)] + P[X_1(F) > Y_1(F) \mid X_1(E) < Y_1(E)]\, P[X_1(E) < Y_1(E)], \qquad (3)$$

earthquake failure probability plus earthquake survival and fire failure probability. The probability $P[X_1(F) > Y_1(F) \mid X_1(E) < Y_1(E)]$ conditions fire failure on earthquake survival allowing earthquake deterioriation to affect fire failure probability.

What Good is Operations Research After an Emergency?

There are many Operations Research methods useful after an emergency:

1. Management of resources (50,65,52),
   a. perishable inventories (24),
   b. transportation and distribution (27, 29, 34, 40, 41, 65, 67),
   c. rationing (47),
   d. cannibalization of spare parts (44, 45),
   e. feasible resource allocation (66).
2. Models of contagion, epidemic, and fire,
   a. stochastic process models of epidemics (68),
   b. Markov process models of fire spread in 2D and 3D (26, 68),
3. Models of control of emergencies
   a. Markov decision processes for control of fires (4, 5, 6, 7, 8, 9, 11),
   b. dynamic lifeline analysis to construct the optimal network after damage (16, 17, 18, 19, 20, 21, 22),
   c. bottleneck transportation problems (27),
4. Search (70).

Because there are so many methods, I'll describe only feasible resource allocation.

The typical resource allocation problem is to find the levels of activities x_j, $j=1,2,\ldots,n$, to maximize some profit function where p_j is the profit per unit of activity j

$$z = \underline{p}^T x = \sum_{j=1}^{n} p_j x_j \tag{4}$$

subject to constraints

$$\sum_{j=1}^{n} a_{ij} x_j \leq b_i \quad i=1,2,\ldots m \tag{5}$$

$$x_j \geq 0. \tag{6}$$

The b_j are available resource quantities, the a_{ij} are the consumption rates of resource i per unit of activity j, and the product $a_{ij} x_j$ is the amount of resource i used by activity x_j. This problem is called a linear program. The constraints define a convex set in the vector space spanned by x. The set may be empty if resources are insufficient to satisfy intermediate production constraints.

For example, there may be a limited amount of unpolluted water which can be used in three activities, drinking by humans, watering agriculture, and drinking by livestock. The variable x_1 represents the amount of water for drinking by humans so its input-output coefficient $a_{11}=1$ and its profit may be assumed to be $p_1=1$. The variable x_2 represents the level of agricultural activity. Its input output coefficient a_{12} is the water consumption per unit of agricultural activity. The profit p_2 per unit of agriculture is greater than from livestock, p_3.

There may be other constraints which depend on population size that define the minimum levels of combinations of activities required for survival; e.g.

$x_1 \geq b_1$ (water required by population)

$a_{22}x_2 + a_{23}x_3 \geq b_2$ (calories required by population)

After an emergency, the problem may be to find a feasible set of activity levels to support the population.

The data for feasible resource allocation exists except for the amounts of resources and the population. As soon after an emergency as resource and population estimates become available, the feasibility problem can be solved and solutions recommended to resource managers. If no feasible solutions exist, sersitivity analyses can show which resources are most needed and how much.

Conclusions

Operations Research is ready and waiting to help after emergencies. One reason it has been used so little is no longer applicable, the lack of computer support. I recommend that emergency managers prepare the data, the programs, the operations researchers and themselves to use the support Operations Research can provide after emergencies.

References

1. D. L. Mitchell, An Optimization Study of Blast Shelter Deployment, Vol. I-III, Lambda, OCD-PS-66-113, 6609 AD--659377-9
2. W. S. Jewell and R. W. Shephard, Operations Research in Forest Fire Problems, National Academy of Sciences - National Research Council Pub. 949, O.R. Center #172-19, U.C. Berkeley (1961).
3. P. Casamajor, Wildland Fire Problems, O.R. Center #172-26, U. C. Berkeley, (1962).
4. G. Parks, Analytical Models for Attack and Control of Wildland Fires, O.R. Center #63-6, U.C. Berkeley, (1963).
5. R. J. Swersey, "Parametric and Dynamic Programming in Forest Fire Control Models," Ops. Res. 12(5), 781-783, (1964).
6. G. Parks, Computer Simulation of the Attack and Control of Wildland Fires, O.R. Center #63-16*, U. C. Berkeley, (1963).
7. D. P. Heyman, Least Cost Allocation of Fire Suppression Equipment, O.R. Center #64-4, U.C Berkeley, (1964).
8. G. Parks, "Mathematical Investigation of The Attack and Control of Wildland Fires," Man. Sci., 10(4), (1964).
9. G. Parks, "The Development and Application of an Analytical Model for Initial Attack of Wildland Fires," Man. Sci., 10(4), 760-766, (1964).
10. W. S. Jewell, Forest Fire Fighting Models, O. R. Center #65-29*, U. C. Berkeley, (1965).
11. A. McMasters, Wildland Fire Control with Limited Suppression Forces, O. R. Center #66-5, (1966).
12. R. Chandrasekaran and R. W. Shephard, "Optimal Strategies of Fire Fighting by Fire Breaks", Proc. 4th International Conf. on Ops. Res., Boston, (1966).

13. R. Chandrasekaran, Optimal Control Policies for Fire Fighting in Fire Breaks, O. R. Center #67-35, U. C. Berkeley, (1967).
14. C. R. Glassey and R. M. Karp, Optimal Search for Pollution Sources, O. R. Center #72-1, U. C. Berkeley, (1972).
15. G. Aumann, Catastrophes on Lattices, O. R. Center #77-4, U. C. Berkeley, (1977).
16. R. E. Barlow, A. Der Kiureghian and V. Satyanarayana, "New Methodologies for Analyzing Pipeline and Other Lifeline Networks Relative to Seismic Risk", Proc. ASME Century II Pressure Vessels and Piping Conf., San Francisco, O. R. Center #80-5*, U. C. Berkeley, (1980).
17. V. Satyanarayna, Multi Terminal Network Reliability, O. R. Center #80-6*, U. C. Berkeley, (1980).
18. V Satyanarayana and J. N. Hagstrom "A New Formula and an Algorithm for the Reliability Analysis of Multiterminal Networks", IEEE Trans. on Rel, R-30(4), 325-334, (1981).
19. R. K. Wood, Efficient Calculation of the Reliability of Lifeline Networks Subject to Seismic Risk, O. R. Center #80-13, U. C. Berkeley, (1980).
20. V Satyanarayana "A Unified Formula for the Analysis of Some Network Reliability", IEEE Trans. on Rel., (R-31), O. R. Center #81-8*, U. C. Berkeley, (1982).
21. Panoussis, G., Seismic Reliability of Lifeline Networks, No. R74-57, Department of Civil Engineering Research, Massachusetts Institute of Technology, Cambridge, Massachusetts, (1974).
22. Taleb-Agha, G., Seismic Risk Analysis of Lifeline Networks, No. R75-49, Department of Civil Engineering Research, Massachusetts Institute of Technology, Cambridge, Massachusetts, (1975).
23. G. O. Weslovs and R. F. Love, "The Optimal Location of New Facilities Using Rectangular and Distances", Opns. Res. (19)1, 124-130, (1971).
24. S. Nahmias, "Perishable Inventory Theory: A Review", Opns. Res. (30)4, 680-708, (1982).
25. W. S. Jewell and A. B. Willoughby, A Study to Analyze and Improve Procedures for Fire Damage Assessment Following Nuclear Attack, Parts I & II, AD 286943, (1960).
26. P. V. Phung and A. B. Willoughby, Prediction Models for Fire Spread Following Nuclear Attacks, AD 613359, (1965).
27. U. Derigs "On Three Basic Methods of Solving Bottleneck Transportation Problems", Nav. Res. Log. Quart, (29)3, 505-515, (1982).
28. Alexander, Michael N., J. Brooks Ferebe, Paul J. Grim, Leonard S. Lebow, Stephen D. Senturia, and Ann M. Singleterry. "Effect of Population Mobility on the Location of Communal Shelters," Opns. Res. (6), 207-231.
29. Kolesar, Peter, and Edward H. Blum. "Square Root Laws for Fire Engine Response Distrances, Management Sci., (19), 207-231.
30. Toregas, Constantine, Charles ReVelle, and Ralph Swain, "Reply to Rao's 'Note on the Location of Emergency Service Facilities'", Opns. Res. (22), 1262-1267.
31. Toregas, Constantine, Ralph Swain, Charles ReVelle, , and Lawrence Bergman, "The Location of Emergency Service Failities", Opns. Res. (19), 1363-1373.

32. Bentz, Richard, et al. "Some Civil Defense Problems in the Nation's Capital Following Widespread Thermonuclear Attack", Opns. Res. (5), 319-350.
33. Kelleher, Grace J. "A Damage-Limiting Shelter-Allocation Strategy", Opns. Res. (15), 211-220.
34. Faulkner, "Determining Ship Routes to Minimize Fallout Dosage", Opns. Res. (10), 799-807.
35. Chaiken, Jan M., and Richard C. Larson," Methods for Allocating Urban Emergency Units: A Survey", Management Sci. (19), 110-130.
36. Valinsky, David, "A Determination of the Optimum Location of Fire-Fighting Units in New York City", Opns. Res. (3), 494-512, (1955).
37. Wilkins, C. A., J. A. Shaw. and A. Keane., "A Comparison of Estimates of Nuclear Bomb Casualities From Two Different Urban Models", Opns. Res. (17), 923-925.
38. Rivas, J. Roberto, and Dale F. Rudd., "Man-Machine Synthesis of Disaster-Resistant Operations", Opns. Res. (23), 2-21, (1974).
39. Everett, Hugh, III, and George E. Pugh. "The Distribution and Effects of Fallout in Large-Weapon Campaigns", Opns. Res. (7), 226-248, (1959).
40. Stearns, S. D., "A Mathematical Model for Strategic Movement", Opns. Res. (12), 239-254, (1964).
41. Kolesar, Peter, Warren Walker, and Jack Hausner, "Determining the Relation Between Fire-Engine Travel Times and Travel Distances in New York City", Opns. Res. (23), 614-627, (1975).
42. Kolesar, Peter, and Warren E. Walker., "An Algorithm for the Dynamic Relocation of Fire Companies", Opns. Res. (22), 249-274, (1974).
43. Hunter, Jeffrey J., An Analytical Technique for Urban Casualty Estimation from Multiple Nuclear Weapons", Opns. Res. (15), 1096-1108, (1967).
44. R. M. Simon "The Reliability of Multi-component Systems Subject to Cannibalization " Nav. Res. Log. Quart. (19)1, 1-14, (1972).
45. D. Khalifa, V. M. Hottenstein and S. Aggrawal, "Cannibalization Policies for Multistate Systems", Ops. Res. (25)6, 1032-1039, Nov. (1977).
46. M. Stade, "Cost Effectiveness of Water Bombers in Forest Fire Control", Can. Ops. Res. J. (5)1, 1-18, March (1967).
47. A. Kaplan, "Stock Rationing". Man. Sci. Theory, (15)5, 260-267, (1969).
48. Anejia, Y. P. and K. P. K. Nair, "Multicommodity Network Flows with Probabilistic Losses", Man. Sci., (28)9, 1080-1086, (1983).
49. Peterson, D. W. et. al, Development of a Dynamic Model to Evaluate Economic Recovery Following a Nuclear Attack, Vol. I & II, Pugh-Roberts Assoc., Inc., ADA 098 587 and ADA 098 588, (1980).
50. Hill, G. A. et al, Managing the U. S. Economy in a Post Attack Environment: A System Dynamics Model of Viability, Vol. II, Analytical Assessments Corp., ADA 087708, Oct. (1979).
51. J. B. Hallan, "A Simulation Model of an Emergency Medical System", Proc. Symp. on Post Attack Recovery from Nuclear War, 67-91, AD672 790, (1967).
52. Bickley, L. J. and E. S. Pearsall, "Estimates of the Potential of the United States Economy Following a Nuclear Attack", 245-273, Proc. Symp. on Post Attack Recovery from Nuclear War, 67-91, AD672 790, (1967).

53. Seal, H. L., Stochastic Theory of a Risk Business, Wiley, New York, (1969).
54. George, L. L. and J. E. Wells, "The Reliability of Systems of Dependent Components", Proc. ASQC Quality Congress, San Francisco, (1981).
55. George, L. L. and J. E. Wells, "Loss of Load Probability for Systems of Dependent Transmission and Generation Components", Proceedings, Reliability Conference for the Electric Power Industry, IEEE, Portland, April (1981).
56. Ramachandran, G. "Extreme Value Theory and Earthquake Insurance", Trans. 21st Int'l Congress of Actuaries, (I), 337-355, Zurich and Lausanne (1980).
57. Ramachandran, G., "Extreme Value Theory and Fire Insurance", Trans. 21st Int'l Congress of Actuaries, (III), 695-707, Zurich and Lausanne, (1980).
58. Johansen, P. "Mathematical Models Regarding Fire and Consequential Loss", Skandinavian Actuarial Journal, 229-234, (1978).
59. Lemaire, J. "Exchange de Risques Entre Assureurs et Theoree des Jeux", ASTIN Bulletin, (9), 181-190, (1977).
60. Ramachandran, G. "Extreme Value Theory and Large Fire Losses", ASTIN Bulletin, (7) 293-310, (1975).
61. Shpilberg, D. C. "The Probability Distribution of Fire Loss Amount", J. of Risk and Insurance, (64)1, 103-115, (1977).
62. Morrison, G. N., J. M. Kallis, L. A. Stratton, I. R. Jones, and A. L. Lena, RADC Thermal Guide for Reliability Engineers, RADC-TR-82-172, Rome Air Development Center, AFSC, Griffiss AFB, NY 13441, June (1982).
63. Bevensee, R. M., H. S. Cabayan, F. J. Deadrick, L. C. Martin and R. W. Mensing, Characterization of Errors Inherent in System EMP Vulnerability Assessment Programs, UCRL-52954, Lawrence Livermore National Laboratory, Livermore, CA 94550, (1980).
64. Wells, J. E., L. L. George, and G. E. Cummings, Seismic Safety Margins Research Program, Phase 1 Final Report, Systems Analysis (Project VII), NUREG/CR2015, Vol. 8, UCRL-53021 Vol. 8, Lawrence Livermore National Laboratory, Livermore, CA, (1981).
65. Hillier, F. S. and G. J. Lieberman, Operations Research, Holden-Day, San Francisco, (1967).
66. Dantzig, G. B., Linear Programming and Extensions, Princeton University Press, (1963).
67. Gaver, D. P., J. P. Lehoczky and M. P. Perlas, "Service Systems with Transitory Demand", in Logistics, Vol. 1, M. A. Geisler, Editor, North Holland/American Elsevier, New York, (1973)
68. Cox, D. R. and H. D. Miller, The Theory of Stochastic Processes, Wiley, New York, (1965).
69. Schmidt, Jr, L. A., A Parametric Study of Probabilistic Fire Spread Effects, Inst. for Defense Analyses Paper P-1372, AD-e500113, (1979).
70. Stone, L. D. The Process of Search Planning: Current Approaches and Continuing Problems", Opns. Res. 31(2), pp207-233, (1983).

*Copies are no longer available. The original is in the O. R. Center Library, 3113 Etcheverry Hall, University of California, Berkeley.

FLAMMABILITY TESTING
STATE-OF-THE-ART

by

John de Ris
Factory Mutual Research Corporation
Norwood, Massachusetts 02062

ABSTRACT

Traditional material flammability tests are discussed in terms of their empirical foundation and oversimplified interpretation of fire phenomena. More recent rate-of-heat-release tests overcome some of these problems by measuring a material's response to different levels of fire exposure. However, no existing small-scale tests are sensitive to the radiant emission from the material's own flames. This radiant emission controls large-scale fire hazards. As a result, existing flammability tests cannot be expected to adequately characterize large-scale hazards. Some new approaches to this problem are discussed and a specific bench-scale test method is suggested which may overcome the identified problems of existing test methods.

BACKGROUND

Traditionally, the flammability of a building material has been evaluated by measuring its: 1) ease of piloted ignition; 2) ability to propagate a small creeping flame in the presence of an external radiant source; and/or 3) ability to propagate a larger under-ceiling fire as measured by the ASTM-E84 "tunnel test" which exposes a 25 ft (7.62 m) long sample to a sizeable propane ignition source. This latter test is legally recognized by most building codes. Since the piloted ignition and creeping flame spread phenomena are closely related and depend on similar material properties they are often jointly evaluated by the ASTM-E162 test apparatus which measures the creeping spread rate and extent of maximum flame travel under conditions of a spatially decreasing external radiant flux.

These tests were developed about thirty years ago at a time when building materials where based primarily on cellulose which has a limited range of flame properties. Also, at that time, lacking a basic understanding of fire behavior, it was implicitly assumed that all materials could be ranked on a single flammability scale based on some standard test which subjects a material to a single representative fire environment. In view of the need for some flammability assessment procedure and the absence of obviously contradictory full-scale (or loss) data this oversimplified approach appeared justified at its time. This traditional philosophy has now outlived its usefulness.

FULL-SCALE TESTING

Around 1970, after experiencing unexpectedly severe losses involving newly introduced fire retarded plastics, various full-scale corner tests were run to check their flammability rankings suggested by the ASTM-E84 test (Castino, 1975). A lack of correlation was observed which was particularly troublesome for those fire-resistant insulation materials having a flame spread rating

less than 25. The ASTM-E84 ranking is based primarily on the extent of flame travel normalized so that red-oak has a rating of 100 and cement-board a rating of zero. Apparently modern polymeric materials and especially fire-resistant foam insulations do not properly fit on this ranking scale.

This lack of correlation has lead to a wide-spread mistrust of current standard flammability tests and the reluctant suggestion that one can only rely on full-scale tests for flammability assessment. Consistent with this full-scale test philosophy the ISO (International Standards Organization) and ASTM are developing a "Standard Method for Testing Wall and Ceiling Materials and Assemblies" (ASTM, 1980) which exposes a material to a large 176 kW propane burner flame placed in a lower corner of an 8 ft x 12 ft x 8 ft high (2.4 x 3.6 x 2.4 m) room whose wall and ceilings are lined with the material. The outcome of these corner/room tests is strongly dependent on the rather arbitrarily chosen heat release rate of the ignition source. For exposure heating rates above some (material dependent) critical value the fire will undergo a dramatic transition to flashover when the heat release rate from the burning wall material becomes comparable to the exposure fire heat release rate. Exposure fires smaller than this critical value are insufficient to initiate flashover and usually cause only local damage. Test engineers welcome such clear-cut go/no go tests because they have an indisputable outcome. However, a result from a single test run with a given exposure is relatively uninformative to a potential user interested in the outcome involving other levels of exposure. A potential user probably wishes to rank materials according to their exposure which will just cause run-away ignition (e.g. flashover) of the material. Unfortunately, at present, it is not possible to determine this critical exposure for a given material from a single full-scale test.

Full-scale tests are also very expensive, difficult to reproduce, and require such large quantities of sample materials that they cannot be considered for screening new materials under development. Finally full-scale tests, being empirical, give little guidance for assessing hazards in related situations. Often small changes in geometric details have a profound effect on the outcome of a fire. In conclusion, full-scale tests are generally regarded as essential for corroborating the general claims of standard flammability test methods, but cannot serve as a substitute because of their complexity, cost and large material requirements.

FIRE PHENOMENA

It is now generally recognized that various materials can have markedly different flammability rankings in different situations depending on such factors as: 1) fire scale; 2) imposed heat flux levels; 3) geometric arrangement; 4) the presence of other nearby materials, and 5) the temperature, pressure and degree of vitiation of the surrounding atmosphere. Fires generally involve synergistic couplings between a material and its environment. Also, different fire scenarios are often governed by qualitatively different burning mechanisms which in turn are controlled by different combinations of material properties. It is important to understand these differences in burning mechanisms when interpreting flammability test results. In particular, it is important to appreciate the effects of fire-scale, if one wishes to infer full-scale fire behavior from small standard flammability tests.

SMALL-SCALE

The steady (constant area) burning rate of a small-scale fire is controlled by the convective heat transfer from the flames. Small-scale flames are not thick enough to emit significant radiation. As a result their mass transfer rates are primarily controlled by the heat required to vaporize unit mass of fuel. The overall heat release per unit area is given by the product of the mass transfer rate and the heat of combustion of the fuel volatiles. Other factors controlling small-scale burning rates depend only on geometry for typical organic fuels burning by natural convection in air at atmospheric pressure. The important fuel property - namely the heat required to vaporize unit mass of fuel - can be directly measured by Tewarson's (Tewarson, 1980) well known "FM Flammability Apparatus" which measures the fuel-mass-loss-rate and heat-release-rate under different applied radiant exposures.

Flame-retardants acting by inhibiting gas-phase reactions can significantly reduce, or even prevent, burning at small-scale. The effectiveness of such retardants has often been inferred from the LOI (Limiting Oxygen Index) test which measures the critical ambient oxygen concentration that is just sufficient to permit downward creeping flame-spread on a small sample. Because this test is convenient and requires only a very small test sample, it is widely used in the chemical industry during material development. Unfortunately, the test results can be very misleading because large-hazardous-scale-fires are not significantly influenced by such gas-phase flame retardants (because large-scale flow times are so much longer than reaction times). Innumerable disappointments have occurred in recent years when supposedly non-flammable fire-retardant polymers burned vigorously in large-scale tests. For example, PVC plastics which usually have an excellent LOI rating burn more rapidly at large-scales than acrylics which generally have a poor LOI rating. Also, the flame-retardants encouraged by this test tend to significantly increase the smoke output and toxicity of a fire.

Fire-retardants which act by encouraging char-formation in the solid-phase can be very effective at all fire scales. By preventing transfer of carbon to the gas-phase they are triply effective by: 1) providing a thermally insulating char layer; 2) reducing the gas-phase heat-release-rate and resulting flame heights; and 3) reducing the flame luminosity and consequent radiant heat transfer which is of dominant importance at large-scales. It is speculated that some of these retardants act by encouraging the polymerization of the fuel vapors as they flow through the chemically active char layer (Parker, 1982). The effectiveness of these char-enhancing retardants can be evaluated by a rate-of-heat-release (RHR) apparatus which measures the transient combustion heat release per unit area of a material subjected to a controlled radiant flux. Tewarson's "FM Flammability Apparatus" and Smith's "Ohio State Apparatus" are well known examples of such RHR tests. Tewarson uses a 10 cm diameter sample and Smith uses a 25 x 25 cm square sample. In both cases the material requirements are small enough to permit testing at a variety of imposed flux levels. However, neither test explicitly measures the flame luminosity or radiated fraction of heat release. As a result, one should not directly extrapolate the test results to large-scales where radiation from the flames is a controlling factor.

Many modern polymeric materials are retarded by the simple addition of inert fillers which increase the heat required for fuel gasification and often leave a porous char-like insulating residue. These effects can be measured by the above mentioned RHR tests. In addition, some fillers incorporate a significant amount of water of hydration, which upon vaporization may possible reduce soot formation and flame radiation. Unfortunately, the current lack of a flame radiation test has prevented measurement of this latter effect.

The rate-of-heat-release test is particularly useful for examining charring flame-retarded materials such as polyurethane or PVC foams. Such materials can have a distinctly non-linear response to an imposed heat flux. Figure 1 shows the peak response of various polyurethane foams (NFPA Handbook, 15th Ed., pg. 4-7). Notice the changes in rankings for various imposed heat fluxes. At very low flux levels the material surface temperature does not increase sufficiently for significant gasification. Above some critical flux level gasification occurs at a rate sufficient to support piloted ignition. Once ignition occurs the sample receives heat both from the external radiant source and the flames themselves. The added heat transfer from the flames often decreases with increasing rates of gasification leading to a less than linear increase of heat release rate with increasing imposed flux.

A rate-of-heat-release (RHR) test has the advantage of providing several important flammability parameters from a single test run versus time. Figures 2a and 2b show a typical RHR test arrangement and results (Ostman, 1982). The sample receives a uniform radiant heat flux. Measurement of oxygen depletion in the exhaust is now typically used to infer the rate-of-heat-release (Huggett, 1980). The initial time delay prior to gasification provides a measure of the ease of ignition. The rapid increase to the peak heat-release-rate is controlled by the material's heat of gasification. The subsequent decrease in heat-release-rate is due to increasing char insulation; while the final secondary peak results from acceleration of the pyrolysis wave as it approaches the thermally insulated back-surface of the sample. Figure 2b shows curves for several externally imposed fluxes. It simulates the effects of flame radiation in much larger fires. The heat flux actually received by the solid is augmented by the heat transfer from the flames produced by the sample itself. All of the above transient phenomena are being actively studied by various fire research groups (Delichatsios and de Ris, 1983). A possible criticism of most current rate-of-heat-release tests is their external radiant heat source. Gas panel radiant heat sources provide heat over a typical infrared wavelength range but their flux levels are too low for realistic view factors; whereas quartz heaters provide plenty of heat but at unrealistically short wavelengths. Solid fuel response times are known to be quite sensitive to the imposed wavelength (Welker, 1969). Improved infrared gas fired radiant heaters using newly available high temperature ceramics may resolve this problem.

Except for the characterization of flame radiation, it is now generally believed that the rate-of-heat-release measurement provides the most meaningful characterization of large-scale flammability.

Before closing this discussion of small-scale fire phenomena, one should mention the wide body of research on the creeping flame spread associated with downward and horizontally propagating fires. This phenomenon is reasonably

well understood for both flame-retarded and non-retarded materials having a smooth surface. It is addressed in part by the LOI test. Also Quintiere, in a series of studies, has shown that the ASTM-E162 flammability apparatus can be used to evaluate downward creeping flame spread rates under the influence of external radiation (Quintiere, et al, 1982). In particular, one can measure the minimum external flux required to sustain propagation. A similar apparatus and technique is now widely used for evaluating carpet flammability. While these advances are significant for the general flammability problem, the creeping fire spread phenomenon is not of central importance to most large-scale fire hazards. The marginal creeping flame-spread is governed by local chemical kinetics, gas phase diffusion and solid conduction, whereas the critical condition for large-scale upward fire spread is governed by solid ignition, the duration and intensity of rate-of-heat-release and the flame radiative heat feed-back. The associated phenomena are quite different and should not be expected to correlate.

LARGE-SCALE

As the scale of a fire increases, the flames become thicker and have more material which can radiate. In general, the radiative heat transfer from flames to adjacent surfaces exceeds convective heat transfer for flame heights exceeding 30 centimeters (Orloff, de Ris, Markstein, 1975). For organic fuels this radiation comes primarily from soot in the flames which makes them appear brightly luminous. Generally, the pyrolysis vapors from man-made polymeric materials are high in carbon content and produce more soot than cellulosic fuels whose pyrolysis vapors have a significant amount of oxygen already bound to the carbon atoms. Fuels which generate copious amounts of smoke tend to have highly radiative flames and have higher large-scale burning rates. The black smoke is thought to arise from the flames losing so much heat by radiation that they are extinguished locally by this radiant loss.

All present day small-scale flammability tests attempt to simulate large-scale fire environments by imposing an independently controlled external radiative flux onto the fuel sample. This external flux generally dominates the radiation from the sample's own flames; so that the measured results are insensitive to the sample's own flame radiation and cannot be expected to provide a complete evaluation of the material flammability at large-scales. This insensitivity is advantageous insofar as it can yield a clear picture of the solid response to a controlled external environment. But it leaves out the essential ingredient - namely the flame radiation which typically represents 80% of the heat feedback at large-scales (Orloff, Modak, Alpert, 1977).

How should we cope with these problems? Clearly we cannot do away with standard flammability tests. If possible, we should have tests which require relatively small samples - say 30 cm square or even less - to encourage testing by industry involved in developing new materials. Of course results from such tests must be corroborated at full-scale for a selection of representative fuels. These problems appear surmountable as will be described below.

Rate-of-heat-release tests are clearly essential and several such tests are under development at various fire research institutions. The test measures

the rate of combustion energy released per unit sample area versus time when subjected to various levels of externally supplied radiation. It is essential to evaluate material at various levels of irradiance because many materials have a strong non-linear response. Also, because charring materials typically have a strongly decreasing transient heat release subsequent to ignition, one should evaluate both the peak rate of heat release, maximum average rate-of-heat-release over selected time intervals (say 1, 2, 3 and 5 minutes) as well as the cumulative heat release. Results from these rate-of-heat-release tests can be directly used for estimating the evolved transient heat release rate and corresponding flame heights for the material when subjected to a known source fire in different practical situations of interest.

Knowledge of the rate-of-heat-release leads directly to estimates of flame heights. In general, both laminar and turbulent flame heights are controlled only by the fire geometry and the actual heat release rates and not by other fuel properties such as its stoichiometric requirements (Masliyah and Steward, 1970; Schug, Manheimer-Timnat, Yaccarino and Glassman, 1981).

To evaluate whether the evolved flames are powerful enough to significantly add to the exposure heat flux, and thereby induce a self-propagating wall or corner fire, one must evaluate the radiative properties of the flames. These properties are the effective flame radiation temperature T_f and the absorption-emission coefficient k_f which is essentially proportional to the amount of soot per unit volume. The radiation emitted per unit volume is equal to $4 \sigma k_f T_f^4$ where σ is the classical Stefan-Boltzmann constant.

The accompanying Figure 3 shows a scientific flammability apparatus being constructed at FMRC to evaluate these flame radiative properties for fire-resistive charring wall materials. The charring material on the left is subjected to an externally controlled radiant flux. The transient rate of heat release is measured by chemically sampling the gases leaving the top of the enclosure. A water-cooled heat transfer plate measures the total (radiative plus convective) heat feedback from the flames. It is shielded from the radiant heat source by a series of radiation baffles, so that it measures only the heat flux from the flames. In addition, we have built a dual radiometer which looks through the flames from the side in order to simultaneously measure both the effective flame radiation temperature T_f and absorption-emission coefficient k_f.

This apparatus is not intended as a standard flammability test. It is clearly too sophisticated for widespread use. It is a scientific apparatus intended to provide an in-depth analysis of the radiative properties of a few selected fire-resistive fuels; so that we can provide a rigorous scientific foundation for a subsequent simplified standard material flammability measuring apparatus. It also is intended to provide the basic flame property data needed for the development of mathematical models predicting corner and room flashover. In addition, provision has been made for providing vitiated air to the enclosure for studying the effects of oxygen depletion on flame radiation. This apparatus is the outcome of a long-range research program aimed at providing a basic scientific understanding of flame radiation in fires.

NBS is currently developing a similar but simpler test apparatus which measures the total radiative-convective heat feedback flux from the upper flames. While it is not placed within an enclosure and consequently is not suitable for evaluating the effects of vitiation, it may eventually lead to a standard test method.

A SUGGESTED BENCH-SCALE FLAMMABILITY TEST

As discussed above, flammability (or fire hazard) of a material at large-scale is governed by three principle factors: 1) its piloted ignition time in response to an imposed heat flux; 2) the subsequent rate-of-heat-release of its pyrolysis vapors in response to the imposed heat flux; and 3) the radiant emission from the flames resulting from the burning of these pyrolysis vapors.

We have already discussed several test devices which can evaluate the rate-of-heat-release and ignitability of a material. Here we discuss a proposed test concept which in addition may evaluate the radiant emission. The suggested apparatus is also sufficiently compact to be placed on a laboratory bench.

As shown in Figure 4, the test examines a buoyant laminar (candle-like) diffusion flame produced by the pyrolysis vapors emerging from the heated test sample. As explained later, the ignition and rate-of-heat-release measurements are directly inferred from the resultant flame height and should produce results similar to existing test methods with the advantage of decoupling the flame heat-feedback from the pyrolysis process.

Of greater significance the test concept allows one to infer the expected radiant emission from material flames at large-scale. It does this by measuring the fuel's so-called "smoke-point". Recent research at FMRC shows there is a close correlation between large-scale flame radiation and the smoke-point for various hydrocarbon fuels*. The smoke-point is conventionally defined as the maximum height a buoyant laminar flame can attain without releasing soot (i.e. smoke). The aircraft industry has traditionally used the smoke-point of commercial fuels as a measure of their relative smokiness and as well as their radiant output. Standard test methods exist for evaluating the smoke-point of liquid and gaseous fuels. The present concept extends these methods to solid fuels.

It is well-known that the radiation from both large- and small-scale diffusion flames comes principally from their luminous soot. This soot is both formed and oxidized within the flames. Fuels which produce more soot radiate more intensely. The radiative heat loss cools the flames and, if given enough time, can induce local radiative extinguishment accompanied by release of cold soot in the form of visible smoke. By increasing the fuel supply to a small candle-like flame, one increases its flame height and residence time,

*Specifically the peak soot absorption coefficient in a 50 kW pool fire and the radiative fraction from a buoyant turbulent fuel jet ranging over 10-50 kW are both tightly correlated with the fuel smoke- point (Markstein, 1983).

resulting in an increased fractional radiative heat loss. A sooty fuel such as propylene can maintain only a relatively short buoyant flame (2.9 cm high) without release of visible smoke; where as a less sooty fuel like propane can support a much taller (16.2 cm) diffusion flame without smoke emission (Shug, et al, 1981). These candle-like flames at their smoke-points release approximately one fifth of their chemical energy in the form of radiation. In the case of hydrocarbon fuels, this heat loss reduces the flame tip temperature to about 1550°K at which temperature soot oxidation rates are significantly reduced (Markstein, 1983). Smoke-point heights are easily measured because the flame undergoes a sudden transition to sooting and release of smoke. Measured smoke-points are independent of apparatus details provided the fuel is supplied at a given temperature and provided the buoyant flame is: well ventilated, shielded from stray laboratory air currents by a chimney, and not subjected to excessive induced forced ventilation (Schalla and Hibbard, 1957).

The accompanying figure shows the suggested measuring apparatus for solid fuels. A patent disclosure has been submitted. It is intended to simulatan-eously measure both the transient heat-release-rate and sootiness of the pyrolysis vapors emerging from a test sample (say 4-6 cm in diameter) placed in an oven at the start of a test run. Auxilliary supplies of fuel and inert gases are added to the pyrolysis vapors under feedback control to maintain a constant overall heat-release-rate and degree of flame sootiness. In general, for organic fuels, the heat-release-rate of a laminar buoyant diffusion flame is directly proportional to its height, regardless of the fuel chemical composition or presence of added inert gas (Shug, 1981). Consequently, as the rate-of-heat-release from the pyroylysis vapors increases, the excess fuel controller will reduce the excess fuel supply while maintaining a constant flame height as seen by the radiometer. This reduction in excess fuel supply provides a direct measurement of the sample's instantaneous heat-release-rate. The subsitution technique should be both rapid and precise.

Similarly, the flame can be maintained in its marginal smoke-point state by a smoke detector which increases the supply of inert gas (say N_2) as the pyrolysis vapors increase in sootiness. An increase in inert gas flow suppresses soot formation without influencing the flame height (Shug, 1981). The added inert flow provides an instantaneous measure of pyrolysis vapor sootiness. The respective heat-release-rate and sootiness measurements are presumably independent of one another and can be performed simultaneously throughout the test run. Certainly the heat release measurement should be independent of the simultaneous soot-point measurements. Recently Calcote and Manos (1983) showed that the relative ranking of hydrocarbon fuels in terms of their sootiness in diffusion flames is not particularly sensitive to the measurement technique. This suggests that the relative sootiness of fuels will not depend importantly on the sample size, or the base point supply rates of excess fuel and nitrogen.

At present, the suggested test concept is in its early stages of develop-ment. Further data is needed for relating large-scale radiant fluxes in various fire situations in terms of measured fuel smoke-points. So far we have only used hydrocarbon fuels for evaluating the test concept. We do not know whether the principles can be extended to fuels having gas-phase chemical retardants. Also considerable effort will be required to develop a standard test method.

In spite of these caveats, one has little choice but to further investigate this suggested flammability test; because there are no other suggested alternative tests designed to assess flame radiative properties. Its bench-scale size and minimal material requirements should make it very attractive to the chemical industry; thereby eliminating the principal impediment to the development of truly fire-resistive materials.

REFERENCES

1. ASTM, "Standard Method for Room Fire Test of Wall and Ceiling Materials and Assemblies," ASTM Subcommittee E-5.13, Draft No. 6, August 1980.
2. Calcote, H.F. and Manos, D.M., "Effect of Molecular Structure on Incipient Soot Formation," Combustion and Flame, Vol. 49, No. 1-3, 1983.
3. Castino, G.T., Beyreis, J.R. and Metes, W.S., "Flammability Studies of Cellular Plastics and Other Building Materials Used for Interior Finishes," Underwriters Labs, Subject 723, 1975.
4. Delichatsios, M.A. and de Ris, J., "An Analytical Model for the Pyrolysis of Charring Materials," presented at the CIB-14 Meeting, Boras, Sweden (May, 1983).
5. Fisher, F.L. and Williamson, R.B., "Intralaboratory Evaluation of a Room Fire Test Method," UCB-FRG 82-1, University of California, Berkeley, 1982.
6. Huggett, C., "Estimation of Rate of Heat Release by Means of Oxygen Consumption Measurements," Fire and Materials , Vol. 4, No. 2, 1980.
7. Markstein, G.H., "Measurements on Gaseous-Fuel Pool Fires with a Fiber-Optic Absorption Probe," FMRC Technical Report 83-BT-1, March 1983.
8. Markstein, G.H., "Soot Formation, Radiant Emission and Absorption in Laminar Ethylene and Propylene Diffusion," Technical Report in preparation, July 1983.
9. Markstein, G.H., "Buoyant Plume Radiation," work in progress.
10. Masliyah, J.H. and Steward, F.R., "Radiative Heat Transfer from a Turbulent Diffusion Buoyant Flame with Mixing Controlled Combustion, Combustion and Flame, Vol. 13, pp. 613-625, 1969.
11. NFPA Fire Protection Handbook, 15th Edition, pp. 4-7, 1981.
12. Orloff, L., de Ris, J. and Markstein, G.H., "Upward Turbulent Fire Spread and Burning of Fuel Surfaces," Fifteenth Symposium (International) on Combustion, The Combustion Institute, pp. 1285-1294 (1975).
13. Orloff, L., Modak, A.T. and Alpert, R.L., "Burning of Large-Scale Vertical Surfaces," Sixteenth Symposium (International) on Combustion, The Combustion Institute, 1979.
14. Ostman, B., "Rate of Heat Release from Building Materials," FoU-Brand 1981/1982, Fire Research and Development News, Sweden.
15. Parker, J.A. and Kourtides, D., "Optimization of Fire Blocking Layers for Aircraft Seating," 7th International Conference on ire Safety, 1982.
16. Quintiere, J.G., Harkleroad, M. and Walton, W., "Measurement of Material Flame Spread Properties," NBSIR 82-2557, National Bureau of Standards, August 1982.
17. Schalla, R.L. and Hibbard, R.R., " Smoke and Coke Formation in the Combustion of Hydrocarbon-Air Mixture," Basic Considerations in the Combustion of Hydrocarbon Fuels with Air, Chapter IX, Report 1300, NACA, 1957.

18. Schug, K.P., Manheimer-Timnat, Y., Yaccarino, P. and Glassman, I., "Sooting Behavior of Gaseous Hydrocarbon Diffusion Flames and the Influence of Additives," Combustion Science and Technology, Vol. 22, pp. 235-250, 1980.
19. Smith, E.E., "Heat Release Rate of Building Materials," Ignition, Heat Release, and Noncombustibility of Materials, Ed. A.F. Robertson, ASTM Technical Publication 502, (1971).
20. Tewarson, A., "Heat Release Rate in Fires," Fire and Materials, Vol. 4, pp. 185-191, 1980.
21. Welker, J.R., Wesson, H.R., Sliepcevich, G.M., "Ignition of Alpha-Cellulose and Cotton Fabric by Flame Radiation," Fire Technology, Vol. 5, pp. 59-66, (1969).

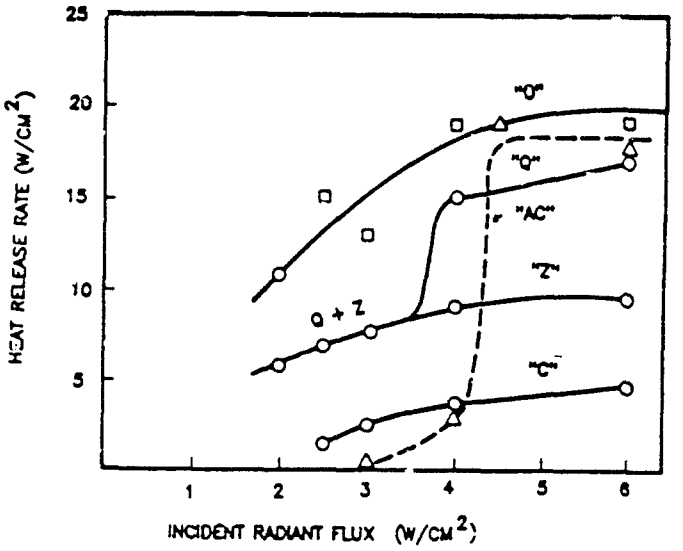

Figure 1: Heat Release Rate of Some Fire-Retarded Polyurethane (Coded According to Castino et al, 1975).

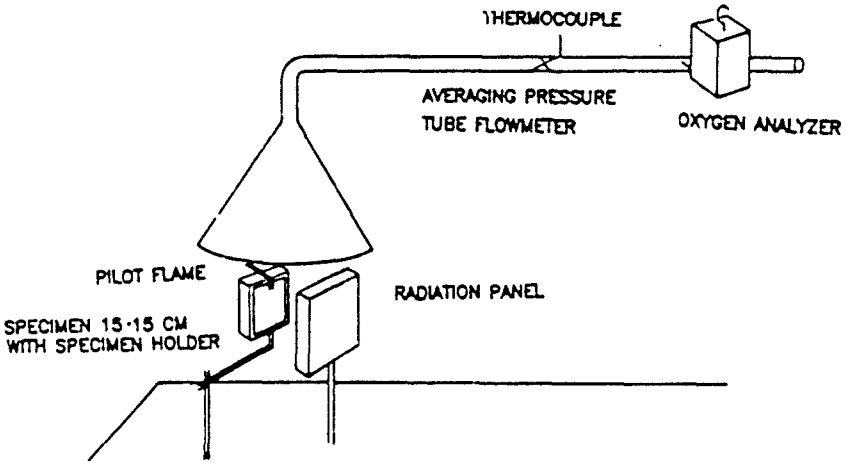

Figure 2A: Typical Rate-of-Heat-Release Apparatus (Ostman, 1982).

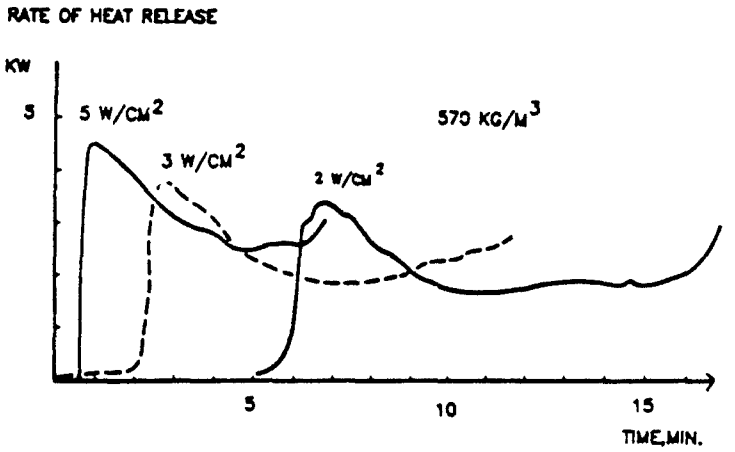

Figure 2B: Typical Rate-of-Heat-Release Curves versus Time for Charring Fuels (Ostman, 1982).

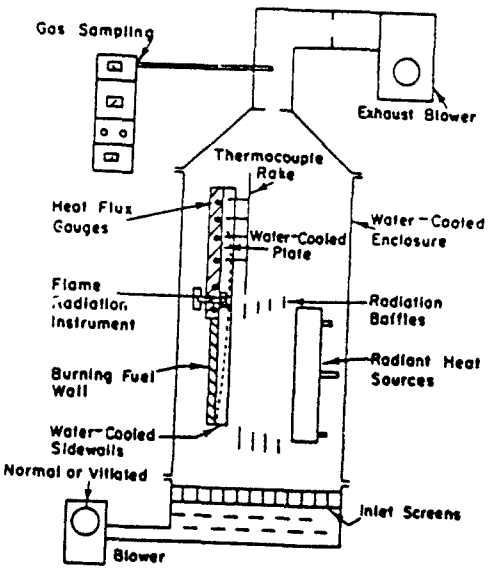

Figure 3: Material Flammability Apparatus of Measuring Flame Radiation in a Vitiated Atmosphere.

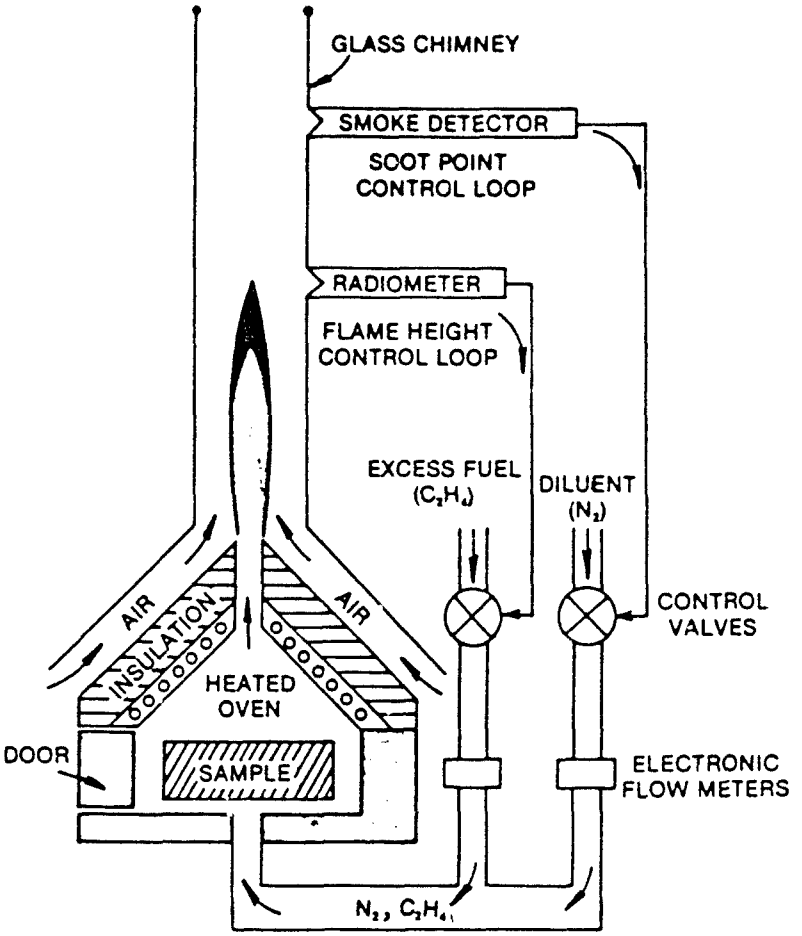

MATERIAL FLAMMABILITY TEST

Figure 4: Suggested Bench-Scale Material Flammability Apparatus for Measuring Both Rate-of-Heat Release and Flame Radiation.

SESSION IV

STRUCTURAL RESPONSE B

RELIABILITY OF ENGINEERED BASEMENTS AS BLAST SHELTERS

A. Longinow*, J. Mohammadi**, R.R. Robinson***

INTRODUCTION

This paper presents a method for predicting the reliability (probability of nonfailure) of basement shelters when subjected to the blast effects of a single nuclear weapon in its Mach region. The method is described with reference to a reinforced concrete basement shelter whose roof slab is the weakest structural component. This is generally the case in weak-walled conventional buildings when the first floor over the basement is at grade and the peripheral basement walls are not exposed but are in contact with the soil. In such basements, partial or total collapse of the slab results in casualties. Casualties would be produced by debris from the collapsed slab, the building above, and by pressure build-up within when the shelter envelope is breached. The objective then is to determine the probability of roof slab collapse and on this basis to determine the probability of people survival. The paper presents the method of analysis and illustrates its application by means of an example problem.

STRUCTURAL ANALYSIS

The form of structural analysis performed is described in Reference (1). The reinforced concrete slab is modeled as a single degree of freedom system whose flexural resistance is a piecewise linear function. The resistance function, see Figure 1, relates the flexural slab resistance to the deflection at its midpoint. Since shear is a possible mode of failure, the analysis is also concerned with peak dynamic reactions distributed along the edges of the slab.

The blast load is approximated by a function having an instantaneous rise to peak overpressure, followed by an exponential decay, see Figure 2. It has the following form (Reference 2).

$$F(t) = F_1(1 - t/t_d)e^{-t/t_d} \qquad (1)$$

where F_1 = peak overpressure

t_d = positive phase duration of the overpressure

The spacial distribution of the blast load is assumed to be uniform over the surface of the slab.

Since both the loading and resistance are complex functions, it was

* Associate Professor, Department of Civil Engineering, Illinois Institute of Technology, Chicago, IL 60616

** Assistant Professor, Department of Civil Engineering, Illinois Institute of Technology, Chicago, IL 60616

*** Senior Research Engineer, IIT Research Institute, Chicago, IL 60616

necessary to use a numerical procedure to obtain the peak midpoint deflection and the peak dynamic reactions. The primary equations used in the analysis are the following.

$$K_{LM}M_t\ddot{y} + R(y) = F(t) \tag{2}$$

where K_{LM} = the load-mass factor (Reference 1)

M_t = the total mass of the slab

$R(y)$ = flexural resistance

$F(t)$ = load=time history, see Equation (1)

$$V(t) = C_1R(y) + C_2F(t) \tag{3}$$

where $V(t)$ = the dynamic reaction along the given edge (a or b) of the slab, see Figure 3

C_1, C_2 = constants whose values depend on the aspect ratio of the slab

PROBABILITY OF FAILURE

In the case of two failure modes, the probability of slab failure, $P(F)$, is (Reference 3)

$$P(F) = 1 - [1 - P(F_b)][1 - P(F_v)] \tag{4}$$

when the modes are independent, and

$$P(F) = \max [P(F_b), P(F_v)] \tag{5}$$

when the modes are highly correlated. In Eqs. (4) and (5), $P(F_b)$ is the probability of failure due to flexure, and $P(F_v)$ is the probability of failure due to shear. The actual probability of failure is between these two bounds.

Probabilities of failure due to flexure and shear were each computed using the following expression

$$P(F) = 1 - \Phi\left\{\frac{\ell n(\tilde{r}/\tilde{s})}{\sqrt{\ell n[(1 - \Omega_R^2)(1 - \Omega_S^2)]}}\right\} = 1 - \Phi\left[\frac{\ell n\tilde{\theta}}{\zeta_\theta}\right] \tag{6}$$

where $\Phi(\ )$ = the cummulative density function of the standard normal distribution

$\tilde{r}$ = the median value of the resistance parameter in flexure or shear

$\tilde{s}$ = the median value of the load parameter in flexure or shear

Ω_R, Ω_S = coefficients of variation of the resistance and load parameters respectively

$\tilde{\theta}$ = median safety factor

ζ_θ = total degree of dispersion of the safety factor

For the case of flexural response the median safety factor $\tilde{\theta}$ is taken as the ratio of y_m/y_p, where y_m is the ultimate (collapse) midpoint deflection of the slab, see Figure 1, and y_p is the midpoint deflection at a given load. The value of y_m is taken as 0.15a, where "a" is the short span dimension of the slab (Reference 4).

For the case of shear response, the median safety factor is taken as the ratio of v_m/v_p, where v_m is the ultimate unit shear capacity of the slab and v_p is the corresponding shear stress at a given load. The shear stress is computed at the periphery of the slab by the use of dynamic reactions mentioned earlier. The ultimate unit shear capacity of the slab is based on the following formula which is the standard ACI (Reference 5) formula modified as suggested in Reference 6.

$$v_m = 1.5(2\sqrt{f'_{dc}}) \tag{7}$$

where $f'_{dc} = 1.25f'_c$ = the ultimate compressive strength of concrete increased to account for the increase in strength due to dynamic loading conditions (Reference 1)

SAMPLE APPLICATION

Figure 3 shows the plan view of a reinforced concrete slab whose reinforcing steel extends over and beyond the supports. Supports are continuous along the edges of the slab. The reinforcement in the short direction is $0.27(\text{in})^2/\text{ft}$ ($572\text{mm}^2/\text{m}$) and in the long direction is $0.19(\text{in})^2/\text{ft}$ ($402\text{mm}^2/\text{m}$). The slab is 9-in (228.6mm) thick. The compressive strength of concrete, f'_c = 3000 psi (20.7 MPa) and the yield strength of reinforcing steel, f_y = 60,000 psi (414 MPa).

In performing the analysis, the following parameters were treated as random variables, i.e., F_1, t_d, f'_c, f_y, A_s (cross-sectional area of reinforcing rods), d(effective depth of the slab).

Coefficients of variation of the basic parameters were obtained from available experimental data (Ref. 4, 7, 8). Corresponding coefficients of variation of slab resistance, peak deflection and peak shear stress were determined on the basis of a first order approximation, Reference 3.

This slab was analyzed when subjected to a series of blast loads of increasing intensity with durations corresponding to a 1-MT surface burst. Results of the analysis are shown in Figure 4 and Figure 5. Figure 4 shows the probabilities of failure in flexure and shear taken separately and determined on the basis of Eq. (6). Figure 5 shows the bounds on the probability of failure computed on the basis of (4) and (5).

SUMMARY AND CONCLUSIONS

A method for predicting the probability of failure of structures by considering multiple failure modes was formulated. It was applied to the analysis of a reinforced concrete slab when subjected to a uniformly distributed blast load over its surface. Currently available criteria for failure due to flexure and shear (Ref. 4 and 6) were used in predicting the probability of failure.

This method is capable of considering all major components of a structure, the respective failure modes of each component, and of predicting the probability of failure of the structure as a whole.

ACKNOWLEDGMENT

This study was supported by the Federal Emergency Management Agency under Contract EMW-C-0374.

REFERENCES

1. Biggs, J.M., "Introduction to Structural Dynamics", McGraw-Hill Book Company, 1964.

2. Glasstone, S., Ed. "Effects of Nuclear Weapons", U.S. Government Printing Office, Washington, D.C. 1964.

3. Ang, A.H. -S., et al., "Uncertainty and Survivability Evaluations of Design to Airblast and Ground Shock", For U.S. Army Construction Engineering Research Laboratory, Contract DACA-88-73-C-0040, A.H. -S. Ang Associates, Urbana, IL., June, 1974.

4. Wiehle, C.K. and Bockholt, J.L. "Dynamic Analysis of Reinforced Concrete Floor Systems", Contract DAHC20-71-C-0292 for Defense Civil Preparedness Agency, Stanford Research Institute, May, 1973.

5. "Building Code Requirements for Reinforced Concrete", (ACI318-77) American Concrete Institute Standard, 1977.

6. Crawford, R.E., et al., "The Air Force Manual for Design and Analysis of Hardened Structures", Air Force Weapons Laboratory, Albuquerque, NM., October, 1974.

7. Mirza, S.A., et al., "Statistical Description of Strength of Concrete", ASCE, Journal of the Structural Division, ST6, June, 1979.

8. Mirza, S.A., et al. "Variability of Mechanical Properties of Reinforcing Bars", ASCE, Journal of the Structural Division, STS, May 1979.

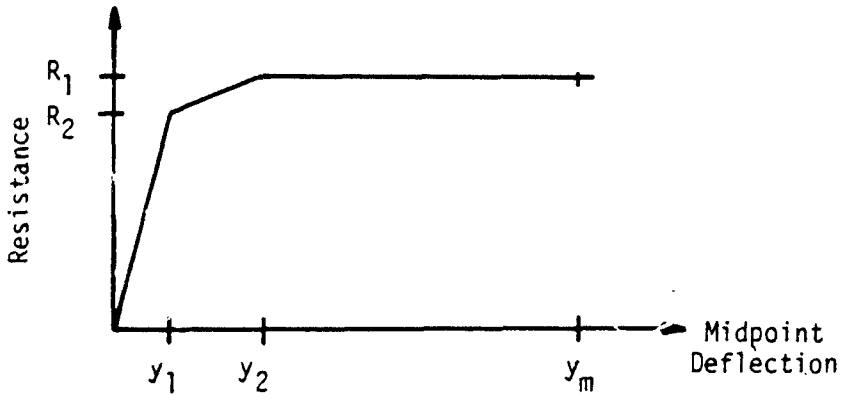

Fig. 1 Resistance Function*

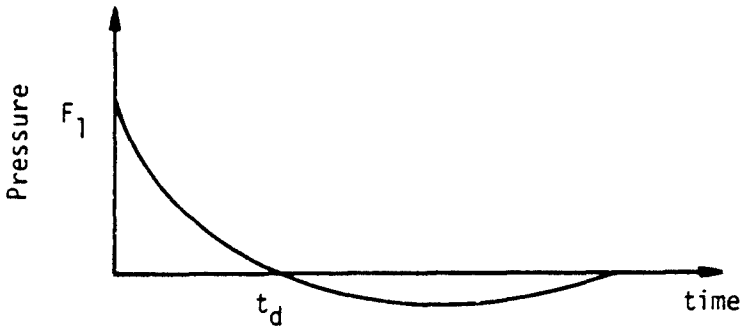

Fig. 2 Load Function

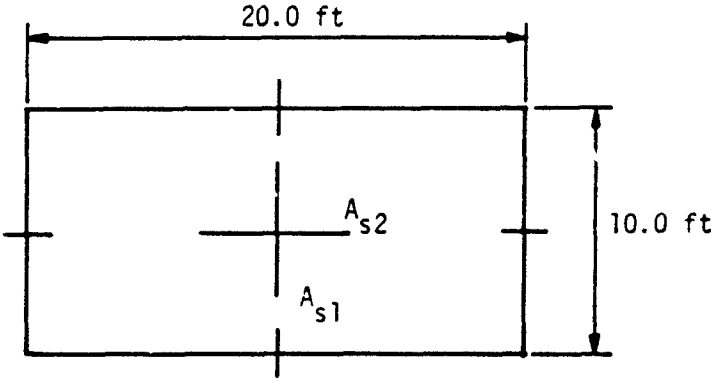

Fig. 3 Slab Dimensions

*R_1, y_1 = Resistance and deflection at the end of the elastic range

R_2, y_2 = Resistance and deflection at the end of the elasto-plastic range

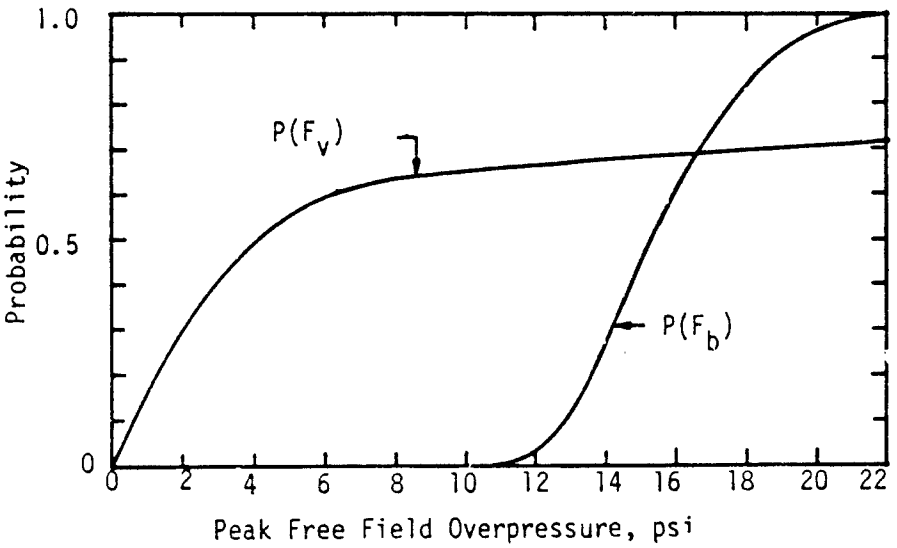

Fig. 4 Probabilities of Failure Due to Flexure and Shear

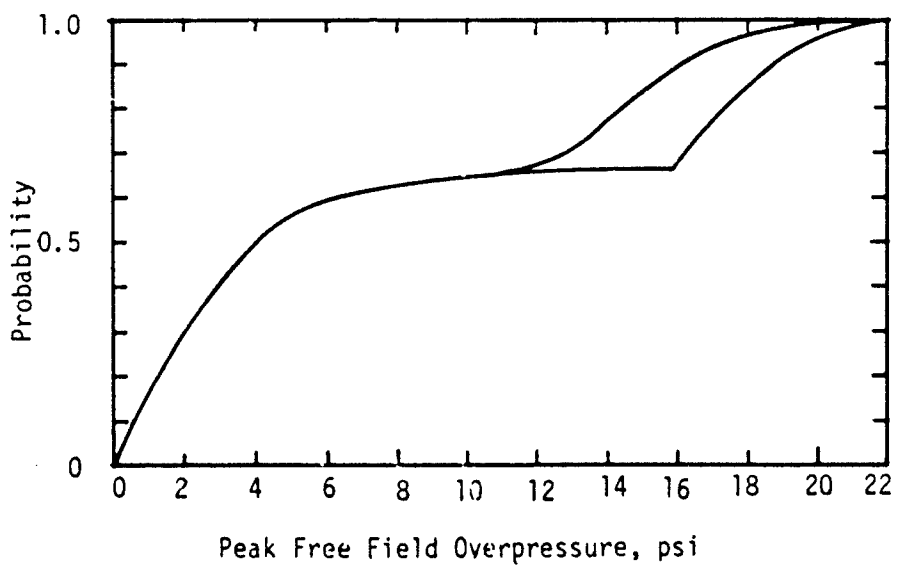

Fig. 5 Bounds on the Probability of Slab Failure

RELIABILITY OF RESIDENTIAL BASEMENTS AS BLAST SHELTERS

A. Longinow* and J. Mohammadi**

INTRODUCTION

This paper describes an analysis method for predicting the probability of failure of a wood-framed basement when subjected to a static, uniformly distributed load. The analysis considers the primary failure modes of each framing member and determines the probability of failure for each mode acting alone. The failure probability of the system as a whole is then bounded. The upper bound is determined on the assumption that the failure modes are independent, while the lower bound is determined on the assumption that the failure modes are perfectly correlated. The analysis is described with reference to an example problem.

DESCRIPTION OF THE STRUCTURE

Plan and elevation views of the wood-framed basement are shown in Fig. 1 and Fig. 2 respectively. The basement is lined with concrete block walls on footings. The floor is a thin concrete slab. The original framing system consists of joists supported by basement walls and girders, which are in turn supported by five wood columns. The flooring, consisting of two layers of 1-in. thick boards is nailed to the joists (Ref. 1).

This basement is an improvised shelter against the effects of blast. To this end, the original framing is strengthened by incorporating a studwall at the center of each of the two joist spans. There is one stud column under each joist in each span. The windows into the basement are blocked off and the protruding basement walls are mounded up to the level of the flooring. Sizes of the framing members considered in the analysis are given next.

Joists: 1.625-in by 5.625-in with an average spacing of 24.12-in
Girders: 5.5-in by 6.75-in
Columns: 4.0-in by 8.0-in
Studwalls: Columns 2.0-in by 4.0-in with bracing at midheight
The material is Jack Pine.

STRUCTURAL ANALYSIS

The joists are continuous over the girders and the studwalls are simply-supported at the basement wall. Experimental results (Ref. 1) indicate that flooring nailed to joists does not result in full composite action between the joists and the flooring and therefore the joists are analyzed as being independent of the flooring.

Girder 1 is simply-supported on column 1 and column 3 and is continuous over column 2. Girder 2 is simply-cupported on column 3 and the basement wall and is continuous over columns 4 and 5. The columns are analyzed

* Associate Professor, Department of Civil Engineering, Illinois Institute of Technology, Chicago, Illinois 60616
** Assistant Professor, Department of Civil Engineering, Illinois Institute of Technology, Chicago, Illinois 60616

as pin-ended. The extent to which the girders and the studwalls provide flexible supports for the joists is neglected. The loading consists of pressure applied uniformly normal to the floor surface.

Computed stresses are compared to ultimate (incipient failure) stresses which were determined based on a load duration of 1 sec (Ref. 2). To this extent the results approximate the load carrying capacity of the structure when subjected to a uniformly distributed dynamic loading (Ref. 3). These ultimate stresses are given as follows (Ref. 2):

F_b = Rupture (Bending) Strength = 7,100 psi

F_c = Compression Strength Parallel to the Grain = 6,050 psi

F_v = Shear Strength Parallel to the Grain = 750 psi

E = Modulus of Elasticity = $1.35(10)^6$ psi

PROBABILISTIC ANALYSIS AND RESULTS

The framing system is analyzed when subjected to a series of loadings of increasing intensity. At each loading a probability of failure is estimated as being between two bounds. Upper bound failure probability $P(F^*)$, is determined on the assumption that conditions between different components are such that the failure modes are independent. Lower bound failure probability $P(F')$, is determined on the assumption of perfect correlation between components and is based on the highest failure probability of one failure mode occuring in some one component of the system. These bounds are defined as follows:

$$P(F^*) = 1 - \prod_{i-1}^{n} [1 - P(F_i)] \qquad (1)$$

$$P(F') = \max[P(F_1), P(F_2), \ldots, P(F_n)] \qquad (2)$$

where $P(F_i)$, $i = 1, n$ are individual failure mode failure probabilities occuring in the various components. In the analysis of joists and girders, failure modes considered were flexure and shear. In the case of columns and studwalls the only failure mode considered was buckling. For the purpose of illustration, the failure probability of a joist is calculated next.

FAILURE PROBABILITIES OF JOISTS

A joist can fail in flexure or in shear. If these two modes are independent of each other then the failure probability of the joist is

$$P(F_j) = 1 - [1 - P(F_1)][1 - P(F_2)] \qquad (3)$$

On the other hand, if the two modes are perfectly correlated, the failure probability is

$$P(F_i) = \max[P(F_1), P(F_2)] \qquad (4)$$

Expressions (3) and (4) bound the actual failure probability. In (3) and (4), $P(F_1)$ and $P(F_2)$ are failure probabilities due to flexure and shear

respectively. They are computed as follows:

$$P(F_i) = 1 - \Phi\left(\frac{\ell n \theta_i}{\Omega_{\theta_i}}\right) \tag{5}$$

where Φ ( ) = standard normal distribution

$\bar{\theta}_i$ = the mean safety factor in flexure or shear

Ω_{θ_i} = coefficient of variation of the mean safety factor in flexure or shear

$$\bar{\theta}_1 = \bar{N}_{g1}\bar{F}_b\bar{S}/\bar{M} \tag{6}$$

where $\bar{N}_{g1}$ = correction factor on the flexure formula

$\bar{F}_b$ = modulus of rupture

$\bar{S}$ = section modulus = $bh^2/6$, where b and h are the width and depth of the cross-section

$\bar{M}$ = maximum moment acting on the joist

$$\Omega_{\theta_1} = \sqrt{\Omega_{g1}^2 + \Omega_{F_b}^2 + \Omega_S^2 + \Omega_M^2} \tag{7}$$

where the parameters inside the radical are coefficients of variation of 1) correction factor on the flexure formula, 2) modulus of rupture, 3) section modulus, 4) maximum moment.

Assuming perfect correlation between "b" and "h", the coefficient of variation of "S" can be computed from

$$\Omega_S = \sqrt{\Omega_b^2 + 4\Omega_n^2 + 4\Omega_b\,\Omega_h} \tag{8}$$

where Ω_b and Ω_n are coefficients of variation of "b" and "h" respectively.

$$\bar{\theta}_2 = 2\bar{N}_{g2}\bar{F}_v\bar{A}/3\bar{V} \tag{9}$$

where $\bar{N}_{g2}$ = correction factor on the shear formula

$\bar{F}_v$ = shear strength parallel to the grain

$\bar{A}$ = cross-sectional area of joist = bh

$\bar{V}$ = maximum shear acting on the joist

$$\Omega_{\theta_2} = \sqrt{\Omega_{g2}^2 + \Omega_{Fv}^2 + \Omega_A^2 + \Omega_V^2} \tag{10}$$

where the parameters inside the radical are coefficients of variation of 1) correction factor on the shear formula, 2) shear strength, 3) cross-sectional area of joist, 4) maximum shear.

Assuming perfect correlation between "b" and "h", the coefficient of variation of "A" can be computed from

$$\Omega_A = \sqrt{\Omega_b^2 + \Omega_h^2 + 2\Omega_b\,\Omega_h} \tag{11}$$

The values of N_{g1} and N_{g2} and the coefficients of variation of p, b, h, N_{g1}, N_{g2}, F_b and F_v were estimated on the basis of available data and engineering judgment. Estimated and computed parameters used in computing $P(F_1)$ and $P(F_2)$ are listed in Table 1. From (5) and data in Table 1:

$$P(F_1) = 1 - \Phi\left[\frac{\ell n(3.79/\bar{p})}{0.354}\right] \tag{12}$$

$$P(F_2) = 1 - \Phi\left[\frac{\ell n(3.898/\bar{p})}{0.317}\right] \tag{13}$$

The failure probability of the joist system is represented in Fig. 3. The upper bound was determined using (3). The lower bound was determined from (4) and is the failure probability due to shear, $P(F_2)$.

Note, that when all joists are identical and subject to the same load distribution and intensity, then conditions between the joists are perfectly correlated. On this basis the failure probability of the joist system is presented by the failure probability of one joist.

The failure probability of the entire framework, considering the joist system, girders and columns, is represented in Fig. 4. The upper bound was determined on the basis of (1) and the lower bound on the basis of (2). The lower bound is the failure probability of the stud-wall located in the east span, see Figure 1.

CONCLUSIONS

The results of the analysis are an upper bound at least because the flexibilities of the girders, the columns and the studwalls are neglected when calculating the response of the joists.

Note that the bounds on the failure probability for the system are fairly close together (See Fig. 4). Therefore the upper bound can conservatively be taken as the failure probability for the system.

ACKNOWLEDGMENT

This paper is based on a study which was supported by the Federal Emergency Management Agency, Washington, D.C. under Contract EMW-C-0374.

REFERENCES

1. Longinow, A. and Joyce, R.P., Load Tests of a Wood Floor Over a Basement, Contract DCPA01-78-C-0223, for Federal Emergency Management Agency, IIT Research Institute, Chicago, Il., June 1980.
2. Wood Handbook, Agriculture Handbook 72, Forest Products Laboratory, U.S. Department of Agriculture, Revised August 1974.
3. Gabrielsen, B.L. Blast Upgrading of Existing Structures, for Defense Civil Preparedness Agency, Contract DCPA01-77-C-0205, Work Unit 1127G, Scientific Service, Inc. Redwood City, California, January 1979.

Table 1. Parameter Values Used in Sample Problem

$M^* = 9759\bar{p}$ lb-in	$\Omega_M = 0.20$
$V^* = 891\bar{p}$ lb	$\Omega_V = 0.20$
$b = 1.625$-in	$\Omega_b = 0.07$
$h = 5.625$-in	$\Omega_h = 0.07$
$N_{g1} = 0.95$	$\Omega_{g1} = 0.03$
$N_{g2} = 0.95$	$\Omega_{g2} = 0.03$
$S^{**} = 5.585(\text{in})^3$	$\Omega_S = 0.21$
$A = 7.313(\text{in})^2$	$\Omega_A = 0.14$
$F_b = 7100$ psi	$\Omega_{F_b} = 0.20$
$F_v = 750$ psi	$\Omega_{F_v} = 0.20$
$\theta_1 = 3.790/b$	$\Omega_{\theta_1} = 0.354$
$\theta_2 = 3.898/b$	$\Omega_{\theta_2} = 0.317$

* The joist is supporting a uniformly distributed line load equal to $16\bar{p}$ per inch, where $\bar{p}$ is in psi.

** The section modulus was calculated using a depth equal to 0.8h to account for possible notches or knots.

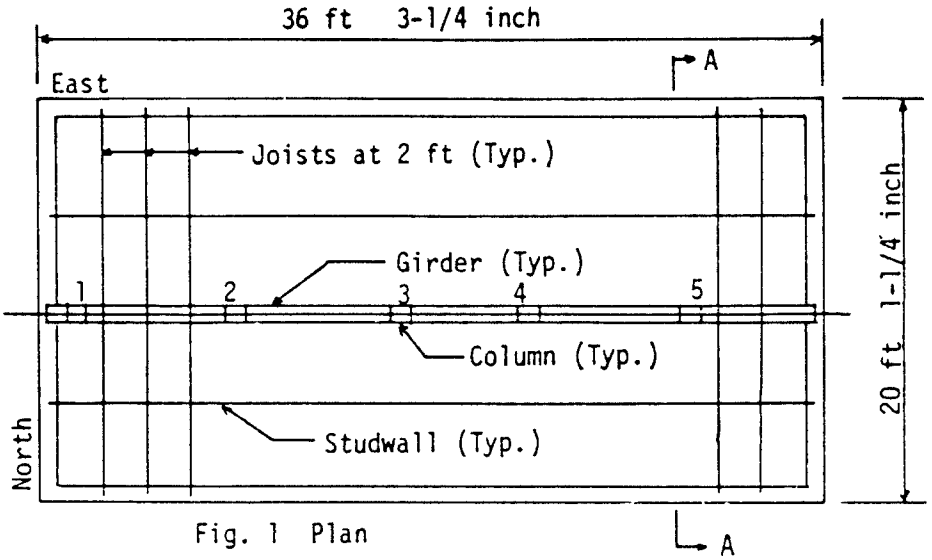

Fig. 1 Plan

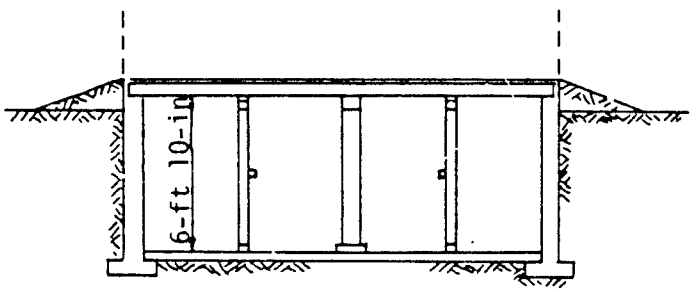

Fig. 2 Section A-A, Elevation

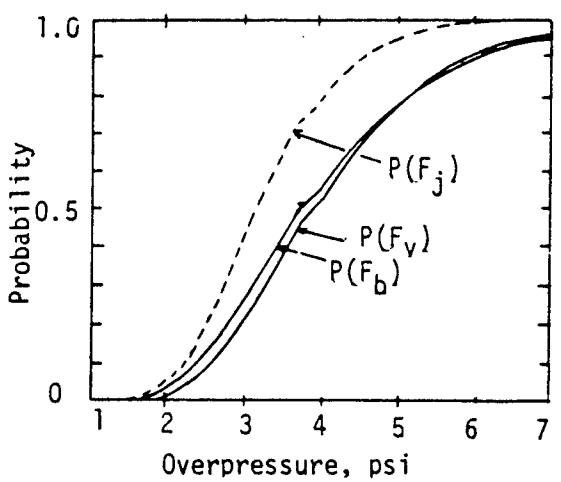

Fig. 3. Probability of Joist Failure

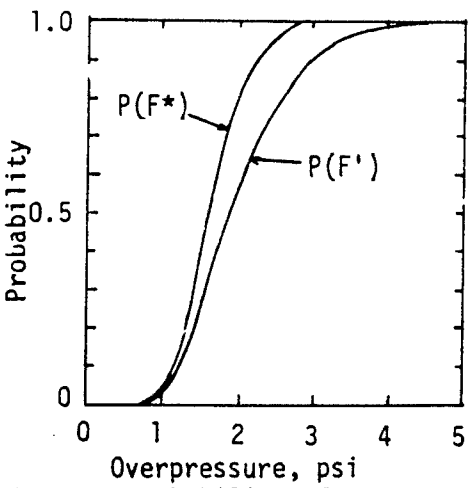

Fig. 4 Probability of System Failure

DESIGN VALIDATION EXPERIMENTS FOR THE KEY WORKER BLAST SHELTER

By
S. A. KIGER and T. R. SLAWSON
USAE Waterways Experiment Station (WES)
Vicksburg, MS

ABSTRACT

Design calculations for the blast shelter included the effects of soil arching. In the past, soil arching has been ignored for dynamic loads at shallow burial depths; however, recent test data indicate structural loading is significantly reduced by arching, even at very shallow burial depths. The result is a more efficient structural design than was previously thought possible.

Experiments to be conducted on 1/4-scale structural elements during June through October 1983 will provide loading and response data for the structural design. Specific design parameters that will be investigated include depth of burial, backfill soil specifications. concrete strength, and the effects of multiple weapon detonations. Static testing, using the Large Blast Load Generator facility at WES, will be conducted in the laboratory. All dynamic testing will be performed at remote field sites using a High-Explosive Simulation Technique known as a Foam HEST to simulate nuclear overpressures. Instrumentation will document the overpressure loading, free-field stresses and motions in the backfill, interface loads on the buried structure, structural deformations, and instructure shock levels. Results from these experiments will be used to validate and/or improve the blast shelter design and the computational procedures used for the design calculations.

INTRODUCTION

This research program is jointly sponsored by the Federal Emergency Management Agency (FEMA) and the Defense Nuclear Agency (DNA), and is being conducted by personnel in the Structural Mechanics Division of the Structures Laboratory at WES.

Key worker shelters will be used to house personnel operating critical industry within high-risk areas of the country during and after a nuclear attack. Current civil defense planning calls for the evacuation of nonessential personnel to safe (lower risk) host areas, and the construction of approximately 20,000 to 40,000 shelters to protect the key workers remaining behind. Both deliberate- and expedient-type shelters are planned. The current deliberate shelter designs are 100- and 400-man capacity, and the expedient shelter designs are 20- to 30-man capacity. The specifications require that the shelters be capable of resisting the blast loading, radiation, and associated effects at the 50 psi overpressure level for a 1-Mt weapon. The FY83 research program will concentrate on supporting the design of a deliberate facility. Expedient shelter design concepts will be tested in FY84.

Computational procedures developed in the DNA sponsored Shallow Buried Structures research program at WES have been used for design calculations. Therefore, the shelter designs take full advantage of the load mitigating effects of soil-structure interaction, the initial capacity increasing effects

of inplane thrust loads in the structure roof, and large deflection membrane resistance of the roof slab. These effects allow a much more cost efficient design than would otherwise be possible. However, careful attention must be given to backfill specifications, to assure that the soil friction forces required for soil arching will occur, and to concrete strength and reinforcement details, to assure that the roof can respond as a membrane without premature failure.

The USAE Huntsville Division (HND) is responsible for the shelter designs. The floor plan of the HND 100-man shelter design is shown in Figure 1. This research program will evaluate the design details used in this 100-man blast shelter.

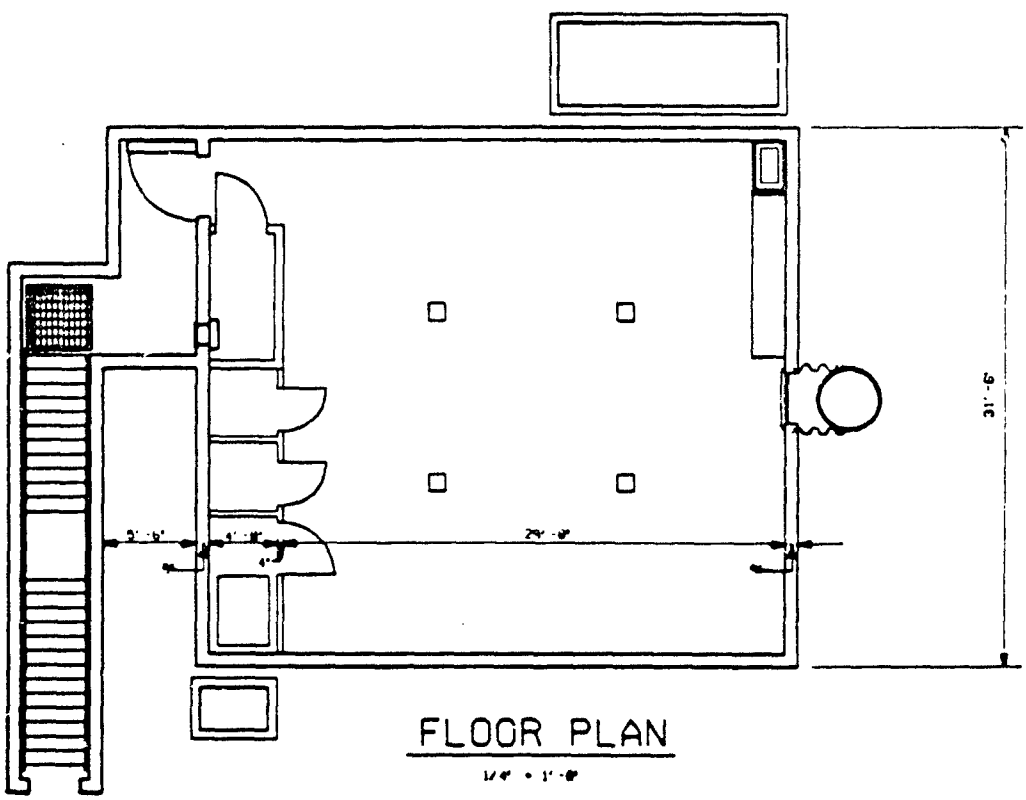

Figure 1. 100-man blast shelter from Mr. Paul LaHoud, USAE, Huntsville Division.

OBJECTIVES

(1) Verify computational procedures used for design calculations: The calculational methods are based on structural response data collected in test at 2,000 to 10,000 psi. These data need to be verified at the 50 psi overpressure level.

(2) Evaluate structural design concepts: Test data will be used to evaluate design concepts, such as the use of corrugated sheet metal to form the roof and protect against fragments, and the effectiveness of the beam-column

construction supporting the concentrated loads that will be arched onto the roof beams.

(3) Investigate and recommend minimum allowable concrete strength specifications: To take full advantage of soil arching, the structure is relatively flexible and large roof deflections are expected. However, the concrete must be strong enough to prevent bond failure at the roof supports when the roof is responding in the membrane mode.

(4) Investigate and recommend backfill specifications: Because soil arching is assumed in the design calculations, it is very important that a high shear strength backfill be used. However, to minimize cost, the backfill specifications should be as unrestrictive as possible.

(5) Develop structural response computational procedures to predict response from multiple weapon detonations: Two of the test structures will be retested to obtain response and loading data from multiple loadings, and to document large response failure modes.

(6) Evaluate stirrup reinforcement configuration: Reinforcement ties between the tension and compression rebar mats can significantly increase the moment capacity of a cross section and improve the roof performance as it responds in a tensile membrane mode. The increased moment capacity results from the increased concrete confinement provided by the stirrup reinforcement. As the roof responds into the tensile membrane mode, the stirrup ties will confine the cracked concrete and force the two reinforcement mats to respond as a unit. In practice, placing these ties is a labor intensive, costly, item. Therefore, alternate, easily installed, stirrup configurations will be evaluated.

TEST PLAN

A series of static and dynamic tests, using 1/4-scale box structures and box structural elements will be conducted. Static tests using the Blast Load Generator facilities at the WES and dynamic tests using a High-Explosive Simulation Technique (HEST) to simulate nuclear overpressures at a remote field test site will be performed. In addition to the two test structure types shown in Figure 2, a one-way slab element will be used for the shear stirrup

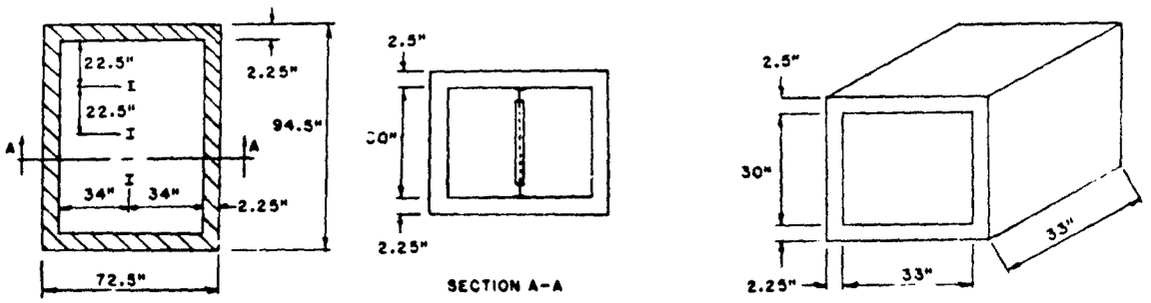

a. Type 1 Element

b. Type 2 Element

Figure 2. Test elements.

configuration tests. The Type 1 structure will be used to investigate roof-wall interaction, the girder-column design, and the girder-wall interaction. The Type 2 element will be used to investigate concrete strength, backfill types, and effects of depth of burial. Reinforcement details for both Type 1 and 2 elements are shown in Figure 3.

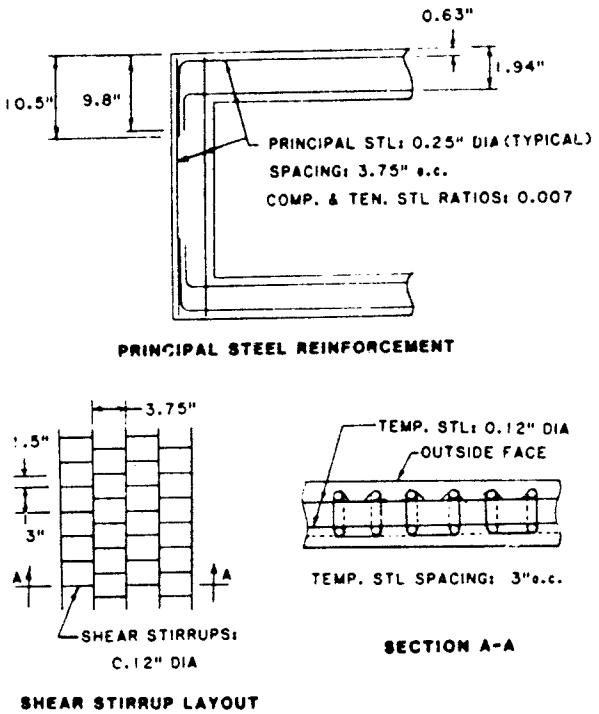

Figure 3. Steel reinforcement details.

Table 1 presents a test matrix showing the parameter to be investigated and number of tests. The Type 1 element will be a baseline test. The first static and dynamic test on Type 2 elements will have the same test configuration as the Type 1 element tests, to establish a basis of comparing the results of the remaining Type 2 element tests to the baseline tests.

Approximately 500 channels of data will be recorded during these tests. Airblast gages will document the overpressures generated by the Foam HEST, soil stress gages will be used to measure the free field stress environment, interface pressure gages will record the magnitude and distribution of pressure on the roof, walls, and floor of the structure, and strain, deflection, and acceleration gages will document structural response.

ANALYSIS

Several pretest calculations have been performed. Iso-damage curves for design level damage (maximum roof deflection equal 5% of roof span), and for severe damage (maximum roof deflection equal 20% of roof span) are shown in Figure 4. Numbers shown on the curves are ranges (in ft) at which the indicated overpressure occurs from a surface burst. The structural configuration

Table 1. Test matrix.

Test Parameters	Element Type	f'_c psi	Backfill	DOB ft	Number of Tests Static	Number of Tests Dynamic
Baseline	1	4000	Sand	1	1	1
Baseline	2	4000	Sand	1	1	1
Concrete strength	2	2500	Sand	1	1	1
Backfill type	2	4000	*	1	2	2
Depth of burial	2	4000	Sand	0	1	1
Multiple hits**	1 or 2	4000	Sand	1	0	1 or 2
Alternate shear stirrup designs	Slab	4000	Sand	0	6-10	0

* Two alternate backfill types are to be tested.

** Multiple hits will be made on a previously tested Type 1 or 2 element.

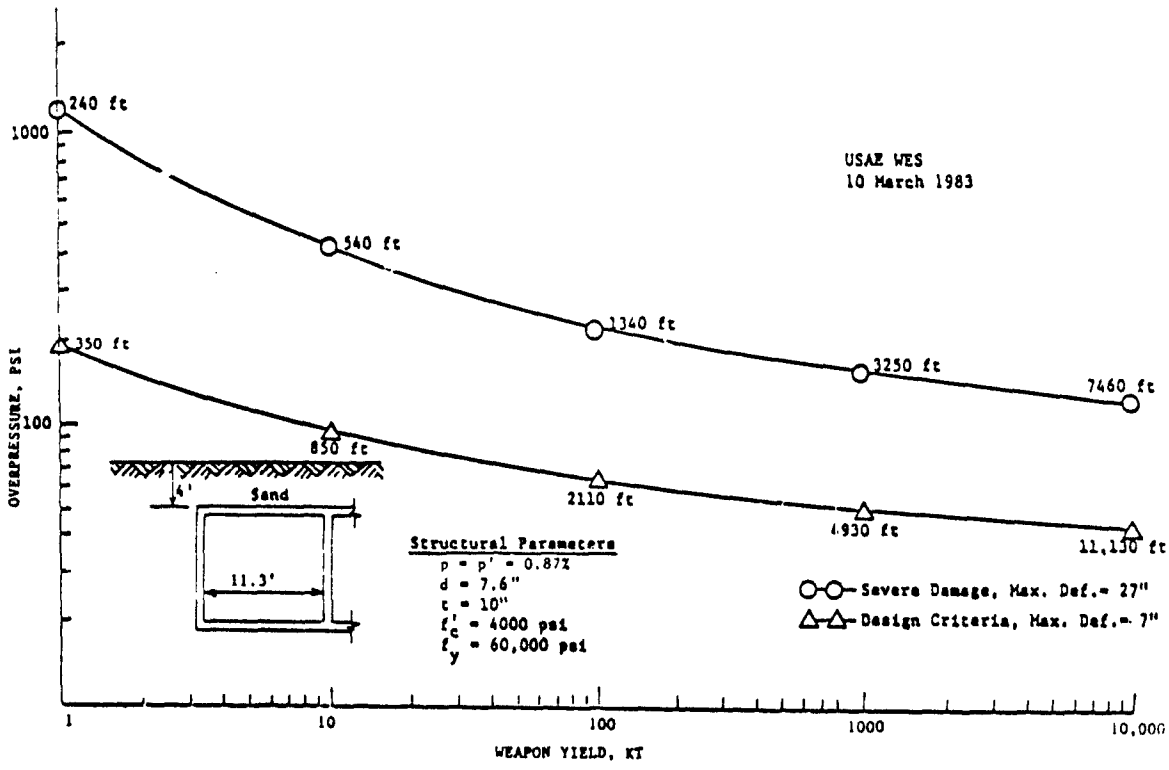

Figure 4. Iso-damage curves for 100-man capacity key worker blast shelter.

and structural parameters are shown in Figure 4, where p is percent of reinforcement steel, d is the effective depth of the roof, t is the total thickness of the roof, f'_c is the compressive concrete strength, and f_y is the yield strength of the reinforcement steel. In Figure 5 the structure described in Figure 4 is analyzed in sand and clay backfill materials at various depths-of-burial (DOB). The angle ϕ (PHI) is the angle of shear capacity for the backfill soil. The computer program RCCOLA (1) was used to investigate the effect of shear stirrup spacing. Results of this analysis indicate that a 6 in. stirrup spacing will assure flexural response without a premature shear failure.

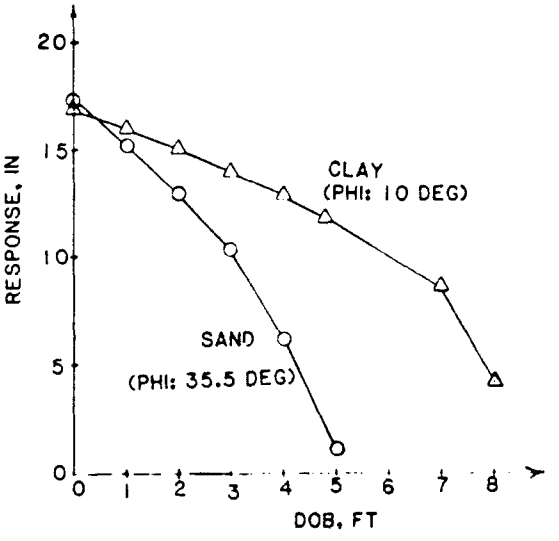

Figure 5. Response vs. depth of burial for a 1 mt weapon at an overpressure of 50 psi for two backfills

REFERENCES

1. S. A. Mahin and V. V. Bertero, RCCOLA, A Computer Program for Reinforced Concrete Column Analysis; User's Manual and Documentation, Department of Civil Engineering, University of California, Berkeley (1977).

STRUCTURAL RESPONSE OF THE SATCOM ANTENNA TO A BLAST LOADING

Joseph M. Santiago & Bahaaeldin I. Shehata

U.S. Army Ballistic Research Laboratory
Aberdeen Proving Ground, Maryland

ABSTRACT

The accuracy of the ADINA finite element program in modeling the transient response of a dish shaped antenna has been evaluated. Computed strain histories were compared with strain gage records from a simulated nuclear blast test performed on the antenna. With an 839 degrees-of-freedom finite element model, the program reproduced the salient features of the response, although a close correspondence between computed and test results was not realized. The study, however, did demonstrate that the model is sufficiently accurate for survivability estimates.

I. INTRODUCTION

A shock tube test simulating a nominal 2.5 psi nuclear blast was performed on the SATCOM antenna and strain gage records were collected. The corresponding pressure loading was determined in a series of tests on a scale model of the antenna's reflector. The loading data were used in the ADINA finite element model of the antenna to calculate the strain histories at the gage locations. The accuracy of the finite element model was evaluated by comparing the computed strain histories with the strain gage records.

II. SATCOM ANTENNA

The SATCOM antenna is a component of the AN-GSC-86 satellite communication ground terminal developed by the U. S. Army Satellite Communication Agency (SATCOM). The antenna consists of a dish shaped reflector connected at the back to the tracking mechanism which is supported by a quadrupedal truss assembly. The reflector itself comprises a 1.22 m (4 ft) diameter center section to which the tracking assembly attaches, and four identical petal sections that attach to the periphery of the center section and to each other to form a rigid, paraboloidal dish 2.44 m (8 ft) in diameter. Figure 1 illustrates this arrangement and also indicates schematically the monocoque construction of the reflector, consisting of front and rear skins which attach every 15^{0} to radial ribs, with circumferential rings capping the component sections along their common interface.

III. SHOCK TUBE TESTS

Two series of tests were performed at the shock tube facility. In the first series a sample of the actual antenna was exposed to a series of progressively larger blast waves emanating from the open end of the BRL 2.44 m (8 ft) diameter shock tube (1). The antenna was mounted facing the

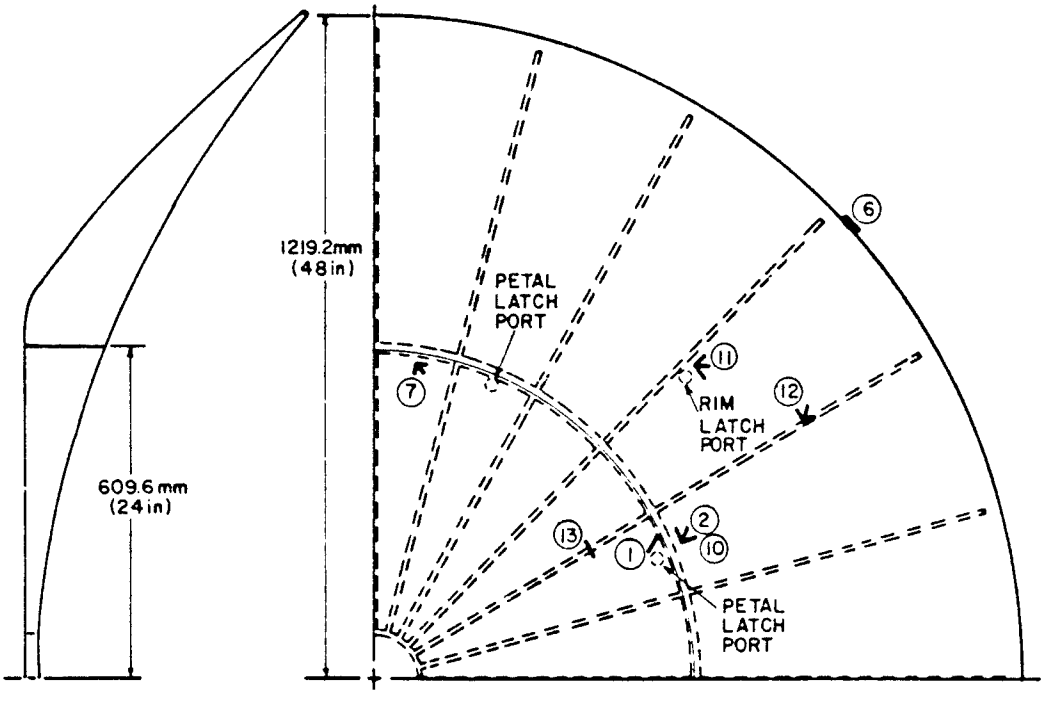

Figure 1. Front view of the upper-right quadrant and cross-section of the SATCOM antenna reflector.

open end along a line 24° to the side of the tube axis. Strain gages were cemented to the skin of the reflector at locations 1, 2, 6, 7, 10, 11, 12, 13 in the upper-right quadrant as indicated in Figure 1. The strain records chosen for comparison were from the last test of the series, in which the antenna at a distance of 12.2 m (40 ft) from the open end was exposed to a 17.2 kPa (2.5 psi) free-field blast.

The second series of tests was performed on a scale model of the reflector at a corresponding location outside the BRL 0.575 m (22.6 in) diameter shock tube (2). The purpose was to determine the loading function for the finite element analysis from pressure measurements on the model. The model was scaled in proportion to the ratio of the shock tube diameters (0.575/2.44 = .236). A row of pressure transducers was imbedded along a radius flush with the front and rear faces, as illustrated in Figure 2.

The model was located at a scaled distance of 2.87 m (9.4 ft) from the open end of the shock tube and subjected to a free-field pressure of 13.8 kPa (2.0 psi) in a series of tests in which the row of transducers was rotated by increments of 45°. It was found that the pressure distribution varied little with angle, so that the profiles along the vertical radius depicted in Figure 2 typify those found along the other radial directions. This result made it convenient to use an axisymmetric loading function obtained by circumferentially averaging the experimental pressure data.

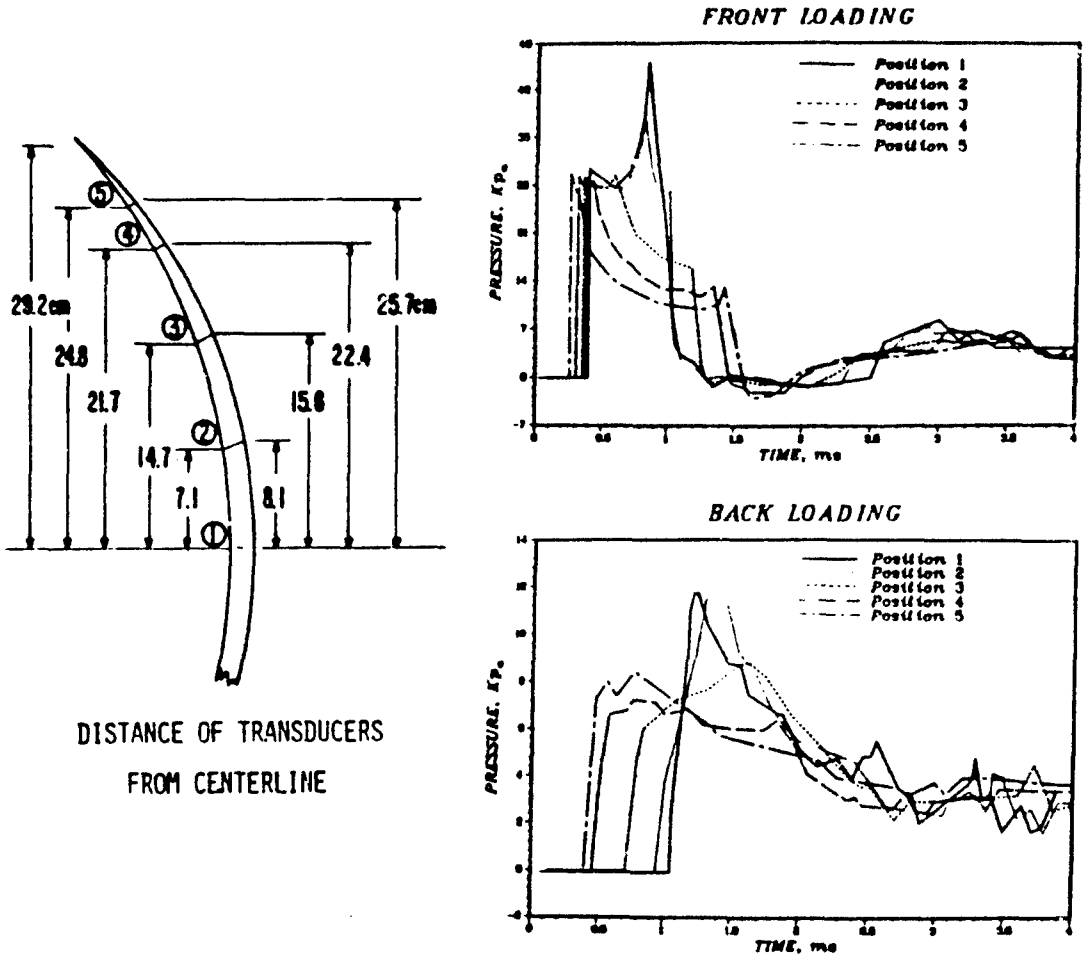

Figure 2. Location of transducers on scale model and corresponding pressure records along a vertical radius.

Of the elements available in the ADINA finite element program (3), the three-dimensional plane stress element was chosen as the most suitable for modeling the sheet metal construction of the reflector. Use of an axisymmetric loading function allowed us to take advantage of the two planes of structural symmetry of the reflector to model only one quadrant, as illustrated in Figure 3. The rim and petal latchings were simulated by having the reflector components share common nodes at their points of attachment. Assuming that the tracking and support assembly was rigid compared to the reflector, the nodes at the points of attachments to this assembly were fixed. Except at the common nodes connecting the petals to the center section, the elements employed 4 nodes. This resulted in the reflector being modeled by a total of 342 elements, using 306 nodes with 839 degrees-of-freedom.

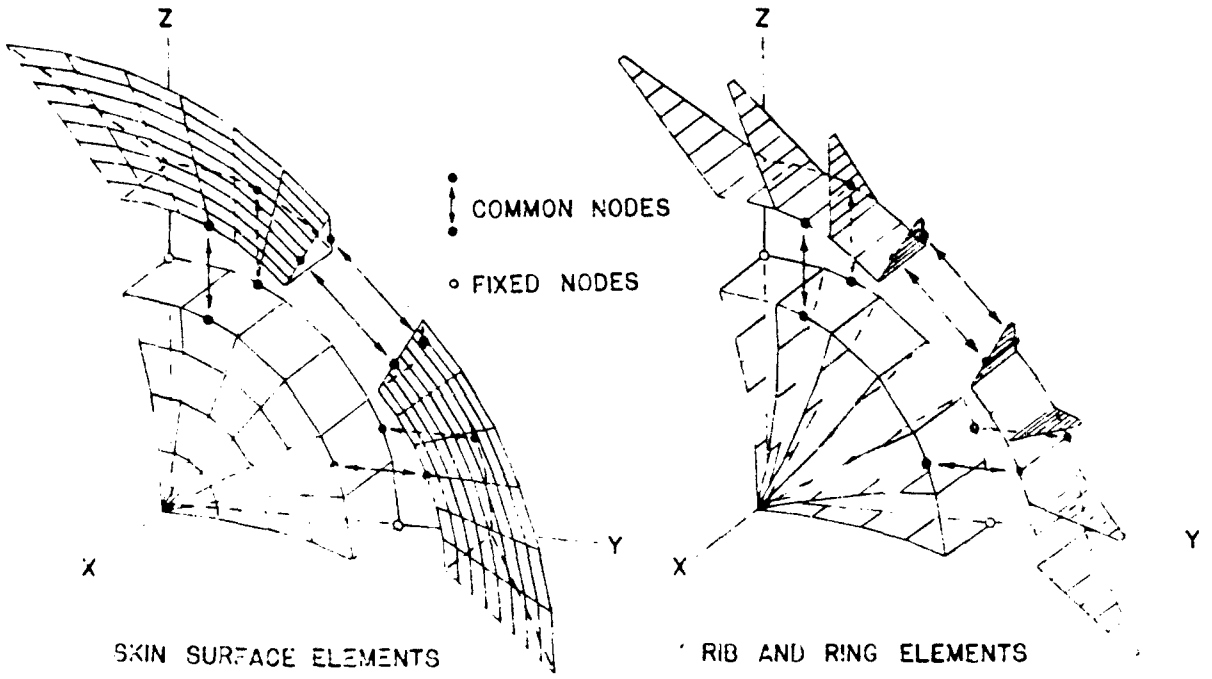

Figure 3. Exploded views of the finite element model of the upper-right quadrant of the reflector.

Since the recorded strains were well within the elastic limit, a linear analysis sufficed. Hence, only the elastic constants for the aluminum,

Young's Modulus = 68.95 GPa (10^7 psi) & Poisson's Ratio = 0.3

had to be specified. The thickness of the center section elements was taken as 1.613 mm (0.0635 in) and the petal elements as 1.359 mm (0.0535 in), and the density was set equal to 2768 Kg/m^3.

In addition to the loading data being circumferentially averaged, as already mentioned, these data were extended by interpolation over the entire surface of the reflector to provide full-field pressure histories for the analysis. Moreover, the pressure levels had to be proportionally scaled from the nominal 13.8 kPa of the model tests to the 17.2 kPa of the full-scale test, and the time scale had to be expanded by a factor of 1/.236 to account for the difference in loading times between the model and the antenna. Also, since the expansion only provided data for the first 16 ms, while it was intended to compare strains over the first 50 ms, the last recorded values of the pressures were maintained constant till the end.

The long duration of 50 ms made it advisable to choose the Newmark implicit time integration method. Employing the default values of the Newmark parameters (a = 1/4 and w = 1/2), the calculation was carried out for a total of 50 cycles using a time step of 1.0 ms, and the strain histories at points corresponding to the gage locations were computed.

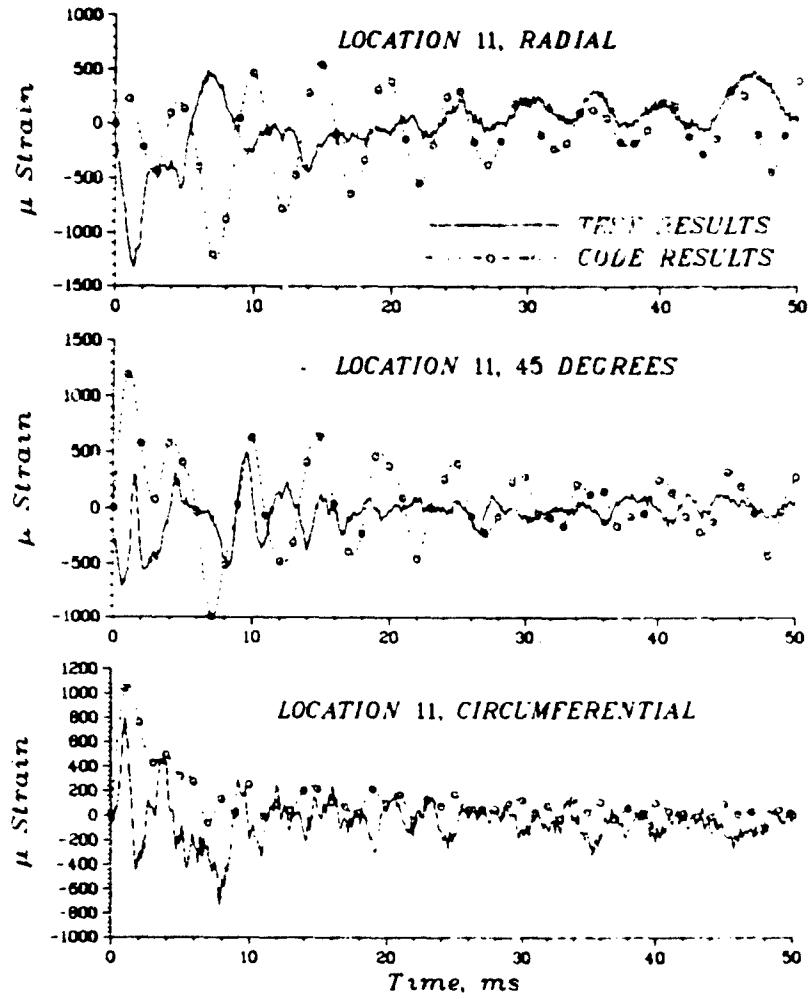

Figure 4. Comparison of computed and recorded strain histories at strain rosette location 11.

V. COMPARISON OF RESULTS

We focus on a comparison with the three strain histories recorded by the rosette at strain location 11 (see Figure 1). The degree of correlation, as shown in Figure 4, is typical of that achieved at the other locations, in that the computed results more-or-less capture the prominent features of test results, although the details, especially near the beginning, are missed. By comparing periods and ranges of amplitude in the table below, we see that correspondence is closest in the radial and circumferential directions and somewhat poorer at 45^0.

In general, it was found that computed and experimentally determined amplitudes and frequencies at all gage locations were of the same order, although the curves did not agree very closely over the entire interval. Nonetheless, the correlation is surprisingly good when we consider, in addition

Gage Direction	Period (ms)		Range of Amplitude (microstrain)	
	Test	ADINA	Test	ADINA
Radial	5	5	-1350 + 500	-1210 + 537
45°	2.6	5	- 730 + 500	-1000 +1190
Circumferential	2.7	2.1	- 750 + 800	- 98 +1040

to the modest size of the finite element model and the aforementioned simplifications, the structural details that were unaccounted for and the uncertainty in the loading function. For example, no attempt was made to reproduce the details of the latching mechanisms. Moreover, the analysis completly neglected the contact interactions at component interfaces. As for the loading data, unaccountable discrepancies between the free-field records from the full-size and model tests (1, 2) suggest that significantly different loadings were experienced by the reflector and the model.

In summary, the comparison does show that even with a fairly crude representation of the antenna, the ADINA finite element model reproduced the salient features of the response. The study certainly demonstrated the adequacy of ADINA model in determining survivability, confirming that the antenna is capable of surviving a 17.2 kPa blast.

REFERENCES

1. R. Abrahams, B. P. Bertrand and R. J. Pearson, Blast Tests of a Mobile Satellite Tracking Antenna and of Two Model Antennas, USA Ballistic Research Laboratories, Aberdeen Proving Ground, Maryland, BRL MR 2661 (August 1976).

2. B. P. Bertrand and R. R. Abrahams, Quarter Scale SATCOM Antenna Blast Loads, USA Ballistic Research Laboratory, Aberdeen Proving Ground, Maryland, ARBRL-MR-0286 (September 1978).

3. K. -J. Bathe, ADINA - A Finite Element Program for Automatic Dynamic Incremental Nonlinear Analysis, Acoustic and Vibration Laboratory, Mech. Engr. Dept., M.I.T., Cambridge, Massachusetts, Rpt. 82448-1 (1975) (Revised 1979).

STRUCTURAL DEBRIS EXPERIMENTS AT OPERATION MILL RACE

John R. Rempel, James E. Beck and Robert G. McKee

Abstract. Structural debris patterns as determined by the mechanisms of building collapse under airblast loading have been studied experimentally at MILL RACE, White Sands, N.M. Three near full-size buildings were instrumented to observe deflections, accelerations and air pressures and exposed to two different regimes of incident blast pressure produced by HE simulating 1 kt, viz., 10 and 30 psi; after the shot enough wall debris was located and identified to provide estimates of debris movement. Two of the test buildings were unreinforced, load-bearing masonry, one located at each of the two incident overpressures. The third building was made of reinforced concrete panels and was exposed to approximately 25 psi. Preliminary estimates of the effect of arching on debris energy and distribution are presented.

INTRODUCTION

Knowledge of airblast debris distribution has many uses in civil defense planning. Moving debris is itself a hazard to structures and people; it may influence fire initiation and spread and its ultimate resting place will determine access to and usefulness of the site after attack. And certainly in regions of high blast overpressure the most plentiful kind of debris will be that originating in the buildings of the area. For the purpose of studying the production of structural debris three near full size buildings of two different types were exposed to airblast during the MILL RACE event in the pressure regime 10 to 30 psi. These buildings were instrumented with pressure and deflection gages and accelerometers to document the airblast loadings and the structural response. Final resting places of some of the debris also was recorded. Preliminary analysis of these data has told us how these particular kinds of buildings come apart in an airblast and where their parts go. More complete data than we can report here can be found in DNA Project Officer's Report 7077 soon to be published.

DESCRIPTION OF THE BUILDINGS

Two of the structures were nearly identical load-bearing masonry retangular buildings facing ground zero, one at 10 psi free-field overpressure and the other at 30 psi. Plan dimensions were 16 by 12 feet, the short dimension aligned with the radius from ground zero. Height was 8 feet. The front wall contained two windows 40 by 32 inches in dimension. A heavy overburden on all four walls was supplied by a reinforced concrete ceiling 10 inches thick. There was a door in one sidewall.

The third building was a reinforced concrete "tilt-up" scaled down by a factor of two from an actual industrial design and located at approximately 25 psi. Dimensions were 13 by 17 feet in plan and 6 feet 8 inches in height. Ceiling was made of reinforced concrete "Double Tee" beams four feet on center. The structure was held together with embedded welding plates.

POST-SHOT SURVEY

Airblast effects on the two load-bearing buildings were dramatically different. While 10-psi destroyed all walls and brought the ceiling down on the floor slab, the

30-psi blast blew front and sidewall material nearly 200 feet off the site, overturned the ceiling slab and carried it downwind of the floor slab.

Sidewalls at both sites travelled directly laterally (i.e., perpendicularly to the direction of the blast) in focussed streams while rear walls moved rearward. At 30-psi the rearwall was punched out by interior pressure and its fragments displayed a pattern on the ground devoid of evidence of hinging at the horizontal supports at top and bottom and only slight evidence of hinging at the vertical side articulations. At 30-psi the front wall however showed strong pivoting about horizontal junctures; the top half was lofted and outdistanced all other debris downwind. The bottom half appeared to have been pushed down into the floor after pivoting around its articulation with the floor slab. It barely travelled off the floor slab.

Although the tilt-up building suffered catastrophic collapse also, the rear wall was left standing after the shot. In fact, it showed no evidence of deformation except in a localized area impacted by a front wall fragment. The front wall and ceiling failed in bending; the sidewall connectors all ruptured or pulled out of the concrete. The side walls all were found outside the building; all but one appeared to have failed initially at the upper articulation and then fell exterior face down immediately next to its original location.

INSTRUMENTATION

Each structure contained six air pressure and three wall deflection gages. The pressure gages were located to produce information about wall and ceiling loads; the deflection gages were intended to show wall motion in response to these loads. There was one deflection gage attached to a central point in the front, rear and one sidewall of each building. To document the interaction of a wall and its overburden, three vertical accelerometers were placed in the two masonry buildings: one in the ceiling directly over the front wall, a second in the middle of the ceiling, and a third in the footing directly under the front wall. A fourth observed horizontal displacement of the front wall parallel with a deflection gage.

Useful data was obtained from every gage. When these data are combined with the results of the post-shot debris survey, the movements of all structural components during building collapse can be deduced.

GAGE RESULTS

Gage records show front walls moving steadily rearward. In the masonry building at 30-psi peak acceleration is reached in 7 to 8 ms and collapse is complete in 13 to 14 ms. "Collapse" here means that central deflection has equaled wall thickness. At the 10-psi masonry building acceleration lasts two to three times as long as at 30-psi and the front wall has collapsed in approximately 21 ms. In the reinforced building front wall collapse requires 22 ms. The final speeds of the central fragments can be calculated from the slope of the deflection gage records.

In all three buildings the sidewalls initially move inward then travel outward to collapse. The sidewalls in the two unreinforced buildings move inward between two and three inches before reversing direction; the reinforced sidewalls come in only 1.5 inches. The rear walls all behave differently. In the unreinforced building at 30 psi the rear wall moves directly outward at approximately half the speed of the front wall in the

same building. In the unreinforced building at 10 psi rear wall collapse is marginal and appears to be influenced by ceiling behavior.

INERTIAL ARCHING

McDowell, McKee and Sevin (1) during the 1950's showed that a masonry wall panel held tightly in a rigid frame developed arching forces under horizontal load, that is, the rotation of the wall created an opposing reaction in the frame. McKee and Sevin (2) applied the theory to walls impacted by nuclear airblast to account for their strength. Wiehle and Bockholt (3, 4) extended the idea to a wall loaded vertically by a static weight. Wiehle speculated that the actual stabilizing moment would be larger than that calculated from the weight of the overburden since wall rotation must accelerate the overburden upward. The present experiments with unreinforced masonry clearly show simultaneous front wall flexure and upward ceiling acceleration under the airblast impact on the front wall. This occurs despite the initial downward pressure of airblast on the ceiling. Preliminary calculations suggest that the stabilization is limited by crushing of the masonry and that an iterative, self-consistent calculational procedure should be capable of predicting it quantitatively.

The simplest evidence for the existence and magnitude of this stabilizing moment is seen in Table 1, which presents the gage data for all three front walls along with predictions based on Wiehle's response model using the dead load carried by the wall. For the two masonry buildings the Table demonstrates that actual behavior lags predictions, that is, front walls collapse later and with less kinetic energy than predicted. In sharp contrast, predictions for the reinforced front wall, whose response is controlled by the properties of steel and by its own mass and not by in-plane load, are quite accurate.

From double integration of the accelerometer traces the elevations of the front edge of the ceilings carried by the front load-bearing walls at the moment of collapse of the front walls are approximately 0.62 and 0.85 inches for the 30-psi and 10-psi sites, respectively. In the absence of crushing, rotation of the front wall segments, as illustrated in Figure 1, should raise the front edges of the ceilings approximately 1.2 inches. For this we assume four symmetrical crushing zones, one at the top and bottom of each of the two rotating blocks that make up the front wall as it approaches collapse.

Allowing for approximately 0.126 inches of elastic compression (to the elastic limit) there were approximately 0.45 inches and 0.68 inches of crushing in the front walls at the 30- and 10-psi sites, respectively. The energy dissipated in this crushing can be estimated indirectly from the data. The airblast in displacing the front wall does work of seven kinds:

(1) pushes the ceiling upward against air pressure
(2) gives kinetic energy to the front wall
(3) gives kinetic energy to the ceiling
(4) increases the potential energy of the ceiling
(5) causes the elastic compression of the front wall
(6) (probably) puts elastic energy into bending the ceiling
(7) contributes energy to the crushing of the front wall

The airblast work on the front walls and the first five dissipations above have been estimated (by hand) from the analogue data. The results are shown in Table 2. The

final two (righthand) columns of Table 2 list (a) the crush energy calculated as the residual energy after subtracting from the airblast input the first five energy losses above and (b) crush energy as estimated from measured compressive strength of the masonry units (i.e., 1310 psi on the gross area), the distance of crush, and the area of the unit. The order of magnitude agreement between the final two columns suggests that it may eventually be possible to quantify the crushing process.

Table 3 lists the energy distributions found in the two buildings. Although more energy was dissipated in crush at the 30-psi site than at the 10-psi building, this form of loss amounts to approximately the same percent of the total input at both. The difference in the sites appears in the relatively large elastic component at the low pressure location. The Table indicates that the influence of the downward airblast on the ceiling is relatively minor in both cases.

In a rigid frame, crushing depth in this wall would presumably be 1.2 inches, corresponding to an order of magnitude estimate of crushing work equal to 192,000 ft-lb. This is slightly less than the airblast input at the 30-psi site but considerably more than the input at the 10-psi location, suggesting that at both overpressures rigid arching should be an extremely effective stabilization against airblast. Inertial arching appears to be intermediate between the case discussed by Wiehle and Bockholt on the one hand and that discussed by McKee and Sevin on the other.

CONCLUSIONS

We are looking forward to more precise examination of the experimental data than so far undertaken. We believe it will confirm our tentative conclusions that the stability of the load-bearing wall is enhanced by inertial arching but the major effect of the phenomenon for our purposes may be the reduction of the kinetic energy of the wall fragments on collapse.

This work was supported by the Federal Emergency Management Agency under contract EMW-C-0583, work unit 4113, through a subcontract with SRI International.

References

1. E. L. McDowell, K. E. McKee and E. Sevin, "Arching Action Theory of Masonry Walls," Paper 915, Proc Am. Soc. Civil Eng., March 1956

2. K. E. McKee and E. Sevin, "Design of Masonry Walls for Blast Loading," Paper No. 2988, Trans. Am Soc. Civil Eng., Vol 124, 1959.

3. C. K. Wiehle and J. L. Bockholt, Summary of Existing Structures Evaluation Part I: Walls, Stanford Research Institute, November 1968.

4. C. K. Wiehle and J. L. Bockholt, Existing Structures Evaluation Part IV: Two-way Action Walls, Stanford Research Institute, September 1970.

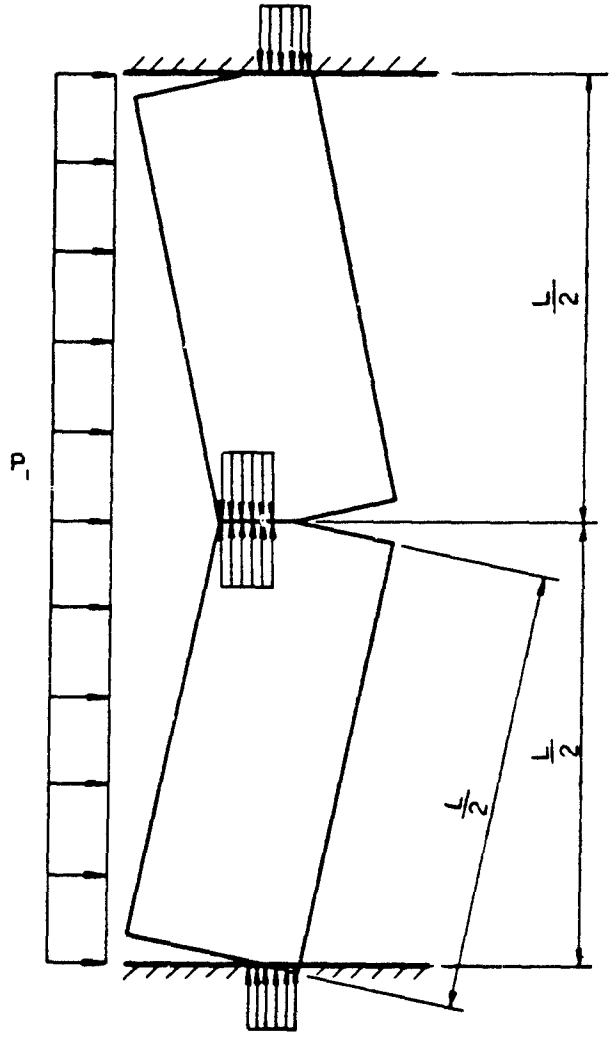

Figure 1 Assumed Arching Behavior of Masonry Wall.

TABLE 1
COLLAPSE OF UNREINFORCED FRONT WALLS

EXPERIMENT NO.	ACTUAL TIME OF COLLAPSE* (MS)	ACTUAL SPEED (FT/S)	COMPUTED TIME OF COLLAPSE* (MS)	COMPUTED SPEED (FT/S)
5401	13.	67.	8.5	127.
5403	26.5	29.	19.5	53.
5402	22.	35.	25.	36.

* Time of collapse = Time central deflection equals wall thickness

TABLE 2
UNREINFORCED FRONT WALL ENERGY DISSIPATION

Site	Time to Collapse (ms)	Average Net Pressure (psi)	Vertical Displacement (in)	Energy (1000 ft-lb) Airblast Input	Airblast Ceiling	Ceiling Potential	Ceiling Kinetic	Wall Kinetic	Elastic	Crush (a)	Crush (b)
DNA5401 (30-psi)	13.5	36.4	0.62	197	11.8	0.46	3.11	80.9	10.0	90.8	81.8
DNA5403 (10-psi)	26.5	12.8	0.85	69.2	5.48	0.68	0.941	16.2	10.0	35.9	35.8

TABLE 3
UNREINFORCED FRONT WALL ENERGY DISTRIBUTION

	DNA5401 (30-psi)	DNA5403 (10-psi)
clg airblast	6.1 %	7.9 %
wall K.E.	45.	23.
clg K.E.	1.6	1.4
clg P.E.	0.24	1.2
elastic	5.1	14.
crush (est.)	42.	52.

AIR GUN TEST FACILITY

H. Napadensky, E. Swider, T. Waterman and R. Pape
IIT Research Institute, Chicago, IL

ABSTRACT

This paper describes a facility that is potentially useful in providing data for models to predict the effects of nuclear explosions on cities. IIT Research Institute has a large air gun facility capable of launching heavy items of a wide variety of geometries to velocities ranging from about 80 fps to 1100 fps. The facility and its capabilities are described, and "city model" problem areas capable of investigation using the air gun are presented.

INTRODUCTION

A unique, large air gun facility exists at IITRI which is capable of launching virtually any shaped object weighing hundreds of pounds. This facility can be used to study what happens to building debris or building contents after a nuclear explosion. Specifically, testing can answer the questions that currently require assumptions in the analytical models.

1. How do different types of debris break-up on impact with the ground?

2. How much bouncing occurs after the debris initially impacts the ground?

3. What do debris piles really look like? What is their bulk density, for example?

4. If a section of wall or a furniture item is burning while it is being lofted, is it extinguished or is the burning accelerated?

The large air gun (Figure 1) has over one million foot pounds of energy available. Thus, we have launched 500 lb objects to 500 fps and 50 lb objects to 1100 fps. Currently two gun tube sizes are available, 8 in. and 12 in. diameter. (The gun was designed to accommodate up to a 24 in. diameter barrel.) We have launched 1 ft long cylinders and 20 ft long telephone poles; we have launched I-Beams (the I-Beam was outside the gun tube), concrete rubble, and other shapes. We see no problem with launching a full size couch or arm chair (burning or not burning during launch), wall section, etc. by using the same methods that were used to launch I-Beams.

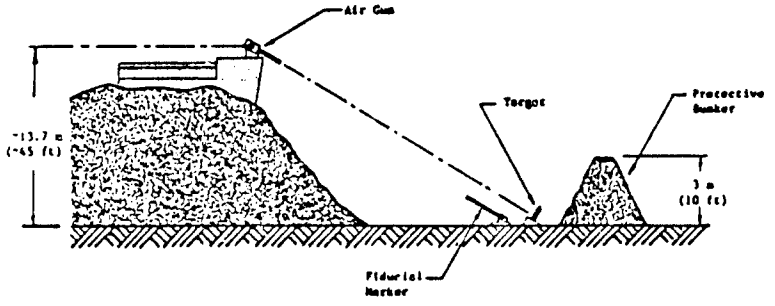

Figure 1. Typical range set up for 12 inch diameter air gun test

A second smaller air gun (4-in. diameter tube) can be fired in tandem with the larger gun. Firing the two guns with any time separation desired can answer such questions as effects of burning debris impacting non-burning debris and vice versa.

VELOCITY RANGE

Figure 2 shows empirically derived velocity curves for several projectile weights as functions of gun chamber pressure. A least squares curve fit of experimental data was used as the basis for these curves:

$$v = 280p^{0.449} M^{-0.495} \qquad (1)$$

where p is the chamber pressure (psig) and M is the projectile mass (lb).

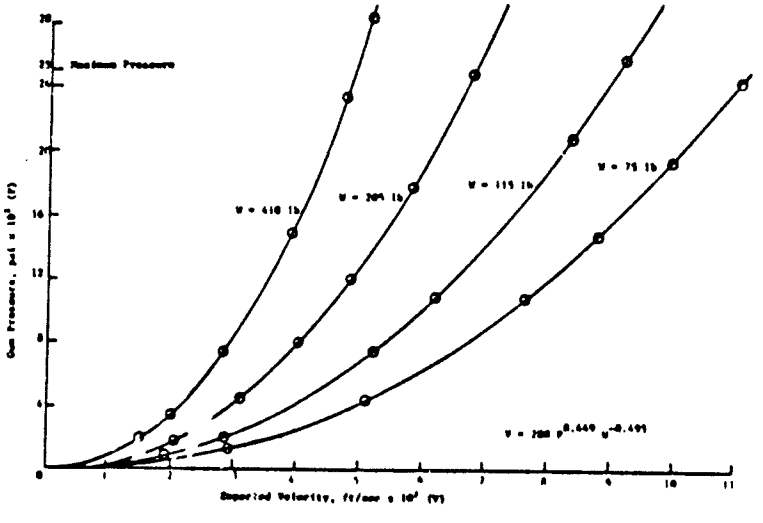

Figure 2. Air Gun Capability

This relation is for tests in which the projectile is positioned almost at the back end of the gun barrel, causing it to receive nearly the full chamber pressure initially during a shot. In order to see what other options are available to modify the pushing action of the gun, an analytic expression for projectile velocity has also been derived:

$$v = f \; 2 g_c \left(\frac{P_1 V_1 + P_2 V_2}{M} \right) \ln \left(1 + \frac{XA}{V_1 + V_2} \right) + 2X \left(g \sin\Theta - \mu g \cos\Theta - \frac{g_c P_2 A}{M} \right) \quad (2)$$

where g_c is the dimensional constant, P_1 is the chamber pressure, P_2 is the ambient pressure, V_1 is the chamber volume, V_2 is the initially ambient volume of gas behind the projectile, M is the projectile mass, X is the projectile position in the gun barrel relative to its initial position, A is the gun barrel cross-sectional area, g is the gravitational acceleration, Θ is the gun tilt angle relative to the horizontal, μ is the projectile-barrel friction factor, and f is a correction factor to account for non-ideal effects (on the order of 0.8 to 0.9). This equation shows us that although P_1 and M are the dominant parameters defining the projectile velocity v, the final velocity and rate of acceleration can also be influenced by the ambient volume behind the projectile (V_2), the barrel length (X), the barrel cross-section (A), and the tilt angle (Θ). The barrel length and cross-section are somewhat fixed by the apparatus available, but the initial ambient volume (V_2) behind the projectile can be altered more easily. By cutting a large hole in the rear opturator in the pusher tube (see Figure 3), the internal volume of the pusher tube can be added to V_2. This makes it possible to achieve lower projectile velocities as well as provide a "softer" push to the projectile. It is estimated that a 400 pound projectile (e.g., 200 pound furniture item plus 200 pound pusher assembly) could be given velocities between about 83 and 500 fps. A 200 pound projectile (e.g., 100 pounds for the item plus 100 pounds for the pusher assembly) could be given velocities between about 117 and 680 fps. It should be noted that the pusher tube in Figure 3 is inserted into the gun barrel. It can be made to separate from the launched item (e.g., I-beam) after the launch.

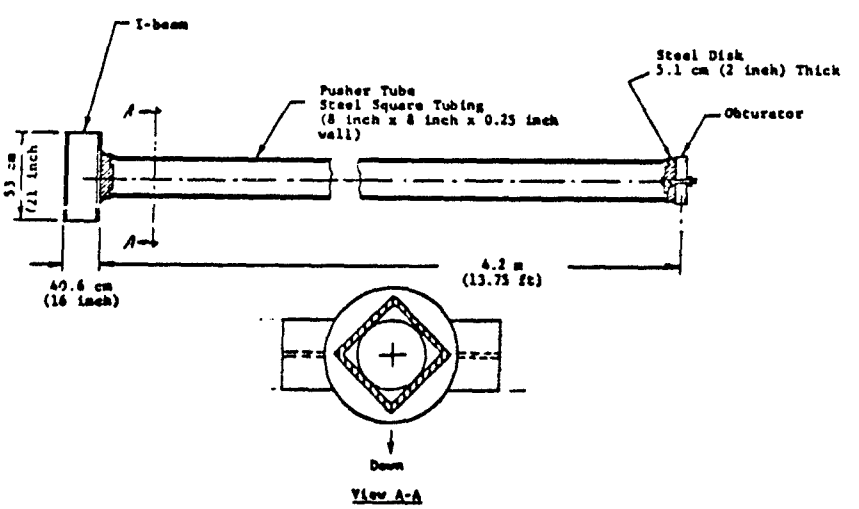

Figure 3. I-beam Projectile with Pusher Tube for 12 inch Diameter Air Gun

ACCELERATION OF ITEM

Using Equation 2, the acceleration of the projectile during its launch can be estimated. A typical acceleration curve is shown in Figure 4 (400 pound projectile with an initial chamber pressure of 500 psig). The actual acceleration duration will be longer than the estimated value due to the effects of mechanical part movements and flow through orifices such as a hole in the rear opturator on the pusher tube. However, it is expected that the actual acceleration duration is within 0.2 or 0.3 seconds. Although this is a short time period, the push is extremely gentle compared to conventional guns. For example, thin-walled liquid filled FAE* cannisters have been accelerated to high velocities using the air gun with no damage to the cannisters.

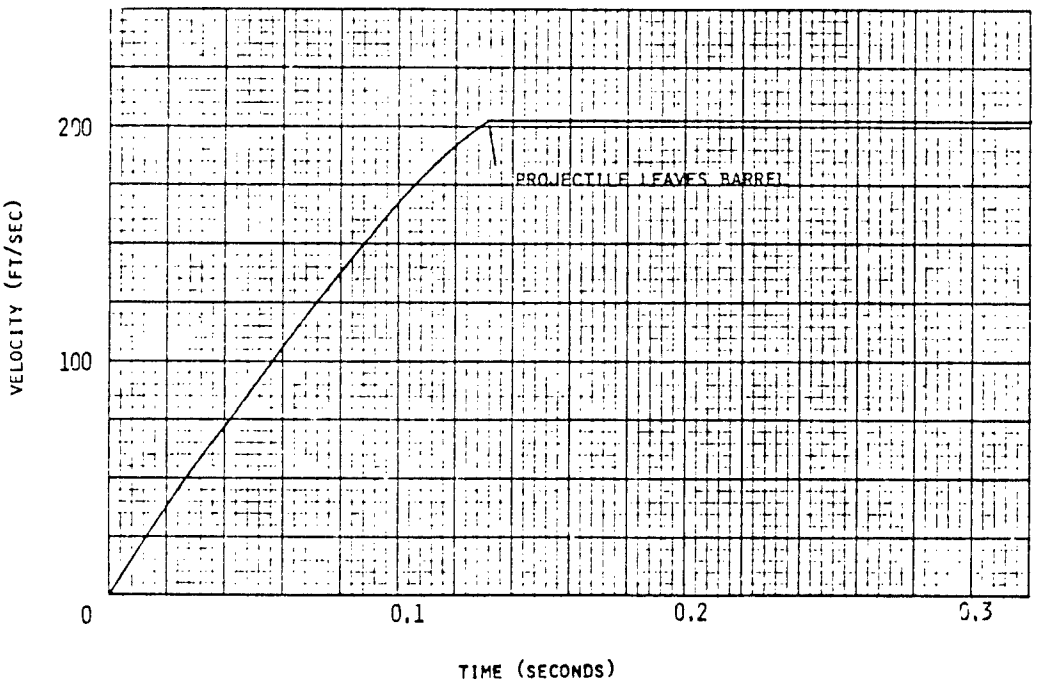

Figure 4. Typical Calculated Air Gun Acceleration Curve
400 lb. Projectile, Initial Pressure 500 PSI

---

* Fuel-air Explosion Weapon System

NUCLEAR EXPLOSION MODELING NEEDS

The large air gun is seen to address two categories of problems useful in city fire modeling. First, to determine how furniture or structural items break up, bounce, and form debris piles, the absolute velocity of the item relative to the ground must be produced. It should also be noted, for this category of problems it is clear that the gun would have to be taken off of its 45 foot bunker and put at ground level in order to obtain the proper interaction with the ground surface.

The second category of problems is concerned with extinction or enhancement of fires in items by the relative velocity between the item and the wind following the shock front. The high pressure and high velocities immediately following the shock front may in itself extinguish the fire. The air gun facility cannot reproduce the high pressures. Therefore, the facility can only address those cases where the initial pulse will not extinguish the fire. Then, the subsequent wind effects on the fire can be realistically investigated using the air gun. In this case, the gun can be used either in its current position on top of its bunker or at ground level.

Figure 5 shows absolute velocities for several furniture items and the relative velocity for a sofa estimated for a 1 MT weapon at the 5 psig peak overpressure distance from ground zero. These represent the low end of velocities of interest, since structures will not break up at much lower peak overpressures. Figure 6 shows the extreme change in wind velocity as one moves closer to ground zero. Therefore, much higher absolute and relative velocities can be expected in the region of interest. The air gun facility can be used to accelerate heavy items (200 to 400 pounds, including pusher arrangements) to velocities from about 83 to 680 feet per second, a range of extreme interest in modeling debris activity from nuclear explosions in cities. The facility can be a valuable tool to support such modeling activities.

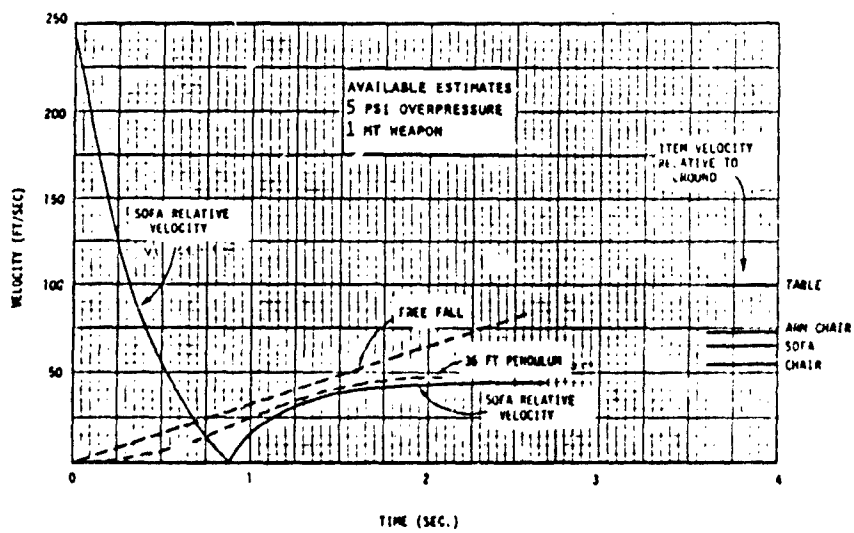

Figure 5. Relevant Velocity Profiles for 1MT Weapon at 5 psi overpressure

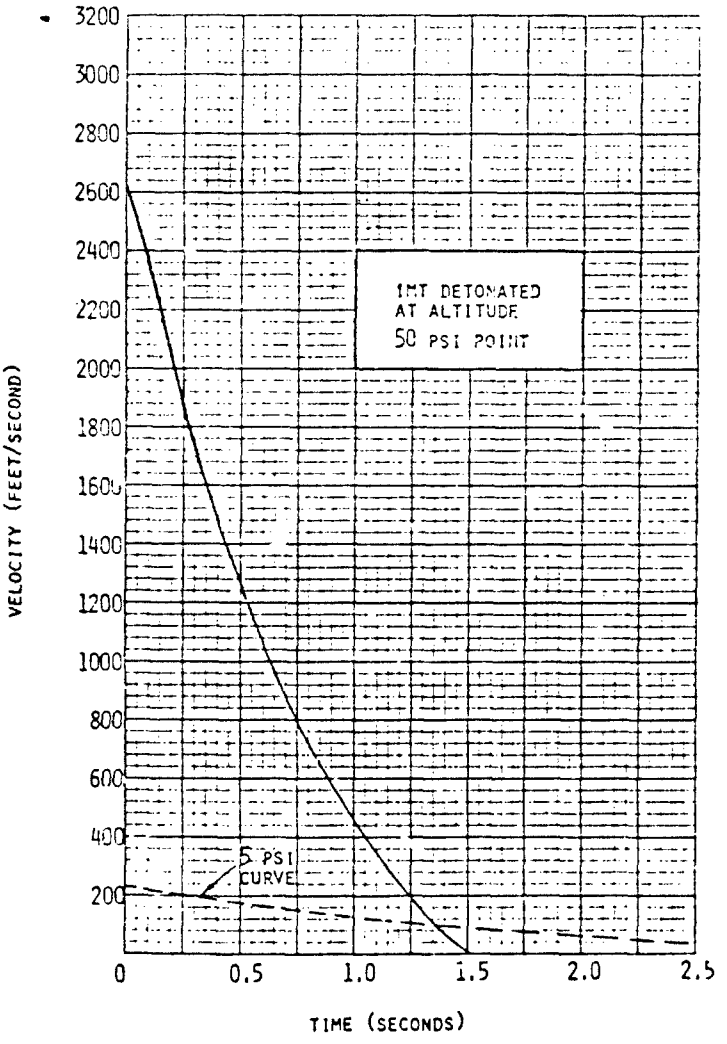

Figure 6. Comparison of Wind Following Blast from 1 MT Weapon at 5 and 50 psi Peak Overpressure Locations

"SWPI Shelter Testing Plan"

presented by

William Baker
Southwest Pesearch Institute

Text not available for publication.

SESSION V

FIRE SPREAD

A HEAT CONDUCTION ANALOG MODEL OF URBAN FIRE SPREAD

Thomas A. Reitter
Lawrence Livermore National Laboratory
P. O. Box 808, L-140
Livermore, CA 94550 U.S.A.

Introduction

In the development of computational models for use in civil defense planning, one must always be conscious that the goal is a practical tool. The product must not be prohibitively expensive in time or moncy.

It was in this spirit that the heat conduction analog model of urban fire spread was conceived and investigated. This work proceeded from the observation that many fire spread phenomena have at least a superficial similarity to transient heat conduction phenomena, and from the recognition that well-developed and maintained heat conduction codes and associated graphics are available.

The intent of this preliminary investigation was to get some idea of the virtues and limitations of the model by developing it sufficiently for use on simple test problems. The practical problem of ultimate interest is the estimation of the rate and extent of fire spread across fuel distributions that are continuous (debris fields) or discontinuous (standing buildings with various amounts of damage), or a combination of both types.

Previous models of fire spread have been of two basic types. One type is completely stochastic.[1,2] The second type of fire spread model may be described as deterministic on a microscale and statistical on a macroscale.[3]

There are so many variables, even for the limited case of fire spread among similar buildings, that many compromises have to be made. With this in mind, it does not appear unreasonable to circumvent the detailed modeling by use of a few parameters that can be adjusted to agree with experiment or fire experience.

Concept of the Heat Conduction Analog Model

Consider an array of buildings of various types of construction, occupancies, and physical condition. Wind is negligible, separations are such that fire spread by radiation across the streets is possible in some cases. At t=0, some of the buildings suffer ignition of sustained fires. Following an induction period during which fire spreads within the affected buildings, the burning buildings become intense heat sources as the fires reach their peak burning intensity, with flames shooting out of windows and over the roofs. If the configuration and obscuration factors, fire susceptibilities, etc. are appropriate, neighboring buildings may be ignited, creating new heat sources while the original ones are dying out.

If one thinks of the burning buildings as heat sources releasing a prescribed amount of energy in some prescribed fashion, and the non-burning buildings are seen as potential heat sources separated by regions of various heat capacities and temperature-dependent thermal conductivities, one can imagine representing the spread of fire by the spread of heat in a transient heat conduction problem. Thermal conductivities can be modified to give expected fire spread rates and to

favor spread in expected directions. We would expect that a building very susceptible to ignition would light faster than a less susceptible neighbor. This can be reflected in the specific heats assigned to the buildings. We would also expect a building exposed to several burning buildings to ignite faster than a building exposed to only one. Heat conduction automatically provides for this effect, at least qualitatively.

It should be clear already that we are no longer dealing with actual physical properties. One starts with plausible base values, then adjusts some parameters to get agreement with experiment and physical expectations. The only parameters not subject to change are: geometrical layout of the urban area, the fuel values and burn characteristics of the buildings, and the (approximate) time for fire spread between neighboring similar structures.

Implementation of the Model

The code used to test the model is the 2-dimensional version of TACO, a finite element, transient heat conduction code that has been developed over several years and is in general use at LLNL.

Each element in TACO has an associated material, which in turn has a specified density, specific heat, thermal conductivities (the conductivity may be orthotropic), and heat generation rate. The specific heats, conductivities, and heat generation rates may be time or temperature dependent. The timestep in transient problems may be varied according to the rate of temperature change, or interactively between timesteps.

While conduction is usually not important in fire spread between buildings, the model is in the bizarre position of using conduction to model radiative and convective heat transfer. A more difficult incongruity in the model is the use of a continuous process (heat conduction) to represent a spatially discontinuous one (fire spread between buildings). Spread across debris fields is a much better match to the model. It has not been studied for lack of data, and because it was recognized that the model had to be able to do the discontinuous problem to justify its development. The procedure is as outlined below.

1. For each "material" in the problem, choose densities, specific heats, and thermal conductivities typical of non-conductors (e.g., wood, asphalt, soil). Modify c_p and k as necessary to get physically plausible results.
2. Choose heat generation rates to approximate expected values for corresponding building types and occupancies; modify to simulate effects of damage.
3. Get approximate value for threshold ignition temperature for each building type by calculating its adiabatic temperature, the temperature it would reach if all the heat generated by its burning went into self-heating. Divide this by four to get an idea of the maximum temperature that a burning building can give any of its neighbors. Lower this by 15-20% to account for some conduction.

4. Allow random fluctuations in threshold temperatures about the mean value for each finite element of the type. (I.e., assign each building element a threshold temperature in the range $[\theta-\delta\theta, \theta+\delta\theta]$). This is to reflect differences in building conditions and contents, obstructions, and the heat generation rates of neighboring buildings.
5. Give material between buildings temperature-dependent thermal conductivity of form $k = k_0(1+\alpha T^3)$, where k_0 is the intrinsic conductivity. This form is chosen in analogy with the radiation heat transfer coefficient and to force fire spread to occur near peak burning rates. Make materials between buildings orthotropic, with temperature-dependent conductivity in the direction normal to buildings to account for the rapid decrease of radiation configuration factors laterally.
6. Run test problems of homogeneous building types, modifying α's and the specific heats of materials between buildings and α's, c_p, θ, $\delta\theta$ of building types to approximate expected rate of spread for given building separation. For maximum sensitivity, the separation should be about that for 50% spread probability.
7. Using parameters chosen in step 6, check spread probabilities at other separations (e.g., at 20% spread probability). Some iteration between steps 6 and 7 may be appropriate to make slight improvements.

Test Runs

Only very simple cases have been run. By running simple problems one has some idea of what is physically plausible. The uniform, square grid most commonly used is shown in Fig. 1. "Buildings" consisted of 4 elements. Only one building type was used. Floor area and the heat generation rate were chosen to approximate wooden barracks burned at Camp Parks[5]. (Fig. 2 shows the heat generation rate used). Building separations of one or two elements, corresponding to 12.9m or 25.8m, were chosen to ensure significant spread probabilities.[6,7] The building material was given an isotropic, temperature-dependent thermal conductivity so large that spread within a building generally occurred. No effort was made to approximate expected spread rates within a building. (In any problem of realistic size buildings would almost certainly be represented by a single element so this is not a major area of concern.) The material between the buildings consists of four types of "asphalt". They have the same density and nearly the same c_p, but different thermal conductivities. Most are strongly undirectional. Some, in corners or at misaligned buildings are temperature-dependent but isotropic. Some have a low, constant, isotropic conductivity reflecting their expected lack of participation in fire spread due to their location.

Within the parameter space for which any spread within or between buildings occurs, the results are sensitive to changes in c_p's, α's, θ, and $\delta\theta$. The values used for the examples are given in the Table. This is not necessarily an optimum set, as there was not enough time to investigate all possibilities. These parameters gave the desired spread probability across a 12.9m separation of about 45% (5 out of 11 chances) in a test configuration.

The effects of a constant ambient wind have been simulated in some runs by adding a term to the thermal conductivity of all elements. The wind is taken as the positive X-direction without loss of generality since the urban grid could be rotated by an appropriate amount if desired. Since thermal conductivity is bidirectional by nature, it is necessary to know the direction of the temperature gradient at each element in order to know the appropriate sign of the effective conductivity due to the wind. That is, if the temperature increases in the X-direction, the effect of the wind should be to retard heat flow Conversely, if the temperature decreases in the X-direction, the wind should augment the heat flow.

The appropriate form of k_W is not known, nor is there data available for calibration. The test problems were run with $k_W = BW$ for $W \leq W_0 = 3.76$ m/s, and $k_W = BW_0 (W/W_0)^{\beta}$ for $W \geq W_0$. B and β are viewed as empirical constants. The choice of W_0 is to reflect the empirically-derived demarcation between stationary and moving mass fires. In the test problems, B = 500 and $\beta = 1.25$. If suitable data were available, B and β would be modified to give the appropriate downwind rate of spread, then compared with the upwind rate.

Results

For the test problems initial ignitions were chosen to see the effects of interactions, or 10% - 30% of the buildings or elements were chosen at random for initial ignition. Some of the results are shown in Fig. 3 and 4.

An important observation is that the spread of fire appears physically plausible in time and space. That is, fire spread events can be attributed to one or more neighboring burning buildings near or a little past peak burning intensity.

Even with only 10% building or element ignitions generally all buildings eventually ignite for the basic urban area used here. This basic urban area, however, has building separations of only 12.9 or 25.8 m and only one type of building--there are no fire resistive types which might stop fire spread. Not all burning buildings in the test problems cause spread. In some cases most of the spread can be traced back to one or two of the initially ignited buildings. Recall also that the parameters were chosen to give about 50% spread across a 12.9 m separation. It is known from Schmidt's work that with a spread probability of 50% or more there is generally unlimited spread.[2]

Some problems were run with a break of 38.7 m through the center of the problem area. Fire failed to cross this break in some cases or barely managed to cross it in others. More work is needed to ensure appropriate spread probabilities for various separation distances.

For one test problem (10% random element ignitions), the initially ignited elements were fixed but different sequences of random numberswere used to choose the threshold ignition temperatures. Qualitatively similar results were obtained for fraction of buildings burning vs. time.

A constant wind had plausible effects of speeding spread downwind and slowing or preventing upwind spread. Lack of data for adjusting empirical constants prevents any useful conclusions other than that the technique used appears promising.

Conclusions

While this preliminary effort has been very limited in scope, it has shown that the heat conduction analog model can produce plausible results for discontinuous fire spread. Given suitable information on fire spread in a constant wind or spread due to firebrands, it may be possible to incorporate these effects. Fire spread across debris fields should be simpler to treat than the discontinuous case. Modeling of fire-induced winds and related mass fire development appear to be beyond the range of the model.

Credibility is a more immediate problem. An important test would be to run an improved version of the model against other fire spread models. This would also provide a comparison of problem set-up and computation times. Such a comparison should indicate whether this model has advantages justifying further development.

References

1. P.V. Phung, A. B. Willoughby, AD-613359, Prediction Models for Fire Spread Following Nuclear Attack, Jan. 1965.
2. L. A. Schmidt, AD-A081387, A Parametric Study of Probabilistic Fire Spread Effects, Sept. 1979.
3. L. W. Weisbecker, H. Lee, AD-713418, Evaluation of Systems of Fire Development, Aug. 1970. This compares the IITRI, URS and SSI models.
4. P. J. Burns, UCID-17980 Rev. 2, TACO2D - A Finite Element Heat Transfer Code, Jan. 1982.
5. C. P. Butler, AD-716327, Measurements of the Dynamics of Structural Fires, Aug. 1970.
6. A. N. Takata, F. Salzberg, AD-684874, Development and Application of a Complete Fire-Spread Model, June 1968.
7. A. N. Takata, AD-695636, Power Density Rating of Fire in Urban Areas, April 1969.

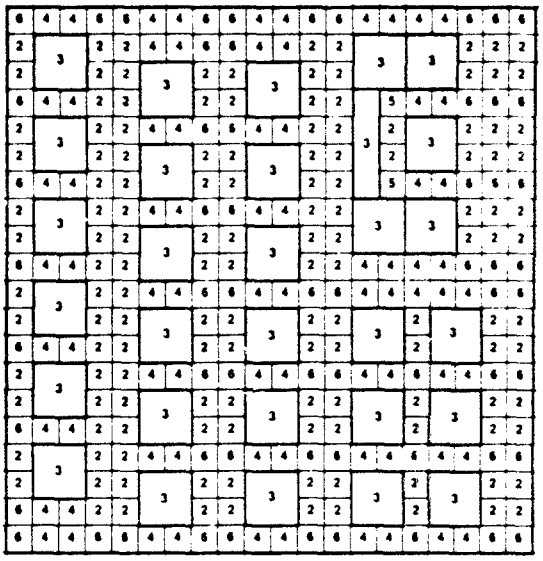

Fig. 1. Problem layout used for most problems.

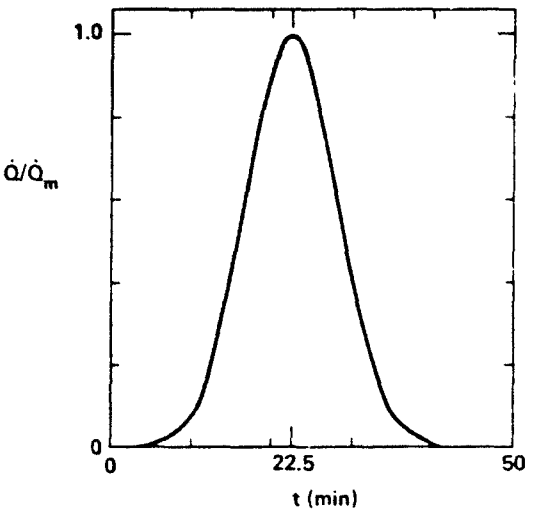

Fig. 2. Heat generation rate for buildings.

$\theta = 140, \quad \delta\theta = 40$

Material No.	ρ	c_p	γ_x	γ_y
1	2500	1600	$1 \cdot 10^{-3}$	$1 \cdot 10^{-3}$
2	1900	60	$1 \cdot 10^{-3}$	0.0
3	720	850	$1.6 \cdot 10^{-2}$	$1.6 \cdot 10^{-2}$
4	1900	60	0.0	$1 \cdot 10^{-3}$
5	1900	60	$1 \cdot 10^{-3}$	$1 \cdot 10^{-3}$
6	1900	100	0.0	0.0

$k = k_0 (1+\alpha T^3)$, k_0=0.6 for all materials
timestep = 2 minutes for problems without wind, variable otherwise.

Table of parameters used in test problems. (All units are S.I.)

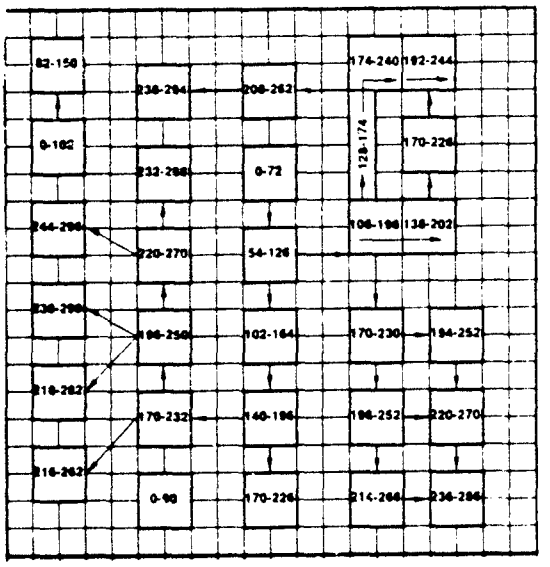

Fig. 3. 10% building ignitions. Here and in subsequent figures the numbers are the times (in minutes) during which the "buildings" burned.

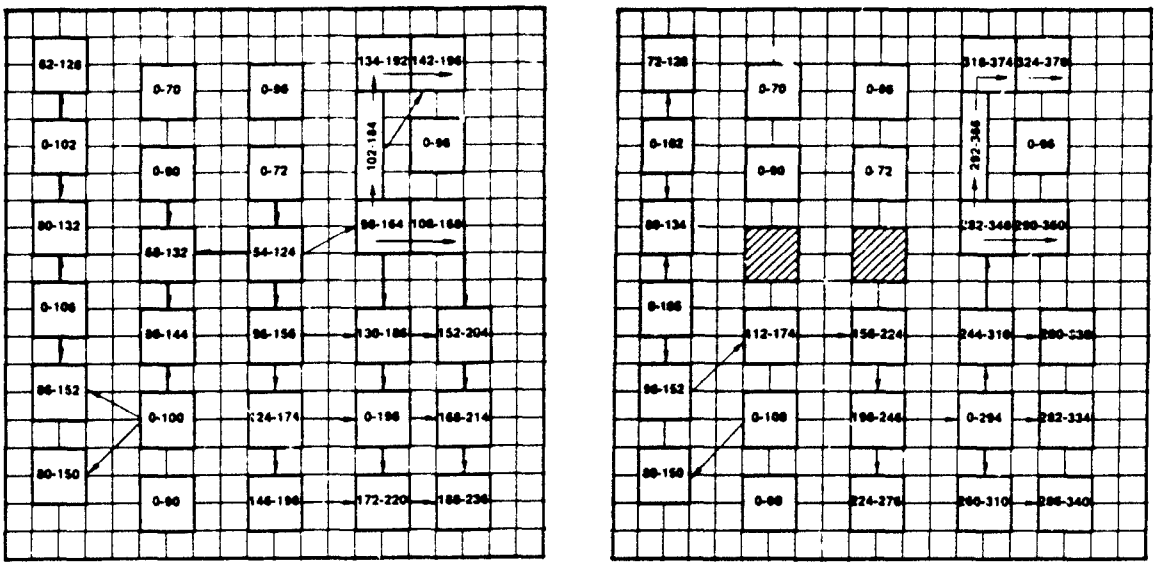

Fig. 4. 10% element (33% building) ignition. On left, all buildings have C_p = 850; on right, two hatched buildings have C_p = 8500. Note delay in fire spread caused by failure to ignite.

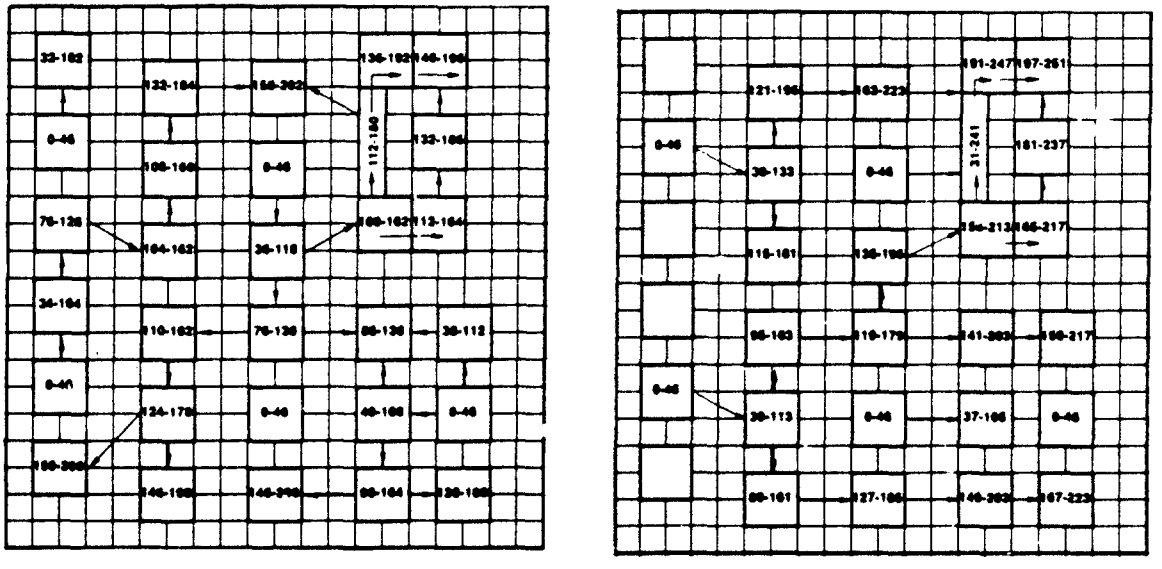

Fig. 5. Effects of a 9 m/s "wind" for 17% building ignition. (The parameters for the effective conductivity due to wind have not been fit to data.)

MOVING BOUNDARIES - A NUMERICAL MODEL

S.-W. Kang

Lawrence Livermore National Laboratory
P.O. Box 808
Livermore, California 94550

FEMA Asilomar Conference
May 30 - June 3, 1983

ABSTRACT

A numerical model for time-dependent moving-boundary phenomena is constructed, with a view towards application of the method to calculation of the fire-spread characteristics in urban environments.

A. INTRODUCTION

Determination of the physical characteristics involved in the blast-propagation and the fire-spread phenomena during nuclear attack is important for civil defense programs in terms of planning and minimizing damages and casualties. A complete understanding of the phenomena will require concentrated and considerable time and effort. The enormous complexities involved in these phenomena have in the past necessitated a piece-meal approach to the problem.

The present paper investigates the possibility of a simplified approach on modelling the blast propagation and the fire-spread processes in terms of mathematical equations describing moving fronts. Across these fronts, there exist precipitous changes in the physico-chemical properties of the flow medium. The moving-boundary concepts have been previously applied to other situations, such as combustion problems, multi-phase problems and coal drying problems (Refs. 1-7). The present approach and the numerical code developed therefrom represent a first-approximation analysis, and hopefully these will be modified or expanded for a more detailed study in the future.

B. ANALYSIS

A time-dependent, one-dimensional (spherical, cylindrical, Cartesian) transport problem under the assumptions of "lumped" parameters in front of, and behind the moving fronts in the flow field is studied. These lumped physical parameters, such as thermal conductivity and density, need not be

constant with time. The governing equations describing the moving-front phenomena are the conservation equations of the global mass (or density), the constituent components, the momentum, and the thermal energy with appropriate boundary conditions (transient or steady).

The main thrust of the present analysis is to investigate the possibility of adapting the moving-front approach to the fire-spread and the blast-propagation history under nuclear-attack situations; therefore, the conservation equations mentioned above may not be directly applicable. Nevertheless, these equations form a basis for exploring the feasibility of model adaptation to the problems of present interest. For the sake of completeness and illustration, the relevant conservation equations specialized to the spherical coordinate system are included below.

Global mass conservation:

$$\frac{\partial \rho}{\partial t} = - \frac{1}{r^2} \frac{\partial}{\partial r} (r^2 V_r \rho)$$

Component conservation:

$$\frac{\partial S_i}{\partial t} = - \frac{1}{r^2} \frac{\partial}{\partial r} (r^2 V_r S_i) + \phi_i$$

Momentum conservation:

$$\rho \frac{DV_r}{Dt} = \frac{1}{r^2} \frac{\partial}{\partial r} (r^2 \bar{\mu} \frac{\partial Vr}{\partial r}) - \frac{\partial p}{\partial r}$$

Energy conservation:

$$\overline{\rho c} \frac{\partial T}{\partial t} = \frac{1}{r^2} \frac{\partial}{\partial r} (r^2 \bar{k} \frac{\partial T}{\partial r}) - V_r (\Sigma_i S_i C_i) \frac{\partial T}{\partial r} + \Sigma_i \phi_i Q_i$$

where

$$\phi_i = e^{\bar{W}_i} - e^{B_i/T} .$$

The term ϕ_i denotes the i-th component species production rate, ρ the global density of the medium, t the time, r the spherical radius, V_r the radial velocity, S_i the i-th component mass fraction, p the static pressure, T the temperature, k the mean "thermal conductivity." This term may be regarded as one of the parameters to be appropriately used in considering fire-spread scenario. The term C_i denotes the specific heat of component i, and Q_i the heat release due to phase change of component i. The diffusion term in the component conservation equation is taken to be negligibly small in

comparison to the convective flux and the heat-generation effects in the present moving-front problem. In cases where the thermal-radiation effects are sizable, the radiation heat flux term can be added to the energy conservation equation. Other effects, where deemed important, can also be included in these equations.

In solving these equations, available numerical computer codes (Refs. 8-9) were utilized for describing a moving-front case in a semi-infinite region. This problem was chosen to demonstrate the versatility of the present approach in other coordinate systems in addition to the spherical conservation equations presented earlier. The results obtained are as follows.

C. RESULTS AND DISCUSSION

The time-dependent moving front problem in a semi-infinite flow medium was solved with the following initial and boundary conditions and lumped property values. The term F(t) signifies the location of the moving front measured from X = 0, a boundary where we prescribe a sudden increase in temperature and maintains it at T_0. This high temperature, taken to be 1273 K in the present example, represents a source of thermal transport potential for the medium ($o \leq x < \infty$), generating a moving front and changes in the property values as the front (called "havoc front") moves inward from X = 0 as a function of time. Other conditions used in the example are:

$0 \leq x \leq F(t)$, i.e., behind the moving front;

$$\bar{k} = 1.1(10^3) \text{ [J/m - Sec - K]}$$

$$\overline{\rho c} = 1.3(10^6) \text{ [J/m}^3 \text{ - K]}$$

$F(t) < x < \infty$, i.e., undisturbed region:

$$\bar{k} = 2.1(10^6) \text{ [J/m - Sec - K]}$$

$$\overline{\rho c} = 2.6(10^6) \text{ [J/m}^3 \text{ - K]}$$

$X = 0$; $T = T_0 = 1273$ K, $Z = 0$

$X \to \infty$; $T = T_\infty = 273$ K, $Z = 1.0$,

and the $Q_f = 2(10^6)$ [J/kg], denoting the "latent" heat of phase change of the medium z. The "activation-energy barrier" B used was $8(10^3)$ K and the "reaction-rate coefficient" W was taken to be 10.0. The results obtained on LLL CRAY Computer are presented.

Figure 1 describes the temperature distributions as a function of time in a semi-infinite region, in which the boundary condition used was a constantly maintained temperature at a prescribed location in the field, (i.e., X = 0). At a certain critical value (Tc) at 400° C, the thermal properties were assumed to undergo precipitous changes, such as ablation, releasing or absorbing latent thermal energy in the process. This then delineates the "havoc front" characterizing the moving boundary in the field creating vastly

different transport phenomena in front of and behind the demarkation. The movement history of this havoc front (S_1) is shown in Fig. 2.

In the present illustration, the havoc front may be considered to represent the fire-spread front, moving inward at a certain speed whose magnitude depends upon various thermodynamic properties and initial conditions used in the problem.

The present analysis can also generate a second havoc front along with the first front. This has potential application in the fire-spread studies where some materials may undergo radical property changes at a higher critical temperature (T_2) than the lower critical temperature (T_c) at which some fraction of the medium has already experienced drastic changes. Solutions were obtained for W = 90.0, and B = $3(10^4)$ K. This is shown in Fig. 3.

These results indicate that the moving front speed under prescribed boundary conditions (such as the temperature differential between X = 0 boundary and X = ∞) is a function of various thermodynamic properties of the medium. Of these, a dominant dependence of the movement speed on the "reaction term" in the component conservation equation was observed. In particular, the parameters W_i and B_i are identified as significant factors in determining the movement speed of the i-th component. This is illustrated in Fig. 4. The figure shows that a certain B_i - W_i combination exists for which the speed of the havoc front (i.e., fire spread front) is identical, but that change in either W_i or B_i produces change in the movement behavior. Specifically, increasing W_i for constant B_i brings about an increase in the front speeds. The magnitude of B_i (which may be regarded as an activation energy barrier) is indirectly related to the magnitude of the critical temperature, a thresh hold temperature for drastic change in the medium. Thus, Fig. 4 may be used as a guide in calibrating the movement speed for a given problem, where the critical temperature--and, therefore, the value of B--is inferred based on the makeup of the medium and the magnitude of W can be adjusted to fit experimental data. This W-B pair then may be applied to other problems with comparable medium compositions in calculating the havoc-front movement history. It goes without saying that judicious choice of the various lumped property values is required in utilizing the approximate approach taken in the present analysis.

REFERENCES

1. Wilson, D. G. Solomon, A. D. and Boggs, P. T. Moving Boundary Problems, Academic Press, N.Y. (1978).

2. Sikarskie, D. L. and Boley, B. A. "The Solution of a Class of Two-Dimensional Melting and Solidification Problems," Int. J. Solids Structures, Vol. 1, pp. 207-234 (1965).

3. Crank, J. and Gupta, R. S., "Isotherm Migration Method in Two Dimensions," Int. J. Heat Mass Transfer, Vol. 18, pp. 1101-1107, (1975).

4. Tsang, T. H., "Modeling of Heat and Mass Transfer During Coal Block Gasification," Ph.D. Thesis, Univ. of Texas (1980).

5. Gregg, M. L. Campbell, J. H. and Taylor, J. R.," Laboratory and Modelling Investigation of a Colorado Oil-Shale Block heated to 900° C," Fuel, Vol. 60, pp. 179-188 (1981).

6. Kashiwa, B. A. and Harlow, F. H., "An Investigation of Simultaneous Heat and Mass Transfer in Subbituminous Coal," Proc. 15th Intersociety Energy Conversion Eng'g Conf., AIAA, Vol. 2, pp. 1311-1314, (1980).

7. Kang, S.-W. and Levatin, J. L., "Transient Boundary-Layer Flows in Combustion Environments," AIAA Paper 81-0349, AIAA 19th Aerospace Sciences Conf., January (1981).

8. Madsen, N. K., "PDEPACK Uer's Guide" Lawrence Livermore Nat'l Laboratoy Report, UCIR-1027, March (1975).

9. Sincovec, R. F. and Madsen, N. K., "Software for Nonlinear Partial Differential Equations," ACM Trans. on Math Software, Vol. 1, No. 3, pp. 232-260, Sept. (1975).

FIGURE 1.

TEMPERATURE DISTRIBUTION HISTORY IN A REBIUM WHEN SUBJECTED TO A THERMAL FLUX

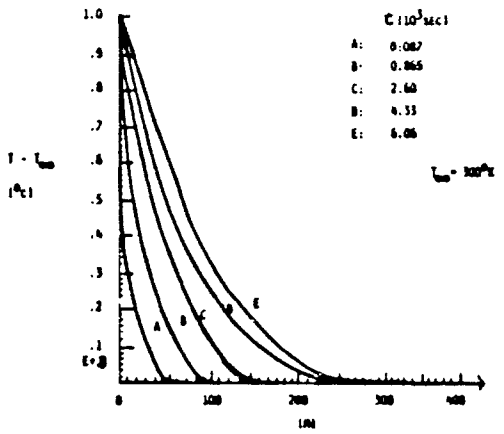

FIGURE 2. MOVING FRONT HISTORY - I

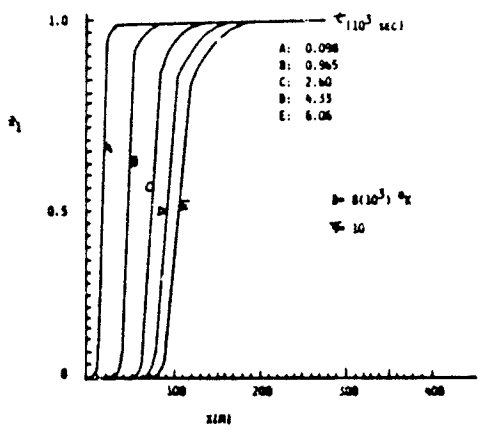

FIGURE 4. EFFECTS OF REACTION PARAMETERS ON MOVING FRONT SPEED

FIGURE 5. MOVING - FRONT HISTORY - II

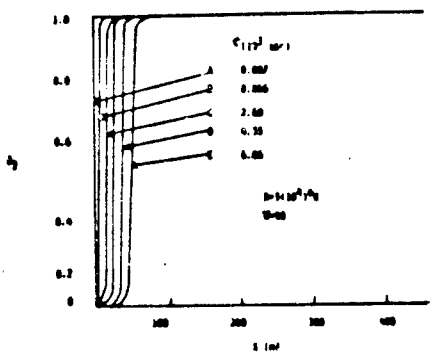

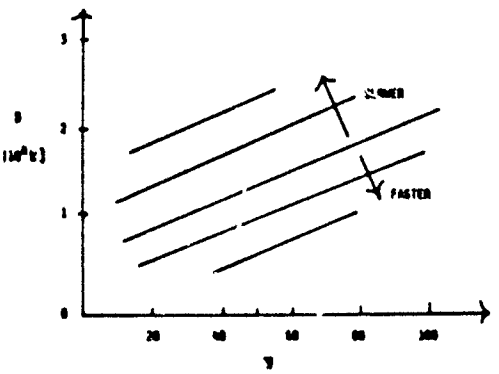

BURNOUT OF LARGE-SIZED WOODY FUELS

Hal E. Anderson
Research Physicist

USDA Forest Service
Intermountain Forest and Range Experiment Station
Northern Forest Fire Laboratory, Drawer G
Missoula, MT 59806

ABSTRACT

The burnout of large-sized woody fuels, 1 to 6 inches thick, is being measured at the USDA Forest Service Northern Forest Fire Laboratory in Missoula, Mont. Physical properties of the fuel bed are varied to determine thresholds for interactive burning, periods of flaming and glowing combustion, and the accuracy of a mathematical model that describes combustion during the flaming phase of burnout. Critical fuel properties include loading, fuel size, and spacing--the distance between outside edges of pieces of the same size. This work is being related to the heat loads on the site and the fire effects on physical and biological features of urban and rural situations.

INTRODUCTION

Research on fire behavior in wildland fuels in the 1930's was directed toward rate of spread and resistance to control (1, 2). As work continued through the 40's, 50's, and 60's, additional knowledge was developed and fire danger rating systems were formulated (3, 4, 5). Ignition, rate of spread or area growth, and flame length were among the variables considered as the fire danger rating was developed. During the 1960's and 70's, work progressed on developing models of fire behavior and these were incorporated into the current National Fire Danger Rating System (6, 7).

The needs of the resource specialist, however, extend beyond expressions of fire danger to greater detail of fire behavior and effects; therefore additional aids are still being produced (8, 9, 10). This work has culminated in a set of mathematical models for estimating the forward rate of fire spread, the rate of perimeter and area growth, flame length, fire line and area fire intensity, fuel consumption rate, and burnout of fuels.

Because the basic fire behavior mathematical model only considers fuels less than 3 inches in diameter, another model, BURNOUT (9), was developed to estimate fire behavior after the initial fire front has passed. The random array of fuel sizes in a fuel bed are considered in terms of their individual burning times, the spacing of pieces of each size, and the planform projection overlap of fuel pieces of equal size and smaller. The amount of load loss and the rate of loss is summed for the fuel sizes by means of a universal burnout function and its derivative based on the burn time for the flaming phase of combustion. The model predicts the fuel consumption and provides a time history of the fire intensity in mixed fuels, including large fuels found in logging slash, wind-thrown timber, or debris from blast effects, earthquakes, and other catastrophies. The burnout model was developed using the weight loss data generated during the Flambeau series of burns. The model estimates fire behavior and fire effects, not only in

wildland situations, but also for urban sites where blast and secondary ignitions can pose serious fire hazards (11).

PURPOSE OF CURRENT WORK

Although forest fire behavior research has generated several useful products for fire specialists, some uses have been hampered because current fire spread models do not consider fuels larger than 3 inches in diameter. Specialists know that large fuels are an important consideration in management plans, but they have had no means of quantification. The results of modeling heat release per unit area and burnout time have not been exercised enough to determine their applicability.

Ongoing research will provide methods for assessing the impact of the fire behavior of large-sized fuels on the site (fire effects) and aiding man's response to actual or expected fire behavior (fire and resource management). Four areas of effort are involved:

1. Testing the theoretical burnout model against experimental fires to confirm the model and define areas of deficiency.

2. Determining the fire behavior associated with the physical properties of large-sized fuels, explaining their role in fuel bed burning processes, and describing the heat flow to the surroundings.

3. Identifying the significant roles of large-sized fuels in fire behavior and coupling these functions to site and resource activities so fire effects can be assessed.

4. Identifying the fire behavior features of large-sized fuels associated with the fire front, the flaming combustion phase, and the glowing combustion phase.

PLANS AND PILOT TESTS

A series of burns has been started in our combustion laboratory. Fuels range from 1 inch (2.54 cm) to 6 inches (15.24 cm) and fuel area loadings from 3 to 40 lb/ft^2 (14.65 to 195.3 Kgs/m^2). The first series used fuel beds of excelsior, 1/4-inch (0.63 cm) sticks, and 1-inch (2.54 cm) square sticks on a load area of 2 square feet (0.186 m^2). The next four beds were constructed on load areas of 16 square feet (1.49 m^2). The largest sized fuel piece in each successive fire was 1-, 2-, 4-, or 6-inch (2.54, 5.08, 10.16, 15.24 cm) dimensioned lumber. The physical properties are presented in table 1.

Evaluation of the burnout model will involve determining the fractional weight loss rate of each size class to the overall weight loss rate observed during the history of the fire. In addition such things as the fuel spacing in each size class will be studied to confirm or modify the assumed threshold spacing for interaction that results in mutual burning. The flaming phase and the glowing phase of the combustion process will be measured so flame height computations based on mass loss rate can be adjusted for mass loss due to glowing combustion. Other observations relate the burnout to the radiant heat received at a point away from the fire and to the heat flow into the medium beneath the fuel bed.

Table 1.--The physical properties of the fuel beds burned in the first series. Spacing defines the fuel separation for a given size in terms of their thickness, t.

BURN NUMBER	Total fuel load lbs/ft^2	Depth ft	Excelsior fuel load lbs/ft^2	1/4-inch and spacing lb/ft^2:xt	1-inch and spacing lb/ft^2:xt	Large-size fuel		
						Thickness in.	Layers and spacing no.:xt	Fuel load lb/ft^2
1T1-4	3.88	1.08	.11	1.02:5t	2.74:3t	--	---	---
1T1-5	3.47	1.08	.13	.80:5t	2.54:3t	--	---	---
2T11-1	10.79	1.08	.11	.98:5t	2.77:3t	2	3:1.5t	6.94
2T6-1	21.94	2.75	.15	2.43:5t	6.33:3t	4	3:2.7t	13.04
3T13-1	27.50	3.08	.14	1.00:8t	2.88:5t	6	3:1.5t	23.48

After this first series of fires is analyzed, we will develop a cycle of burns where spacing and loading by size class are altered to complete the investigation of the burnout model. We plan to investigate the effect of timber type upon burning and perhaps the effects of fuel moisture content. As we gain information on the fire behavior of large-sized fuels, field studies are planned utilizing prescribed burns to extend the research findings to operational situations. This phase will depend on the availability of manpower and operating budget. Approximately 1 year has gone into this study; another 3 years are needed.

RESULTS OF WORK TO DATE

The burnout model's fractional weight loss rate is based on a modified "top hat" burning rate history. During the first third and the last sixth of the weight loss for each fuel size, the burning rate is assumed to change linearly with time, while the center portion of the burnout curve has a nearly constant rate. The weight loss data were converted to a fractional loss rate and compared to the model predictions (fig. 1). Although predicted burning rates are in agreement, the flaming times are longer than those experienced in the laboratory. The flaming period usually runs 20 minutes or less, but the model predicts about 17, 35, 67, and 98 minutes for the 1-, 2-, 4-, and 6-inch (2.54, 5.08, 10.16, 15.24 cm) sticks, respectively. The glowing combustion phase, which is not considered in the burnout model, continues for a much longer period: more than 2 hours for the 1-, 2-, 4-inch (2.54, 5.08, 10.16 cm) sticks, over 5 1/2 hours for the 6-inch (15.24 cm) sticks, at an initial moisture content of 6 percent.

Energy release rates on the 16-ft^2 (1.49 m^2) beds during the flaming period of the finer fuels ranged from (229 to 522 Btu/ft^2-s (621 to 1416 Kcal/m^2-s). After burnout of the 1/4-inch sticks, the fractional weight loss rates show no consistent burnout rates for the large-sized fuels, but generally exhibit a decreasing rate, with abrupt shifts as fuels are rearranged when the bed structure begins collapsing. The fractional weight loss rate

ranges from 0.1 and 0.01 min.$^{-1}$ during flaming and from 0.01 and 0.001 min.$^{-1}$ during the glowing phase.

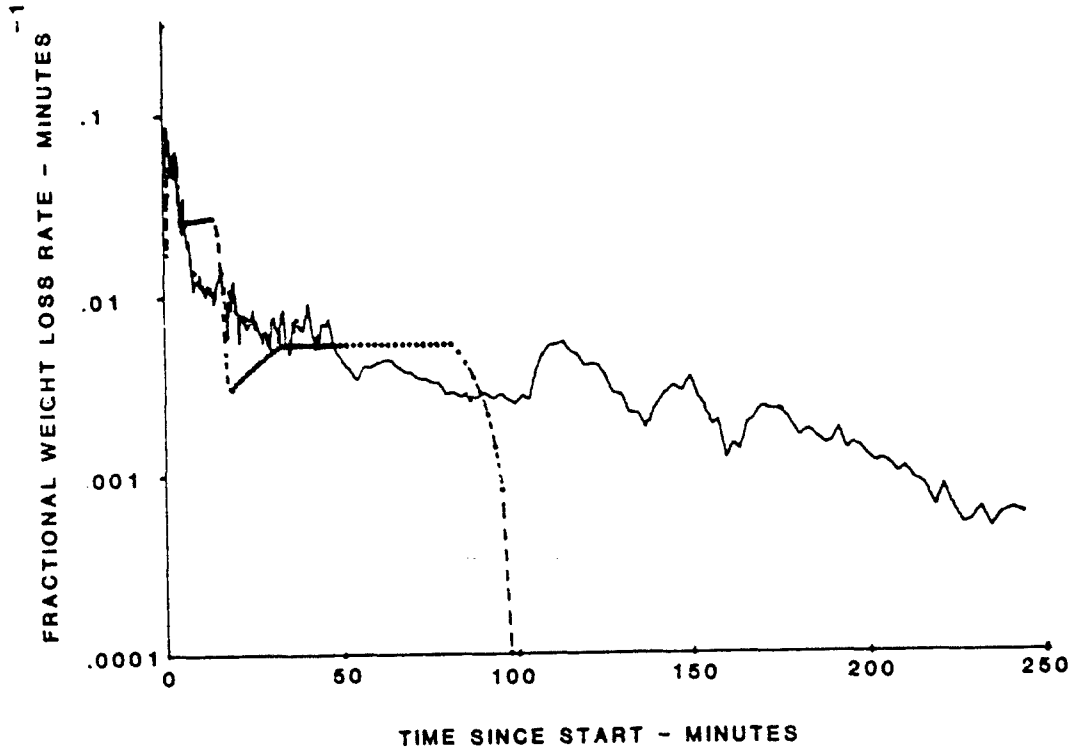

Figure 1.--Fractional weight loss rates are determined from strain-gage weight-loss measurements and compared to mathematical model output (dashed line) for a burnout theory.

Thermal gradients into a sand substrate beneath the fuel bed are measured with two arrays of thermocouples arranged vertically at 1-cm spacings. This information will be related to physical and biological functions that indicate the fire's effect on the site. The maximum temperature gradient in the first centimeter of sand averages about 1,567°F/in (325°C/cm); the peak occurs during the flaming phase. The maximum sand surface temperature experienced was 1,420°F (771°C) occurring more than 1 1/2 hours after the fire start. The total time for heat flowing into the sand has ranged from 55 to over 200 minutes. The heat flux into the sand did not exceed 2.92×10^3 Btu/ft^2-hr (0.22 cal/cm^2-s) (fig. 2).

The flames generated from a bed of woody debris are part of the hot gas plume that can carry embers and that contribute to the radiant heat load adjacent to the burning area. Therefore flame heights are measured visually and photographically. These data have been compared with a model of flame height used in estimating firebrand lofting (12). The model uses the weight loss rate to predict flame height. This allows us to estimate when glowing combustion becomes a significant part of the weight loss and also allows us to check the flame height model's accuracy. Peak flame heights occur within the first 2 minutes of the fire and are underestimated by the model; however, the flame heights associated with the 1-inch burnout are accurately

predicted. Flame height is overestimated for the burnout of the larger fuels because of the glowing combustion contribution to weight loss. In addition we are correlating the radiant heat to the flame height and weight loss data to develop interpretative guides for the radiation environment.

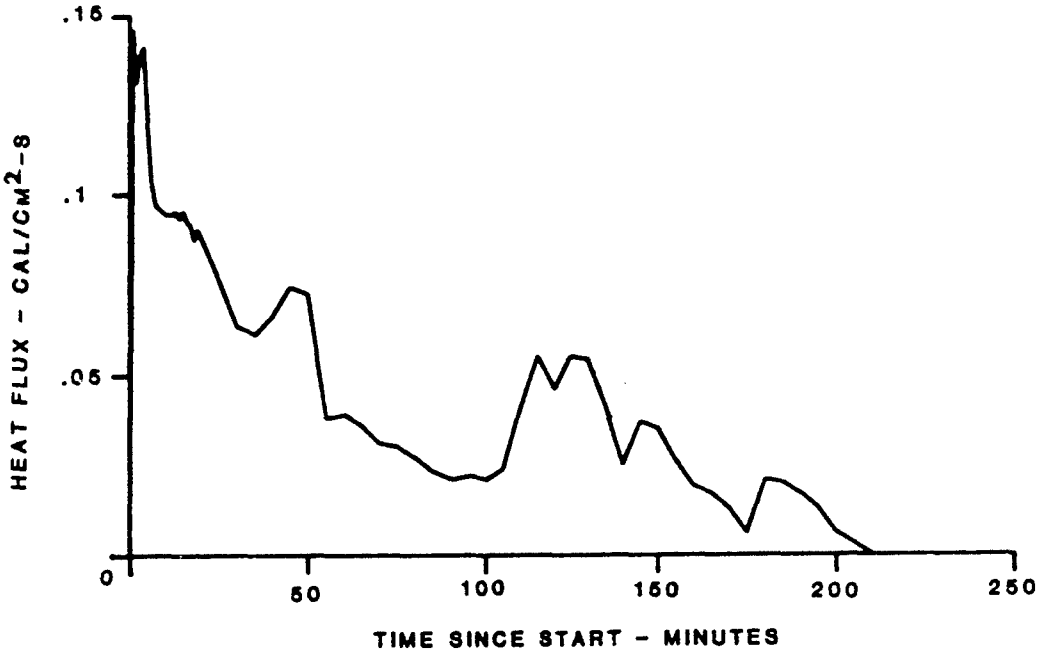

Figure 2.--Heat flow into the surface of a dry sand layer determined by an array of thermocouples. Thermal conductivity of dry sand was determined to be 0.487 mcal/cm-s-°C

SIGNIFICANCE OF RESULTS

These initial burns suggest the spacing of large-sized fuels must be closer than assumed in the burnout model in order to have mutual and interactive burning. Fuels of a given size probably have to be within 1.5 diameters of each other for interactive burning, but the critical spacing is at least a function of fuel size and the number of vertical layers involved. It is doubtful that two layers of fuel elements of the same size would interact to maintain flaming combustion while three or four layers probably would interact at spacings 1.5 diameters or less.

The glowing combustion phase is an important aspect of the burnout of a fuel bed. Glowing starts exerting its influence early in the fire history and continues 10 to 20 times longer than the flaming phase. Glowing will have a major effect upon the site, being lethal to soil organisms and causing physical changes in soil properties.

The experimental burns and associated field studies will provide numerical checkpoints for establishing bounds of energy release rates and flame heights that can be experienced. Consideration of the glowing combustion phase, the heat flow conducted below the fire, and heat radiated or convected away from the fire will be useful in restricting access to the area, establishing shelter needs, and estimating the potential for fire-induced winds.

Results from experimental fires such as have been described provide data for describing the burning regimes and intensities expected during the growth and decay of fires in rural and urban situations.

REFERENCES

1. J. R. Curry and W. L. Fons, "Rate of Spread of Surface Fires in the Ponderosa Pine Type of California," Journal of Agriculture Research. 57:4, (1938).

2. L. G. Hornby, "Fuel Type Mapping in Region One," Journal of Forestry 33(1), 67-70 (1935).

3. H. W. Beal, Forest Fire Danger Tables, Department of Mines and Resources, Ottawa, Canada (1946).

4. U. S. Department of Agriculture, Forest Service, The Wildland Fire Danger Rating System (1968 ed.), 108 p., Pacific Southwest Forest and Range Experiment Station, Berkeley, California (1958).

5. A. G. McArthur, Fire Behavior in Eucalypt Forests, Leaflet No. 107, 36 p., Forest Research Institute, Canberra, Australia (1967).

6. R. C. Rothermel, A Mathematical Model for Predicting Fire Spread in Wildland Fuels, USDA Forest Service Research Paper INT-115, 40 p. Intermountain Forest and Range Experiment Station, Ogden, Utah (1972).

7. John E. Deeming, James W. Lancaster, Michael A. Fosberg, and others. The National Fire-Danger Rating System, USDA Forest Service Research Paper RM-84, 53 p. (rev.), Rocky Mountain Forest and Range Experiment Station, Fort Collins, Colorado (1974).

8. Frank A. Albini, Estimating Wildfire Behavior and Effects, USDA Forest Service General Technical Report INT-30, 92 p, 74 ref., Intermountain Forest and Range Experiment Station, Ogden, Utah 84401 (1976).

9. F. A. Albini, Computer-based Models of Wildland Fire Behavior: a users' manual, 68 p., USDA Forest Service, Intermountain Forest and Range Experiment Station, Ogden, Utah (1976).

10. Andrews, Patricia L., A System for Predicting the Behavior of Forest and Range Fires, In: Proceedings 1983 SCS Conference on Computer Simulation in Emergency Planning, January 27-29, San Diego, California (1983).

11. T. A. Reitter, D. B. McCallen, and S. W. Kang, Literature Survey of Blast and Fire Effects of Nuclear Weapons on Urban Areas. Final report, June 1982, Lawrence Livermore National Laboratory, 7000 East Avenue, Livermore, California 94550 (1982).

12. F. A. Albini, Spot Fire Distance from Burning Trees--a Predictive Model, USDA Forest Service General Technical Report INT_56, 73 p., Intermountain Forest and Range Experiment Station, Ogden, Utah (1979).

WIND-AIDED FLAME SPREAD ACROSS STREWN DEBRIS

G. Carrier, F. Fendell, and R. Fleeter

TRW Space and Technology Group, Redondo Beach, CA 90278

Design of a laboratory experiment, to support further development of an already initiated theoretical model of wind-aided flame spread through a fuel matrix of large porosity, is presented. The design goals include delineation of a well-defined fuel matrix, careful control of the combustion environment (air flow and radiation), capacity for varying parameters (including fuel element type, matrix geometries, and introduction of upslope), and provision for attaining steady-state rate of spread (if one exists). If the model, given initial credibility by the laboratory experiment, is corroborated by field-scale data, then the model may be used with more confidence for predicting the movement in time of a fire front (with current position specified), through a partially combustible debris field of known topographical and aerothermochemical properties, under given meteorological conditions.

INTRODUCTION

The spectacular urban fires of modern times have usually been associated with the occurrence of strong sustained winds (London, 1666; Lisbon, 1775; Moscow, 1812; Chicago, 1871; Boston, 1872; Baltimore, 1904; Tokyo/Yokohama, 1923; Bandon, Oregon, 1936; Tokyo, 1945). Many of the memorable wildlands fires also were consequences of wind-aided flame spread (Miramichi River Valley, New Brunswick, Canada, 1825; Peshtigo, Wisconsin, 1871; Hinkley, Minnesota, 1894; Cloquet, Minnesota, 1918; Tillamook, Oregon, 1933; Shoshone National Forest, Wyoming, 1937; Victoria, Australia, 1939; Maine, New Hampshire, 1977; Sundance Mountain, Idaho, 1967; Victoria, Australia, 1983). This list is hardly exhaustive. What it suggests is that ignition often occurs in heavily fuel-laden areas in times of drought, but it is the coincidence of persistent winds of appreciable speed that causes a "blow-up." The arising of strong winds precipitates a startling run that ends only when the wind subsides, combustible matter is exhausted, or precipitation arrives. Clearly it is the wind-aiding, not the mode of ignition, that is the key common factor in most fire catastrophes.

What is missing in analysis of urban-scale fires is the capacity to predict with confidence the rate of flame spread, given the vertical and horizontal distribution, size distribution, exothermicity, and moisture content of the fuel; the nature of the topography; and the wind magnitude and direction,† the temperature, and the relative humidity as a function of pressure of the ambient atmosphere. If information were available on how fast the fire front will advance in a direction normal to the local front, then tracking of

†The "residue" left behind the fire front can serve to retard and divert the on-coming wind, such that the wind within a city or forest is reduced from the wind at the leading edge. On the other hand, narrow streets can constrict available passageway, so the flow can speed. Thus, the low-level modification of winds within an urban area is a complicated issue. Still, the first step remains obtaining the rate of spread, given local values of the pertinent meteorological, topographical, and aerothermochemical parameters; then the problem may be addressed of estimating appropriate local parameters (so that the local advance in time, from current position, of a given fire front may be executed).

the expected fire position at future time (given its position at the current time) becomes a relatively simple exercise. What is limiting is not computer storage or graphical display. What is limiting to meaningful prediction is reliable quantitative formulation of the physical processes controlling spread. (Spread rate from ignition site is also key insight in structure fires.)

The need for spread-rate information becomes more crucial as the rate becomes faster: escape times and countermeasure times are reduced. The fastest spread is almost invariably associated with wind-aiding: upslope spread exceeds downslope spread, spread under a sustained breeze exceeds spread in a calm. The accelerated spread can be owing to several factors: hot product gases blown downwind preheat uninvolved fuel in the fire path; more-distant transport of lofted firebrands is likely; bent-over plumes may ignite downwind fuel by contact or by enhanced radiative transfer (better view factor).

Interest here concentrates on an urban environment blasted into disarray. The debris-strewn setting has a far more continuous distribution of combustible material than the fire-code-satisfying preblast city. It should also be noted that interiors of (possibly partially toppled) structures are likely to be opened. While the similarity certainly should not be carried too far, the urban setting attains some of the properties of a wildlands setting, with ground-level combustibles playing the role of understory fuel (slash, litter, grass, brush, down woody matter) and the still-standing structures playing the role of overstory fuel (tree crowns); however, whereas ladder fuels linking understory and overstory fuels in a wildlands setting are often limited (lichen, dead or low branches, young trees, smaller trees), there is no lack of ladder fuels in the urban setting (there is no third story without a first and second story). Now, in a forest setting, one usually envisions flame spread through the large-pore fuel matrix of the understory, with an occasional crown being taken; in extremely severe, high-wind conditions a "wall" of flame takes all the readily combustible fuel from understory to overstory in one tall front; only very rarely (if ever) does flame race from crown to crown, either in the absence of an understory fire or far in advance of the surface-level fire (1). Though the taking of a crown is spectacular, aside from radiative transfer the event may not be that much more significant than the exothermicity contributed by reaction of a comparable mass of understory fuel. One point very much worth noting is that it is the small-diameter, thin, leafy matter that is dried out and consumed as the fire front passes, and hence is pertinent to rate of front progression; the thicker fuels are dried out and consumed on a longer time span, and thus react after the front has passed (if ever consumed at all).

The complexity of wind-aided fire spread through a porous, vertically extensive fuel bed lies partly in the fact that the reactants are initially in different phase, and partly in the fact that the intensively burning zone (separating the downwind preheat zone from the upwind burn-up zone) involves strongly buoyant convection. Thus, one must keep track of heat lost to drying out and gasification that may not be recovered, but one must also discard one-dimensionality for two-dimensionality. In fact, the buoyant updraft forms a barrier to the oncoming flow in two dimensions, and at least forms an obstacle about which oncoming flow is diverted in three-dimensional situations. Now, if the oncoming wind is strong enough, it should be able to blow over the convective column, whereas for not so strong a wind the column should

remain fairly vertical.* Since the strength of the updraft is related to the rate of fuel consumption, and since the rate of fuel consumption increases with the crosswind, the plume posture is a complicated matter. However, if the entrainment from the downwind side is overwhelmed by the crosswind strength (2), the plume should be blown over such that the fire is confined to the surface-layer fuels only, as far as burning at the front is concerned. Trying to state more than this soon becomes so convoluted that the need for experiment should be manifest.

MODEL ACCREDITATION BY LABORATORY EXPERIMENT

It is suggested that laboratory-scale experimentation should precede field-scale tests. The laboratory-scale experimentation permits attaining much data relatively quickly and relatively inexpensively, so appreciable parametric variation and considerable repetition (to check for error) is possible. There is likely to be better environmental definition, and more extensive and sophisticated diagnostic instrumentation, and better isolation of constituent components, in the laboratory than in some remote, possibly hostile, field environment. Conversely, relatively few data points are furnished by large-scale field tests, and these are obtained sometimes with long-time intervals; there is always a temptation to change too many parameters from one test to another, and there is almost never adequate redundancy, so field tests are in danger of becoming anecdotes (isolated events of uncertain reproducibility).

An oft-quoted argument against laboratory experimentation in fire science is that sometimes relatively few parameters can be assigned the values that they have in the field. Thus, one usually cannot carry out an experiment on laboratory scale, and by use of dimensional analyses, predict definitively what would occur in the field. However, if one could demonstrate, by comparison against a wide range of experimental data, that the theoretical model could predict (as accurately as required for the user's needs) physical events from boundary/initial conditions, then the model is given credibility. The wider the range, the greater the credibility. Of course, if the range of experimental data is not great enough to encompass the actual field situation of ultimate interest, the corroboration of the model remains incomplete: the model could still fail in the field. Thus, in the practical world of highly

---

*The wind is constant neither in magnitude nor in direction. Hence, use of the fire-front-propagation insight gained here will probably entail invoking a (well-justified) quasisteady approximation. That is, the propagation of flame normal to the front depends only on the component of wind instantaneously normal to the front, even though that wind is varying in magnitude and direction. During calms the fire may diminish in intensity, such that fire is confined to the understory. In fact, for the elliptical, preferred-axis shape of a wind-aided front, the fire at the flanks tends to have a weak aiding wind normal to the front, and "crowning" is less likely than at the head (3). As the wind freshens beyond some minimum, the fire may again enter the overstory along most of the front. Thus, as the front passes, it is quite likely that some tall structures may be left unconsumed because of wind variability and fuel combustibility--though these structures may be consumed later, well behind the front.

complicated, interdisciplinary phenomena, there remains an important role for engineering judgment.

This discussion would not be complete without reference to the desirability of ultimately utilizing results from the periodic burns on 500 X 500 ft. sections of coniferous stands carried out in the Canadian National Forest over the past decade by Brian Stocks of the Great Lakes Forest Research Center, Canadian Department of the Interior, Sault Sainte Marie, Ontario, Canada. These burns in heavily fuel-laden sectors provide an apparently unique opportunity to study large-scale wind-aided flame spread under relatively well characterized conditions, although motion-picture photography is presently the major mode of documentation.#

DESIGN OF LABORATORY EXPERIMENT

Since a model for wind-aided flame spread has been fairly well outlined (4), but even the most closely related experiments (5 - 9) are not appropriate for present needs, attention is limited to the design of a suitable, well-defined, easily repeatable experiment.

What is sought is a propagating one-dimensional wind-aided fire front in a basically two-dimensional flow through a precisely defined fuel matrix of large "porosity". There is to be relatively little constraint on air motion within the matrix, pyrolyzing to yield the combustible hydrocarbon vapors that burn exothermically with oxygen. (Only in later, more complicated versions would one consider initiating the experiment such that a two-dimensional fire front exists.)

The fuel bed is to consist of vertically suspended strips of thin combustible material (e.g., strips of paper); the separation between strips may be taken to be constant initially, such that the rows and columns of strips define a rectangular checkerboard (the number of rows is not in general equal to the number of columns). One may alter the "porosity" by (say) halving the separation between strips. However, if one homogeneously added more fuel loading to elements of the rarer matrix such that the total fuel loading equaled that of the denser matrix, the anticipation here is that the difference in flame spread rates might not be very large: details of the porosity are not believed to be crucial. The ability to incline the entire matrix at a constant angle to the horizontal, for purposes of adding upslope effects, would be desirable.

All the strips in the first row are to be ignited simultaneously by use of gas-jet-type diffusion flames. (For a two-dimensional experiment, one would ignite just the central few strips in the first row.) The key

---

#In the experiments conducted to date, the entire leading edge of the section perpendicular (more or less) to the wind direction is ignited simultaneously. It is suggested that only the (say) right half of the leading edge be ignited in at least one future test, for purposes of checking lateral-edge effects during wind-aided spread.

information sought is the rate at which the (hopefully) one-dimensional front moves from row to row. The number of rows should be enough to permit the initial transient to decay and a steady rate of flame propagation to be achieved, if a stable steady rate exists--there is no guarantee. But certainly the number of rows must be at the very least half again as many as are involved in the moving-front structure, from preheating through vigorous burning to residual burn-out. How many rows this is must be found empirically, but provision for hundreds of rows is advisable. The other key information sought is at what (constant) wind the flames of the vigorously burning zone are blown flat so no front can be defined.

It should be appreciated that much information about suitable properties for the test matrix can be obtained only by trial and error. Also, one must consider the fuel-loading in terms of the air flux past the matrix: one should be aware if the experimental conditions approach an oxygen-starved burning.

Space prevents listing of parameters, but two final issues are noted--topics deferred because they require particular attention. The first issue is achieving a uniform wind across the rows and down the columns (aside from perturbations owing to the fuel matrix itself and the burning thereof). If one employs just any nozzle to produce a wind, then the jet expands and slows (to conserve momentum flux) with distance from the nozzle exit, such that the speed experienced (say) half-way down the matrix may be reduced appreciably from that experienced by the leading row (independently of any perturbation caused by the matrix). Hence, achievement of a steady fire-front propagation is precluded. A response is to enclose the experiment in a duct. The floor always produces a boundary layer--probably an effect one wants to retain because of its relevance to the practical situation. The ceiling would restrain the buoyant gases, and possibly interfere with the downwind portion of the experiment--so the ceiling should be in place only upwind of the fire front. Sidewalls would restrain the spreading of the stream and thus serve the useful purpose of preserving the cross-sectional area; one should allow for the turbulent boundary-layer growth on these (nearly) parallel sidewalls. Most of the matrix elements should not lie in the sidewall boundary layer, even at the trailing row of the matrix.

The other issue concerns the radiation, the role of which in transport of heat increases with spatial scale, such that radiative transfer may be appreciably more important in the urban-scale fire than it would be in the small laboratory apparatus. However, it is well worth noting that it is quite feasible to add radiative heat input via an external source to examine the nature and magnitude of the laboratory-flow response.

This discussion of wind-aided flame spread through a uniform fuel matrix is concluded with the following two observations. First, perhaps not enough emphasis has been placed on the possibly highly variable thickness of the flame structure, the streamwise length spanning the domains of (1) preheating and thermal degradation; (2) pyrolysis and vigorous flaming with buoyant ascent; and (3) burn-up of the char residue left after pyrolysis is complete. For close spacing in a high wind, there may be only partial burn-up as the flame front passes, and burn-out occurs only long after flame passage; conversely for widely spaced elements in a modest wind, the fuel elements may burn almost individually and the "wave structure" is smaller. Second, since only a

fraction of the debris is combustible in a blasted urban environment, the other inert portion perhaps serving as a heat sink-source repository, perhaps the homogeneous addition of such inert mass to the fuel matrix ought to be considered ultimately.

ACKNOWLEDGMENT

The authors are grateful to technical monitors Mike Frankel and Tom Kennedy for the opportunity to pursue this investigation. This work was supported by the Defense Nuclear Agency under contract DNA001-81-C-0111.

REFERENCES

1. C. E. Van Wagner, "Conditions for the Start and Spread of Crown Fire," Canadian Journal of Forestry Research 7, 23-34 (1977).

2. G. I. Taylor, "Fire under the Influence of Natural Convection", in International Symposium on the Use of Models in Fire Research (National Academy of Sciences - National Research Council Publication 786, Washington, D.C., 1961), pp. 10-28.

3. D. A. Haines, "Horizontal Roll Vortices and Crown Fires," Journal of Applied Meterorology 21, 751-763 (1982).

4. G. Carrier and F. Fendell, "Crown Fires," Engineering Science Laboratory, TRW Space and Technology Group, Redondo Beach, CA (1982), report 38095-6001-UT-00.

5. W. L. Fons, H. B. Clements, and P. M. George, "Scale Effects on Propagation Rate of Laboratory Crib Fires," in Ninth Symposium (International) Combustion (Academic, New York, NY, 1963), pp. 860-866.

6. H. E. Anderson and R. C. Rothermel, "Influence of Moisture and Wind upon the Characteristics of Free-Burning Fires," in Tenth Symposium (International) on Combustion (Combustion Institute, Pittsburgh, PA, 1965), pp. 1009-1019.

7. J. B. Fang and F. R. Steward, "Flame Spread through Randomly Packed Fuel Particles," Combustion and Flame 13, 392-398 (1969).

8. H. W. Emmons and T. Shen, "Fire-spread in Paper Arrays," in Thirteenth Symposium (International) on Combustion (Combustion Institute Pittsburgh, PA, 1971), pp. 917-926.

9. F. R. Steward and K. N. Tennankore, "The Measurement of the Burning Rate of an Individual Dowel in a Uniform Fuel Matrix," in Eighteenth Symposium (International) on Combustion (Combustion Institute, Pittsburgh, PA, 1981), pp. 641-646.

MODELING URBAN FIRE GROWTH

T.E. Waterman and A.N. Takata
IIT Research Institue
Chicago, Illinois

ABSTRACT

Under FEMA Contract DCPA01-79-C-2065, IIT Research Institute (IITRI) employed existing models for debris transport and fire behavior to assess the value of existing blast/fire/people survivability data. Presentations at prior Asilomar Conferences have addressed debris transport and overviewed survivability results. The purpose of this presentation is to examine potential weaknesses of the fire spread model.

The IITRI Urban Fire Spread Model as well as others of similar vintage were constrained by computer size and running costs such that many approximations/generalizations were introduced to reduce program complexity and data storage requirements. Simplifications were introduced both in input data and in fire growth and spread calculations. Modern computational capabilities offer the means to introduce greater detail and to examine its practical significance on urban fire predictions.

Selected portions of the model are described as presently configured, and potential modifications are discussed. A single tract model is hypothesized which permits the importance of various model details to be assessed, and, other model applications are identified.

INTRODUCTION

Prediction of the fire behavior of an urban area subjected to a nuclear attack is necessary for evaluating damage, casualties, and the effectiveness of countermeasures. Indeed, fires grow and spread over an extended period of time, and this growth can be strongly modified both by preattack passive countermeasures and by human actions taken during the relatively long trans-attack period. Furthermore, the initiation and growth of new fires in a specific local area are affected not only by their immediate surroundings, but by fire development over a much broader area in terms of firebrands, winds, air quality and gross radiation levels, including factors from or related to mass fire development.

Even a cursory examination reveals that large numbers of parameters and processes are involved. These mandate computer assessment if any level of detail is to be preserved. Conceptually, computer modeling of urban area fires is straightforward. It involves programming the processes and inputing pertinent data parameters describing the urban area. However, the various processes interrelate and the number of structures in an urban area is quite large. Thus, the calculations become complex and extremely voluminous.

The major development of computerized urban fire spread models occurred in the late 1960s (1)(2)(3). Each employed various techniques, primarily of a statistical nature, to make calculations manageable within the available computer memories. Each benefitted from lessons learned in an earlier attempt by IITRI to produce a more deterministic model (4). This earlier model treats weapon initiation of fires from a probability point of view, considered

necessary as furniture locations in rooms were assumed not to be predictable. Fire spread and other input data were treated deterministically, prescribing go or no-go conditions. Firebrands were of stated concern, but not introduced into the model; fire spread was solely by radiation.

The basic philosophy developed in the early model was to apply calculated ignition probabilities to local city areas called tracts (several blocks of relatively uniform characteristics) by Monte Carlo techniques. Spread across tract boundaries was to be assessed by similar means. The results of repeated computational exercises (computerized fire experiments) were to be used to develop analytical approximations of fire spread within tracts and across various tract boundaries. These, in turn, were to be fitted together by Monte Carlo methods to form the overall model for urban fire spread.

Unfortunately, computer capabilities in the early 1960s were such that the time required for one fire spread calculation in a tract of 100 buildings equalled or exceeded that which would occur in the real fire. Considering the number of runs required to attach statistical significance to the results for just one tract, the problem of examining an entire city becomes obvious. The solution at the time was to develop an interim model for minimum expected damage which considered fires not to spread across streets. In this simplified form, the model was employed by the National Military Command Systems Support Center to estimate fire damage and, with some assumptions, casualties. Also, it served as the starting point for Firefly (3). Potential benefits of this early model, as yet not exploited, are the detailed inter- and intra-building fire spread calculation techniques and the extensive sensitivity studies performed and reported (4).

POTENTIAL MODEL DEFICIENCIES

The more recent IITRI model (1) will be examined here. It has been modified over time to include effects of fire suppression efforts (5) and blast-suppressed ignitions (6) and to refine prediction of spread by firebrands (6). Most recently, the model was adapted for use in regions of moderate blast damage (7). None of these modifications/adaptations have changed the basic procedures for assessing primary ignitions or radiation fire spread. Potential model deficiencies in these areas are illustrated. Note in addition that the model does not presume to calculate mass fire behavior. It does, however, provide output of heat release and active fire locations with time for input to future mass fire development criteria or models.

Primary ignition calculations presently assume all buildings have one wall directly facing ground zero. This tends to maximize the interior room areas supplied with critical ignition energies in those rooms exposed to the thermal pulse; but, minimizes the number of rooms "seeing" the pulse. The assumption thus overestimates the number of rooms receiving primary ignitions of furniture (Figure 1) and underestimates the number of rooms where draperies and curtains are ignited. Since draperies and curtain ignitions appear more prone to blast-wave extinctions, it is not clear whether the net effects of the above assumption are high or low at any given building orientation and distance to ground zero.

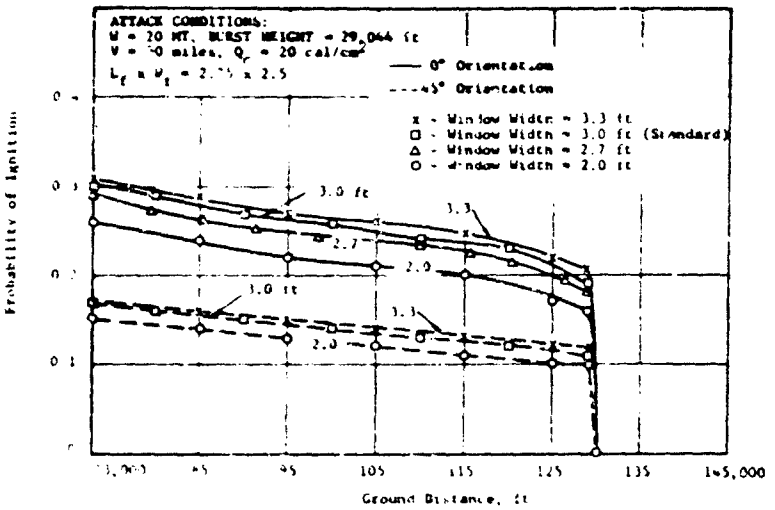

Figure 1. Probability of a chair being ignited as a function of window width, distance and orientation to ground zero. (4)

The impacts of assumptions introduced into radiation fire spread modeling are not so simply described and readily assessed. First, note that radiation fire spread depends on many factors, including separation of radiant source(s) and target, target susceptibility to ignition, presence or absence of pilots (sparks, brands, open flames), and intensity of the radiant sources. Also, the intensity of each radiant source (burning building) is a function of time, number and location(s) of ignition(s) and resistances to fire spread within the burning building; and, the radiant exposure on a single target may be the net (or total) exposure due to several radiant sources.

The present IITRI model (1) incorporates this variety of information, but the detail is lost as the model uses statistically distributed times of active burning (assumed to represent most likely times of peak radiant strength*), ignition susceptibility for target materials, and building separations (based on surveys of "typical" actual areas). Indeed, the model has been criticized by Schmidt (8) for arbitrarily increasing all building separations in relation to the number of "burned out" buildings with time. Unfortunately, the true impact of this latter assumption is still not known; the analysis presented by Schmidt retains many other, related assumptions of the IITRI model.

While concerns such as these raise some question about the adequacy of model-predicted ultimate fire damage, of comparable importance is the fact that the present IITRI model (and its contemporaries) does not permit detailed time-based, building-by-building analysis of local fire development and spread. This somewhat limits the confidence placed on model-based measures of the effectiveness of suppression activities, and places strong constraints on use

* The same technique, but a different time distribution, is applied to firebrand generation.

of the model to characterize the fire vulnerability of specific local areas of interest such as key industries or regions immediate to key worker shelters. The figures (4) illustrate details of fire development and spread lost in the statistical nature of the models in current use.

The building employed for the following examples is a three-story multi-family apartment, the typical Chicago six-flat with two apartments per story sharing a common front entry and stairwell, with somewhat independent rear entries. Rear doors open to independent rear porches which share a common open rear stairwell. Figures 2 and 3 illustrate the effects of different numbers and locations of ignitions on the subsequent history of fire development within the building (time from ignition to significant involvement of the ignited compartment, and fire resistance of interior barriers, fixed for these examples).

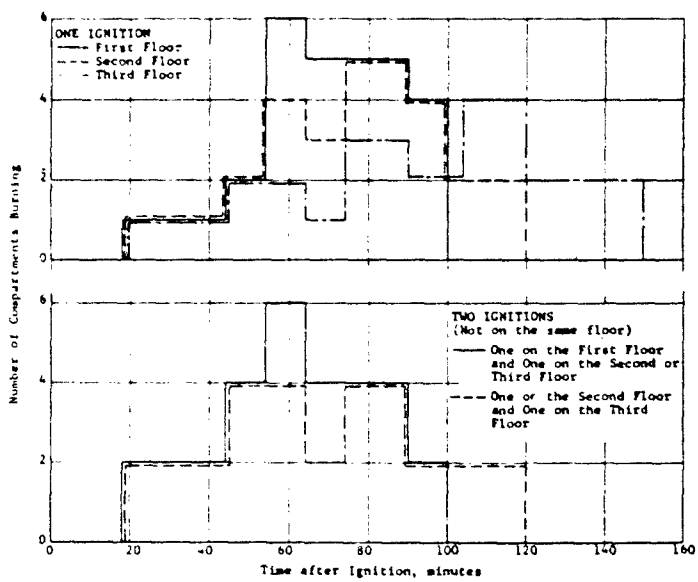

Figure 2. Effect of location of one or two ignitions on compartment burning in "six-flat". (4)

The strength of the radiant source formed by a burning building is a function of which compartments are burning and whether or not internal ceiling-floor constructions or ceiling-roof constructions are still intact. Drawing on experimental results generated in a supporting effort (9), examples of radiation intensities on a target 20 ft from the building are illustrated in Figure 4. In all of the stated examples, fire spread throughout each apartment was considered to be relatively unhindered (open doors) with major delays (closed doors, other barriers) to spread between apartments. This can be generally considered to be the case; thus, the assumptions of the current model (1) in this regard have some affect on results for single family residences, but much greater impact on results for apartments, condominiums, and hotels.

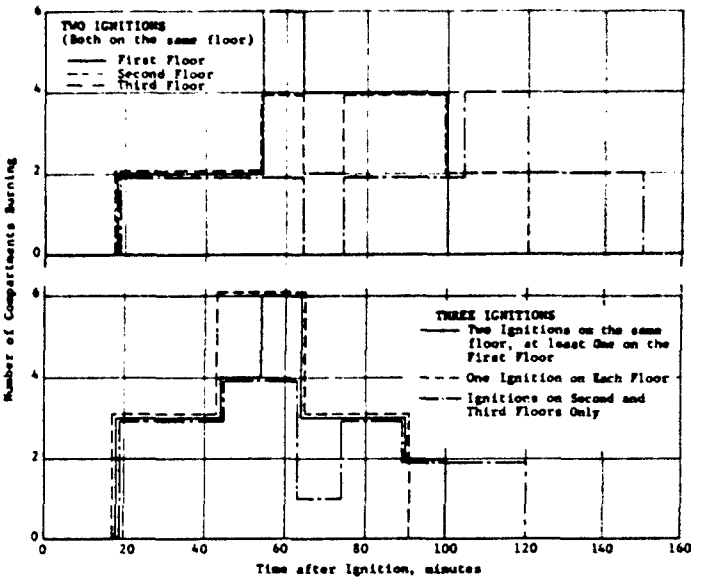

Figure 3. Effect of location of two or three ignitions on compartment burning in "six-flat". (4)

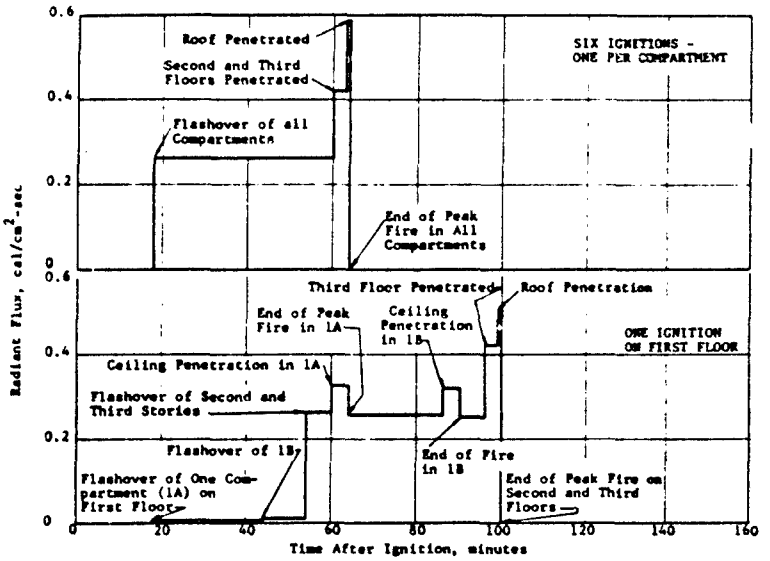

Figure 4. Calculated Radiation from the Front of a six-flat for two ignition patterns. (4)

Not all model weaknesses are computer related. We still have many uncertainties related to our basic knowledge of the phenomena. Among the many inadequacies are: (1) affect of residual heat from the weapon pulse on fire growth to room flashover; (2) affect of exposure fires on fire growth in ignited room or building; (3) detailed characterization of firebrand escape from fire plume, trajectory near target; and (4) local wind variation.

RECOMMENDED MODEL DEVELOPMENT

A new model should be constructed taking advantage of the speed and storage capacity of modern computational facilities. The model should address, at first, a localized urban area similar to the previously used "tract". By initially considering a local area instead of an entire city, the model can incorporate greater detail than may be practical for the entire city as a whole, even with modern computers.

The model should be constructed, to the degree possible, in a deterministic manner, modularly designed for ready modification of selected input or calculation processes as these are deemed inadequate by state of the art information or weaknesses identified by exercising the model. On a local area basis, the model lends itself particularly to parameter sensitivity analysis to define the importance of the various levels of detail included, and to examine the need of further refinement, where data or "physics" are lacking. At this level of development, the model also can be used to examine fire spread through areas of various structural types, structural mixes, building density, and damage levels to provide a "Fire Vulnerability Index" for local assessment of fire danger levels, perhaps comparable to the blast "vulnerability numbers" presently in use.

At this level of development, the model can assess the effects of wind, humidity and precipitation on local fire growth. Through certain assumptions regarding the upwind boundary, a first level of "conflagration potential" can be addressed. At the very least, levels of wind and heating required to significantly affect downwind fire spread can be identified.

Upon satisfactory development of this detailed local area model, it could be applied to the entire city in a manner compatible with its complexity and utility. In its simplest use, it could be applied to selected local areas under the influence of a general urban fire described by the present urban fire models (1)(2)(3), or with some refinement suggested as critical by the above-mentioned sensitivity analyses. In essence, it could be introduced into blast-fire analyses such as those performed by IITRI under work unit 2564D (7).

Should size and complexity of this new "local area" model permit, it could completely replace the present "tract" model and be used to describe all tracts in the entire urban fire area in detail, or at selected levels of detail.

To complete all aspects of model development and application will require a significant expenditure of time and effort. It appears reasonable to target the "local area" model development and some measure of sensitivity analysis as the first goals. Armed with the information and insight so obtained, the remaining course of action and ultimate goals may be refined and defined more precisely.

REFERENCES

1. A.N. Takata and F. Salzberg, Development and Application of a Complete Fire-Spread Model: Volume I, Development Phase, IIT Research Institute, OCD Work Unit 2538B, Contract N0022867C1498 (Jun 1968).

2. S. Martin, R. Ramstad and C. Colvin, Development and Application of an Interim Fire-Behavior Model, URS Research Company, Burlingame, California, URS-674-3 (Apr 1968).

3. J.W. Crowley, et al, Firefly - A Computer Model to Assess the Extent of Nuclear Fire Damage in Urbanized Areas, Systems Sciences Inc, Bethesda, Maryland, (May 1968).

4. F. Salzberg, M.M. Gutterman and A.J. Pintar, Predictions of Fire Damage to Installations and Built-Up Areas from Nuclear Weapons: Phase III, Theoretical Studies, IIT Research Institute for National Military Command Systems Support Center, Contract DA-49-146-XZ-021 (Jul 1965)--phase I initiated in 1959.

5. A.N. Takata, Mathematical Modeling of Fire Defenses, OCD Contract DAHC20-70-C-0209, (Feb 1970).

6. A.N. Takata, Fire Spread Model Adaptation, IIT Research Institute, DCPA Work Unit 2538G, Contract DAHC20-72-C-0152 (Oct 1972).

7. A. Longinow, T.E. Waterman and A.N. Takata, Assessment of Combined Effects of Blast and Fire on Personnel Survivability, IIT Research Institute, FEMA Work Unit 2564D, Contract DCPA01-79-C-0265 (Jun 1982).

8. L.A. Schmidt Jr, A Parametric Study of Probabilistic Fire Spread Effects, Institute for Defense Analyses, IDA Paper P-1372, (Sep 1979).

9. T.E. Waterman, et al, Prediction of Fire Damage to Installations and Built-Up Areas from Nuclear Weapons: Phase III, Experimental Studies - Appendices A to G, IIT Research Institute for National Military Command Systems Support Center, Contract DCA-8, (Nov 1964).

SESSION VI

BLAST/FIRE AND RELATED TOPICS

BLAST/FIRE INTERACTION SCALING

by

Murty Kanury
Department of Aerospace and Mechanical Engineering
University of Notre Dame
Notre Dame, IN 46556

ABSTRACT

Hypotheses are formulated of the process of interaction between an airblast and fires supported by liquid fuels and wood cribs. A map of blast weakness versus fire strength is conceived on which the regime of fire extinction by the blast can be delineated from the regime where the fire will sustain the blast. The fire strength is described for liquid fuels primarily by the heat of combustion; and for wood, it is mainly described by the preburn time. The concept is substantiated by the SRI shocktube data.

INTRODUCTION

Thermal radiation from the fireball would cause spontaneous ignition of various combustibles at all stations where the fluence of energy is sufficiently high. As the thus started fires grow, the blast wave would arrive to perturb the fires with its associated transient pressure, flow and temperature disturbances. The purpose of the research synopsized in this paper is: to develop scaling rules governing the behavior of the blast-impacted-fires; to apply these rules to the available experimental data on blast/fire interaction; and to thus elicit upon the nature of this interaction. A synopsis as this paper is, complete details are available in (1).

Fires supported by hydrocarbon liquid fuel pools (known as Class B fires) and by charring solid fuels such as wood (known as Class A fires) are of specific interest in this study. Since the wood pyrolyzates are composed mostly of a variety of gaseous hydrocarbons, the wood flame combustion chemistry characteristics are expected to be essentially similar to those of liquid hydrocarbon flames. Additionally, however, if the flame were annihilated to permit approach of oxygen to the hot char surface of wood, glowing combustion would ensue. Thus, a scrutiny of blast effects on flames and on glowing surfaces constitutes the essential scientific content of this study.

BLAST INTERACTION WITH FLAMES

A steadily burning pool fire is disturbed by a blast wave through the manifestation of one or more of the following phenomena.

(a) Annihilation of spacial gradients of species, temperature and velocity by the increased molecular and turbulent transport is expected to lead to excessive thermal as well as species dilution in the reaction space.

(b) Energy feedback from the flame to the condensed phase fuel will be reduced due to physical displacement or deformation of the flame resulting in both a decay in fuel vapor supply to the gas phase and a reduction of the temperature of gas phase near the fuel bed. The chemi-

cal kinetic rate is drastically reduced as a result.

(c) If the wind is feeble, energy feedback to the fuel bed may be augmented by the wind bringing the flame closer to the surface so that the blast imposition would augment the fire intensity contrary to the consequences of (a) and (b) above.

(d) Energy feedback to the fuel bed will be enhanced due to flame-holding in the recirculatory zones.

(e) The fuel bed may be mechanically broken up to possibly aggrevate the fire in intensity by transforming the bulk fuel into a spray. Fragmentation of the fuel bed might also aid to dissipate the energy content of the fuel in the tray to an ineffectually low average level.

(f) Pressure change will result in a shift in combustion chemical kinetics. The kinetic rate for combustion of hydrocarbons in air varies nearly as proportional to the square of pressure. The pressure change also alters the fluid dynamics to increase the coefficients of heat and mass transfer. The net effect of these two opposing actions of increased pressure can not be drawn without a detailed study. Additionally, since the pressure rise associated with a blast wave is temporally variant, arguments based on static imposition of a pressure rise might become invalid in the dynamic behavior of a blast-impacted flame.

(g) The shockwave is also associated with a temperature rise due to isentropic compression of air. This too is a transient phenomenon which may exert some effect on the chemical kinetic aspects of the flame.

(h) In all practical situations of blast wave generation by the explosion of a weapon, a thermal radiation pulse is involved which would promote continued vaporization of the fuel bed even as the energy feedback is mitigated from the disappeared flames. Even more important is the thermal radiation pulse from subsequent weapon bursts. The issue of multibursts is ignored here.

Inasmuch as most of the above-enumerated effects can be condensed, they fall into one or more of the three global altercations: thermal dilution, fuel vapor dilution and oxygen enrichment of the gas phase space where once the flame stood. The dilution effects figure dominantly in the fate of flaming while the oxygen enrichment has a role to play in glowing combustion of charcoal.

Based on an algebraic analysis of the fuel species and energy conservation, the following relation is derived in (1) to relate the gas temperature θ to the energetic strength q^* of the flame, blast weakness P^*, and fuel surface temperature θ_i.

$$P^* = \frac{(\theta-\theta_i)\exp(1/\theta)}{q^*-(\theta-\theta_i)} \qquad (1)$$

where $\theta \equiv RT/E$, $\theta_i \equiv RT_i/E$, $P^* \equiv k_0\ell/u$ and $q^* \equiv Rh_cY_{Ai}/EC_{pg}$. ($E/R$, k_0, h_c and T respectively are the activation temperature, preexponential factor, enthalpy of combustion and temperature of the flame reaction. Y_{Ai} and T_i are mass fraction of fuel and its surface temperature. C_{pg} is gas specific heat; ℓ is fuel bed dimension and u is blast-induced velocity.) Equation (1) indicates that there exists a P^* for any given q^* and θ_i at which the reaction can not sustain itself, i.e., θ falls catastrophically to result in extinction. The higher the q^* (i.e., the more stronger the flame is energetically), the lower is P^* (i.e., the stronger is the blast wave) to cause extinction. Figure 1 shows the P^* vs q^* map in which fires and blasts corresponding to the area under the curve are expected to represent extinguish-

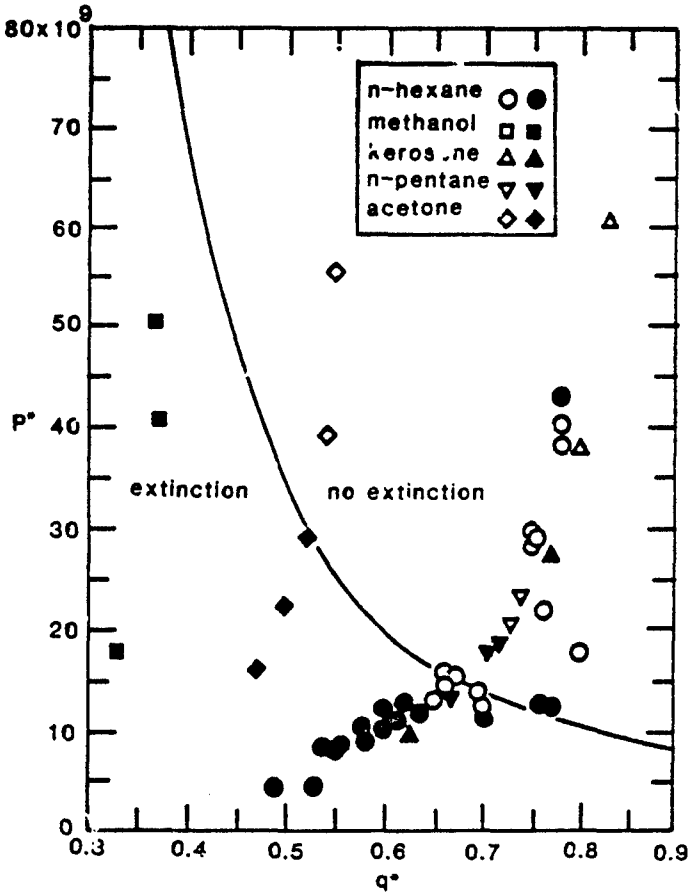

Figure 1: Extinction (filled symbols) - No Extinction (open symbols) Correlation for Class B Fires with No Barriers.

ment. The shock-tube (Class B, no-barrier) fire data obtained by Martin and Backovsky (2-4) are shown in this figure (open and closed symbols respectively for unextinguished and extinguished fires) to demonstrate that the extinction regime can indeed be delineated according to our hypothesis. Upstream barriers, behind which recirculation of flow is possible, are shown in (1) to render the fire more blast resistant.

BLAST INTERACTION WITH WOOD FIRES

Whereas the flaming combustion of wood cribs follows the same patterns as described above, there are at least two special features to be noted. It is known that the longer a wood crib fire burns, the more established it becomes, mainly due to the transient conductive heating and pyrolysis. Based on analyses of transient pyrolysis of wood sticks (5), the characteristic time to completely burn a stick of wood of thickness b is given by $t^\circ = Ab + Bb^2$ where the A is a function of pyrolysis energetics and kinetics, heating rate and wood specific heat and B is essentially the inverse thermal diffusivity of wood. Typically, A ≈ 260 sec/cm and B ≈ 30 sec/cm^2. The fire strength then can be expressed as a ratio of (pre)burn time t to the characteristic time t°. Since the wood flames appear to be similar to hydrocarbon flames, we expect the blast interaction with wood flames to obey the same rules as Class B fires on a blast weakness P* versus fire strength q* map provided $q^* \equiv \tau$ is

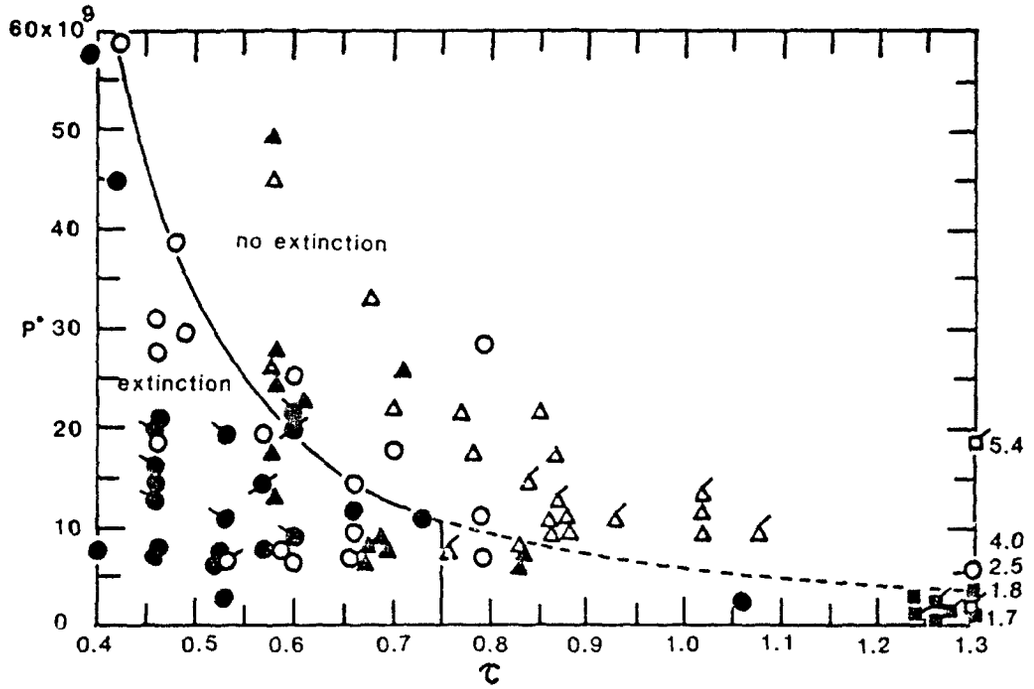

3/4" stick cribs: ● extinguished. ○ sustained. ◕ extinguished, glows, no reflash. ◕ extinguished, close to reflash. ◎ reflashed.

3/8" stick cribs: ▲ extinguished. △ sustained. ◭ reflashed.

shredded paper trays: ■ extinguished. □ sustained. ◪ rekindled. ◪ rekindled upon blowing air.

Figure 2: Extinction- No Extinction Correlation of Class A Fires.

taken to be proporational to t/t^*. With $\tau = 2.7\ t/t^*$, the shock-tube data of (3) and (4) are shown in Fig. 2 to demonstrate that weak, short-preburn, fires impacted by strong blasts are prone to extinction.

SRI experiments also indicate that beyond a critical preburn time of about 170s, the crib fire becomes altogether blast-proof. Based on wood pyrolysis kinetics literature, the time taken for complete charring of a wood element surface is shown in (1) to be also about 170s under conditions typical of crib burning. Beyond this time: (a) the pyrolysis process will become completely submerged within the solid, less vulnerable to any extinguishment actions in the gas phase; and (b) the surface char is so richly carbonaceous as to effectively glow with the oxygen attacking it after the flame is extinguished. This intense glowing maintains or even accelerates the subsurface pyrolysis. As the blast effects subside and glowing tends to cease, the system passes through the flaming ignition state at which a reflash is imminent. If, on the contrary, the preburn time is short, the surface would be only partially charred; the resultant glowing, being less intense, fails to perpetuate the pyrolyzate production; the flaming ignition state is not encountered as the system cools down; and the reflash is absent. Based on this description, for τ exceeding that corresponding to preburn time = 170s, the fire is to become blast-proof. Figure 2 shows this critical fire strength parameter to be $\tau = 0.75$.

Such factors as recirculation of flow behind the sticks within the crib to stablize the flame are discussed in (1) as the reasons underlying the scatter in Fig. 2.

CONCLUSION

The scaling approach appears to provide a systematic framework with which an improved understanding of the blast/fire interaction mechanisms can be gained from the experimental observations. The influence of blast on both Class B fires with and without barriers and Class A fires over a range of preburn times appears to be describable on a blast weakness P* versus fire strength q* map.

REFERENCES

1. A.M. Kanury, "Responses Mechanism: Blast/Fire Interactions," Final Report, contract EMW-C-0366, FEMA WU 2564 H, University of Notre Dame, Notre Dame, Indiana, (March 1983).

2. S.B. Martin, "Experiments on Extinction of Fires by Airblast," Annual Report, Contract DCPA01-79-C-0245, FEMA WU 2564A, SRI International, Menlo Park, California, (January, 1980).

3. J. Backovsky, S.B. Martin, and R. McKee, "Blast Effects on Fires," Annual Report, Contract DCPA01-79-C-0245, FEMA WU 2564A, SRI International, Menlo Park, California (December 1980).

4. J. Backovsky, S.B. Martin, and R. McKee, "Experimental Extinguishment of Fire by Blast," Final Report, Contract EMW-C-0559, FEMA WU 2564A, SRI International, Menlo Park, California (March, 1982).

5. A.M. Kanury, "Rate of Charring Combustion in a Fire," pp. 1131-1142, Fourteenth Symposium (International) on Combustion, the Combustion Institute, Pittsburgh, Pennsylvania, (1973).

FLASHOVER MODELING FOR DIRECT COURSE

By: Stan Martin and
Pete Hughes
of Los Alamos Technical Associates

ABSTRACT

The current fire defense doctrine for nuclear attack preparedness is possibly erroneous. The guidance to local planners has been strongly influenced by the concept that fires started by the thermal pulse of the nuclear fireball are initially feeble and quite susceptible to airblast extinction. This concept ignores a potentially crucial observation made during the days of atmospheric nuclear testing, that has since been termed an anomaly. Nevertheless, this observation may provide the explanation for some of the puzzles--the contradictions of experimental tests vis-a-vis historical fact--that have for years persisted about the incendiary consequences of nuclear explosions in or near urban complexes.

Operation DIRECT COURSE offers an opportunity to resolve a part of the quandary. The question to be answered is whether fires of the rapid fire-growth-to-flashover type, as associated with nuclear thermal-pulse scenarios, are as susceptible to extinction as the current doctrine supposes. This paper describes an experiment designed to gain an answer to that question.

INTRODUCTION

The currently accepted models of the incendiary effects of nuclear explosions in urban areas focus on fire starts in rooms, the underlying assumption being that fires in rooms will dominate the outcome. Unquestionably, fires in rooms constitute a category of special interest in fire growth dynamics. The enclosure not only serves to limit air supply to the fire, but it conserves a portion of the heat released by the fire to intensify it, often leading to a relatively abrupt involvement of the entire room and its contents in an event called "flashover." Viewed operationally, as well as in straight forward damage assessment terms, flashover is a critical endpoint to the development of the incipient fire. The nuclear-effects predictive models customarily treat the incipient fire, prior to flashover, as a feeble--and therefore blast-sensitive--stage in the growth of the fire. Full-scale tests of incipient room fires that were conducted in the Ft. Cronkhite blast tunnel in 1970 (1) consistently resulted in blowout thresholds only slightly higher than 2 psi. Even under airblast conditions failing to extinguish it, the conventionally modeled fire is perceived to be still quite easily extinguished by prompt action of the first-aid firefighting sort, up to the onset of flashover (2). There is good reason to believe, however, the conventional wisdom may be wrong.

During the ENCORE event (3) of Operation UPSHOT/KNOTHOLE in 1953, a furnished room, its window facing the fireball, flashed over in less than a minute after exposure to a thermal fluence of about 25 cal/cm^2. The building was rapidly destroyed by a fire that did not blow out despite an incident air

blast of about 6 psi or higher peak overpressure. A conclusion that the ENCORE response, rather than being an anomaly, is the more realistic situation to expect--as opposed to the slow buildup of fire from a feeble and airblast-vulnerable start--could go a long way toward providing the explanation for some of the puzzling inconsistencies between experimental results and the historical experiences. Should such a conclusion be substantiated by further research, it could significantly impact current perceptions of the dynamics and threat potential of fire caused by nuclear explosions. In turn, it might lead to modification of civil defense planning, calling for reexamination of such operational concepts as crisis relocation, the choice and design of risk-area shelters, and the efficacy of preattack fire-defense preparations and both trans-attack and post-attack firefighting strategies.

THE EXPERIMENT

OBJECTIVES

The objective of the room-fire experiments at DIRECT COURSE is to determine the susceptibility to blowout of fires that are dynamically comparable to the ENCORE response. The tests are to be conducted to reveal effects of fire intensity, representing differences in time intervals between fire initiation and blast wave arrival.

SCOPE

This experiment comprises the test of four separate blockhouses (of non-responding design), furnished as a representative urban occupancy, with fire initiated by propane gas supply. Two distinct variations are planned: (1) a room fully flashed over prior to shock arrival; (2) a room experiencing rapid heat buildup at the time of shock arrival, but not yet flashed over. Two blockhouses, one of each of the two fire-state variations, will be located together in the DIRECT COURSE test bed at a distance expected to experience a peak overpressure of 7 psi. An additional variation (1) blockhouse will be located to experience a 9 psi overpressure, and an additional variation (2) blockhouse, to receive 3 psi.

Details of the experiment are given in a companion paper to be presented at this conference. This paper focuses on the requirement for reliably achieving the prescribed fire state at the instant of blast wave arrival and on the theoretical/empirical basis for selecting the experimental conditions to ensure that this requirement is met.

EXPERIMENTAL RATIONAL

DESIGN CONSTRAINTS

Dynamic similarity to the ENCORE event requires rates of rise in temperatures that are not ordinarily encountered in growing fires. To properly simulate exposures to the high thermal radiation fluxes from a nuclear fireball, large rates of heat release within the room must be provided in some alternative manner, and the duration of heat supply must be short. By comparison,

the development of quasi-steady flow of air into, and combustion products out of, the room is a much slower process. Accordingly, even after flashover occurs, conditions in the room that influence its fire behavior continue to change with time. Therefore, the elapsed time between flashover and shock arrival must be controlled by experimental design. In the room fires that have not yet reached the flashover stage by the time the blast wave impacts them, predictable conditions can be achieved only by close control of the rate of fire growth and the elapsed time from fire initiation to shock arrival.

BACKGROUND CONSIDERATIONS

In designing the room fire experiments for DIRECT COURSE, the following factors have been considered:

- It is desirable to relate these experiments to the blockhouse tests at ENCORE (a 27-KT yield airburst, at a height of 2425 ft) that were fielded by the U.S.F.S. Forest Products Laboratory.
- It is also desirable to relate these experiments to the reduced-scale model experiments conducted at SRI in 1978 for the Products Research Committee (PRC, see Ref. 4), because of the potential this offers for predicting flashover conditions and unsteady characteristics of compartment-fire growth. This would require designing the DIRECT COURSE experiments to retain geometric similarity and to preserve the magnitude of several non-dimensional parameters pertaining to fuel supply and convective flow.
- Several other experiments are expected to have a bearing on the design of the DIRECT COURSE room fire experiments. (See, as examples, Refs. 5 through 10).

Further elaboration is given below.

Details of the ENCORE Blockhouses

The ENCORE Blockhouses had approximate inside dimensions of 9½ ft width, 13 ft depth, and 8 ft ceiling height. The single opening, a window, was 6 ft wide and 4 ft high, centered in the front wall, its soffit about 2 ft below the ceiling. Accordingly, each FPL blockhouse had a plan area of about 123 ft^2 (11.5 m^2) and a volume of about 988 ft^3 (27.9 m^3). The volume of room air above the window soffit was about 246 ft^3 (7 m^3), and the (Kawagoe) ventilation factor of the window was 2.46 (mks units)*. It is estimated that during the (2 second) thermal pulse prior to shock arrival, the window transmitted 5 x 10^5 calories to the room interior (about 2 megajoules), and that flashover occurred in about 30 seconds.

---

*The significance of this is that, once steady flow through the room is established, ventilation sets a limit on the rate of heat release in the room to a value in the range 2 x 10^5 to 7.3 x 10^5 cal sec^{-1} (roughly 1 to 3 megawatts).

The PRC Model

The PRC model was roughly a third-scale counterpart of the ENCORE blockhouses. Among the PRC experiments, the configuration that best simulated ENCORE was the one used in the 14 tests numbered 40 through 57, in which a window of 18-inch width and 17-inch height was used, having a 9-inch ceiling-to-soffit drop.

The PRC enclosures were lined with insulating wallboards (Kaowool M-board and Marinite XL) and heated with a propane-fueled diffusion flame burner. The propane supply rate ($\dot{m}_v$) was held constant in each test; but, from test to test, varied over the range from 0.3 to 2.0 SCFM (about 0.28 to 1.84 g/sec). The shortest estimated times to flashover conditions were 40 to 45 seconds, achieved only when Kaowool M-board insulated the walls and ceiling. Test No. 51 was judged to have arrived at flashover conditions in 52 seconds. In this test, the propane supply rate was 1.38 g/sec ($\sim$ 15.2 kcal/sec rate of heat release, $\phi \equiv \dot{m}_v/1.6W_oH_o^{3/2} = 6.6 \times 10^{-3}$)*, with the burner positioned in the middle of the floor. Extrapolation to 30 seconds (the approximate time to flashover in ENCORE blockhouse No. 1) would require 2.2 g/sec propane flow ($\sim$20 kcal/sec heat release rate, $\phi = 10.6 \times 10^{-3}$).

Over long periods of heating, the heat released in the PRC enclosures was divided roughly equally between convected enthalpy flow out of the window and heat stored in the upper region of the room (hot gases and flames trapped under the ceiling, above the soffit, and heated ceiling and upper wall boards). At early times in such situations, however, a disproportionate share goes into heating the upper portion of the room, and the heat losses are relatively independent of window size, being more dependent on an area of the ceiling (specifically on the scale-factor squared and either the interface heat-transfer coefficient, h, or the thermal inertial, kpc, of the wallboard) than on volume of the room (i.e., scale-factor cubed and heat capacity of the air). For cases like ENCORE, we may be justified in disregarding h also.

DESIGN FACTORS

The enclosure design is a full-scale approximation to the FPL blockhouse that was exposed to the ENCORE nuclear airburst, retaining as much as possible of the geometry, thermal, and flow properties of the PRC model. Because of the remaining uncertainties about the role of the thermal properties of wall and ceiling insulation, we plan to use Kaowool M-board for this purpose. Most of the PRC experiments were conducted with this material. It is quite serviceable, and due to its low thermal inertia, it offers the prospect of rapid flashover with relatively low expenditure in fuel supply. For the DIRECT COURSE blockhouses, a window identical in size and geometry to the ENCORE case has been selected, and it is planned that they be furnished following the description published in the WT-Report (Ref. 3). The following material is provided in justification of the selected design.

*The constant 1.6 is in mks units.

Blast Filling

To minimize the effects of the particular details of the pressure-time history that acts on the experimental enclosures at DIRECT COURSE, and, by so doing, making as generally applicable as possible the results, e.g., independent of explosion yield, the room filling time should be kept short in comparison to the duration of the airblast overpressure. Rempel (11) notes that most room filling situations lie in the regime that cannot be simplified as approximate to either the case in which the opening is such a large part of the wall that the blast wave passes into the room with only slight perturbation or the case in which the opening is so small that filling is not a shock process at all. With the admonition that any simplified method of calculation requires independent checking, Rempel (11) offers the following as an approximate estimate of the time of room filling (in ms): V/2A, where V is the room volume in cubic feet and A is the area of the window in square feet. He notes that this is an empirical relationship in which the dimensions cannot be changed willy-nilly. This predicts for the FPL blockhouses at ENCORE a filling time of about 20 ms. Even if we scale the volume up (with a scale factor of 3) from the PRC model to 1296 ft^3, the filling time increases to only 27 ms. Within this time period, we can expect the free-field overpressure at DIRECT COURSE to decay to no less than 80% of the peak value, reasonably approximating a time-invariant external pressure. At the same time, since the window opening is ¼ of the area of the shock-incident wall, substantial effects of the transmitted shock can be expected within the room.

Fuel Supply

To achieve flashover in a period of roughly 30 sec, the fuel supply rate needs only be scaled from the PRC tests in accordance with the change of enclosure dimensions. Flashover in 30 sec was extrapolated for the conditions of the PRC tests (with Kaowool M-board) to a fuel supply rate of 2.2 g/sec (propane). Further scaling to a 12 ft x 12 ft plan area, increases the supply rate by a factor of nine (x9) to about 20 g/sec, or a gaseous propane supply rate of about 21 SCFM.

Although the convective flow providing the continued oxygen supply to maintain a well ventilated fire develops slowly in relation to the growth of the fire, sufficient air is contained in the room volume to ensure the required release of heat within the enclosure itself.

EXPECTED RESULTS

From the results of the Ft. Cronkhite experiments, we might reasonably expect all of the blockhouse fires at DIRECT COURSE to be extinguished, since the expected overpressures will exceed 2 psi. However, differences between the two experiments in states of fire development are graphic; it is unlikely that the flames will be extinguished in all cases. Possibly none will be, but we expect that at least one, hopefully two or more, will be extinguished, if not permanently, at least for an observable time. Often when flames are extinguished, a smoldering fire persists to rekindle a flaming fire. Depending on a variety of factors, including wind currents, this can happen quickly, be delayed for an hour or more, or fail altogether. Whether rekindle

occurs, and if so, how long it takes, can influence the formulation of civil defense doctrine in the future; its determination by post-shot observation is, therefore, an important technical objective of this experiment.

Finally, as a bonus, these room fire tests, even without blast effects, will extend the range of fire dynamics experience to help confirm the general validity of room fire scaling rules.

REFERENCES

1. T. Goodale, Effects of Air Blast on Urban Fires, Final Report, OCD Work Unit 2534I, URS Research Co., San Mateo, CA, URS 7009-4(1970) AD723 429.
2. DCPA Attack Environment Manual, Chapter 3: What the Planner Needs to Know About Fire Ignition and Spread, DCPA Research Directorate (1972).
3. H. D. Bruce, Incendiary Effects on Buildings and Interior Kindling Fuels, WT-774, Report to the Test Director, Operation UPSHOT/KNOTHOLE, U.S. Forest Products Lab., Madison, WN, (1953).
4. S. B. Martin and S. J. Wiersma, An Experimental Study of Flashover Criteria for Compartment Fires, SRI Final Report to the Products Research Committee, SRI Project No. PYC6496 (April 1979).
5. K. Kawagoe, Fire Behavior in Rooms, Building Research Institute, Report 27, Tokyo (1950).
6. T. E. Waterman, Determination of Fire Conditions Supporting Room Flashover, DASA 1886 (1966).
7. P. H. Thomas, Some Problem Aspects of Fully Developed Room Fires, ASTM STP 614, A. F. Robertson, Ed., (1977).
8. B. Hägglund, R. Jansson and B. Onnermark, Fire Development in Residential Rooms After Ignition from Nuclear Explosions, F.O.A. Rapport C 20016-D6 (A3), Stockholm, Sweden (1974).
9. P. H. Thomas and M. L. Bullen, "On the Role of Ease of Room Lining Materials in the Growth of Room Fires," Fire and Materials, Vol 3, p 68 (1979).
10. B. J. McCaffrey, J. G. Quintiere, and M. F. Harkleroad, "Estimating Room Temperatures and the Likelihood of Flashover Using Fire Test Data Correlations," Fire Technology, Vol 17, p 98 (1981).
11. J. R. Rempel, "Room Filling from Air Blast," Appendix E to Technical Report: Feasibility Study of Slanting for Combined Nuclear Weapons Effects, OCD Work Unit 1154E, Stanford Research Institute, Menlo Park, CA (1971).

SPONTANEOUS IGNITION OF SOLIDS SUBJECTED TO LINEARLY TIME-DEPENDENT RADIANT EXPOSURE

by

A. Murty Kanury, Pravinray D. Gandhi and Stanley B. Martin

Department of Aerospace and Mechanical Engineering
University of Notre Dame
Notre Dame, Notre Dame 46556
and
Stan Martin & Associates
860 Vista Drive, Redwood City, CA 94062

ABSTRACT

The important problem of spontaneous ignition of solids heated by temporarily variant thermal radiant exposure is studied. Available data are examined in the light of a simple heat balance analysis to find that the observed behavior is predictable. An exposition of the elements of this general problem of ignition is made to realize that further research is required to predict the ignition behavior of realistic solids under realistic reradiative and free convective loss conditions.

INTRODUCTION

Little, if any, quantitative knowledge exists about the important problem of the spontaneous ignition response of a combustible solid subjected to time-wise ramped thermal radiative exposure. Martin (1) developed some preliminary experimental data by exposing blocks of wood to a transiently varying radiant flux. In one set of data (2), the source of radiation is a model room compartment in which a propane burner, remote from the target, continuously pumps combustive energy to transiently heat the room which then radiates to the target. The radiant flux in this set up varies with time in the early phases, more or less linearly, in the range of $r = 10^{-2} - 10^{-1}$ W/cm^{2}s. In the second set of data, the source of radiation is an electrically powered heater which is manually programmed to yield flux rate ramps in the range $r = 10^{-1} - 10^{0}$ W/cm^{2}s. In both these test series, the time to ignition t_{ig} of the wood block is noted as a function of the exposure flux rate.

These data are presented in Fig. 1. The time to ignition is noted to decrease with increasing flux rate according to

$$t_{ig,exptl} = 17.6\ r^{-2/3} \qquad (1)$$

where time is in seconds and ramp rate is in W/cm^{2}s. Also presented in Fig. 1 are the same data but manipulated to obtain the flux at ignition (rt_{ig})(W/cm^2) as dependent on the rate of heating rate r. If it were not for the dynamics of the heating and ignition processes, one expects this critical flux to be independent of the ramp rate r. The data, however, show that ignition occurs at a lower flux when the ramp rate is low, approximately according to $rt_{ig} = 17.6\ r^{1/3}$.

The question addressed in this paper is this: Is it possible to predict, from a theoretical basis, the constant of proportionality and the power 2/3 appearing in Eq. (1) as

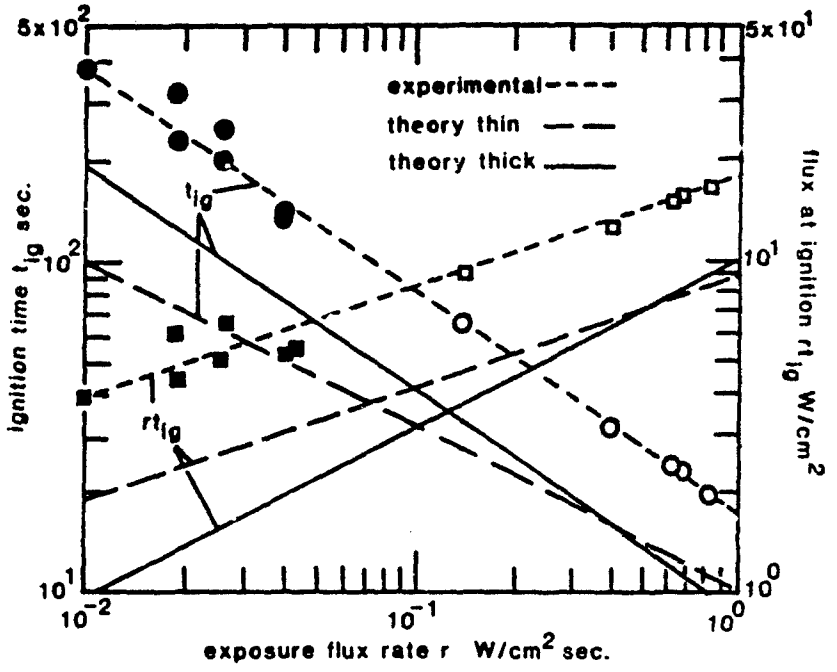

Figure 1: Ignition Time●○ and Flux at Ignition■□ as Dependent on the Exposure Flux Rate.
Open Symbols Data from (1).
Filled Symbols Data from (2).

dependent upon the various thermal and physical properties of the system?

ANALYSIS

Thin Slab:

Consider a target of thickness ℓ, conductivity K_s, density ρ_s, specific heat C_s and initial temperature T_i exposed for time t equal to and greater than zero to a heat flux (W/cm^2) ramped linearly as $j=j_0+rt$, where the ramp rate r has units of flux per unit time, i.e., W/cm^2 sec.

If the target is thermally thin, its temperature will be uniform throughout its thickness. This time-dependent temperature $T_s(t)$ is given by an energy balance.

$$\rho_s C_s \ell (T_s - T_i) = a_s \int_0^t (j_0 + rt)dt + \text{losses} \qquad (2)$$

The left hand side represents the increase in energy content of the solid whose volume per unit surface area is ℓ. The integral in the first term on right hand side is the amount of energy arriving at the surface in time t; a fraction a_s of this is absorbed by the surface, a_s being an absorptivity constant. There are four types of 'losses' to be considered. Losses from the backface of the slab are absent if it is perfectly insulated. As the solid becomes warmer, the front face begins to transiently reradiate to its surroundings. It also experiences a transient natural convection process

by which further energy is lost. Additionally, the pyrolysis of the solid to produce combustible gases may involve an energy sink. All these four types of losses are ignored in the present work. Parenthetically, it is important to note that the very same transient free convection process which tends to slow down the heating of the solid also brings into the boundary layer the oxygen required for oxidation of the pyrolyzates to eventually culminate in a flame. Equation (2), integrated under these simplifications, leads to

$$\rho_s c_s \ell (T_s - T_i) = a_s (j_o + rt/2)t \quad (3)$$

If attainment of a critical temperature $T_s = T_{ig}$ is taken as the criterion for ignition, the ignition time is obtained from from Eq. (3) by simply setting $t = t_{ig}$ when $T_s = T_{ig}$. Since flux ramps generally start with $j_o = 0$,

$$t_{ig,thin} = \{2\rho_s c_s \ell (T_{ig} - T_i)/a_s\}^{1/2} r^{-1/2} \quad (4)$$

Thick Slab:

If the slab considered above were thermally thick, internal spatial temperature gradients exist. As heating progresses, progressively thicker will be the heated layer of the solid near the exposed surface. This thermal layer thickness δ_s: (a) delineates the depth beyond which stations within the solid do not know that the surface is experiencing heating; (b) determines the characteristic temperature gradient in the solid; and (c) determines the rate at which the solid energy content increases. Taking temperature to vary linearly within the solid from T_s at the surface to T_i at the depth δ_s from the surface, the time-dependencies of the surface temperature T_s and the thermal penetration depth δ_s are coupled by

$$K_s (T_s - T_i)/\delta_s = a_s (j_o + rt) \quad (5)$$

Ignoring all the losses as in the case of thin slab, the energy conservation is given, with the linear temperature distribution within the solid, by

$$\rho_s c_s (T_s - T_i)\, \delta_s/2 = a_s (j_o + rt/2)t \quad (6)$$

Assuming $j_o = 0$, resolution of Eqs. (5) and (6) for δ_s and T_s leads to $\delta_s = \sqrt{(K_s t/\rho_s c_s)}$ and $(T_s - T_i) = \sqrt{(a_s^2 r^2 t^3/K_s \rho_s c_s)}$. With the critical temperature criterion, ignition time is thus given by

$$t_{ig,thick} = \{K_s \rho_s c_s (T_{ig} - T_i)^2/a_s^2\}^{1/3} r^{-2/3} \quad (7)$$

DISCUSSION AND CONCLUSIONS

Taking wood properties to be those of typical fir, $\rho_s = 600$ kg/m^3, $C_s = 2720$ J/kg K and $K_s = 0.12$ W/mK, and taking ignition temperature to be about 900 K and the typical thin sample thickness to be 5×10^{-4}m with $a_s = 1$, Eqs. (4) and (7) can be reduced to

$$t_{ig,thin} = 9.9\, r^{-1/2} \quad (4a)$$

$$t_{ig,thick} = 8.9\, r^{-2/3} \quad (7a)$$

where, as in Eq. (1), the time is in seconds and ramp rate is in W/cm^{2}s. These results are also shown in Fig. 1.

Both thin and thick body models predict the trend of shorter the ignition time at larger ramp rate. Even more interestingly, the thick body model successfully predicts the observed inverse 2/3-power dependence of ignition time on ramp rate. While the trend and sensitivity are thus captured by the thick body analysis,

the predicted ignition time is consistently about half the measured. An absorptivity of 0.5 would raise the constant 8.9 in Eq. (7a) to 14.1, still underpredicting by about 20%. Variations in the thermal properties can perhaps account for this discrepancy.

Even more importantly, the assumed linear temperature profile in the solid inherently tends to underestimate δ_s and (T_s-T_i) at any given time. Thus a more rigorous solution of the conduction problem is expected to result in a shorter time to ignition under a given set of conditions. Pyrolysis endothermicity, and heat losses by radiation and natural convection point towards a longer time to ignition. The magnitudes of these improvements, however, can not be estimated without obtaining a complete solution.

It is surprising that the thick body behavior is retained over the relatively wide range of the tested ramp rate. Conceptually, one would expect that low heat fluxes and flux rates make even thick solids behave as thin. The r value representative of this transition from thick to thin solid behavior is apparently smaller than 10^{-2} W/cm^{2}s.

The present agreement between thick body analysis and experiment is quite fortuitous. There is no assurance that this agreement will persist for taller and shorter target slabs and for larger or smaller ramp rates. This pessimism is not without reason. The development of thermal reradiation from the heated surface, evolution of the natural convection boundary layer adjacent to the surface, pyrolysis of the solid, mixing, of the pyrolyzates with air in the boundary layer and the thermal runaway of the mixture, are all highly transient but essential aspects of the problem. The simple result given by Eqs. (4a) and (7a) can not be expected to be so versatile as to capture the extreme nonlinearities involved in the total transient problem. In fact, such crucial phenomena as critical heating below which ignition is impossible can not be predicted without accounting for at least some of these enumerated transient aspects. In (3), for instance, the authors have developed a model for the transient heating of thin vertical slabs by constant radiant flux to discover some important quirks of the boundary layer development and heat loss from the surface. A threshold heat flux (dependent upon the solid height as well as the reradiant loss), below which ignition is impossible, has been determined in this reference.

Other aspects of the total problem of spontaneous ignition of solids subjected to time-wise varying exposure radiant flux are currently being investigated.

REFERENCES

1. S. B. Martin, "Prediction of Ignition Thresholds During Ramp Heating," Paper presented at the ASTM Committee E-5 Conference entitled Polymeric Material Behavior in Fire, Toronto, Canada, (June, 1982).

2. S. B. Martin, and S. J. Wiersma, "An Experimental Study of Flashover Criteria for Compartment Fires," Final Report, SRI Project PYC 6496 submitted to the Products Research Committee, SRI International, Menlo Park, CA, 94025 (April, 1979).

3. A. M. Kanury, S. B. Martin, and P. D. Gandhi, "Transient Heating of a Thermally Thin Vertical Solid Slab in Air by a Constant Uniform Radiant Flux," paper to be presented at the 1983 ASME/AIChE National Heat Transfer Conference, Seattle, WA (July, 1983). To be published in the symposium volume.

ELECTROMAGNETIC RADIATION PROPAGATION IN LARGE FIRES

Thomas Y. Palmer
SWETL, Inc.
Fallbrook, California 92028

ABSTRACT

Experimental measurements of electromagnetic radiation propagation in the visible, infrared and radar frequencies indicate that the primary obscuration effects are due to very small smoke particles, spectral absorption by carbon dioxide with water vapor and temperature generated temperature inhomogenities. Visibility is reduced to tens of feet, IR attenuation coefficients are on the order of one km^{-1}, while radar was foreshortened by one percent with from three to nine minutes of beam bending.

GLOBAL-SCALE OBSCURATION BY MASS FIRE SMOKE

William T. Kreiss and Thomas Y. Palmer
Physical Dynamics, Inc.
La Jolla, California 92037

I. INTRODUCTION

Fire has been a major weapon in wars for centuries. In a conflict involving nuclear weapons, major fires wil form and their smoke will effect later weapon effectiveness and the post attack environment. A recent issue of AMBIO (11), the journal of the Swedish Acadamy of sciences presented "a realistic assesment of the possible human and ecological consequences of a nuclear war"(sic). It covered a large number of topics including the effects of nuclear weapons, fallout, smoke obscuration, weapon targeting, etc., - each section being written by a "specialist" in that area. This issue is being widely cited and quoted in reviews (c.f. JDA,1982 Pain, 1983) and has been edited and reproduced as a book, (Peterson and Hinrichen, 1982). It proposes that widespread forest and industrial fires would occur after a nuclear war, spreading far beyond the areas ignited by the prompt radiation. We propose to examine this premise.

II. THE FIRE-SMOKE SCENERIO

Crutzen and Birks, (1982) considers smoke from oilwell, oil storage and wildland fires. There is an almost complete absence of references to fire research literature literature, but they assumed that all ignitions will automatically spread and continue to burn for at least two months. This assumption ignores the evidence of the past. During the nineteenth century steam locomotives were prolific generators of sparks and embers in all areas of the United States, yet mass fires and conflagrations only occurred in areas where fuel conditions and weather were conducive to such fires. In what follows we attempt to arrive at a more realistic assesment of the probability of country-wide mass fires and conflagrations during a nuclear war.

III. PAST MASS FIRES

The analysis of the probality of large-scale mass fires and conflagrations is obviously one which must arrive at joint probability densities of fires occurring simultaneously over widely seperated areas. This is a problem in Baysian statistics, which states that the probability of fire occurring in another area given that it has occured in a given area is:

$$P(B_i|A) = \frac{P(B_i)\ P(A|B_i)}{\sum P(B_i)\ P(A|B_i)}$$

where $i = 1,1,\cdots\cdots$ or k

It is usually assumed that the probability densities are independent, while here, they are obviously not since they are weather and climatically related by a series of events which lead to drought and high winds. But, for the purposes of this preliminary study it was assumed that the correlations of weather and climate between the diverse areas was weak enough to ignore correlations.

The initial analysis used the United States fire spread statistics prepared by Chandler

et al, (1963). We used a minimal fire spread rate of three meters per hour as the criteria for the continuation of any particular fire. The various data sets studied included California Oregon and Washington. There was no set of data pairs from any of these three states that had a joint probability greater than twenty percent, even at the afternoon time of largest spread rates.

Since this data could not be directly related to large fire events, because of the shortness of the record, a second study of the joint probabilties of observed large disaster fires were undertaken. This data was derived from various sources including Brown and Davis (1973) and Pyne, (1982). It covered 150 years of fire experience in the United States. The results are presented in Table I.

AREA	JOINT PROBABILITIES FOR FIRES FOR ONE YEAR, Percent
Southern California	6.5
Pacific Northwest	4.7
Northern Rockies	7.7
Lake States	0 (since 1933), 9.8 (prior to 1933)
South	81.0(since 1930), 0. (prior to 1930)

Table I. Conditional probabilities of a large disaster fire occurring in any of the given areas, given that one has occurred during that year in the first given area.

In this study, the fire areas in the United States were chosen as southern California, the Pacific Northwest, the northern Rockies, the Lake States and the South. The data was grouped on a yearly basis, no attempt being made to develop smaller intervals or areas. Conditional probabilities were computed for each area, given that a large fire had occurred in another area during the same year.

IV. ANALYSIS AND CONCLUSIONS

Two of the areas required special consideration--the Lake States and the South. Prior to the 1930's logging was extensive in the Lake States, providing a large amount of litter and slash to carry a fire. In the South however pioneer burning practices in removing the forests to provide large cleared areas (deserts in 19th Century parlance) permitted very little buildup of burnable material on the ground. In the 1930's logging practically ceased in the Lake States, while it became extensive in the South, with the attendent accumulation of slash and low growth on the ground. It seems apparent that this demonstrates an increased fire hazard if there are trash accumulations in large cities.

In general, these results show that the probability of simultaneous ignitions resulting country-wide large fires and conflagrations by any even, including steam locomotives, nuclear weapons, incendiaryism (or whatever) has a low probability of causing widespread mass fires. It follows that the probability of the production of large amount of obscuring smoke sufficient to cause a large climatic is limited although visibilities may be lowered. In general measurements of electromagnetic at longer wavelengths than abou 1 micrometer will relatively unaffected by smoke (Palmer, 1981a,b)

This study could be refined and expanded significantly by using both smaller areas and time intervals and more accurate definitions of the fire hazard based upon fire danger ratings. It is apparent that fire may be identified with drought periods and high winds and further study should include these factors.

V. REFERENCES

Brown, A. A. and Davis, K.P,, 1973. Forest Fire, Control and Use, 2nd Ed., McGraw-Hill, N.Y. 686p.

Chandler, C.C., Store, T. S., Tangred, C.D., 1963. Prediction of fire spread following nuclear explosions. USDA Forest Service PSW Stn, PSW-5, Berkeley, CA.

Crutzen, P.J. and Birks, J.S., 1982. The atmosphere after a nuclear war, twilight at noon. Ambio 11, p 114-174.

JDA, 1982. Physics Today, 35 (10) p17.

Paince, C., 1983. The aftermath of nuclear war. Science, 220, p812-814.

Palmer, T. Y., 1981a. Large fire winds gases and smoke. Atmos Env. 15, p2079-2090.

Palmer, T. Y., 1981b. Visible infrared(IR) and microwave propagation in and near large fires. Proce. SPIE, Atmospheric effects on electro-optical, infrared and millimeter wave systems performance, R. B. Gomez, Ed., Aug 27-28, 1981, San Diego, CA, Bellingham, WA p28-30

Peterson, J. and Hinrichsen, D. Eds., Nuclear War; The Aftermath., Pergamon, N. Y., 1982 196pp.

Pyne, S. J., 1982. Fire in America. Princeton Univ. Press, Princeton, NJ, 654 pp.

FIRE IN TARGETING URBAN/INDUSTRIAL AREAS

H. L. Brode and R. D. Small

Pacific-Sierra Research Corporation
12340 Santa Monica Boulevard
Los Angeles, California 90025

ABSTRACT

A preliminary study of the parameters pertinent to considerations of fire in urban targeting illustrated the dominance of some factors and the insensitivity to damage assessments of others. The factors considered, together with the simple assumptions and approximations used in this scoping study supported the assumption that fire may add significantly to the damage to urban/industrial targets. The influence of uncertainties and unknowns were evaluated, and the consequent implications for research were assessed. This work was done in cooperation with RDA (R. Port) for DNA.

INTRODUCTION

Damage from a nuclear weapon burst is usually associated with the blast wave, nuclear radiation, electromagnetic pulse and thermal radiation. Theoretical or empirical relations describing shock wave propagation, diffusion of nuclear radiation and transmission of thermal and electromagnetic radiation are well developed. Translation of each effect to a damage prediction requires analysis of the target response. In general, the correlation of the weapon effect with target damage is non-linear and complex. Most current damage estimates are based on relations describing structural response to shock wave loadings. No such correlations are available to define fire damage.

In general, the prediction of fire damage is no more complex than the prediction of blast damage. The loading and damage of a structure by the blast wave is a complex function of orientation, timing, and strengths of materials. Fire in a target building may develop from ignitions due to thermal loadings or from blast disruption, or from spread from an adjacent burning building. The first two mechanisms relate to weapon effects. Spread relates to established adjacent fires, so that the immediate weapon effect-target response provides only a partial fire damage estimate. Description of the fire development and later time behavior is necessary for a complete damage prediction. Both the immediate weapon effect-target response and the effect of many unchecked fires in a city must be analyzed.

In this paper, many of the factors that may influence the occurrence and development of fires in a target area are considered, and probability of fire damage-range curves are constructed. The analysis includes available relations and criteria for transmission of thermal radiation, ignition criteria, and blast induced ignitions. Fire spread and civil defense actions are approximated. In most cases, a parameter range was created in order to compensate for either a lack of data or an inadequate prediction methodology. Conservative estimates of the parameter values indicate a damage range greater than that for light blast damage. Less conservative estimates produce fire damage radii greatly exceeding comparable blast damage radii.

FIRE DAMAGE RANGE CURVES

THERMALLY-INDUCED IGNITIONS

The basic fire damage-range relation is based on the probability of occurrence of a sustainable ignition. Considering heavy drapes, bedding and overstuffed furniture as representative combustible materials, then for a 1 Mt burst, ignition is likely at a flux level of 22 cal/cm^2 (1). For that value, a target fire resulting in structure destruction is assumed 50% probable. A 90% probability is assumed for 33 cal/cm^2, and a 10% probability for 11 cal/cm^2. The ignition threshold levels increase slowly with weapon yield.

Slant ranges and thus damage (ground) ranges for each threshold level (Q) are calculated from

$$S = \left[\frac{W}{Q}(1 + \beta S/V)e^{-\alpha S/V}\right]^{1/2} \quad \text{mi} \quad .$$

The weapon yield is W (kt), and Q is in cal/cm^2, V is the visibility length (mi) and α, β define the scattering and absorption characteristics of the atmosphere. The basic fire damage-range curve for thermally induced ignitions is shown in Fig. 1. The values 2.0, 1.4 chosen for α, β are recommended by Brode (2). Damage ranges are reduced slightly (3) for α, β = 2.9, 1.9 (4). A much greater influence is the characteristic visibility length. The 50% damage radius increases by a factor of two for the visibility length range of 3 to 48 miles. The variation depends on weapon yield--decreasing for lower yields (3).

The amount of thermal radiation incident on a target may be enhanced by reflection from a ground snow cover or superior cloud deck or attenuated by cloud cover below the burst. A simple multiplicative constant (greater than 1.0 for enhancement, less than 1.0 for attenuation) is used to estimate the influence on damage ranges. Sample results are shown in Fig. 2. Reflection of thermal radiation can increase the damage range by 30%. The thermal reach is halved if 75% of the fireball radiation is absorbed by a cloud layer.

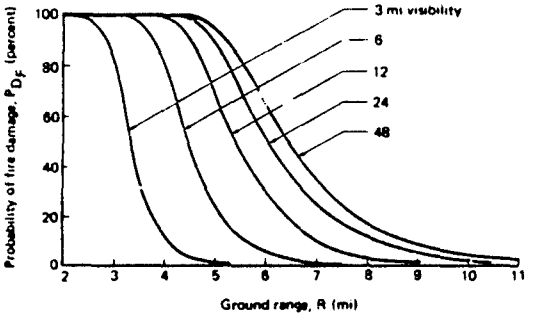

Fig. 1 Fire damage range for various visibility lengths, thermally induced ignitions, W = 1 Mt, α= 2.0, β= 1.4

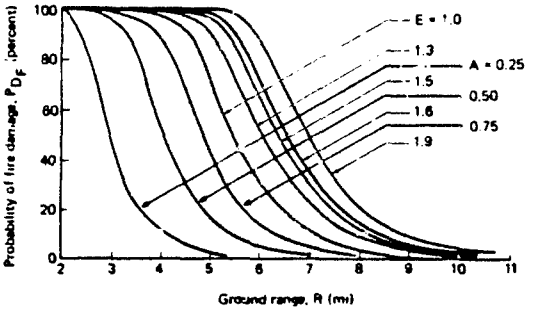

Fig. 2 Fire damage range for various amounts of radiation attenuation A and enhancement E: thermally induced ignitions, W = 1 Mt, V = 12 mi, α= 2.0, β= 1.4

Other factors that may influence the damage-range relation include height of burst and threshold level variations (3). With the exception of ground bursts, the height of burst modifies the results only slightly (less than 5% for scale burst heights between 200 ft/kt$^{1/3}$ and 700 ft/kt$^{1/3}$). Significant changes occur for increased or decreased threshold levels. A 50% decrease in threshold levels doubles the damage areas. Variation of the 10 and 90% values sharply slews the damage range curves. These parameters have been considered in detail by Brode and Small (3).

BLAST-INDUCED IGNITIONS

The blast wave from a nuclear burst may disrupt electrical, open flame and other high-energy fuel sources, starting a substantial number of fires. The methodology of Wilton, Myonuk and Zaccor (5) is used to estimate the probability of a fire start as a function of overpressure, structure type and contents. The applicability of this model may be limited by its assumptions, however, the resulting probabilities agree fairly well with those suggested by the large burned-out regions of Hiroshima and Nagasaki (6, 7).

Figure 3 plots sample fire damage-range curves for several combinations of building types and contents. A light-design structure (type 10) with highly flammable contents (approaching 10) presents a high probability of blast induced fires beyond the 0.5 psi level (13 to 24 miles for a 1 Mt burst). Each damage-range curve assumes a uniform building-contents distribution throughout the target area. Damage ranges shown for the light design structures greatly exceed those for thermally induced ignitions. For those cases, blast-induced fire starts dominate the ignition distribution, and variations in visibility length or the coefficients α, β cannot greatly affect the damage ranges.

COMBINED PROBABILITIES

The damage range curves in Fig. 4 combine the probabilities of ignition by thermal radiation and blast. The indices for building type and contents are fixed (4/7.5) at all ranges, ensuring a homogeneous distribution of buildings. Combining the independent probabilities of thermally and blast-induced ignitions significantly extends the damage-range curves. However, attenuation of the incident thermal energy reduces the probable damage range just slightly, whereas enhancement moderately increases the damage range. Lower building type/contents indices would shift the curves to the left. Inclusion of blast-induced ignitions in the computation of probable fire starts lessens the influence of the visibility length and the attenuation or enhancement of thermal radiation. Those parameters would be more important, however, if the distribution of blast-induced ignitions (as shown in Fig. 4) has been overestimated.

A more specific analysis of the sources of blast-induced fires in Soviet cities would be valuable. Such sources may be electrical, thermal, chemical, mechanical, electrostatic, or gas dynamic. Certain industries, such as paper mills, chemical plants, oil refineries, or power generators, contain obvious potential secondary sources, and could be targeted accordingly. Such features, when identifiable, should be part of the vulnerability considerations, since the ensuing fires are likely to extensively damage some facilities that might otherwise survive the blast. Such was the case for an electric generating station in Hiroshima--though housed in a massive building that survived the blast, the station itself was gutted by fire.

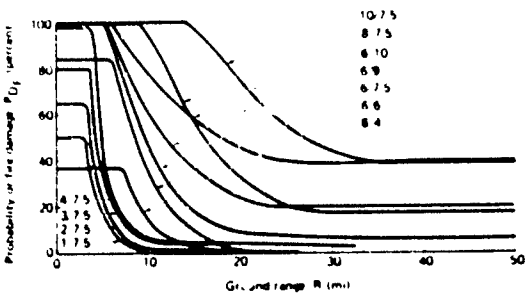

Fig. 3 Fire damage range for various building type contents indices blast induced ignitions W = 1 Mt

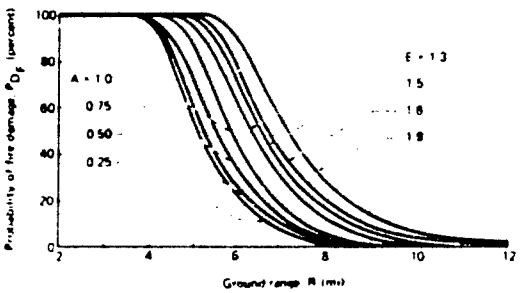

Fig. 4 Fire damage range for various amounts of radiation attenuation A and enhancement E thermally and blast-induced ignitions, W = 1 Mt V = 12 mi d = 2.0 β = 1.4 building type/contents index = 4/7.5

FIRE SPREAD

When many simultaneous fires are ignited in conjunction with considerable blast damage and radioactive fallout, the best civil defense efforts cannot hope to contain them. The added threat of multiple or subsequent bursts will further deter effective firefighting. Under those circumstances, fire spread is limited chiefly by natural boundaries (rivers, lakes) or man-made barriers (open areas such as parks, parking lots, broad boulevards). However, even such firebreaks have not always proved effective against a large fire. The ultimate limit is the fuel bed itself; when there is no more fuel to burn, the fire must stop. Within densely constructed areas, industrial facilities with highly flammable contents, or extensively damaged regions with widely scattered debris, fire is more likely to spread. Contiguous fuel sources are likely to burn completely once numerous fires are started and civil services disrupted.

Consistent with the previous assumptions of our simple, generic fire damage model, a heuristic accounting for fire spread is used. Thus, the model ignores a continuity of structures and the flammability of their contents, the direction of winds and blast waves, and the potential for flammable debris, though all could significantly affect fire spread. Regions between multiple bursts will suffer fire damage, because of a tendency of large fires ignited by multiple bursts to merge with neighboring fires.

Fire spread was included in the damage-range relation by doubling the probability of a fire at each point. Thus, if 50% of the structures are burning, it is assumed that the fire will spread to all adjacent structures. Similarly, ignition in one building in four implies fire damage to 50% of the structures. Results of those calculations are plotted in the fire-damage-range curve in Fig. 5, which combines the probabilities of ignition by thermal radiation and blast, followed by fire spread. The

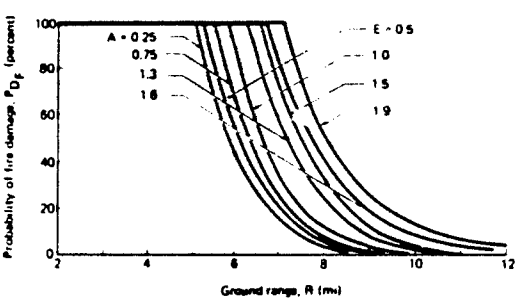

Fig. 5 Fire damage range for various amounts of radiation attenuation A and enhancement E thermally and blast-induced ignitions and fire spread, W = 1 Mt, V = 12 mi, d = 2.0, β = 1.4, building type/contents index = 4/7.5.

modifying effects of enhancement and attenuation of the thermal radiation are also incorporated. At even the largest attenuation factor, complete fire damage extends to the 3 psi region (5 mi for 1 Mt).

COMBINED PARAMETER VARIATIONS

This section develops fire-damage-range curves for multiple-parameter combinations. The nine "independent" variables considered include ignition threshold level, visibility length, transmissivity form, thermal radiation enhancement and attenuation, building type/contents indices for blast-induced fires, probability of fire spread, and the effectiveness of countermeasures against thermally and blast-induced ignitions. Based on the previous parameter excursions, a mean value for each variable was defined. One- and two-standard-deviation bracketing values were then estimated. Interpolation between the mean and $\pm 1\sigma$ deviation ensembles was used to define $\pm 1/3\sigma$ and $\pm 2/3\sigma$ values for each variable (unit standard deviations). The nine "independent" variables were then combined to form $\pm 1\sigma$ and $\pm 2\sigma$ fire-damage-range curves for all the effects.

Table 1 lists the parameter values calculated for each ensemble for both a 50 kt and 1 Mt explosion. Ignition threshold levels were defined for 10, 50, and 90% probabilities of ignition. Worst-case scenarios are represented by the negative standard deviation ensembles. Lower threshold levels corresponding to a greater slant range were used for positive standard deviation sets.

The mean visibility length (11 km) represents a clear day. Positive and negative unit standard deviations span the range of conditions from foggy to very clear days. In view of the uncertainty in the relations describing the transmittance of thermal radiation, mean values of the absorption α and scattering β coefficients were calculated from the average of the values given by EM-1 (4) and Brode (2). The lower estimates of α and β correspond to an increase in damage range and thus were used for the positive standard deviation ensembles. Values corresponding to the EM-1 (4) fit were used for the -1σ ensembles. Intermediate values were obtained by interpolating between the mean and $\pm 1\sigma$ sets.

For each esemble, a degree of enhancement or attenuation of the incident thermal radiation was hypothesized. The values represent the likelihood of modification of the incident thermal radiation. The mean case postulates a greater probability of thermal radiation enhancement, but accounts for a lower probability of attenuation. The worst-case scenarios admit attenuation only and the standard deviation sets ($\geq 2/3\sigma$) admit enhancement only. To determine, for each ensemble, the adjusted incident radiation level necessary to produce a thermally induced ignition, the threshold radiation was divided by a modification factor

$$(1 + E_1)(1 + E_2)(1 - A) \quad ,$$

where E_1 and E_2 represent the percentage enhancement of radiation by reflection from snow cover and a superior cloud deck. The quantity $(1 - A)$ defines the reduction of incident thermal radiation by cloud cover beneath the burst.

Target susceptibilities to blast-induced ignitions are defined for each ensemble using values suggested by Wilton, Myronuk, and Zaccor (5). The

Table 1--Ensembles of parameter values

Parameter	Parameter Value								
	-2σ	-σ	-1.5 kt	-1 kt	Mean	+1 kt	+2.5 kt	+σ	+2σ
50 kt[a] ignition threshold (cal/cm²)									
90% probability	51	38	33	29	24	22	18	15	8
50% probability	34	25	22	19	16	14	11	10	5
10% probability	17	13	11	10	8	7	6	5	3
1 Mt[a] ignition threshold (cal/cm²)									
90% probability	60	47	42	37	33	30	27	25	18
50% probability	40	31	28	25	22	20	18	17	12
10% probability	20	16	14	12	11	10	9	9	6
Visibility length (km)	2	5	7	9	11	22	35	46	92
Transmissivity[b]									
A	3.2	2.9	2.75	2.60	2.45	2.30	2.15	2.0	1.8
B	2.0	1.9	1.82	1.74	1.65	1.56	1.48	1.4	1.25
Thermal radiation enhancement (%)									
Snow	--	--	--	--	10	30	50	70	90
Clouds above	--	--	10	25	27	31	33	40	50
Thermal radiation reduction (%)									
Clouds below	85	75	52	28	5	2	--	--	--
Combined effects[c]	0.15	0.25	0.53	0.86	1.33	1.62	2.03	2.4	2.9
Building type/contents indices for blast-induced fires	3/2.5	3/4	4.66/4.33	5.33/4.66	6/5	6.33/5.33	6.66/5.33	7/6	9/7.5
Probable fire-spread enhancement factor	1.1	1.25	1.5	1.75	2.0	2.3	2.7	3.0	5.0
Reduction of ignitions due to countermeasures (%)									
Thermally induced fires									
Overpressure ≤ 0.5 psi	75	63	58	54	50	43	37	30	10
Overpressure = 2 psi	50	33	31	28	25	22	19	15	5
Overpressure ≥ 5 psi	20	10	7	3	--	--	--	--	--
Blast-induced fires									
Overpressure ≤ 2 psi	80	60	53	47	40	35	30	25	10
Overpressure ≥ 5 psi	80	50	40	30	20	17	13	10	--

[a] Height of burst = 500 ft/kt$^{1/3}$.

[b] $[1 + B(R/V)] \exp [- \alpha(R/V)]$.

[c] The multiplication factor is calculated as follows: threshold/combined effect = adjusted incident radiation.

building type index was varied from 3 (worst case, corresponding to heavy-design-load structures) to a +2σ value of 9 (light wood-frame construction). Similarly, the contents type index assumes values from 2.5 (-2σ ensemble) to 7.5. Average parameter values were used for the mean set.

An enhancement factor was used to determine the increased probability of a target ignition by fire spread. That factor was employed as a multiplication constant for each point in the fire-damage probability distribution. For the -2σ set, fire spread increases the probability of fire damage by 10% and, for the +2σ set, by 500%. The number of structure fires was doubled for the mean case.

The final two independent variables used in each ensemble accounted for the reduction in ignitions due to countermeasures. We distinguish countermeasures against thermally induced ignitions (e.g., reflective window coverings) from those against blast-induced ignitions (e.g., closure of central power and gas supplies). In both cases, the effectiveness of the countermeasures is assumed to be a function of the overpressure--lower overpressures mean fewer ignitions. We assume the countermeasures to be most effective

against the blast-induced ignitions. Their overall effectiveness decreases for the positive standard deviations.

Fire-damage-range curves representing the sum of the nine independent variables are shown in Fig. 6. The summation curves reflect the wide band of parameter values used to construct the ensemble. At the 50% damage level, the range from -2σ to +2σ varies by a factor of 5. The damage range varies by a factor of 2 for the ±1σ band.

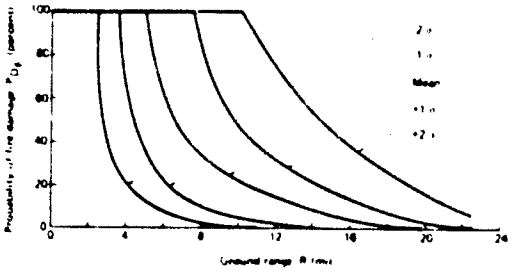

Fig. 6 Fire damage range for all parameters, summation curves, W = 1 Mt

The values selected for each variable were assumed to represent reasonable parameter choices. The positive standard deviation ensembles tend toward an expansion of the fire damage range. The negative ensembles represent a more conservative valuation. In all cases, each parameter choice is subject to confirmation by research. In constructing the ensembles, we chose values that should characterize a range of targets. Selection of a specific target or area should reduce the spread in values for threshold levels, building types/contents indices, and countermeasure effectiveness. Statistical definition of target area weather and local environmental conditions would establish a narrower range of visibility lengths and probabilities for thermal radiation enhancement or reduction. In any event, the mean, ±1σ, and ±2σ damage-range curves should indicate the potential amount of fire damage.

SUMMARY

The sample fire damage-range curves presented in this paper estimate the immediate weapon effects-target response from blast and thermally induced ignitions as well as the longer time damage effects from those fires. Factors such as variable threshold levels, visibility lengths, transmissivity, cloud or snow cover, civil defense countermeasures, and blast induced ignitions were considered. A more complete survey is currently being prepared (3).

In many cases, simple linear predictive methods were used and parameter ranges created in order to estimate a particular effect. Though many approximations are used, the results should indicate the relative sensitivity of the damage-range curve to each effect. Improved estimates can be made as new theories are developed and parameter ranges refined. Topics not explicitly considered in the present study, but may warrant inclusion in further calculations include: blast-flame interactions, specific fire spread mechanisms, fire-wind damage beyond the fire periphery, variable urban structure, and multi-burst effects.

Specific target structures and cities are susceptible to complete destruction by fire. The damage curves and suggested uncertainty bands show that fires from nuclear weapon explosions are quantifiable and predictable. Conservative parameter valuations indicate that fire damage radii exceed those for blast damage. Less conservative--though realistic--parameter values greatly extend the probable fire damage radius. Verification of this trend would enable revision of current targeting and civil defense strategies.

ACKNOWLEDGEMENT

This research was supported by the Defense Nuclear Agency and monitored by Dr. Michael J. Frankel.

REFERENCES

1. S. Glasstone and S. J. Dolan, The Effects of Nuclear Weapons, 3rd Ed., U.S. Department of Defense and the U.S. Department of Energy (1977).

2. H. L. Brode, Fireball Phenomenology, The Rand Corporation, Santa Monica, California, Report P3026 (1964).

3. H. L. Brode and R. D. Small, Fire Damage Estimations for Strategic Targeting, Pacific-Sierra Research Corporation, Los Angeles, California, In Press (1983).

4. Defense Nuclear Agency, Capabilities of Nuclear Weapons, (EM-1), Chapter 3, Part 1 (1972).

5. C. Wilton, D. Myronuk and J. Zaccor, Secondary Fire Analysis, Scientific Services, Inc., Redwood, City, California, Report 8048-6 (1981).

6. H. Bond (Ed.), Fire and the Air War, 1st Ed., National Fire Protection Association, Boston, Massachusetts (1951).

7. R. D. Small and H. L. Brode, Physics of Large Urban Fires, Pacific-Sierra Research Corporation, Los Angeles, California, PSR Report 1010 (March 1980).

THERMAL RADIATION FROM A NUCLEAR WEAPON BURST

R. D. Small and H. L. Brode

Pacific-Sierra Research Corporation
12340 Santa Monica Boulevard
Los Angeles, California 90025

ABSTRACT

The different methods and correlations used to calculate the propagation of thermal radiation are reviewed and compared. A simple method to account for radiation enhancement by reflection from a superior cloud deck or snow cover, as well as attenuation of radiation by cloud cover below the burst is presented. The results show that the thermal "reach" may vary considerably. Additional calculations show that a significant fraction of the thermal energy may be incident after the arrival of the shock wave. Results for a range of weapon yields are presented, and the implications for blast-induced (secondary) fire starts are discussed.

INTRODUCTION

Approximately 35 to 45% of the energy from a nuclear weapon explosion is emitted as thermal radiation. Materials exposed to the fireball may be subject to a rapid increase in temperature. Flammable objects may ignite. The rapid heating of structural materials lowers the effective yield stress and in extreme cases can cause failure of load bearing elements. Lesser heating levels may lead to structure degradation or failure when combined with the subsequent shock wave loading. Low thermal flux levels can damage focussing optical devices that image the nuclear fireball. Retinal eye damage and skin burns occur at very low levels of incident thermal radiation.

In this paper, we review the basic relations describing the calculation of thermal flux from a nuclear fireball and consider some effects that modify the results. A short calculation illustrating the partition of incident energy before and after the shock wave arrival is presented. The results are relevant to the prediction of thermally and blast induced ignitions, shock precursor calculations, and structural response.

THERMAL PULSE

Thermal output from the fireball occurs in two pulses. The time interval of the first pulse is limited by the early shock wave formation (opaque fireball) and only a small fraction of the total energy is emitted. Following the shock breakaway, the fireball is again visible and the major fraction of energy is radiated. The rise to maximum energy output for the first pulse occurs in a few milliseconds and that for the second pulse in hundreds of milliseconds. The following correlations describe the early pulse characteristics as a function of weapon yield W (in kt) and burst altitude to sea-level density ratio η (1):

$$\text{time to first maximum} \simeq 0.10 W^{1/3} \eta^{0} \text{ msec} \qquad (1)$$

$$\text{time to minimum} \simeq 3.8 W^{2/5} \eta^{0} \text{ msec} \pm 35\% \qquad (2)$$

$$\text{time to second maximum} \simeq 50W^{0.2}\eta^{0.42} \text{ msec} \pm 20\% \ . \tag{3}$$

Since the initial pulse is short and contributes little to the total energy release, it is sufficient in most applications to consider the output from the second pulse only. Relations characterizing the time to maximum t_{max}, power maximum P_{max}, and pulse shape P/P_{max}, developed from fits to atmospheric test data and detailed radiation-hydrodynamics calculations (1) through (5) are:

$$t_{max} \simeq 0.05W^{0.42} \text{ sec} \pm 20\% \tag{4}$$

$$P_{max} \simeq 4.5W^{0.6}\eta^{-0.42} \text{ kt/sec} \pm 40\% \tag{5}$$

$$P/P_{max} \simeq \frac{2t^{*2}}{1 + t^{*4}} \ , \quad t^* = t/t_{max} \ . \tag{6}$$

The pulse shape agrees well with that presented by Glasstone and Dolan (6), though the late decay to zero energy output is probably too slow.

THERMAL ENERGY OUTPUT

One method to relate the thermal output to the total weapon energy is through the use of a partition function, f. The total energy available as thermal radiation is thus

$$E_{TH} = fW \ . \tag{7}$$

For visible and infrared radiations from airbursts, Brode (1) suggests the following form for the thermal partition function

$$f = 0.27 + 0.06\eta + \frac{114\eta}{82{,}000\eta^2 + 1} + \frac{0.0085\sqrt{W}}{1 + 0.032\sqrt{W}} \pm 20\% \tag{8}$$

η is the altitude to sea-level density ratio and W is the yield in kt. f increases from 0.35 for heights of burst less than 4500 m to 0.45 for heights of burst greater than 30,000 m.

For surface bursts, the thermal output is complicated by the distorted geometry of the fireball, by the materials engulfed and vaporized within the fireball, and by the obscuration due to dust and smoke clouds raised outside the fireball. For megaton bursts, the output at points on or near the ground from surface bursts is about half that from airbursts, i.e., less than 20% of the total yield.

The emitted thermal energy fraction (for air bursts) can be obtained as a function of time from the following integral of the power spectrum

$$E/E_{TH} = \frac{\sqrt{2}N}{\pi} \int_0^{t^*} P/P_{max} dt^* \ , \tag{9}$$

where N varies with t* as

$$N = 1 - 0.283e^{-1.181/t^*} \quad , \quad t^* \leq 2.5 \tag{10}$$

$$N = 1 - 0.2e^{-0.05t^*} \quad , \quad t^* \geq 2.5 \quad . \tag{11}$$

The coefficient $\sqrt{2}N/\pi$ normalizes the energy fraction to 80% at $t/t^* = 10$. From Eqs. (6), (7) and (9) the thermal energy output as an explicit function of time is

$$E = fW \frac{N}{\pi} \left\{ \text{arctg}\,(\sqrt{2}t^* - 1) + \text{arctg}\,(\sqrt{2}t^* + 1) - \frac{1}{2} \ln\left(\frac{1 + \sqrt{2}t^* + t^{*2}}{1 - \sqrt{2}t^* + t^{*2}}\right) \right\} kt \quad . \tag{12}$$

INCIDENT THERMAL FLUX

The energy flux decreases proportionately with the square of the slant range $\tilde{R}$(km), and as a function of time the incident thermal flux is approximated as

$$Q = 10^{12}\, ET/4\pi\tilde{R}^2 \text{ cal/cm}^2 \quad . \tag{13}$$

For W in kt and $\tilde{R}$ in miles, the total energy output reduces to

$$Q_{TH} = WT/\tilde{R}^2 \text{ cal/cm}^2 \quad . \tag{14}$$

The transmissivity T accounts for the scattering and absorption of radiation in the atmosphere. In general, scattering increases the transmissivity linearly with range, and the absorption decreases T exponentially. Analytic fits to experimental data (Fig. 1) indicate a relationship of the form

$$T = \left(1 + \alpha\frac{\tilde{R}}{V}\right)e^{-\beta\tilde{R}/V} \quad , \tag{15}$$

where V is the visibility length and α and β specify the degree of atmospheric scattering and absorption of the radiation. The visibility length characterizes the state of the atmosphere and varies from 280 m for an exceptionally clear day to less than 1 km for a light-to-thick fog. A clear day is defined as V = 20 m (6). Recommended values for α, β vary from 1.4, 2.0 (1, 6) to 1.9, 2.9 (7). The influence of visibility length and transmissivity form on the effective thermal reach for a 1 Mt burst is illustrated in Fig. 2.

The amount of radiant energy incident on a target can be modified by the presence of cloud cover above or below the burst, and by ground snow cover. Simple estimates can be made using multiplicative factors. For example, a lower cloud deck (below the burst) reduces the energy arrival so that

$$Q_{\text{effective}} = \sigma\, 10^{12}\, ET/4\pi\tilde{R}^2 \text{ cal/cm}^2 \quad , \tag{16}$$

where σ is less than 1.0. Radiation enhancement due to reflection from a superior cloud deck or snow cover may also be calculated from Eq. (16) using

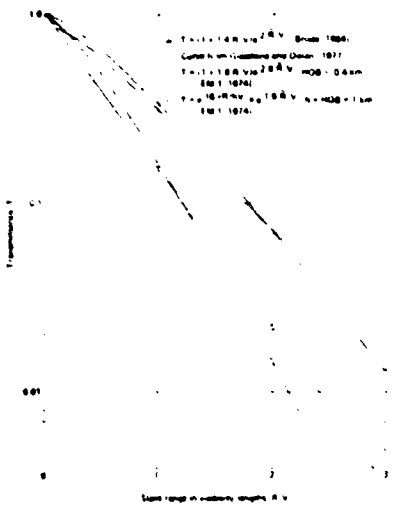

Fig. 1 Standard forms for calculating total visible radiation from airblast

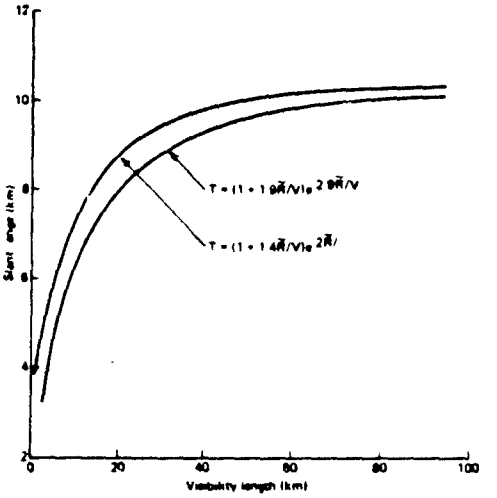

Fig. 2 Slant range vs. visibility length for 1 Mt burst, 152 m scaled height of burst and incident flux level of 22 cal/cm²

values of σ greater than 1.0 but less than 2. The potential change in thermal reach is illustrated in Fig. 3 for a range of attenuation and enhancement factors. For $0.25 \leq \sigma \leq 1.9$, the thermal reach increases by 30% or decreases by 50% from the nominal $\sigma = 1.0$.

LATE THERMAL RADIATION

As the weapon yield increases, the thermal pulse lasts longer and a significant fraction of the radiation may be incident after the shock wave arrival. For scaled ground ranges less than 0.5 kft/kt$^{1/3}$, more than half the thermal energy may arrive after the shock wave. At greater ranges (e.g., 1-5 kft/kt$^{1/3}$) 5 to 20% of the thermal energy follows the shock arrival. The latter values may correspond to low overpressure regions (less than 5 psi). Sufficient energy is available to ignite materials exposed by the blast disruption as well as contribute to the spectra of "secondary" ignitions.

The partition of energy arriving before and after the shock wave may be calculated using Eqs. (10) through (15) once the shock time of arrival is specified. This time can be conveniently calculated from the following analytic fit developed by Brode (8)

$$\text{time of arrival} = W^{1/3} \frac{0.54291 - 21.185R^* + 361.8R^{*2} + 2383R^{*3}}{1 + 2.043R^* + 2.6872R^{*2}} \text{ msec} \quad . \quad (17)$$

The weapon yield, W, is in kt and R* is the scaled slant range in kft/kt$^{1/3}$.

A sample calculation illustrating the energy fraction incident on a target after the shock arrival as a function of weapon yield and scaled ground range is shown in Fig. 4. The influence of the fixed (2.5 kft) height of burst is evident at zero ground range. Close to ground zero, most of radiation arrives after the shock wave for weapon yields larger than 1 Mt. This suggests that even in heavily blast damaged areas, many thermal ignitions will occur. At greater ranges, the amount of late thermal decreases rapidly, though remains significant out to about 3.5 kft/kt$^{1/3}$. For this calculation, the thermal flux corresponding to $E/E_{TH} \sim 0.2$ was 10 cal/cm^2.

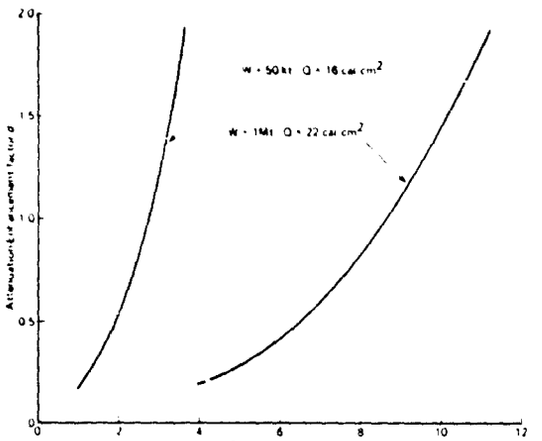

Fig. 3 Thermal reach modified by radiation attenuation or enhancement SHOB = 152 m, V = 19.3 km
$T = (1 + 1.4R/V)e^{2R/V}$

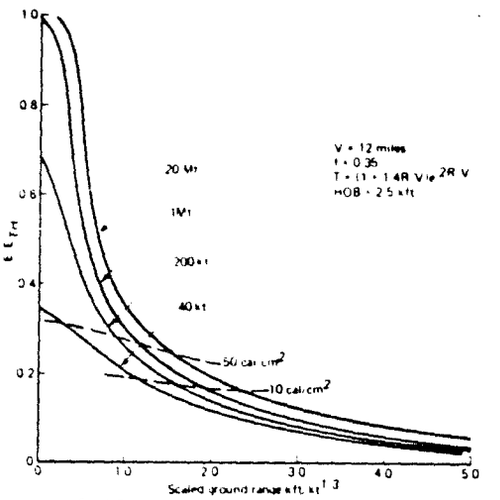

Fig. 4 Thermal radiation fraction incident after shock arrival vs. scaled ground range

SUMMARY AND CONCLUSIONS

The relations presented in this paper for calculation of thermal energy fluxes are based on analysis of weapons tests and detailed radiation-hydrodynamics computations. Many of the analytic forms have uncertainties of 20% or greater. Though atmospheric testing may not be possible, uncertainties involving visibility lengths and transmissivity may be reduced in a test series using high powered light sources. Additional experiments may define the degrees of radiation enhancement and attenuation by snow and cloud cover.

The influence of transmissivity form, visibility length, and reflection or absorption of fireball radiation was explored. Either singly or in combination, these parameters can significantly modify the level of incident thermal radiation. Perturbations about probable values can be used to indicate deviations from expected flux levels. A sample calculation showed that a major fraction of the thermal flux can arrive at a target after the shock wave. Synergistic effects of late thermal and blast disruption may increase the number of "secondary" fire starts.

Analysis of incipient ignitions, fire start distributions, shock precursors, transient thermal loading of structural elements, and personnel casualties depends on the rate and level of incident thermal energy deposition. The functions presented in this note facilitate those calculations.

REFERENCES

1. H. L. Brode, "Review of Nuclear Weapons Effects," Annual Review of Nuclear Science, Vol. 18, pp. 153-202 (1968).

2. H. L. Brode, Fireball Phenomenology, The Rand Corporation, Santa Monica, California, P3026 (1964), (paper presented at the Tripartite Technical Cooperation Panel Meeting, Panel N3, Dorking, England, October 1964).

3. H. L. Brode, Theoretical Description of the Blast and Fireball for a Sea Level Kiloton Explosion, The Rand Corporation, Santa Monica, California, RM2246PR (1966).

4. H. L. Brode, "Gas Dynamic Motion with Radiation: A General Numerical Method," Astronautica Acta, Vol. 14, pp. 433-444 (1969).

5. R. W. Hillendahl, Theoretical Models for Nuclear Fireballs, Lockheed Missile and Sapce Company, DASA 1589 (1965).

6. S. Glasstone and S. J. Dolan, The Effects of Nuclear Weapons, 3rd ed. U.S. Department of Defense and the U.S. Department of Energy (1977).

7. -----, Capabilities of Nuclear Weapons, Defense Nuclear Agency Effects Manual No. 1, DNA-EM-1(N) (November 1974).

8. H. L. Brode, Height of Burst Effects at High Overpressures, The Rand Corporation, Santa Monica, California, DASA 2506 (July 1970).

BLAST/FIRE INTERACTION EXPERIMENTS

Robert G. McKee, Jr.
Los Alamos Technical Associates, Inc.
Albuquerque, New Mexico 87108

ABSTRACT

Los Alamos Technical Associates, Inc. (LATA), under contract to the Federal Emergency Management Agency (FEMA), is fielding three categories of experiments at the DIRECT COURSE H.E. Event. The three categories consist of: 1) constrained debris, 2) unconstrained debris, and 3) room fires.

The overall goal of these experiments is to reduce the present uncertainties in estimates of fire effects of nuclear explosions caused by airblast effects, notably extinction of fires by airblast. More specifically, the experimental objectives are to explore mechanisms of air blast extinction, to test conclusions drawn from shocktube experiments.

The objectives of the three categories of experiment enumerated above are as follows:

1. The objectives of the experiments with constrained debris will be to validate the use of the SRI Blast/Fire Facility as a bona fide source of practical-situation data, and to extend the data base to test conditions that are not readily provided in shocktubes. These variables include: 1) larger areas of exposed debris and, 2) orientation, with respect to both the advanced shock and earth's gravitational field.

2. The addition of "real world" debris in unconstrained configuration provides for data to extend the data base to include more realistic debris mixes, establish blowout criteria for debris that is free to move with the airblast, observe any firebrand production and trajectories, and to observe conditions for rekindling of blast-supressed debris fires.

3. The objective of the room fire experiments is to determine susceptibility of such fires to blowout as a function of fire intensity. The DIRECT COURSE tests may serve to strengthen the conclusion of the Ft. Cronkhite shock tunnel tests. As a bonus, these room fire tests, even without including blast effects, will extend the range of fire dynamics experience to help verify the general validity of room-scaling rules.

Background

1. Debris Fires

The MILL RACE event in September 1981 was initially viewed as an opportunity to verify data taken by direct simulation in the SRI shocktube facility. Unfortunately, the SAI developed thermal pulse accessory was not delivered to SRI in time to allow full simulation prior to MILL RACE. Fires started by brief exposure to a propane burner (used in lieu of the thermal radiation source) in a shredded-filter-paper representation (or idealization) of debris were extinguished in the SRI facility by blast waves that approximated MILL RACE loadings, but definitive data were not obtained. This was compounded by the failure at MILL RACE to acheive unambiguous ignition in the debris specimens exposed to the thermal radiation source (TRS).

Debris fires have been experimentally studied by various investigators. The data most relevant to questions of airblast interaction, prior to the pre-MILL RACE tests by SRI, date from the 1950s; studies conducted at UCLA on wildland fuels and newspaper employed a combined shocktube (actually a blowdown system) and thermal source. The resulting data show a regular, and fairly strong, dependence of extinction thresholds on both preburn time and positive-phase duration.

2. Room Fires

The currently accepted models of the incendiary effects of nuclear explosions in urban areas focus on fire starts in rooms, the underlying assumption being that fires in rooms will dominate the outcome. Unquestionably, fires in rooms comprise a category of special interest in fire growth dynamics. The enclosure not only serves to limit air supply to the fire, but it conserves a portion of the heat released by the fire to intensify it, often leading to a relatively abrupt involvement of the entire room and its contents in an event called "flashover". Viewed operationally, as well as in straight forward damage assessment terms, flashover is a critical end point to the development of the incipient fire. The mathematical models customarily treat the incipient fire, prior to flashover, as a feeble, and therefore blast-sensitive stage in the growth of the fire, and full scale test of incipient room fires that were conducted in the Ft. Cronkhite blast tunnel consistently resulted in blowout thresholds at peak overpressures only slightly higher than 2 psi. Even when the airblast fails to extinguish it, the conventionally modeled fire is perceived to be still quite easily extinguished by prompt action of the first-aid fire-fighting type to the occurence of flashover. The conventional wisdom may, however, be wrong.

During the ENCORE event of operation UPSHOT/KNOTHOLE in 1953, a furnished room, its window facing the fireball, flashed over in less than a minute after exposure to a thermal fluence of about 25 cal/cm^2.

The building was rapidly destroyed by a fire that did not blow out despite an incident airblast of about 6-to-9-psi peak overpressure. A conclusion that the ENCORE response, rather than being an anomally, is the common situation to expect--as opposed to the slow buildup of fire from a feeble, airblast-vulnerable start--could go a long way toward explaining some of the puzzling experimental-results vis-a-vis historical-experience inconsistencies concerning incendiary consequences of nuclear explosions in or near urban complexes. If such a conclusion is borne out by further experimental work, it will significantly impact current perceptions of the dynamics and threat potential of fires caused by nuclear explosions. In turn it will effect civil defense planning, such as crisis relocation, key worker shelter locations, preattack fire-defense preparations, and both trans-attack and post-attack fire-fighting strategy.

Objectives

The overall goal of this program is to reduce the present uncertainties in estimates of fire effects of nuclear explosions caused by airblast effects, notably extinction of fires by airblast. More specifically, the experimental objectives are to explore mechanisms of airblast extinction, to test conclusions drawn from historical and research experience, and to verify data derived from shocktube experiments.

The experiments to be fielded at WSMR consist of the following types:

1. constrained (idealized) debris,
2. unconstrained (real-world) debris, and
3. room fires.

The objectives of the three categories of experiments are as follows:

1. The objectives of the experiments with constrained, idealized debris will be, as they were at MILL RACE, to validate the use of the SRI Blast/Fire Facility as a bona fide source of practical-situation data, and to extend the data base to test conditions that are not readily provided in shocktubes. These variables include (1) larger areas of exposed debris and (2) orientation with respect to both the advancing shock and the earth's gravitational field.

2. The addition of "real world" debris in unconstrained configuration provides for data to extend the data base to include more realistic debris mixes, establish blowout criteria for debris that is free to move with the airblast, observe any firebrand production and trajectories, and to observe conditions for rekindling of blast-suppressed debris fires.

3. The objective of the room fire experiments is to determine susceptibility of such fires to blowout as a function of fire intensity. The DIRECT COURSE tests may serve to strengthen the conclusions of the Ft. Cronkite shock tunnel tests, though that appears less likely today than it would have a decade ago. As a bonus, these room fire tests, even without including blast effects, will extend the range of fire dynamics experience to help verify the general validity of room fire scaling rules.

1. Technical Approach

Debris

Each experiment will consist of five debris pans (1' × 2' × 3"). Four of the units will be located 1.5 m above grade at various angles relative to ground zero. The remaining unit will be located at grade normal to ground zero. Two each of these experiments will be located at the overpressure levels (1, 3, and 7 psi). The two experiments will contain the same fuel but at two different densities. Propane will be used to ignite the debris in each pan. The ignition system will be activated using a spark ignitor or pilot flame and will be terminated prior to shock arrival.

Test Variables

The test variables to be monitored in these six experiments are (1) shock orientation, (2) position in shock wave, at grade and 1.5 m above ground, (3) peak overpressure, (4) preshock burn time, and (5) fire extinguishment threshold.

Instrumentation

The instrumentation will consist of a free field pressure measurement at each station--total of three. Two camera's running at 2,000 f/s and two time lapse (1 f/s) at each station will provide the necessary visual coverage.

Preliminary Tests

Tests will be conducted prior to the September event to determine the desired fuel densities and the preshot burn times needed to obtain the desired fuel burning rates at shock arrival.

2. Unconstrained (Real World) Debris

Each experiment will consist of a 6' × 12' × 6" test bed located at grade at the 1, 3, and 7 psi overpressure levels. The fuel beds will be normal to ground zero and will contain a mixture of various cellulosic materials. As in the Task 1 experiments, ignition will be achieved utilizing a propane system and will be terminated prior to shock arrival.

Test Variables

The test variables to be monitored in these three experiments are (1) peak overpressure, (2) firebrand production and translation, (3) fire extinguishment threshold, and (4) late-time fire rekindling.

Instrumentation

The uncontrained debris experiment utilizes the same free field pressure measurement and camera coverage, since both experiments are located at the same locations.

Preliminary Tests

Tests will be conducted prior to the September event to determine fuel mixture and the preshot burn times needed to obtain the desired burning rates at shock arrival.

3. Room Fires

This experiment is composed of four separate blockhouses (of the ENCORE model), furnished as a representative urban occupancy, with fire initiated by propane gas supply. Two distinct variations are planned: (1) a room fully flashed over prior to shock arrival; and (2) a room experiencing rapid heat buildup (comparable to the ENCORE situation) at the time of shock arrival, but not yet flashed over. Two blockhouses, one of each of these variations, will be located together in the DIRECT COURSE test bed at a distance expected to experience a peak overpressure of 7 psi. An additional variation (1) blockhouse will be located to experience a 9 psi overpressure and an additional variation (2) blockhouse, to receive 3 psi. The room furnishings will be ignited prior to shock arrival utilizing a propane ignition system similar to one used in Tasks I and II.

Test Variables

In addition to blast wave loading, the only intentional variable in this experiment is the intensity of the fire as represented by the two test variations described above. It should be noted that large rates of heat release such as proposed for this experiment, to represent exposures to the high radiation fluxes of a nuclear fireball capable of initiating primary fires in urban interiors, are expected to cause flashover conditions in relatively short times, such as a minute or two.* The development of convective flow of air into the room, in the lower portion of the ventilating opening (e.g., with window), and flow of combustion products and other hot

* Contrast this with the 15 to 20 minute growth periods predicted by current analytical models for initial room fires resulting from nuclear explosions.

gases out of the upper part is a much slower process. Therefore, the flashed over room continues to undergo changing conditions with time, and time elapsed between flashover and shock arrival is a variable that must be controlled by experimental design. In the case of the room fire that has not reached a flashover state prior to shock arrival, the rate of approach must be controlled (by controlling the supply of propane), and the time elapsed between the start of heating and shock arrival will be an even more critical experimental control variable than the counterpart delay in the flashed over rooms. The dynamics of fire growth are fairly predictable and appropriate scaling rules can be derived from full-scale tests and modeling studies.

Instrumentation

For each of the four stations, the instrumentation requirements will consist of: (1) one free field and three internal building pressure measurements (front, side, and back wall); (2) two thermal radiation measurements, one externally mounted viewing the building window and one internally mounted at floor level with a vertical field of view; (3) three temperature measurements, the first located at the ceiling, the second 6 inches below the ceiling, and the third at 2 inches below the window soffit; and (4) one flowrate measurement to monitor propane flow to the burner inside the building. The camera coverage will consist of two cameras one camera will be directed at the window with the remaining camera mounted in the wall for internal coverage.

Preliminary Tests

Tests will be conducted to determine the preburn times needed to obtain the desired burning conditions (flashover and preflashover) at shock arrival.

Results and Conclusions:

None at this time.

SESSION VII

BLAST (MODELING AND SIMULATION)

DIRECT COURSE INDUSTRIAL HARDENING EXPERIMENT AND PREDICTIONS

by A. B. Willoughby and J. V. Zaccor

ABSTRACT

The report describes the background for a practical approach to prepare industry (equipment) to survive a nuclear attack. The status of efforts to assess technical options so far conceived at a forthcoming simulation of a 1 kt weapon are discussed and results predicted.

INTRODUCTION

The Federal Emergency Management Agency (FEMA) has established a continuing program to develop procedures for industry to apply to reduce its vulnerability to nuclear attack. Under the austere civil defense budget, the only practical approach open to FEMA to develop this is through a self-help program that can be implemented effectively by industry upon warning of an impending disaster. To be effective, extremely simple methods will be required that have a significant impact on vulnerability at a minimum expenditure of critical resources (manpower, materials, available time). There are three aspects to developing a truly effective solution: conception, testing of technical effectiveness, and testing of practical feasibility. Field tests such as those scheduled for September 1983 at White Sands Missile Range (WSMR) provide the opportunity to test the technical effectiveness of industrial options that have been conceived. This paper describes the status of the technical assessment of a relatively recently conceived option, the tests planned, and predicted results.

BACKGROUND

Studies conducted by Boeing Corp. at Misers Bluff have demonstrated that industrial equipment can survive drag forces and overpressures at ground ranges where the latter are 300 psi and more, if the equipment is simply buried. However, a realistic assessment of industry options for protecting industrial equipment has shown many plants will have little opportunity to bury equipment as most plants are surrounded by asphalt and concrete surfaces of parking lots, paved loading areas, streets, etc. Moreover, construction equipment to do ground breaking, and dirt moving and hauling, will be in short supply for industrial hardening because this equipment will be needed for creating shelter space. Out of a practical necessity, therefore, some kind of hardening option appeared necessary that could improve equipment survivability using the meager resources most likely to be available.

Other than to collapse under the sudden application of an overpressure, equipment is likely to be damaged principally as a result of impacts that are due to sliding, overturning, building collapse, or missiles. Considerable data already exist on missile velocities as a function of drag forces and missile geometry, and debris studies on wall and building failures can be used in conjunction with this and with material properties to assess the impact damage via the mechanisms of missiles and building collapse. Little information has been developed, however, on sliding and overturning of industrial equipment and related damage. To rectify this, exploratory studies were initiated at the MILL RACE 1 kt weapon simulation event conducted at WSMR, in New Mexico in 1981, to examine overturning and to assess the potential for harnessing the static overpressure to reduce sliding, both under drag forces and at a single ground range (i.e., where the static overpressure from this surface burst was 20 psi). These

studies used artifacts (drums) to simulate industrial equipment and showed that both overturning and sliding under drag forces could be affected rather significantly by simple expedients - for example, clustering items in a group and banding them tightly so that they would act as a unit. Hence, the basic concepts were confirmed through the exploratory tests; additional data are needed now to develop information that can be applied by industry with confidence.

EXPERIMENTAL OBJECTIVES:

The major thrust of the DIRECT COURSE experimental program on industrial hardening is to further verify the clustering concept by:

1. Testing actual equipment clusters under conditions similar to the simulated clusters tested at MILL RACE where 55-gallon drums were used;
2. Testing of an actual equipment cluster inside a frangible structure;
3. Testing of simulated equipment clusters under a wider range of conditions than those used at MILL RACE including:
   a. higher overpressures
   b. larger clusters
   c. materials other than seat belt webbing for securing the cluster
   d. effects of static overpressure on anchoring equipment packages (on dirt and, possibly, water surfaces) against the horizontal dynamic pressure impulse

A secondary objective is to further study the behavior of unhardened equipment under blast loading to help assess vulnerability.

EXPERIMENTAL ARRANGEMENT FOR EQUIPMENT CLUSTER TESTS

Cluster Details

Each cluster will consist of 9 individual items of equipment arranged as illustrated in Figure 1.

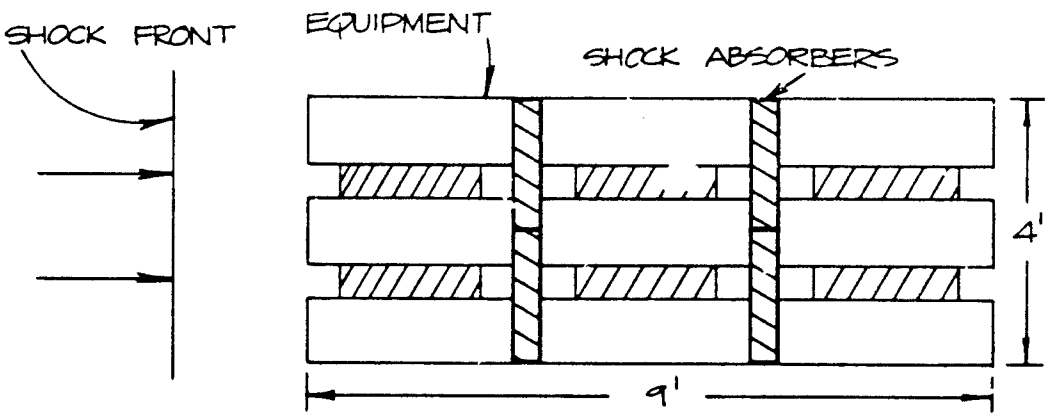

FIG. 1. SKETCH OF ACTUAL EQUIPMENT CLUSTER.

Overall dimensions of a cluster will be 4 ft x 9 ft, and the package will be oriented so that the blast front will impinge on the narrower (4 ft) side; the overall density will be about 16 lb/ft^3. This particular array was selected to model the behavior of a heavy equipment cluster exposed to a 1 Mt weapon. The heavy equipment cluster modeled (one assembled in an earlier demonstration experiment) had a maximum dimension of 20 ft and a density of 50 lb/ft^3 (1). A discussion of the basis of this modeling is given here, in Appendix A.

Cluster Layout

Three of the clusters described will be tested; two of them will be in the open at the 20 psi static overpressure level (Item 1, above), and one will be inside a structure (Item 2, above) at a static overpressure somewhere between 15 psi and 25 psi. The two clusters in the open will be on different surfaces, one on a prepared surface of concrete or asphalt and the other on dirt. The cluster inside the structure will be on a concrete surface and will be slightly modified from those in the open as it will also be exposed to missiles from breakup of the wall, and possibly to structural collapse. The modification will consist of adding shock absorbing material around and on top of the cluster when it is assembled.

Both still and high speed photography will be used to record response.

EXPERIMENTAL ARRANGEMENTS FOR SIMULATED EQUIPMENT CLUSTERS

Cluster Details

For these tests 55-gallon drums will be used to simulate equipment items and clustered in various arrays similar to what was done at MILL RACE (2). Sketches of the arrays that will be tested are shown in Figure 2.

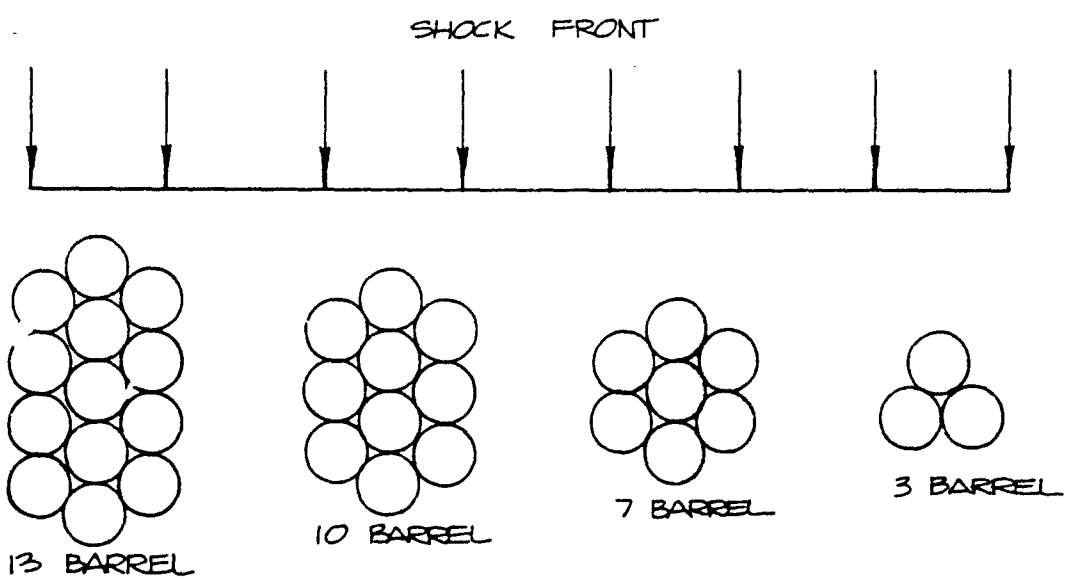

FIG. 2. SKETCHES OF BARREL CLUSTERS.

Cluster Layout

The planned cluster tests are divided into three groups depending on the particular overpressure levels where the cluster is to be located.

Group I - Tests at 30 psi

At three different locations, 7 and 10 barrel arrays will be placed with at least one array being on a stabilized surface so that high speed photographs may be taken. These tests will help to evaluate the overturning and sliding response and the securability of items into larger arrays and at higher overpressures than tested at MILL RACE.

Group II - Tests at 20 psi

A. At one location, three 7-barrel arrays will be secured with more commonly available strapping material than the seat belt webbing used at MILL RACE.

B. At two locations having different types of surfaces, two 3-barrel arrays having half the normal weight will be placed. One of the arrays will be anchored with the expedient soil anchor used at MILL RACE. The objective here will be to determine if the cluster size can be reduced by using soil anchors.

Group III - Tests at 40 psi

At two locations having different surfaces, one 7-barrel and one 13-barrel array will be placed with one surface sufficiently stabilized to permit high speed photographs of the cluster motions. The purpose of these tests is to extend the Group I tests to still higher overpressures and larger clusters.

EQUIPMENT REFERENCE TESTS

To provide reference data on the equipment, individual items will be exposed to static overpressures at the 20 psi ground range.

TEST SUMMARY

Table I provides a summary of the expected test results.

TABLE 1: PREDICTED VELOCITIES AND DISPLACEMENTS OF ARTIFACTS

Test Array	P_o (psi)	I_q (psi-s)	D (ft)	F (ft/s)	V_z (ft/s)	V_o	V_z/V_o	Overturn	Displacement in D
Full scale 1 Mt Heavy Equip.	20	3	20	0.1	14	22	0.64	NO	(D/3)
Direct Course 1 kt Light Equip. Package	20	0.3	9	0.033	9.3	15	0.63	NO	(D/3)
3 Drums	20	0.3	3.7	0.07	10.7	9.5	1.13	probably	(D)
7 Drums	30	0.6	5.4	0.10	10	10	1.0	marginal	(D/2)
10 Drums	30	0.6	6.7	0.10	8.4	13	0.65	NO	(D/4)
7 Drums	40	0.87	5.4	0.10	15	10	1.5	YES	(1.1D)
13 Drums	40	0.87	8.7	0.10	10	15	0.67	NO	(0.3D)

REFERENCES

1. J.V. Zaccor, R.D. Bernard, and R.E. Peterson, Industrial Hardening: 1981 Technical Status-Report, Scientific Service, Inc., Redwood City, California, SSI 8145-7 (September 1982).

2. R.S. Tansley and J.V. Zaccor, Testing of Shelter Design and industrial Hardening Concepts at the MILL RACE Event, Scientific Service, Inc., Redwood City, California, SSI 8115-4 (January 1982).

APPENDIX A

SCALING OF EQUIPMENT CLUSTERS

Calculations given in Reference 1 show that, for truly impulsive loads, the cluster will not overturn nor will it slide more than a distance, D, providing that:

$$D > 1.5[I_q/F]^{2/3}$$

where D = the minimum horizontal dimension of the cluster (ft)
I_q = the dynamic pressure impulse (psi-s)
F = the ratio of the density of the cluster to that of steel
and it is assumed that the height of the cluster is less than 1/3D.

To illustrate the scaling involved, assume it is desired to model in a 1 kt test using real equipment a full scale cluster having a D = 20 and an F = 0.1 exposed to a 1 Mt weapon burst. This means that D and/or F have to be reduced so that the above equation holds for a reduction in I_q of a factor of 10. This could be accomplished, for example, by reducing F by a factor of 10 to a value of 0.01. However, this is an impractically low value of F, as even very lightweight home shop tools have F values ranging from 0.19 to 0.044. On the other hand, the total change could be made in the D factor, which would reduce it by almost a factor of 5 down to slightly more than 4 ft. This would make it virtually impossible to meet the required height-to-depth ratio as well as to include very many items of real equipment.

The most practical approach is to change both the D and the F values; i.e., to reduce both. For example, to simulate the 1 Mt condition in Table 1 on real equipment at 1 kt, the recommended cluster has a D = 9 and an F = 0.033 (see item 2 on Table 1). This combination avoids the problems discussed previously and is convenient to work with. Note that what this type of scaling means is that the model scale case will have the same likelihood of overturning as the full scale case and that in both cases the cluster will slide less than a distance D. Likelihood of overturning means that the model scale cluster will be accelerated to the same fraction of the velocity needed for overturning as the full scale case, which for the clusters selected is about 2/3.

ANALYTIC APPROXIMATIONS TO DYNAMIC PRESSURE AND IMPULSE AND OTHER FITS FOR NUCLEAR BLASTS

H. L. Brode
Pacific-Sierra Research Corporation
12340 Santa Monica Boulevard
Los Angeles, California 90025

ABSTRACT

Recent fits to data and calculational results provide simple analytic approximations to the overpressure and dynamic pressure from nuclear explosions. The analytic forms provide fits as a function of ground range and height-of-burst for time of arrival, peak overpressure, peak dynamic pressure, onset of Mach reflection, duration of positive phase for both dynamic and overpressure, time histories for overpressure and dynamic pressure, dynamic pressure impulse and overpressure impulse (in the positive phase), and other blast parameters.

INTRODUCTION

Recently Kaman AviDyne (KA) produced for the Defense Nuclear Agency (DNA) 3 two-dimensional hydrodynamic calculations of the nuclear blast wave over an ideal reflecting plane at burst heights of 200, 400 and 700 ft/kt$^{1/3}$ (1). These solutions, together with the DNA kiloton standard (2) (using 2H) for a surface burst allow some definition of both overpressure and dynamic pressure as a function of time, burst height, range and yield.

These KA solutions are being studied further to determine their accuracy and limits, and other DNA sponsored calculations are under way. For the present, these KA results appear to provide the best dynamic pressure height-of-burst information. Any subsequent confirmation by independent solutions or other improvements due to experiments or recalculation are likely to be many months in coming. In this note, relatively simple analytic forms which approximate the KA results are presented and compared with calculations.

In the absence of sufficiently detailed calculations and in view of a paucity of relevant measurements, Brode and Speicher (3) invented an analytic approximation to the dynamic pressure from height-of-burst blasts. The first approximation was almost immediately improved (4). The time dependence was based on one-dimensional calculations appropriate for free air or surface nuclear bursts (5) and on various analytic approximations for time-of-arrival and overpressure-time HOB behavior as provided in earlier fits (6,7). An improved description of the height of burst dependence of overpressure, based on both HE data and calculations, was published in late 1981 (8,9).

A "quick fix" analytic approximation for the dynamic pressure, based on the recent KA calculations, was offered in a memo from S. J. Speicher in December 1982 (10). This quick fix is cast in terms of the previous fit to the overpressure as a function of time, burst height, ground range and yield (8).

DYNAMIC PRESSURE AND IMPULSE FITS

In this report, the peak dynamic pressure and the total dynamic impulse in the positive phase are approximated by analytic forms and simple fits to match the KA and 1 KT Standard results. In the regular reflection region, (of

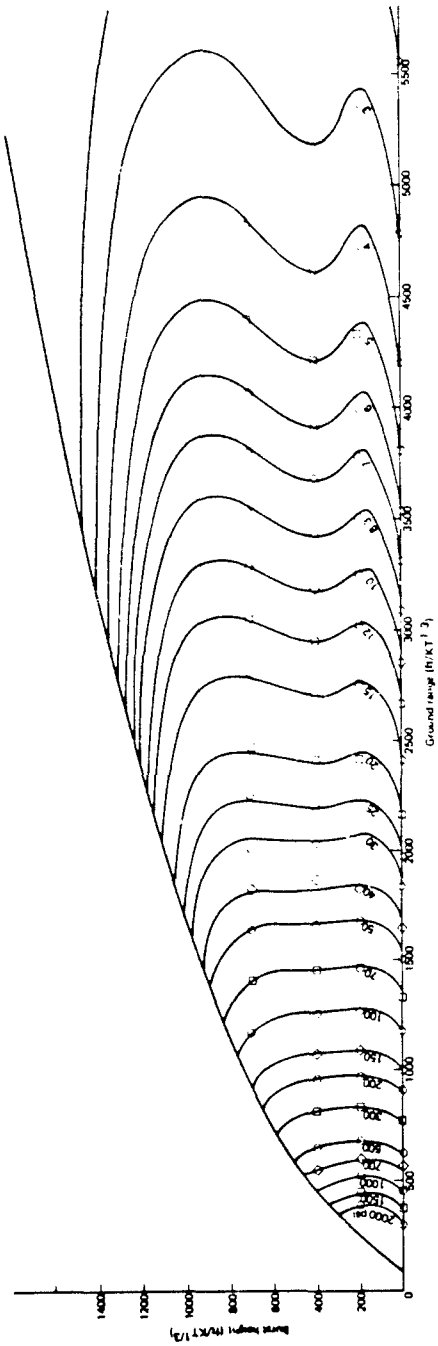

Figure 1--Height of burst fit for peak dynamic pressure

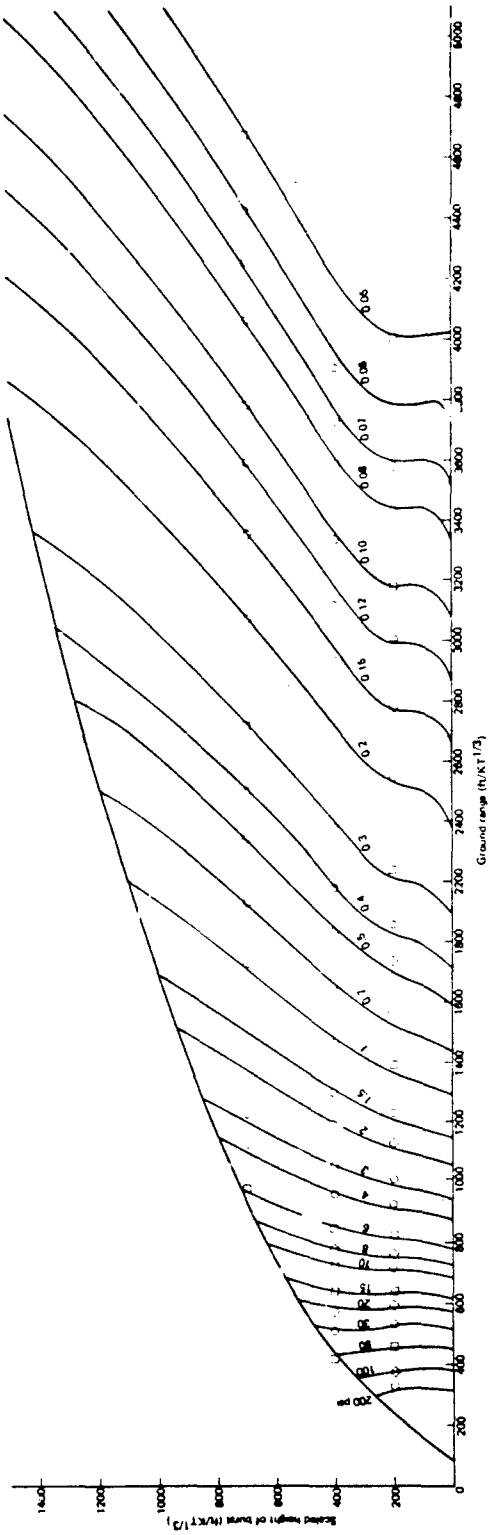

Figure 2--Dynamic impulse fit versus range and burst height

less interest for targeting or damage assessment) the fits are inappropriate, and should be used in the Mach reflection region only.

The fits and comparisons are illustrated in Figures 1 and 2. Tables 1 and 2 compare the differences between the values provided by the fits and the values for 0, 200, 400 and 700 scaled feet HOB from the calculation. In all cases the differences are less than a few percent at variance. As more and better calculations become available, these fits may be amended or replaced, but for now they represent a simple description of the dynamic pressure and dynamic impulse versus height, range and yield.

In evaluating the goodness of these approximations or the accuracy of the detailed calculations, it is well to keep in mind the basic variability of blast data. A review of the peak overpressures as measured on nuclear tests (11) shows scatter of more than ±15% in range for any given peak overpressure. Figure 3 shows one such collection of "data" for 15 psi (scaled to 1 KT) as a function of ground range and burst height. Far fewer and less accurate measurements of dynamic pressure exist, although, these pressures are expected to follow shock (Hugoniot) relations in most of the non-precursed peak pressure regions. An exception is in a portion of the double Mach shock reflection region where second peaks are dominant. In precursor or dust laden blast waves, peak dynamic pressures can exceed the classical shock values by appreciable factors (as much or more than a factor of two). Observed durations and time behaviors are equally variable.

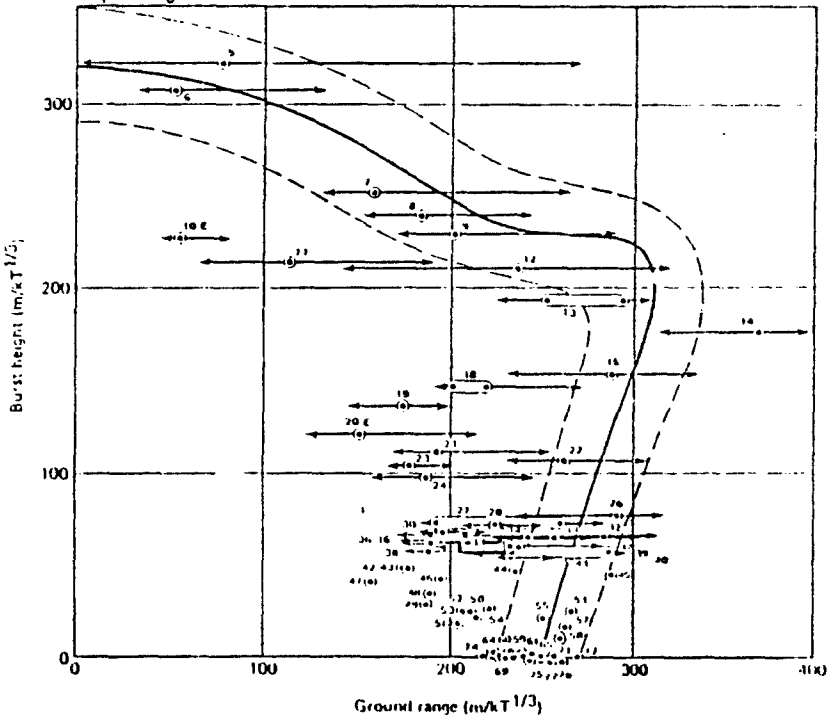

Figure 3 Fifteen psi (103 kPa) nuclear test data versus HOB and range scaled to 1 KT

SOME ADDED USEFUL ANALYTIC APPROXIMATIONS

For shock waves in air (at sea level) all of the conditions at the shock front can be expressed in terms of a single variable, such as peak overpressure. The non-ideal gas behavior of air at high temperatures and pressures

Table 1: Peak Dynamic Pressure, Q_s (psi)

Scaled Ground Range = R ($KFT/KT^{1/3}$), Scaled Burst Height = H ($KFT/KT^{1/3}$)

$$Q_s = \frac{A}{R^4 + .025R^{4.5}} + \frac{C}{R + DR^4} \text{ psi; R,H in } KFT/KT^{1/3}$$

$$A = 2.28 + 12.5H^2/(1 + 1.292H),\ B = 3 + (0.86 + 2.47H)/(1 + 114H^3)$$

$$C = (.21 + 2.2H)/(1 + 200H^3),\ D = (.008 + .24H)/(1 + 260H^3)$$

Valid for : $R > \frac{170(H + .09)}{1 + 337(H + .09)^{1/4}} + 0.914(H + .09)^{2.5}$

Comparison with Kaman Avidyne Calculations (scaled to 1 KT)

HOB (ft)	Max Difference %	Max Difference Q_s (psi)	Average Difference	Net Difference
0	-4	200	0.3 %	-0.3 %
200	+5	200	1.6 %	+1.4 %
400	-2	30	1.1 %	-1.1 %
700	+2	4	0.6 %	+0.5 %

$$\% \text{ Difference} = \frac{(KA) - (FIT)}{(KA)} \times 100$$

Table 2: Dynamic Impulse, I_u^+ (psi-ms)

Scaled Ground Range = R ($ft/KT^{1/3}$), Scaled Burst Height = H ($ft/KT^{1/3}$)

$$I_u^+ = \frac{ER}{F + R^{3.61}} + \frac{G}{1 + 0.22R^2} W^{1/3} \text{ psi-ms; H,R in } KFT/KT^{1/3} \text{ W in KT}$$

$$E = \frac{183(H^2 + .00182)}{(H^2 + .00222)},\ F = 0.00058 \exp(9.5H) + 0.0117 \exp(-22H)$$

$$G = 2.3 + \frac{29H}{(1 + 1760H^5)} + \frac{25H^4}{(1 + 3.76H^6)}$$

Valid for: $R > \frac{170(H + .09)}{1 + 337(H + .09)^{1/4}} + 0.914(H + .09)^{2.5}$

Goodness of Fit: Comparison with Kaman AviDyne Calculations

HOB (ft)	Max Difference %	Max Difference I_u (psi)	Average Difference	Net Difference
0	+7	1000 & 700	2	-1/4
200	+5	2000	1	-1/4
400	+5	2	1/2	+1/4
700	-3	30	2/3	-1/8

$$\% \text{ Difference} = \frac{(KA) - (FIT)}{(KA)} \times 100$$

precludes an ideal gas formulation, but, since the effective specific heat ratio (γ) changes slowly with peak overpressure or shock strengths, empirical fits can be found which follow fairly simple forms. Some such approximate forms for Peak Dynamic Pressure (Q_s), shock velocity (U_s), peak particle velocity (u_s), peak density (ρ_s), shock temperature (T_s) and normal reflection factor (RF) (all shock front quantities that can be described as function of peak overpressure (ΔP_s)) are offered here.

Peak Dynamic Pressure for an ideal gas:

$$Q_s(\Delta P_s, P_0, \gamma) \simeq \Delta P_s^2/[2\gamma P_0 + (\gamma - 1)\Delta P_s] \quad \text{psi} \tag{1}$$

$P_0 \simeq 14.7$ psi at sea level; $\gamma \equiv$ effective specific heat ratio ($1.08 \leq \gamma \leq 1.67$ For $P_0 = 14.7$, $\gamma \simeq 1.4$ for $\Delta P_s < 300$ psi)

$$Q_s(\Delta P_s) \simeq \Delta P_s^2\left[1 + \frac{1}{2}\left(\frac{\Delta P_s}{1000}\right)^2\right]\cdot\left[41 + 0.4\Delta P_s + \frac{1}{10}\left(\frac{\Delta P_s}{100}\right)\right]^{-3} \quad \text{psi} \tag{2}$$

(Eq. (2) accurate to < 5% for $2 \leq \Delta P_s \leq 100{,}000$ psi)

Shock Velocity for an ideal gas:

$$U_s(\Delta P_s, C_0, P_0, \gamma) \simeq C_0[1 + (\gamma + 1)\Delta P_s/2\gamma P_0]^{1/2} \tag{3}$$

C_0 is sound speed ahead of shock, ($C_0 \simeq 1.1$ Kft/sec)

for air ($\gamma = 1.4$):

$$U_s(\Delta P_s, C_0, P_0) = C_0\{(.857 + .006\xi/(1 + .2\xi))\xi + .143\}^{1/2} \tag{4}$$

$$\xi \equiv (\Delta P_s + P_0)/P_0 \tag{5}$$

(Eq. (4) accurate to < 8% for $\Delta P_s < 100{,}000$ psi)

Peak Particle Velocity for an ideal gas:

$$u_s(\Delta P_s, C_0, P_0, \gamma) = C_0(\Delta P_s/\gamma P_0)(1 + (\gamma + 1)\Delta P_s/2\gamma P_0)^{-1/2} \tag{6}$$

(for air, $\gamma = 1.4$, Eq. (6) accurate to < 4% for $1 \leq \Delta P_s \leq 500{,}000$ psi)

Shock Temperature:

$$\frac{\Delta T_s(°C)}{T_0} = \xi\left(\frac{R_0}{R_s}\right)\left(\frac{(\gamma - 1)_s\xi + (\gamma + 1)_0}{(\gamma + 1)_s\xi + (\gamma - 1)_0}\right) - 1 \tag{7}$$

$$R_i = P_i/(\rho_i T_i) \tag{8}$$

for air (T_0 = 273°K, P_0 = 14.7 psi):

$$\Delta T_s/T_0 = (\xi^2 - 1)/[7 + B(\xi - 1)] \tag{9}$$

$$B = 6 + 1.76\xi^{2.5}/[10^5 + 4.38\xi^2] \tag{10}$$

Normal Reflection factor (RF):

$$RF \equiv \frac{\Delta P_r}{\Delta P_s} = \frac{2 + \left(\frac{3\gamma - 1}{2\gamma}\right)\left(\frac{\Delta P_s}{P_0}\right)}{1 + \left(\frac{\gamma - 1}{2\gamma}\right)\left(\frac{\Delta P_s}{P_0}\right)} \tag{11}$$

ΔP_r is reflected peak overpressure from a normally incident shock of peak overpressure ΔP_s in an ambient atmosphere of pressure P_0.

For air at sea level and ΔP_s in psi (6)

$$RF \simeq 2 + \frac{.002655\Delta P_s}{1 + .0001728\Delta P_s + 1.921 \times 10^{-9}\Delta P_s^2} + \frac{.004218 + .04834\Delta P_s + 6.856 \times 10^{-6}\Delta P_s^2}{1 + .007997\Delta P_s + 3.844 \times 10^{-6}\Delta P_s^2} \tag{12}$$

SUMMARY

Simple analytic fits have been developed to describe the results of recent Kaman AviDyne hydrocode calculations. Algebraic relations for the peak dynamic pressure and peak dynamic impulse are presented and compared to the hydrocode results. The simple functions are easily programmable on a hand-held calculator and agree well with the KA calculations. Analytical and empirical relations describing blast wave characteristics are presented and their accuracy noted.

REFERENCES

1. R. F. Smiley, M. A. Tomayko and J. R. Ruetenik, Reflect-4 Code Overpressure, Dynamic Pressure and Impulse Time Histories at the Ground for a 40-KT Burst at 684-FT HOB, Kaman AviDyne, Burlington, Massachusetts, KA TM-136 (9 August 1982).

R. F. Smiley, M. A. Tomayko and J. R. Ruetenik, Reflect-4 Code Overpressure, Dynamic Pressure and Impulse Time Histories at the Ground for a 40-KT Burst at 1368-FT HOB, Kaman AviDyne, Burlington, Massachusetts, KA TM-137 (9 August 1982).

R. F. Smiley, M. A. Tomayko and J. R. Ruetenik, Reflect-4 Code Overpressure, Dynamic Pressure and Impulse Time Histories at the Ground for a 40-KT Burst at 2394-FT HOB, Kaman AviDyne, Burlington, Massachusetts, KA TM-138 (9 August 1982).

R. F. Smiley, J. R. Ruetenik and M. A. Tomayko, Reflect-4 Code Computations of 40 KT Nuclear Blast Waves Reflected from the Ground, Kaman AviDyne, Burlington, Massachusetts, KA TR-201 (1 November 1982).

2. C. E. Needham and J. E. Crepeau, The DNA Nuclear Blast Standard (1 KT), Systems, Science and Software, Inc., La Jolla, California, SSS-R-81-4845 (30 January 1981).

3. H. L. Brode and S. J. Speicher, Analytic Approximation for Dynamic Pressure Versus Time, Pacific-Sierra Research Corporation, Los Angeles, California, PSR Note 315 (May 1980).

4. S. J. Speicher and H. L. Brode, Revised Procedure for the Analytic Approximation of Dynamic Pressure Versus Time, Pacific-Sierra Research Corporation, Los Angeles, California, PSR Note 320 (May 1980).

5. H. L. Brode, Theoretical Description of the Blast and Fireball for a Sea Level Kiloton Explosion, The RAND Corporation, Santa Monica, California, RM-2246-PR (January 1966).

6. H. L. Brode, Height of Burst Effects at High Overpressure, The RAND Corporation, Santa Monica, California, RM-6301-DASA (July 1970).

7. H. L. Brode, "Review of Nuclear Weapons Effects," Annual Review of Nuclear Science (March 1968).

8. S. J. Speicher and H. L. Brode, Airblast Overpressure Analytic Expression for Burst Height, Range and Time-Over an Ideal Surface, Pacific-Sierra Research Corporation, Los Angeles, California, PSR Note 385 (November 1981).

9. S. J. Speicher and H. L. Brode, An Analytic Approximation for Peak Overpressure Versus Burst Height and Ground Range Over an Ideal Surface, Pacific-Sierra Research Corporation, Los Angeles, California, PSR Note 336 (September 1980).

10. S. J. Speicher, Pacific-Sierra Research Corporation, Los Angeles, California, letter to Distribution List, subject: Corrections to Dynamic Pressure "Quick Fix" (21 December 1982).

11. H. L. Brode, Review of Nuclear Test Peak Overpressure Height-of-Burst Data, Pacific-Sierra Research Corporation, Los Angeles, California, PSR Note 353 (November 1981).

BLAST LOADING COMPUTATIONS OVER COMPLEX STRUCTURES

Andrew Mark
U.S. Army Ballistic Research Laboratory
U.S. Army Armament Research and Development Command
Aberdeen Proving Ground, Maryland 21005

and

Paul Kutler
Applied Computational Aerodynamics Branch
NASA Ames Research Center
Moffett Field, California 94035

ABSTRACT

Computational results of shock waves impinging on a truck-like target and the ensuing diffraction flowfield are presented. The Euler equations are solved with MacCormack's explicit finite difference scheme. Computed pressures on the surface of the model compare favorably with experimental results from shock tube experiments. Isopycnics for the diffraction phase are also presented and show the time-dependent development of vortices generated at the various corners of the model.

I. INTRODUCTION

The accurate prediction of the effects of blast waves impinging on vehicles and structures is essential in the design, survivability, and hence effectiveness of these configurations. The problem is stated pictorially in Figure 1. Detailed experimental blast wave interaction data is both costly and difficult to obtain. Moreover, these experiments frequently do not provide a complete picture of the blast wave interaction flowfield. Actual experiments, in fact, only yield pressure data at a few selected points on the models. As a consequence essential design parameters are often difficult to define.

An alternative to the experimental description of the blast wave interaction phenomenon is the use of computational fluid dynamics. This is the approach adopted here. Accurate finite difference simulations offer the possibility of providing design data at a relatively low cost. Such a simulation provides a complete flowfield description that is essential to a fundamental understanding of the fluid mechanics and a necessity for an effective structural design. The numerically generated flowfield data can then be integrated to yield other vital information such as the total loads, center of pressure, and overturning moments.

In the present paper, these "shock-capturing" flowfield simulation techniques have been adapted to the blast wave/target interaction problem for a configuration of a military truck-like shape carrying a communications shelter. For two-dimensional simplicity, the wheels, canvas canopy and windshield have been omitted. Computational results are compared with experimental data from a shock tube.

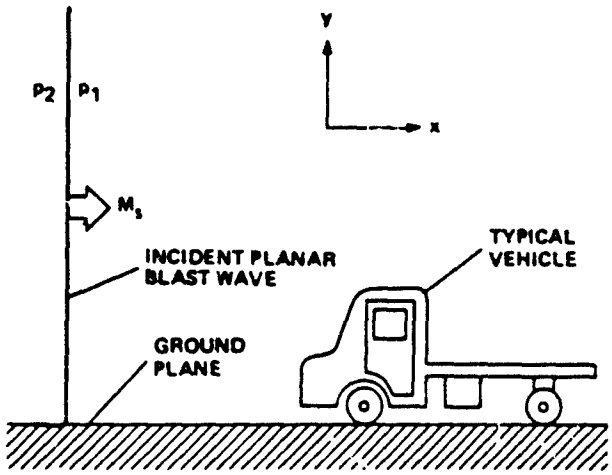

Figure 1. Blast wave-vehicle interaction problem.

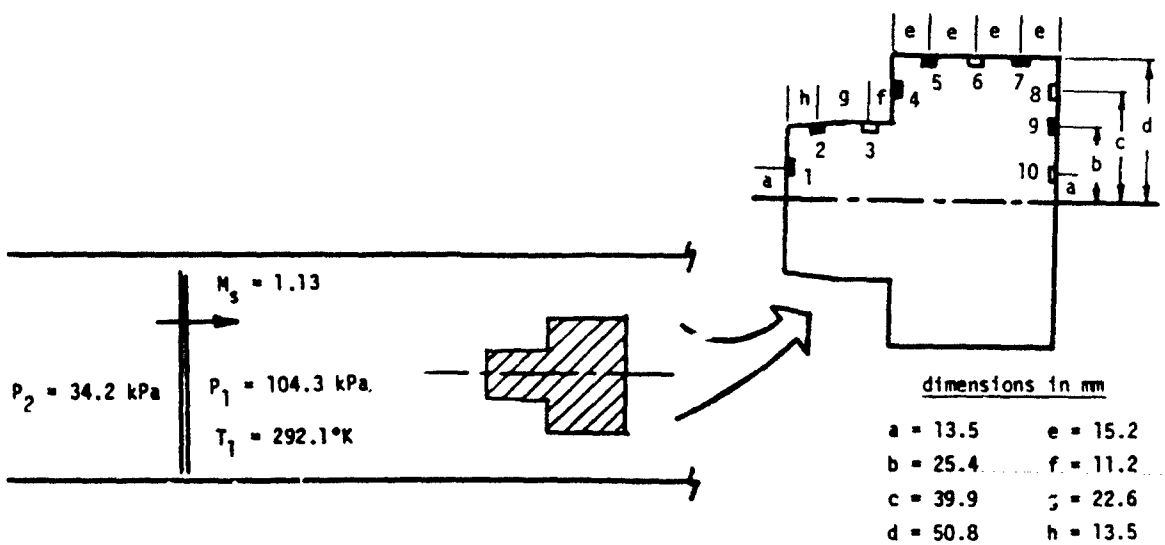

Figure 2. Shock tube experimental conditions for shock wave/truck interaction.

II. THEORETICAL CONSIDERATIONS

Several assumptions are made in the present study of blast wave encounters with targets. The first is that the blast wave is assumed to be planar relative to the target and that conditions behind the wave can be adequately and consistently described. Secondly, viscous effects are ignored. Finally, any effects which result from radiative heating on the target are assumed negligible, and a perfect gas equation of state is employed.

Under the above assumptions, the governing partial differential equations are the unsteady Euler equations which were solved by MacCormack's explicit finite-difference procedure with an additional fourth-order dissipation term (1). This method is a second-order, noncentered predictor-corrector scheme and appears as follows:

$$\bar{q} = q^n - \Delta t(\Delta_\xi E^n + \Delta_\eta F^n)$$
$$q^{n+1} = \frac{1}{2}\left[\bar{q} + q^n - \Delta t(\nabla_\xi \bar{E} + \nabla_\eta \bar{F}) + \varepsilon D^n\right] \tag{1}$$

where $\bar{E}$ implies that the flux vector E is evaluated using elements of the predicted value $\bar{q}$, and Δ and ∇ are the standard forward and backward difference operators. The quantity D represents a fourth-order dissipation term in both directions whose effect is governed by the dissipation constant ε.

III. RESULTS AND DISCUSSION

The physical and computational truck model that was used had no canvas top (cab) or windshield. These are light target components, easily destroyed by small overpressures, and represent an insignificant obstruction to the blast loading. In addition, the wheels were omitted from the model to permit a two-dimensional representation. The overall shape is meant to represent a 2½ ton truck carrying a communications shelter. A physical description of the model with its transducer positions is shown on the right side of Figure 2. This figure also shows a schematic of the test setup used in the shock tube. The model was built with identical mirror halves which were installed in the center of the shock tube, halfway between floor and ceiling. This type of installation avoids the viscous effects behind the shock on a floor mounted model. The Euler equations in the computations more closely approximate this condition. The midplane (or mirror plane) is treated like a symmetry boundary in the computations.

Figure 3 shows comparisons of pressure-time histories between the computations and the experiment. The "noisier" curves in these figures are the experimental results obtained at the Ballistic Research Laboratory by Bulmash (2). Six of the stations around the model are compared. These are indicated by the black dot in each inset figure. The computation was performed assuming free field conditions (no tube wall), so that wall reflections appearing in the experiment are not present in the computations. These occur at approximately 1.5 and 3 ms in Figure 3a. The same waves show up at different times in successive figures, which depend to some extent on the changing flow conditions, but more importantly, on the proximity of the affected surfaces (transducers) to the tube wall.

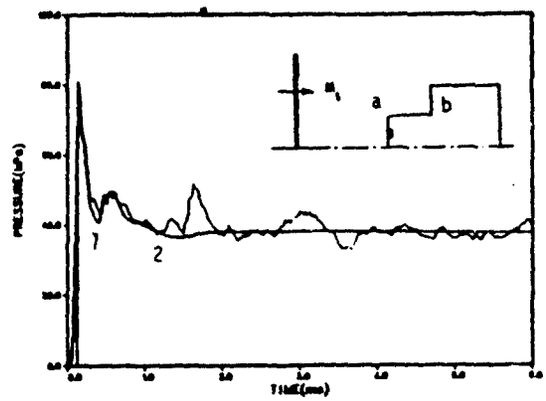

(a) gage location 1

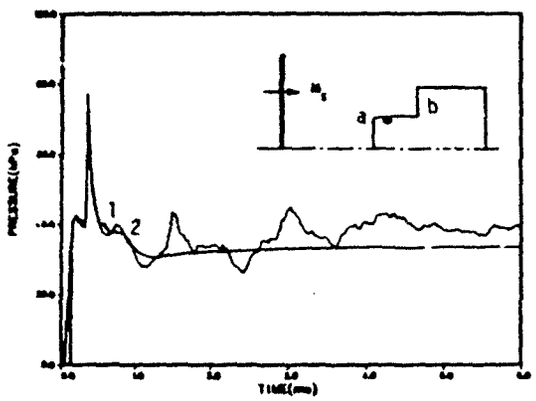

(b) gage location 2

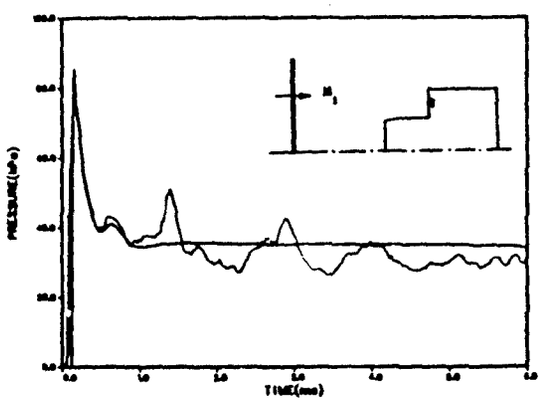

(c) gage location 4

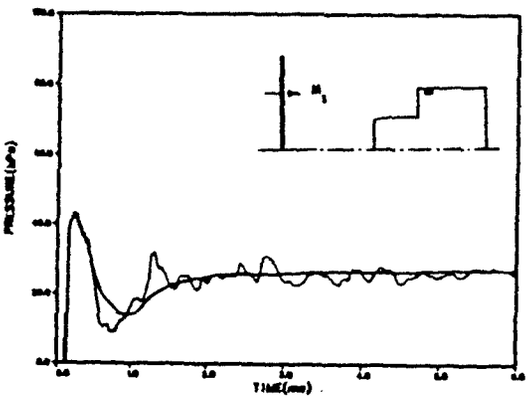

(d) gage location 5

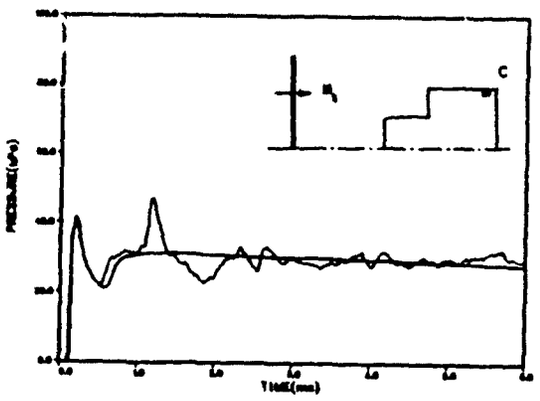

(e) gage location 7

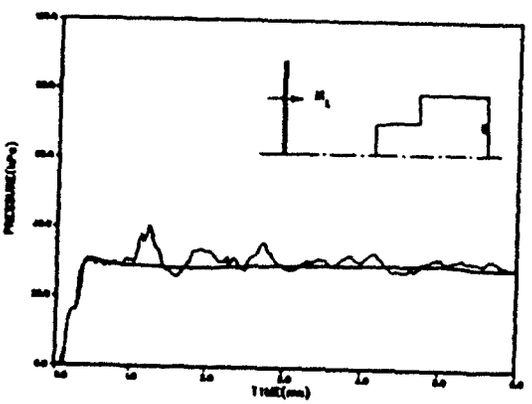

(f) gage location 9

Figure 3. Pressure-time history for blast wave/truck interaction. (Shock strength overpressure = 34.2 kPa)

Much detail is evidenced in the results if one examines the curves closely. As an example, the pressure rise for the early part of Figure 3a is caused by the flow stagnating in front of the truck and the decay is caused by the rarefaction wave generated at corner a and sweeping down the front of the "grill". However as the incident shock continues up the hood of the truck (to which there is a slight incline), a different decay rate is sensed by the transducer at position 1. This decay rate is labeled 1 in Figure 3a. Subsequently, the incident shock hits wall b and reflects with a shock traveling toward position 1. This reflection clearly shows upon the density contour plot of Figure 4c (labeled R2). R2 eventually sweeps past gage position 1 and reflects from the floor resulting in a double peak at approximately .5 ms in Figure 3a. This is also seen in Figure 4e-f (labeled R3). Rarefactions from corner a (primarily) in Figure 3a eventually drop the pressure level to a pseudo-steady level (2 in Figure 3a).

Gage position 2 (Figure 3b) sees a pressure rise to about 40 kPa initially before it senses the reflection from wall b to a level of almost 80 kPa. This pressure is quickly reduced by the rarefaction wave generated at corner a by wave R2 (Figure 4c) as it spills over against the main flow. As it rebounds off the forward part of the floor it creates a small jump (1 in Figure 3b). Finally, R3 generates rarefaction waves at the upper corner of wall b and at corner a which combine to form decay 2 in Figure 3b. Similar waves exist in most plots.

IV. CONCLUSIONS

When comparing computed and experimental pressure-time data the general trend is very encouraging. There are tendencies to show that inclusion of viscosity will improve the computations. The steady-state values of pressures agree well with computations in all of Figure 3 except Figures 3b-c. In Figure 3b the final level is underpredicted and in Figure 3c it is overpredicted. One possible explanation is the viscous vortex set-up between the hood and the front face of the shelter, b. The two locations (2 and 4) probably don't adequately model the slow rotation in that corner. This problem appears to be very similar to the classic driven cavity problem. Pressure gradients normal to the surface are not adequately accounted for.

The computed isopycnics need further development. Shocks, in general, are captured reasonably well and contact surfaces are not. Adequate grid resolution and/or an adaptive gridding scheme should improve our results. Both avenues are being persued.

REFERENCES

1. R. W. MacCormack, "The Effect of Viscosity in Hypervelocity Impact Cratering," AIAA Paper 69-354, Cincinnati, Ohio, 1969.

2. G. Bulmash, "Shock Tube Study of a Two-Dimensional Generic Truck/Shelter Model," BRL Report in publication.

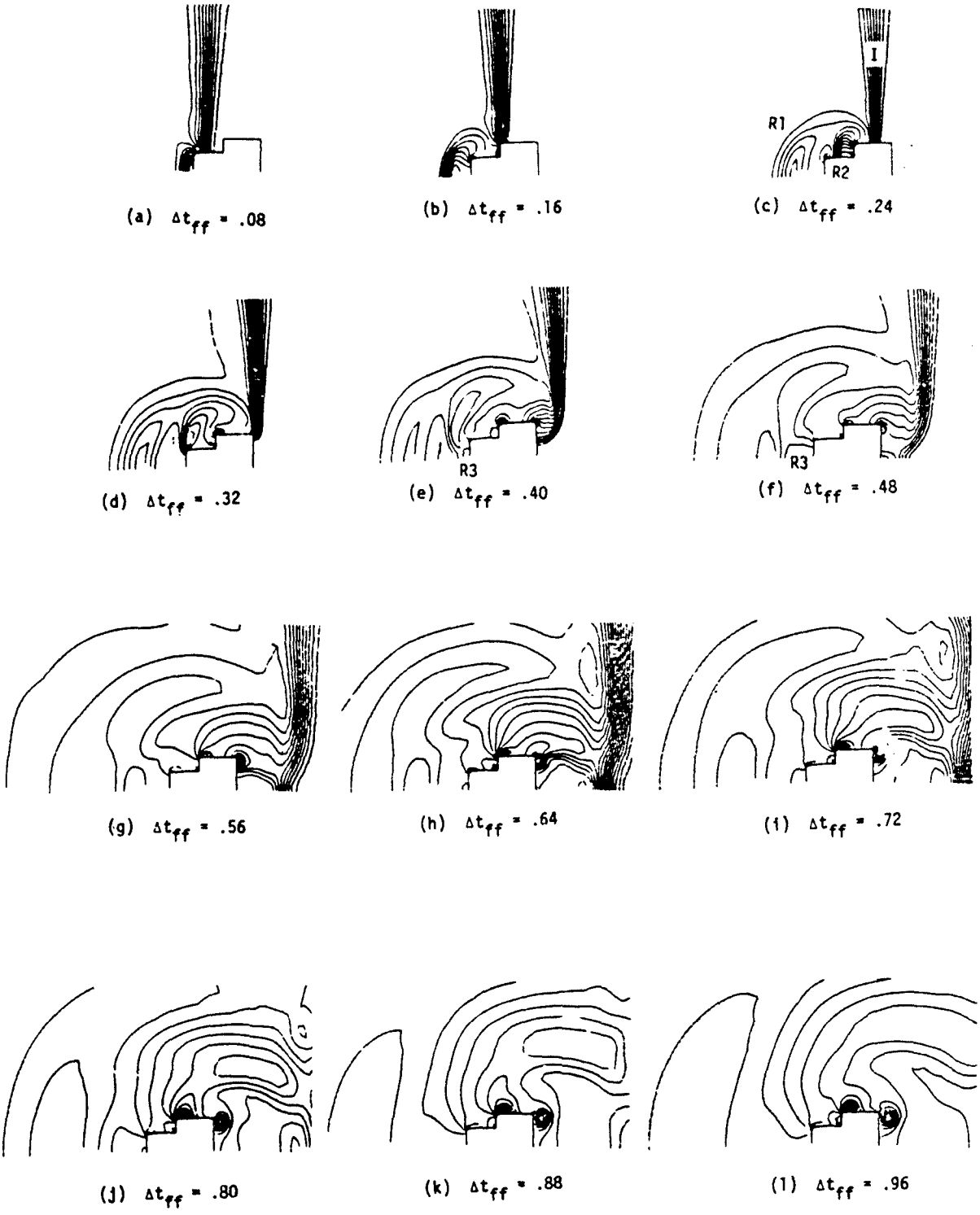

(a) Δt_{ff} = .08 (b) Δt_{ff} = .16 (c) Δt_{ff} = .24

(d) Δt_{ff} = .32 (e) Δt_{ff} = .40 (f) Δt_{ff} = .48

(g) Δt_{ff} = .56 (h) Δt_{ff} = .64 (i) Δt_{ff} = .72

(j) Δt_{ff} = .80 (k) Δt_{ff} = .88 (l) Δt_{ff} = .96

Figure 4. Computed density contours for shock wave/truck interaction. (Times after contacting front face in ms)

DESIGN OF BLAST SIMULATORS FOR NUCLEAR TESTING

Andrew Mark, Klaus O. Opalka and Clarence W. Kitchens, Jr.

U.S. Army Ballistic Research Laboratory
U.S. Army Armament Research and Development Command
Aberdeen Proving Ground, Maryland 21005

ABSTRACT

A quasi-one-dimensional computational technique is used to model the flow of a large, complicated shock tube. The shock tube, or Large Blast Simulator, is used to simulate conventional or nuclear explosions by shaping the pressure history. Results from computations show favorable agreement when compared with data taken in the facility at Gramat, France. Such future shock tubes will include a thermal irradiation capability to better simulate a nuclear event. The computations point to the need for venting of the combustion products since the pressure history will be considerably altered as the shock propagates through these hot gases.

I. INTRODUCTION

There are currently two techniques used to simulate thermal and blast effects produced by tactical nuclear weapons: thermal pulse simulators in combination with blasts produced by high explosives and thermal simulators in special shock tubes. Since the former technique is relatively expensive and is restricted to the simulation of small yield weapons, 1-10 kilotons, the use of specialized shock tube facilities is becoming increasingly attractive. A number of moderate-sized facilities exist in the U.S. and abroad, with the largest at the Centre d'Etudes de Gramat (CEG), France; see References (1) and (2). This facility, shown schematically in Figure 1, is large enough to accommodate full-sized tactical equipment such as tanks and trucks. Its total length is approximately 150 m, with the drivers being about 44 m long. The tunnel width is approximately 12 m at the floor.

A computational technique was used to investigate designs and predict the performance of complex shock tubes, such as the CEG facility. This computational technique is described in the present paper. Data taken by the Ballistic Research Laboratory in recent tests in the CEG facility have been compared with predictions from the present computational technique and used as a point of departure for extrapolating the performance for a possible U.S. facility. Since the present U.S. Large Blast/Thermal Simulator (LB/TS) concept includes a combined thermal and blast simulation capability, the effects of blast wave modification by hot combustion products from a thermal radiation simulator (TRS) are also described.

II. THEORETICAL CONSIDERATIONS

The computational technique employed in this paper is the implicit finite-difference scheme described by Warming and Beam (3). It is applied to the quasi-one-dimensional Euler equations in their weak conservation form.

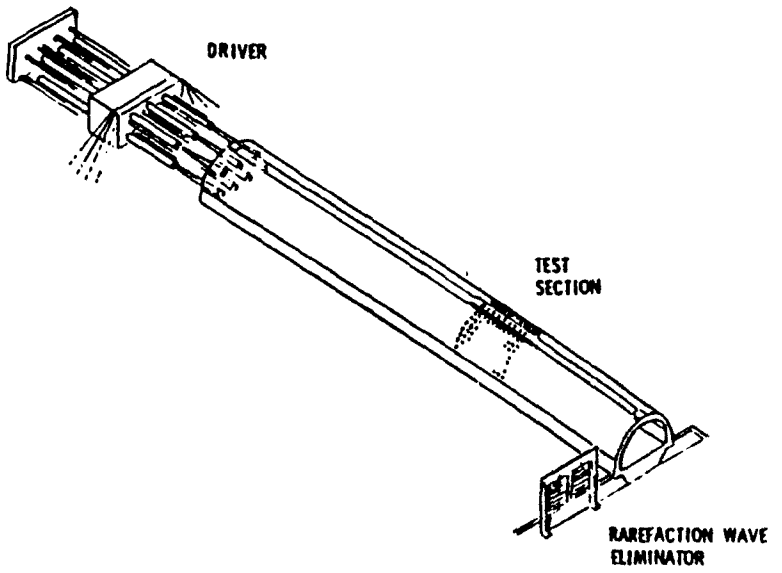

Figure 1. Blast simulator at Centre d'Etudes de Gramat, France.

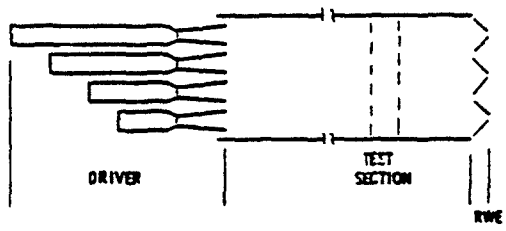

Figure 2. The CEG facility model.

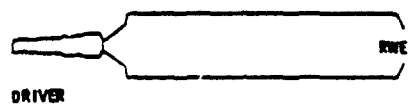

Figure 3. Quasi-one-dimensional computational model of the CEG facility.

This form is retained when the equations are transformed to a uniform computational grid. Central spatial differencing casts the difference equations into a tridiagonal structure which is solved for the increments in the dependent variables at each successive time step with the "delta" form of the algorithm; namely:

$$\left[\bar{I} + \Delta\tau\delta_{\xi}(\bar{A})\right]^{n}_{j} \cdot (\Delta\bar{Q})_{j} = - \Delta\tau\delta_{\xi}(\bar{E})^{n}_{j} \quad \Delta\tau(\bar{h})^{n}_{j}. \tag{1}$$

The reflective boundary at the solid wall of the grid was computed by means of image points, such that $\rho_1 = \rho_3$, $u_1 = -u_3$, $e_1 = e_3$, and $u_2 = 0$. The outflow was computed from one-sided differences at the exit plane.

III. RESULTS AND DISCUSSION

For large shock tubes, the driver must be made of a number of smaller tubes for practical reasons. This is schematically shown in Figure 2. In order to computationally model the facility the crossectional area at any location was simply lumped giving the configuration of Figure 3.

A. COMPARISON WITH CEG DATA

Overpressure histories from the French blast simulator at CEG are available for comparison with the computational results. The experimental record for a case with a peak static overpressure of 52 kPa was matched computationally, and the results are compared in Figure 4. In this figure the smoother, solid line is the computational result whereas the "noisier" curve is the experimental data. In the same figures the dashed lines are the computed dynamic pressures.

The comparisons show that the general features (wave reflections and expansion) of the pressure histories are replicated in the computational simulations. This degree of agreement between computation and experiment however, was obtained only after increasing the initial driver pressure by about 20% and decreasing the driver volume by 30% from the actual conditions used in the CEG tests. Without these two adjustments the overpressure was underpredicted at the start of the pressure-time curve and overpredicted toward the end.

It is indeed surprising that a crude quasi-one-dimensional model can at all approximate the complicated three-dimensional nature of the flow process. Consider, for example, the seven CEG drivers of different lengths. As they are emptied on bursting of the diaphragms, rarefaction waves empty the tubes at different rates. Subsequent compression and expansion waves from the throat and RWE influence the flow differently in these tubes. As they are lumped in the computational model, the influence cannot be the same. Furthermore, the flow at the exit of the driver nozzles experiences a sudden change in area. In the seven driver CEG configuration, the shock waves emerging from each nozzle form a spherical-like shock and coalesce forming a complicated array of Mach Stems and spherical shocks. This array of Mach Stems forms a higher pressure than would result from an equivalent single nozzle such as in

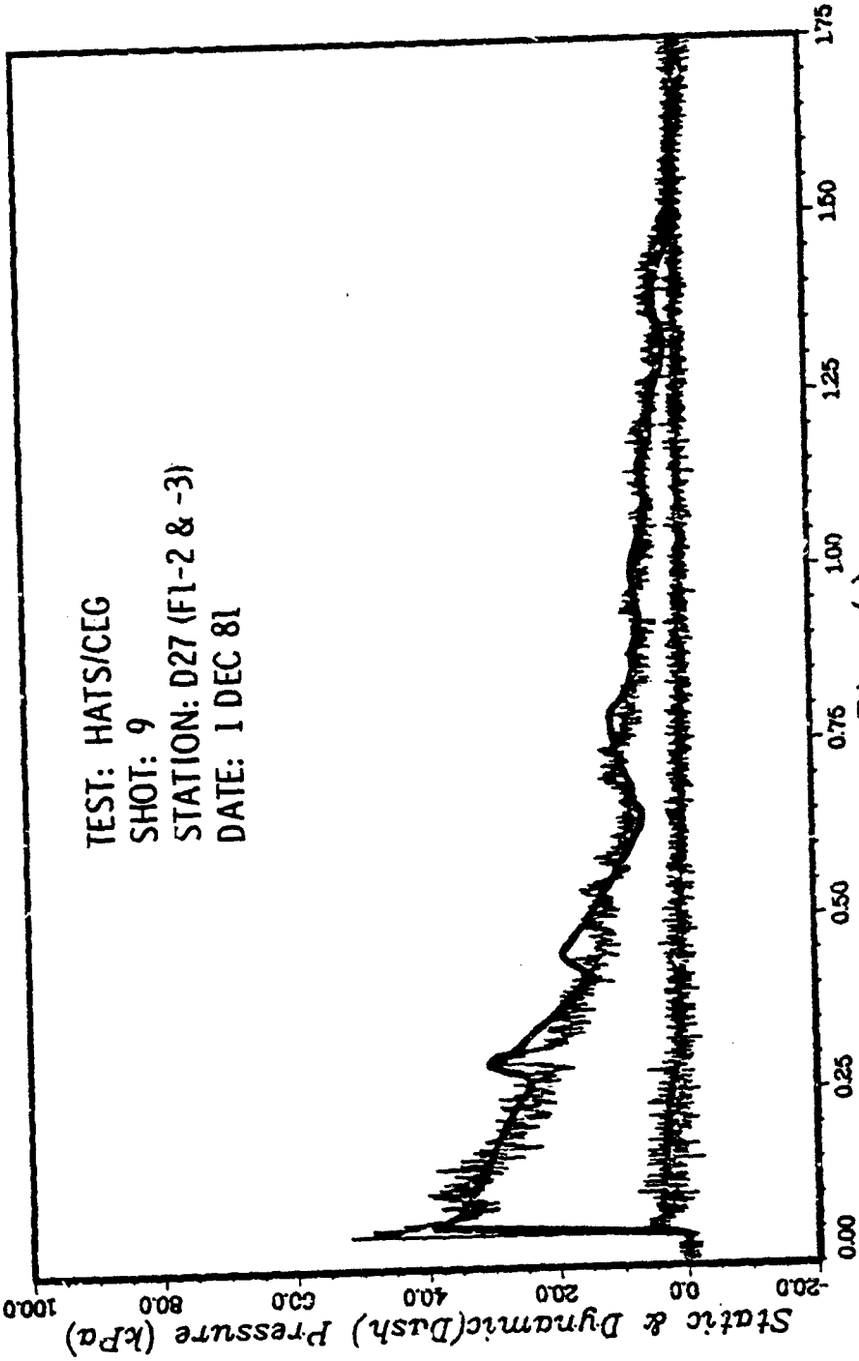

Figure 4. Computed quasi-one-dimensional versus CEG - experimental data comparison of overpressure history for a peak overpressure of 52 kPa (7.5 psi).

our model. This accounts for the adjustment in initial pressure. Losses in a number of locations could account for the volume reduction.

B. INFLUENCE OF THERMAL RADIATION SIMULATOR

Thus far, we have discussed the blast-only modeling aspects of large-scale shock tubes. In order for these shock tubes to be more realistic in simulating nuclear bursts, a thermal source should also be considered. This is true both for the physical and computational shock tube models.

The thermal pulse from a nuclear burst precedes the air blast at the target. For typical distances of interest for tactical equipment from ground zero, the time between the thermal and blast pulses is of the order of 1 second. Adding the capability of thermally irradiating a target and then applying a blast loading is a step closer to a real simulation. This can be done physically by incorporating a thermal radiation simulator in front of the target. The drawback in the physical shock tube is that the hot thermal products may still be in the target area when the shock arrives. As the shock passes through the hot gases its wave characteristics are altered. This section points to the fact that, in attempting to reproduce both the thermal and blast characteristics of a nuclear weapon in a LB/TS, we need to concern ourselves with the thermal radiation simulator combustion products produced within the tube.

One can obtain a qualitative insight into this thermal-blast interaction process by computationally modeling the CEG facility, including a region of remnant thermal combustion products. Such a model is depicted in Figure 5, where the shaded area represents the distribution of hot products and point "A" is the measuring station in the test section. The solid line in Figure 6 represents the predicted static overpressure for the blast-only test, while the dashed line represents a combined thermal/blast test. The hot products were modeled with air having a sound speed 1.73 times the ambient value. The shock wave which arrives at the measuring station is attenuated by about 25 percent in amplitude and arrives somewhat sooner since it traveled for some distance through higher sound speed air. The perturbation on the thermal/blast wave at $t \approx .35$ s occurs because the active rarefaction wave eliminator is now "detuned" for this type of wave. All these anomalies point to the fact that a venting mechanism needs to be incorporated into the design of a LB/TS if realistic combined testing is to be expected.

REFERENCES

1. S. Gratias and J. B. G. Monzac, "The Large-Scale Nuclear Blast Simulator of the Gramat Research Center: Concept, Research, Performance," Proceedings of the Seventh International Symposium on the Military Application of Blast Simulation, Medicine Hat, 13-17 July 1981.

2. S. Gratias and J. B. G. Monzac, "The Large-Scale Nuclear Blast Simulator of the Gramat Research Center: Description and Operational Utilization, "Proceedings of the Seventh International Symposium on the Military Application of Blast Simulation, Medicine Hat, 13-17 July 1981.

3. R. F. Warming and R. M. Beam, "On the Construction and Application of Implicit Factored Schemes for Conservation Laws," SIAM-AMS Proceedings, Symposium on Computational Fluid Dynamics, New York, NY, April 1977.

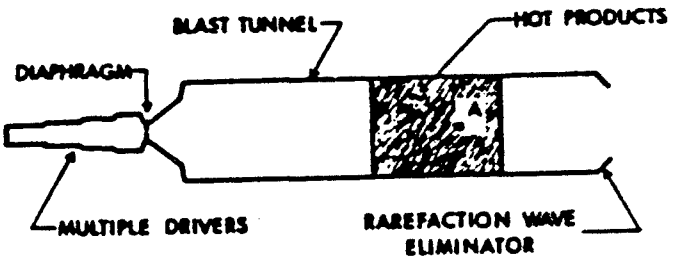

Figure 5. Quasi-one-dimensional computational model of CEG facility with thermal radiation simulator products.

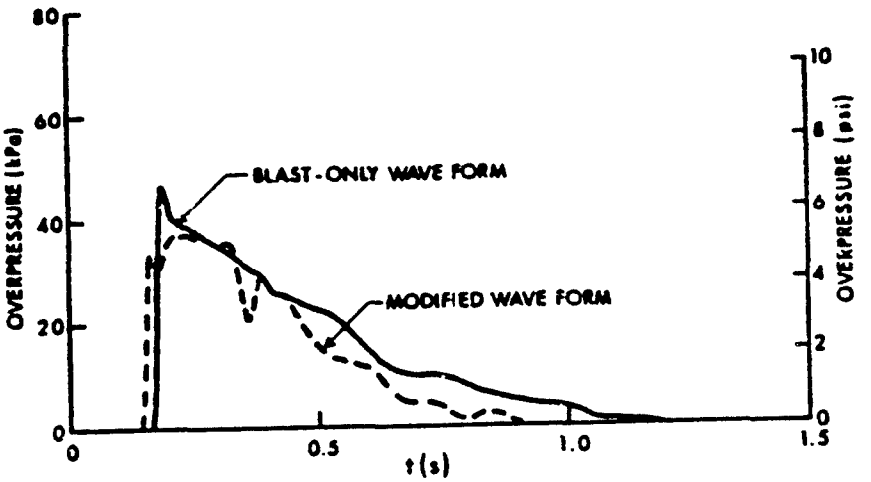

Figure 6. Predicted static overpressure modifications in CEG facility without venting TRS product.

PRELIMINARY NUCLEAR TERRORIST EFFECTS STUDY

by

Terry R. Donich
Lawrence Livermore National Laboratory, Livermore, CA

INTRODUCTION

Earlier studies[1] have looked at the overall problem of nuclear terrorism. It is assumed that the adversary can obtain the necessary people, special nuclear materials, precision machining capability and high explosives materials to accomplish the task of constructing a nuclear device. The nuclear device is assumed to be a small-yield (less than a few tens of kilotons) fission device. Larger yields are also possible.

A nuclear device could be placed in a myriad of urban locations in order to accomplish the goals of the terrorist organization. The simplest location from a technical analysis point of view may be an open street in a simple transporting mechanism such as a trailer or van. Most other locations will add complexity to the problem. For purposes of discussion, we will use the open street location.

For evacuation planning, the device type and expected yield will be very important. Although information about the device type is expected to be relatively easy to obtain, the expected yield will be very difficult to assess. Assuming the device can neither be rendered safe nor disassembled and that a large amount of time is not available for detailed diagnosis, the device must be assumed to have a yield range from just the high explosive yield to the maximum credible yield of nuclear material contained in the device. Even estimating the maximum credible yield requires that a tremendous number of assumptions be made about the nuclear material in the device.

TECHNICAL PROBLEMS ASSOCIATED WITH THE URBAN ENVIRONMENT

In an urban environment, such as Manhattan, with the device on the surface of a street, several mechanisms will come into play that do not exist in the free-field environment. First, the thermal and ionizing radiation output of the device will heat the close surroundings of the device, and some of these surroundings (e.g., buildings on two sides) will emit this energy back into the fireball in an asymmetrical fashion. The shockwave will also build up on the sides of the non-rigid, and possibly collapsing, buildings and be reflected non-symmetrically back into the fireball. The competition of these effects along with the restricted ability of the fireball to "breathe" (i.e., the inrush of cool air is heated causing the fireball to rise) may bring about a strong ballistic component to the rise as opposed to a buoyant rise normally assumed for a small yield fission device. This would have a major effect on the radioactive fallout and dispersal.

The shockwave in the direction of the street (as opposed to the direction of the building) would be channeled and directed down the street. The surrounding buildings and structures would cause drag on this shock front, and depending on the building surfaces, large scale roughness factors may rapidly remove energy from the wave by turbulence build-up. Breakage of glass walls with blast filling of buildings would also remove energy. At street intersections, a pressure relief will occur down side streets and an associated eddy fluid flow and turbulence pattern will build up to remove energy from the shock front. Another problem to be considered might be the collision of shock fronts channeled in different routes in the grid of streets. When this phenomenon occurs, the result will be a loss of shockwave energy that will heat the fluid. Although the problems mentioned above have been studied individually for various fluids, the ability to comprehensively study these effects for a nuclear explosion in an urban environment does not currently exist. If one removes all of the problems above with simplifying assumptions, models are available to coarsely treat the problem. The uncertainty in the results from these models is so large when coupled with the uncertainty in the device yield that it makes the result nearly useless to the emergency planner.

The thermal problem is somewhat easier to analyze. The major considerations are the objects and people in the streets, since this wavelength of radiation energy does not penetrate opaque objects but rather heats them. The temperature of the fireball constrained by the structures of the urban environment when viewed at a distance from the burst probably will not change significantly from the normal 6000K to 7000K and only the cross-sectional area of the radiating surface will have to be considered. The majority of the thermal energy (approximately one-third of the total energy from the device in a free-field environment) will be emitted in a few tenths of a second. At street level, the thermal pulse will come from a volume of luminous gas that will approximate a cylinder filling the area between the buildings and be of a height approximating the radius of the normal free field fireball hemisphere. At times after the thermal pulse, the fireball should exhibit some jetting and movement down the street. This is the result of the pressure created by partial early-time containment on two sides by the buildings, but the buildings will not play a major role in the very early time fireball that gives rise to the thermal pulse. This assumes the yield is 10 kT or less, so the thermal pulse is short.

The fallout problem associated with the urban environment may be the most difficult and overriding in terms of evacuation planning. The problem is to understand the dominant factors in order to determine what fraction of the nuclear debris cloud will rise above the surrounding buildings. As mentioned earlier, the partial blast containment, the radiation and thermal heating of structures, the full involvement of building material in the condensation chemistry, and the "breathing" ability of the cloud will all have an effect on cloud rise. Although recent new fallout models have brought this effect to a level of predictability associated with other nuclear effects in a free-field environment, the effort has never been seriously attempted for an urban environment[2].

A second major problem is to estimate a meteorological surface roughness to be used for an urban environment over large areas that will receive fallout. The surface roughness is used to estimate the turbulence and eddy fluid flow conditions and consequently the air mixing near the ground surface. It should be noted that although fallout a long way downwind does arrive in time lengths of hours, the moderately close fallout (less than one kilometer) can start arriving within a few minutes. Thus, the portion of the population close-in that takes cover during the explosion should not try to outrun the fallout. The rescue effort will have to be well planned and executed to save them. Protection factors of building shielding from fallout may be good enough to protect them for the time needed to plan the area re-entry. In particular, the center areas of midlevel floors in a high-rise building should be reasonably safe.

REFERENCES

1. Northrup, J.A., "The Role of Civil Preparedness in Nuclear Terrorism Mitigation Planning", SSS-R-80-4185, Systems, Science and Software, La Jolla, CA, September 1979.

2. Office of Technical Assessment, U.S. Congress, The Effects of Nuclear War, p. 45 (1979).

FORMAL DISCUSSION SESSION SUMMARIES

The discussion topics were chosen by FEMA Headquarters personnel. The four topics were:

Group 1: Shelter environment in attacked areas, including dust, blast, heat, and debris.

Group 2: Uses and limitations of shock tubes.

Group 3: Utility of computer models for civil defense planning and research.

Group 4: Fire fighting under adverse circumstances.

The thrust for each group was to identify problem areas that had not been addressed adequately in the past. Identification and discussion of these problem areas could result in innovative ideas for research and the application of research methods to solve the problems posed.

SUMMARY

SHELTER ENVIRONMENT IN ATTACKED AREAS, INCLUDING DUST, BLAST, HEAT, AND DEBRIS

Discussion Leader: Chuck Wilton, SSI
Report by: Jim Zaccor, SSI

Our nine-member group addressed these basic questions: What are the problems? What do we need to know? What should we do at MINOR SCALE, that is, the 1985 7-kt blast simulation?

In our deliberations we considered two shelter conditions: 1) upgraded structures, and 2) designed shelters. By upgraded structures we mean those structures which were upgraded to sustain a blast peak pressure of 40 psi. Though we could build structures of 100-psi rating, the consensus was that the cost would be prohibitively uneconomical. We also discussed shelters of lower rating but concluded that 50-psi shelters are adequate and more practical. With the 50-psi shelters, the probability of survival is supposed to be more than 98%, assuming randomly located industry and shelters. In the US, there are few 50-psi shelters; therefore, it is desirable that these shelters be built in all the risk areas. It was also concluded that all future upgrading of the existing structures be targeted for 50-psi overpressure. It is desirable that probability analyses of survival for structures of different ratings also be made available.

Next, we concentrated on the designed shelters. We recognized that until new shelters are designed and built for 50-psi blast loads, upgraded ones might be needed. We also felt that the problems associated with the designed shelters would not be much different from those of the upgraded structures. However, perhaps it is not easy to identify and upgrade the existing structures for shelters. If not upgraded properly it could lead to an uncertain shelter environment at the time of nuclear attack. Once designed shelters exist, we could use the upgraded shelters for the protection of industrial equipment.

We then considered the problem of shelter closure and discussed the tradeoffs associated with a horizontal door that only has to take 50 psi versus a vertical blast door that has to take 190 psi. The differences in weight and cost between horizontal and vertical doors are not significant enough to make horizontal closures worthwhile. Moreover, there is a potential safety problem associated with the fact that people can more easily close vertical doors, while there might be some difficulty in actually getting a 3/4-ton horizontal door to shut properly. Another concern we discussed was the debris that might pile up in stairwells required for vertical closures. Because we realized that this debris problem would make egress more difficult, we concluded that no shelter should be without a second entryway for access and egress.

From this point, we resorted to a generalized casualty function chart (attached) made up by one of the FEMA contractors for another purpose. We concluded that: 1) neither ground shock nor initial radiation would be a problem in our engineered shelters; and that 2) fallout was not a problem

either with properly designed shelters. We felt that a decision process as to when to exit needs to be established so that the occupants are not exposed to fallout.

Siting will be very important. Shelters must be located away from hazardous materials, tank farms, high-rise structures that are debris sources, and high fuel loading areas, which are debris and fire sources. Another consideration is the location of the water tables. For example, in the San Francisco Bay Area there would be few below-grade key-worker shelters that wouldn't have some problem with the high water table which is down about 2 ft all along the Peninsula.

A way to assess the radiation field, particularly if debris piles up on the structure, is necessary because a probe extending just outside the initial structure could wind up under a large debris pile and therefore give a false reading. In addition, one needs to consider how the shelterees will get out if they are under debris, and what kind of communications systems they might be supplied with in order to contact other shelterees or someone in their host area who could rescue them.

The question of design options for dual use was considered, which the industry will probably require if these structures take up space on their property. While we felt that rigid concrete structures would be preferred by the industry, we also recognized that for last-minute quick installations, the corrugated arch would probably be more desirable. In view of this, we decided that it would be well to pursue both types of shelters. Quality of construction would be a concern that would have to be examined because of the probable use of unskilled labor in implementing the shelter program.

Next we looked at the question of life support systems. Heat conduction would not really be a problem, because most fires would be out before heat penetrated through the fallout protection into the shelter. However, where fires occur, there are problems (even in the early stages) resulting from entrainment in the ventilation systems of toxic smokes, gasses, etc. The question of bringing heated air into the shelter where large areas burn and where, perhaps, insufficiency of oxygen might result must be examined as well. The problem of toxic substances entering the ventilation system might be solved via the use of various filters, but the question of the heated air and the insufficient oxygen supply would require considerably more extensive facilities in the shelter. These questions need to be addressed.

Another important area that we considered was the optimum use of soil properties. How do we make use of arching and soil structure interaction (coefficient of earth pressure)? Can the native soil be used as backfill? How different are native soils in different regions? How long does it take the native soil to compact if you build shelters well in advance, before it becomes comparable to the initial material excavated? Soil arching requires a differential compressibility to work. There is the additional question of soil saturation that could make the coefficient of earth pressure equal to one thus losing the benefit of this soil property.

We then addressed the question of what we need to do and what we should do in 1985 with the larger weapon simulation. We agreed that planning, to be completed in 1984, for the 1985 simulation was the most important element.

This effort would require a budget with funds not only to accomplish the planning, but also to do exploratory and parametric tests. MINOR SCALE should be a proof test and not an opportunity for an exploratory program which we felt should be done beforehand. So, before 1985 we need to look at weapon size scaling studies to evaluate scaling effects. We need to know how designed shelters would be expected to perform under a 1-Mt weapon loading. This will mean that we won't be testing at 50 psi in the field at MINOR SCALE, but at a higher overpressure. In addition, it was suggested that 1) we look at a model city at MINOR SCALE, one that extends a few city blocks in both directions, and that 2) two overpressures be used with a fifth or a fourth scale. We should also test expedient shelters at MINOR SCALE. This would include, for example, utility vaults found at intersections in most major cities (and on hand in yards that manufacture and sell those vaults) to identify the failure overpressures for 1-Mt weapons. We also need to test mounded shelters in recognition of the fact that there will be quite a few regions where the high water table will preclude below-grade shelters. And we should design and test key Life-Support systems at MINOR SCALE to see that, in fact, they are adequate.

Connections of structural members are another problem. Many buildings have poor connections, and this needs to be studied again for the upgraded structures to see what potential complications might exist in the upgrading process as a result.

Finally, we decided that somewhere in the program consideration had to be given to amenities in shelters, such as light, food supplies, water, toilet facilities, and auxiliary power.

NOTE: This chart is a modified version of an original provided by Chuck Wilton of SSI under contract No. EMW-C-0678.

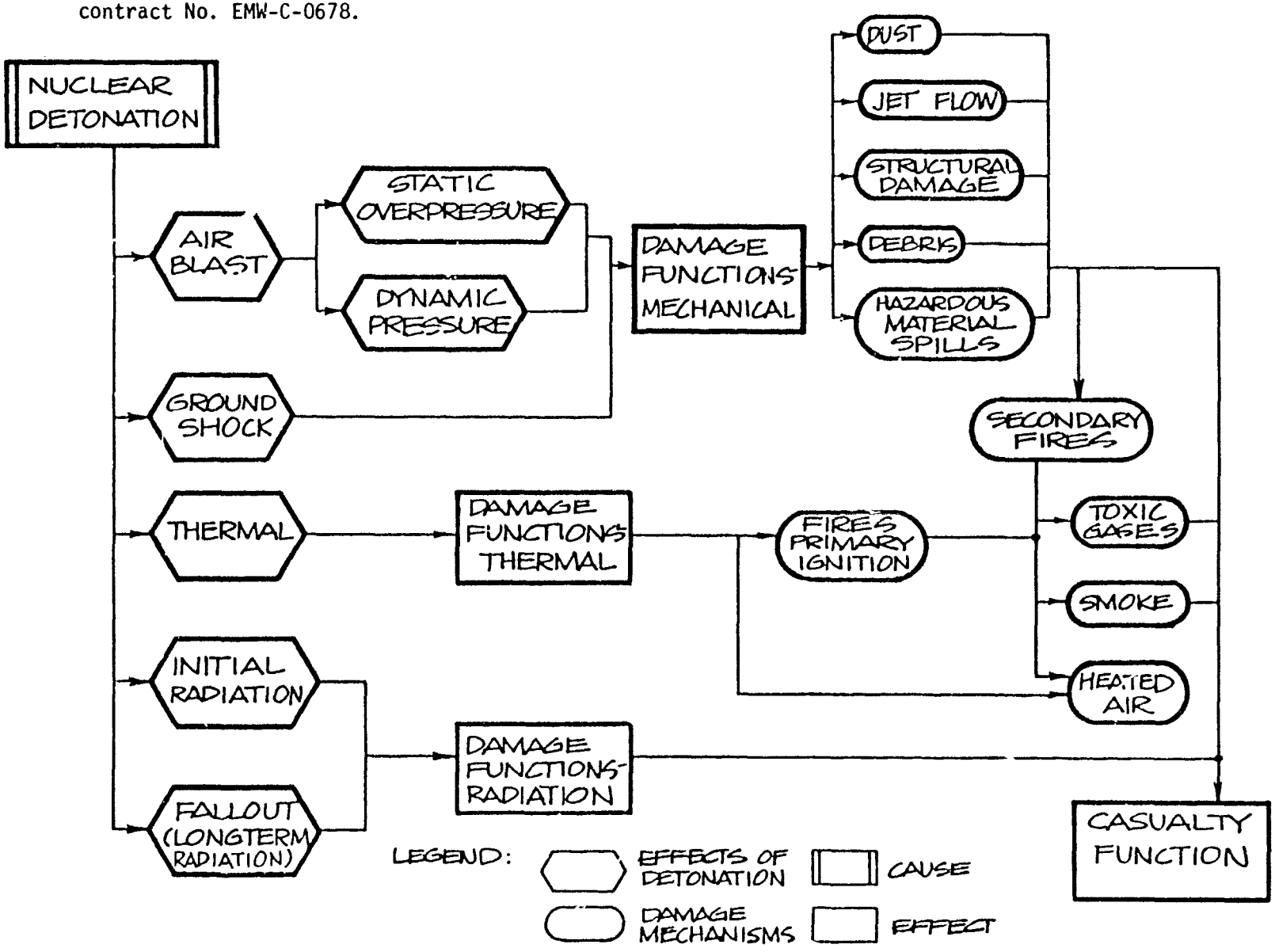

SUMMARY

USES AND LIMITATIONS OF SHOCK TUBES

Discussion Leader: George A. Coulter, BRL

A very brief summary of shock tube description and operation was given for the newcomers to the group. Note was made of facilities at Ft. Cronkhite, BRL, and SRI. It was noted that the DASACON conical shock tube at Dalgren, VA is not in operation although a proposal has been made to reopen it after replacing the explosive driver with a new gas driver. The explosive driver created a great deal of undesirable soot during the operation. It also had been comparatively expensive to test there. Both were drawbacks to its usefulness. A brief description of the large French blast simulator at Gramat was given. Some of the Army's vehicle/shelter combinations have been successfully tested in that facility. A similar facility for the US is presently being planned jointly by BRL, HDL, and DNA. Large-scale testing by FEMA could be accomplished in such a simulator if built.

The group consensus was that a general application of shock tubes could be made to validate analytical techniques, check design procedures, and test system elements. Small-scale systems or models could equally well be tested to advantage in the shock tube. Fundamental blast/fire or ignition/blast reactions could also be studied in a shock tube equipped for this study. In general, shock tubes can be used to support the expedient shelter program and can also be of help in the design of large-scale or full size field tests.

Specific examples of areas where shock tube testing would be helpful in planning for the 1985 large-scale field test are:

1. Fire/blast interactions--
   a. Investigation of fire phenomena.
   b. Barrier/fire interaction studies.
   c. Burning debris/fire brand blast interactions.
   d. Thermal/blast simulation with real time delay.

2. Blast tests--
   a. 1/5-scale building blast tests to compare with field test data.
   b. Shelter and room fill modeling.
   c. Outside shock tube debris study.
   d. Dusty gas problems.

The usefulness of the shock tube is attributed to its repeatability, ease of operation, multiple shot capability, and relatively inexpensive operation (compared to large-scale field tests).

Its limitations are characteristic of specific shock tubes (for example: size at SRI; lack of a thermal source at BRL; and a lower tank pressure limit of 12 psi at Cronkhite). As was noted above with the DASACON, the explosive driver was a liability. The shock duration may be a limitation depending on specific test needs. The tendency to choke the tube exists if the test specimen becomes significant in cross section compared to the shock tube cross section, also. However, in spite of the limitations, shock tubes can be a most useful research tool.

SUMMARY

THE UTILITY OF COMPUTER MODELS FOR CIVIL DEFENSE PLANNING AND RESEARCH

Discussion Leader: Thomas A. Reitter, LLNL

Discussion began on the conflicting models of firestorms. This problem represents an example of a difficult question: how can a model be verified when its results are not accessible to experiment. We agreed that this makes it important to seek out experiments which can, at least in part, exercise the model. This might involve a series of experiments of increasing scale, although this raises the usual questions of scalability.

The suggestion was made that civil defense should concentrate on specific questions related to its needs and responsibilities, rather than seeking general, all-purpose models. This raises the question of how does one develop confidence in limited models if one does not fully understand the relevant phenomena.

This led to a distinction between two classes of models: research and application. A research model studies the physics and chemistry to gain insight into phenomena. These models are scientific models because they can be used to predict new, previously unobserved phenomena, and they can be proven wrong. Application models, on the other hand, should provide a specific answer (number) and a measure of its reliability (variance). Application models meet neither of the requirements of a scientific model, but they can be used to answer operational questions within their limited, verified ranges of validity.

An example of a research model that has become an application model is the Forest Service's fire behavior model. This is now in routine field use in the Forest Service on programmable hand calculators. It is estimated to have required 60 man-years over 12 years at Missoula to develop this from a research model to an application model.

It is generally accepted that civil defense policy should indicate the specific questions to be addressed by both types of models. The British and Swedish civil defense programs, for example, appear to pose very specific questions with the goal of devising actions to minimize loss of life and resources.

A list of policy-based questions by FEMA would provide roles for both types of models.

The group also briefly considered the status of models for some of the high priority research areas identified at last year's conference. The major goal for civil defense was felt to be the characterization of the post-attack environment, especially with respect to gases and dust, inside and near shelters, and throughout the affected areas. To achieve this goal would require progress on more limited questions: ignition criteria for "real" materials (NBS has made recent progress on this for very different materials); debris formation and distribution (little verification, lack of parameter sensitivity studies, no "characterization" debris piles for various types of

buildings subjected to various types of loads); fire spread across debris fields (rate of spread across a given debris field appears possible, but not the combustion of the thicker fuels behind the front); mass fires (two sets of existence criteria for firestorms are available, but none are available for moving-front conflagrations; no detailed understanding of mass fire behavior); multiple-burst effects (except for blast waves, these have only been treated as independent events, and they are not); and the environment in shelters (some work has been done on effects of burning debris above shelters).

A political question, beyond the scope of this conference, was how Congress and the public might be convinced to act on the basis of the results of models.

SUMMARY

FIRE FIGHTING UNDER ADVERSE CIRCUMSTANCES

Discussion Leader: Robert G. Hickman, LLNL

It seems that little in the way of new technology in this area needs to be developed. With regard to debris removal, most fire departments have some limited capability already. Use of tracked vehicles makes no sense, mostly because they can't move through heavy debris. Smothering a fire with soil will work, but dousing with water is better. Because there is so little need for equipment built that employs dirt-smothering methods during peacetime, few (if any) fire departments would buy it for use in situations where water is unavailable.

Nevertheless, there are some things that could be done that would be beneficial. In the area of long-term passive measures, firebreaks could be built into cities, probably in the form of parkways. Likewise, firebreaks could be built around critical facilities, whether they be EOCs, factories, or something else. In the latter cases they might be wide parking lots. Swimming pools or ponds could be located close to critical facilties to provide an emergency water supply for fire fighting. Self-contained sprinkler systems using blast hardened water tanks could be built into critical facilities. They would be tied into the municipal water system only as needed for filling.

On a shorter term, key workers assigned to a particular critical facility could be trained to fight fire in that facility. Urban fire fighters, who are typically water-rich, could be taught the fire fighting tactics of rural fire fighters who are typically water-poor. Then in an emergency, the urban fire fighters might be able to respond more effectively. Fire chiefs should be given a prioritized list of critical facilities within their jurisdictions so that they could become familiar with the facilities beforehand to maximize their efficiency in fighting a fire. In addition, they can use this information to preplan routes to survey the area for fire, since normal telephone service to report fires is not expected to be available during an emergency.

Finally, it was asked if FEMA shouldn't have one person within its civil defense organization be responsible exclusively for fire hardening and countermeasures at critical facilities.

AUTHOR INDEX

DISTRIBUTION

Note: An asterisk (*) designates a conference attendee.

Federal Emergency Management Agency
Attn: Jim Kerr*, Director for Research
National Preparedness Programs
Directorate
Washington, DC 20472 (3 copies)

Federal Emergency Management Agency
Attn: David W. Bensen*
Office of Research
National Preparedness Programs
Directorate
Washington, DC 20472 (45 copies)

Defense Technical Information Center
(DTIC)
Cameron Station
Alexandria, VA 22314 (12 copies)

Oak Ridge National Laboratory
Attn: Librarian
Post Office Box X
Oak Ridge, TN 37830

Los Alamos Scientific Laboratory
Attn: Document Library
Los Alamos, NM 87544

The RAND Corporation
Attn: Document Library
1700 Main Street
Santa Monica, CA 90406

Assistant Director
Energy and Natural Resources
Office of Science and Technology Policy
Executive Office Building
Washington, DC 20500

Assistant Secretary of the Army (RD&A)
Attn: Deputy ASA for (RD&S)
Washington, DC 20310

Chief of Engineers
Department of the Army
Attn: DAEN-RDZ-A
Washington, DC 20314

US Army Training and Doctrine Command
Fort Monroe
Hampton, VA 23651

US Army Combined Arms Combat
Development Activity
Fort Leavensworth, KS 66027

Air Force Weapons Laboratory
Attn: SUL Technical Library
Kirtland Air Force Base
Albuquerque, NM 87117

Air Force Weapons Laboratory
Attn: Civil Engineering Division
Kirtland Air Force Base
Albuquerque, NM 87117

Director, US Army Ballistic Research
Laboratory
Attn: Document Library
Aberdeen Proving Ground, MD 21006

Director, US Army Ballistic Research
Laboratory
Attn: Mr. William Taylor
Aberdeen Proving Ground, MD 21006 (2
copies)

Director, US Army Engineer Waterways
Experiment Station
Attn: Document Library
PO Box 631
Vicksburg, MS 39180

Director, US Army Engineer Waterways
Experiment Station
Attn: Mr. W. J. Huff
PO Box 631
Vicksburg, MS 39180

Civil Engineering Center/AF/PRECET
Wright Patterson Air
Force Base, OH 45433

Mr. Carl Wiehle
Defense Intelligence Agency
Attn: WDB-4C2
Washington, DC 20301

Director
Defense Nuclear Agency
Attn: Michael Frankel*
Washington, DC 20305

Command and Control Technical Center
Department of Defense
The Pentagon
Washington, DC 20301

Oak Ridge National Laboratory
Attn: Emergency Technology Division
Librarian
PO Box X
Oak Ridge, TN 37380

Dr. Conrad Chester
Oak Ridge National Laboratory
PO Box X
Oak Ridge, TN 37380

Dr. Lewis V. Spencer
National Bureau of Standards
Center for Radiation Research
Building 245 - Room C-313
Washington, DC 20234

Mr. Samuel Kramer
National Bureau of Standards
Building 225 - Room B-124
Washington, DC 20234

Mr. William Parker
National Bureau of Standards
Building 224 - Room A-345
Washington, DC 20234

Fire Research Library
National Bureau of Standards
Building 224 - Room A-246
Washington, DC 20234

Dr. John Rockett
National Bureau of Standards
Center for Fire Research
Building 224 - Room B-260
Washington, DC 20234

Dr. Craig Chandler, Director
Forest Fire & Atmospheric Science
Research
US Forest Service
Department of Agriculture
Washington, DC 20013

US Forest Service
Attn: Dr. A. Broido
PO Box 245
Berkeley, CA 94710

Mr. A. P. Brackebush
Forest Fire Research
Northern Forest Fire Laboratory
Missoula, MT 59801

Director
Department of Military Application
Department of Energy
Washington, DC 20545

Director, Army Materials and Mechanics
Research Center
Attn: Technical Library
Watertown, MA 02172

National Council on Radiation
Protection and Measurements
7910 Woodmont Avenue
Bethesda, MD 20014

President
International Association of Fire
Fighters
1750 New York Avenue, NW - 3rd Floor
Washington, DC 20006

National Fire Protection Association
Library
Batterymarch Park
Quincy, MA 02269

Director
Lovelace Foundation
5200 Gibson Boulevard, SE
Albuquerque, NM 87108

Dr. Forman Williams
Department of the Aerospace and
Engineering Sciences
University of California San Diego
La Jolla, CA 03027

Professor A. Murty Kanury*
Department of Aerospace and Mechanical
Engineering
University of Notre Dame
Notre Dame, IN 46556

Professor R. K. Pefley
University of Santa Clara
Santa Clara, CA 95053

Mr. Joseph Minor
Texas Technological College
Lubbock, TX 79408

Mr. Robert Fristrom
John Hopkins Applied Physics Laboratory
John Hopkins Road
Laurel, MD 20707

Mr. Norman J. Alvares
Lawrence Livermore National Laboratory
University of California
PO Box 808, L-442
Livermore, CA 94550

Dr. Clarence R. Mehl
Sandia National Laboratories
Division 7112
PO Box 5800
Albuquerque, NM 87185

Dr. William F. Christian
Underwriters' Laboratories, Inc.
333 Pfingsten Road
Northbrook, IL 60062

Mr. Donald Drzewiecki
Calspan Corporation
PO Box 400
Buffalo, NY 14225

Mr. Richard Laurino*
Center for Planning and Research
2483 East Bayshore, Suite 104
Palo Alto, CA 94303

Mr. John Rempel*
Center for Planning and Research
2483 East Bayshore, Suite 104
Palo Alto, CA 94303

Mrs. Ruth Schnider
Center for Planning and Research, Inc.
2483 East Bayshore, Suite 104
Palo Alto, CA 94303

Mr. Walmer E. Strope
Center for Planning and Research, Inc.
5600 Columbia Pike, Suite 101
Bailey's Crossroads, VA 22041

The Dikewood Corporation
1613 University Boulevard, NE
Albuquerque, NM 87101

Factory Mutual Research Corporation
Attn: Dr. Ray Friedman
1151 Boston-Providence Turnpike
Norwood, MA 02062

Hudson Institute
Quaker Ridge Road
Croton-on-Hudson, NY 10520

Dr. Anatole Longinow*
IIT Research Institute
10 West 35th Street
Chicago, IL 60616

Mr. Thomas Waterman*
IIT Research Institute
10 West 35th Street
Chicago, IL 60616 (2 copies)

Mr. Leo A. Schmidt*
Institute for Defense Analyses
Program Analysis Division
1801 N. Beauregard Street
Alexandria, VA 22311

Dr. Donald Sachs
Kaman Sciences Corp.
1911 Jefferson Davis Highway
Arlington, VA 22202

Mr. Peter S. Hughes*
Los Alamos Technical Associates, Inc.
PO Box 410
Los Alamos, NM 87544 (2 copies)

Mr. Laurence Pietrzak*
Mission Research Corporation
PO Drawer 719
Santa Barbara, CA 93102

Mr. Fred Sauer
Physics International Company
2700 Merced Street
San Leandro, CA 94577

Dr. Dennis Holliday
R&D Associates
PO Box 9695
Marina Del Rey, CA 90291

Mr. Edward L. Hill
Research Triangle Institute
PO Box 12194
Research Triangle Park, NC 27709

Mr. Harvey G. Ryland
Ryland Research, Inc.
5266 Hollister Avenue, Suite 324
Santa Barbara, CA 93111

Mr. Raymond Alger*
SRI International
333 Ravenswood Ave.
Menlo Park, CA 94025

Dr. Jana Backovsky*
SRI International
333 Ravenswood Ave.
Menlo Park, CA 94025

Mr. Clay P. Butler
SRI International
333 Ravenswood Ave.
Menlo Park, CA 94025

Mr. Dick Foster
SRI International
1611 Kent Street
Arlington, VA 22209

Dr. Fred Offensend
SRI International
333 Ravenswood Ave.
Menlo Park, CA 94025

Dr. John Cockayne
Senior Scientist
Science Applications, Inc.
1710 Goodridge Drive
PO Box 1303
McLean, VA 22101

Mr. Marvin Drake
Science Applications, Inc.
1200 Prospect Street
La Jolla, CA 92037

Mr. C. Wilton*
Scientific Service, Inc.
517 East Bayshore Drive
Redwood City, CA 94060 (2 copies)

Department of Fire Technology
Southwest Research Institute
PO Drawer 28510
San Antonio, TX 78284

Mr. Stanley B. Martin*
Stan Martin and Associates
869 Vista Drive
Redwood City, CA 94062

Dr. Francis E. Fendell*
P1/1038
TRW
One Space Park
Redondo Beach, CA 90278

Technology & Management Consultants
330 Washington Street
Suite 613
Marina del Rey, CA 90291

Dr. Matthew G. Gibberts
5424 Lawton Avenue
Oakland, CA 94618

Mr. Kenneth Kaplan
#30 White Plans Court
San Mateo, CA 94402

Mr. H. L. Murphy*
H. L. Murphy, Associates
PO Box 1727
San Mateo, CA 94401

Dr. Don Scheuch
430 Golden Oak drive
Portola Valley, CA 94025

The Information Center
Forest Fire Research Institute
331 Cooper Street
Ottawa Ontario K1A 043, CANADA

Dr. Ing. P. G. Seeger
Forschungsstelle fur Brandschutztechnik
University of Karlsruhe (TH)
75 Karlsruhe 21
Postfach 63380, WEST GERMANY

Dr. Vilhelm Sjolin* (3 copies)
Director of BRANDFORSK
The Swedish Fire Research Board
S-115 87 Stockholm, SWEDEN

Secretaire d'Administration
Ministere de l'Interieur
Direction Generale de la Protection Civile
rue de Louvain, 1
1000 Brussels, BELGIUM

Canadian Defense Research Staff
ATTN: Dr. K. N. Ackles
2450 Massachusetts Ave., NW
Washington, DC 20008 (4 copies)

Director
Civilforsvarsstyrelsen
Stockholmsdage 27
2100 Copenhagen 0, DENMARK

Director de la Securite Civile
Ministere de l'Interieur
18 Rue Ernest Cognac
92 Levallois
Paris, FRANCE

Bundesministerium des Innern
Graurheindorfer Strasse 198
5300 Bonn 1, WEST GERMANY

Ministry of Social Services
11 Spartis Street
Athens, GREECE

Almannavarnir Rikisins
Reykjavik, ICELAND

Stato Maggiore Difesa Civile
Centro Studi Difesa Civile
Rome, ITALY

Civil Emergency Planning Directorate
North Atlantic Treaty Organization
1110 NATO
BELGIUM

Jefe, Seccion de Estudios y Planification
c/Evaristo San Miguel, 8
Madrid-8, SPAIN

Ministero dell Interno
Direzione Generale della Protezione Civile
00100 Rome, ITALY

Directeur de la Protection Civile
Ministere de l'Interieur
36 fue J. B. Esch
Grande-Duche de Luxembourg

Directeur Organisatie
Bescherming Bevoling
Ministry of Interior
Schedeldoekshaven 200
Postbus 20011
2500 The Hague, NETHERLANDS

The Head of Sivilforsvaret
Sandakerveien 12
Postboks 8136
Oslo dep
Oslo 1, NORWAY

Civil Defense Administration
Ministry of Interior
Ankara, TURKEY

Home Office
Scientific Advisory Branch
Horseferry House
Dean Ryle Street
London SWIP 2AW, ENGLAND

*Hal E. Anderson
USDA Forest Service
Intermountain Forest and Range Experiment Station
Northern Forest Fire Laboratory,
Drawer G
Missoula, MT 59806

Gunnar Arbman*
Swedish National Defense Research Institute
Box 27322
S-10254 Stockholm, SWEDEN 631500

W. Baker*
Southwest Research Institute
PO Drawer 28510
San Antonio, TX 78284

Robert B. Barker*
Lawrence Livermore National Laboratory
University of California
PO Box 808, L-389
Livermore, CA 94550

James E. Beck*
James E. Beck and Associates
4216 Los Palos Avenue
Palo Alto, CA 94306

D. Bettge*
Federal Emergency Management Agency
National Preparedness Programs
Directorate
Washington, DC 20472

Art Broyles*
Lawrence Livermore National Laboratory
University of California
PO Box 808, L-10
Livermore, CA 94550

D. Cagliostro*
MS-K555, PO Box 1663
Los Alamos Scientific Laboratory
Los Alamos, NM 87544

George Carr-Hill*
Home Office
Scientific Advisory Branch
Horseferry House
Dean Ryle Street
London SWIP 2AW, ENGLAND

Edward J. Chapyak*
Energy Division
Los Alamos National Laboratory, MS K559
PO Box 1663
Los Alamos, NM 87545

George Coulter*
US Army Ballistic Research Laboratory
US Army Armament Research and
Development Command
Aberdeen Proving Ground, MD 21005

John de Ris*
Factory Mutual Research Corporation
Norwood, MA 02062

Terry R. Donich*
Lawrence Livermore National Laboratory
University of California
PO Box 808, L-97
Livermore, CA 94550

B. Gabrielsen*
Scientific Service, Inc.
517 East Bayshore Drive
Redwood City, CA 94060

Laurence L. George*
Lawrence Livermore National Laboratory
University of California
PO Box 808, L-140
Livermore, CA 94550

Paul J. Hassig*
California Research & Technology, Inc.
20943 Devonshire Street
Chatsworth, CA 91311

Robert G. Hickman*
Lawrence Livermore National Laboratory
University of California
PO Box 808, L-140
Livermore, CA 94550

Sang-Wook Kang*
Lawrence Livermore National Laboratory
University of California
PO Box 808, L-140
Livermore, CA 94550

Edward J. Kansa*
Lawrence Livermore National Laboratory
University of California
PO Box 808, L-451
Livermore, CA 94550

Sam A. Kiger*
ISAE Waterways Experiment Station
Vicksburg, MS 39180

Chi-Yung King*
Lawrence Livermore National Laboratory
University of California
PO Box 808, L-799
Livermore, CA 94550

R. Levine*
National Bureau of Standards
B260 - 224
Washington, DC 20234

Harold J. Linnerud*
Science and Engineering Associates,
Inc.
16 Westford St.
Chelmsford, MA 01824

Robert G. McKee, Jr.*
Staff Engineer/Program Manager
Los Alamos Technical Associates, Inc.
PO Box 410
Los Alamos, NM 87544

L. Lynn Cleland
Lawrence Livermore National Laboratory
University of California
PO Box 808, L-91
Livermore, CA 94550

Garth E. Cummings
Lawrence Livermore National Laboratory
University of California
PO Box 808, L-91
Livermore, CA 94550

Jackie Meeks*
Lawrence Livermore National Laboratory
University of California
PO Box 808, L-140
Livermore, CA 94550

Carol A. Meier*
Lawrence Livermore National Laboratory
University of California
PO Box 808, L-90
Livermore, CA 94550

Camille Minichino*
Lawrence Livermore National Laboratory
University of California
PO Box 808, L-91
Livermore, CA 94550

Thomas Y. Palmer*
SWETL Inc.
PO Box 278
Fallbrook, CA 92028

Ron Pape*
IIT Research Institute
10 West 35th Street
Chicago, IL 60616

Thomas A. Reitter*
Lawrence Livermore National Laboratory
University of California
PO Box 808, L-140
Livermore, CA 94550

Martin Rosenblatt*
California Research & Technology, Inc.
20943 Devonshire Street
Chatsworth, CA 91311

Dr. E. Sevin*
Defense Nuclear Agency
6801 Telegraph Road
Alexandria, VA 22310

Bahaaeldin I. Shehata*
US Army, Aberdeen Proving Ground
(BRL-TBD, BDB)
Ballistic Research Laboratory
Terminal Ballistic Division
Aberdeen Proving Ground MD 21005

Shyam Shukla*
Lawrence Livermore National Laboratory
University of California
PO Box 808, L-90
Livermore, CA 94550

T. R. Slawson*
USAE Waterways Experiment Station (WES)
Vicksburg, MS 39180

Richard D. Small*
Pacific-Sierra Research Corporation
12340 Santa Monica Boulevard
Los Angeles, CA 90025

Brian Stocks*
Great Lakes Forest Research Center
PO Box 490
Sault Ste. Marie
Ontario CANADA

Henry Tovey*
Federal Emergency Management Agency
National Preparedness Programs
Directorate
Washington, DC 20472

Gordon Turnbull*
Home Office
Scientific Advisory Branch
Horseferry House
Dean Ryle Street
London SWIP 2AW, ENGLAND

S. C. Woodson*
USAE Waterways Experiment Station (WES)
Vicksburg, MS 39180

J. Worden*
USAE Huntsville Division
PO Box 1600
Huntsville, AL 35807

J. V. Zaccor*
Scientific Service, Inc.
517 East Bayshore Drive
Redwood City, CA 94060

H. L. Brode*
Pacific-Sierra Research Corporation
12340 Santa Monica Boulevard
Los Angeles, CA 90025

Andrew Mark*
Ballistic Research Laboratory
ATTN: DRDAR-BLT
Aberdeen Proving Ground, MD 21005

Robert F. Perret
Lawrence Livermore National Laboratory
University of California
PO Box 808, L-10
Livermore, CA 94550

GPO 687-002/8078